ARCHITECTURE OF DEEP-MARINE INTERCHANNEL DEPOSITS: ISAAC FORMATION, WINDERMERE SUPERGROUP (NEOPROTEROZOIC), SOUTHERN CANADIAN CORDILLERA

By Leena Davis

Thesis submitted to the
Faculty of Graduate Studies and Postdoctoral Studies
In partial fulfillment of the requirements for a
M.Sc. degree in Earth Sciences

Ottawa-Carleton Geoscience Centre
Faculty of Science
University of Ottawa

The undersigned certify that they have read, and recommend to the Faculty of Graduate and Postdoctoral Studies for acceptance, a thesis entitled: "Architecture of Deep-Marine Interchannel Deposits: Isaac Formation, Windermere Supergroup (Neoproterozoic), Southern Canadian Cordillera) " submitted by Leena Davis in partial fulfillment of the requirements for the degree of Master of Science.

_____

Dr. R.W. (Bill) C. Arnott
Supervisor, University of Ottawa

_____

Dr. Mark Hannington
Chairman of Committee, University of Ottawa

_____

Dr. André Desrochers
University of Ottawa

_____

Dr. Claudia Schröder-Adams
Carleton University

Date: _____

Abstract

The Windermere turbidite system, exposed in the southern Canadian Cordillera, east-central British Columbia, is a continental scale, passive margin, submarine fan system, part of which is well exposed in the Castle Creek study area. Here millimetre- to decametre-scale sedimentological and stratigraphic observations identified five facies in interchannel strata: very thin- to medium-bedded turbidite (F1), thick-bedded turbidite (F2) coarse-tail graded structureless sandstone (F3), mudstone clast breccia (F4) and carbonaceous mudstone (F5) and four architectural elements: channel (AE1), distal levee (AE2), overbank splays (AE3) and crevasse splays (AE4). These elements are assembled into a predictive depositional model that describes the initiation and evolution of sandy splay elements developed in distal levee strata of deep-marine slope channels. These data can be used in hydrocarbon exploration to identify and differentiate splay deposits in core and on seismic, and thereby improve the accuracy of subsurface reservoir models.

Résumé

Le système de turbidites du Groupe de Windermere affleure au sud de la Cordillère canadienne, au centre-est de la Colombie-Britannique. Ces dépôts de marge passive consistent en un cône de déjection sous-marin à l'échelle continentale, dont une partie est bien exposée au site d'étude de Castle Creek. Les observations sédimentologiques et stratigraphiques à l'échelle millimétrique et décamétrique ont mené a l'identification de cinq faciès dans les strates situées entre différents chenaux: turbidites à lits très minces à moyens (F1), turbidites à lits épais (F2), grès massif avec granules à sa base (F3), brèches à clastes de mudstone (F4), et mudstones carbonés (F5); ainsi que quatre éléments architecturaux: chenal (AE1), levée distale (AE2), épandage de plaine (AE3) et épandage de crevasse (AE4). Ces éléments sont assemblés en un modèle de déposition décrivant l'initiation et l'évolution d'éléments d'épandage sablonneux développés dans les strates de levée distale de chenaux marins profonds sur la pente continentale. Ces données peuvent être utilisées pour l'exploration d'hydrocarbures afin d'identifier et différencier les dépôts de cône d'épandage dans les carottes de forage et les images séismiques, et ainsi améliorer la précision des modèles de réservoirs en sous-surface.

Extended Abstract

In the Castle Creek study area (southern Canadian Cordillera, east-central British Columbia), millimetre- to decametre-scale sedimentological and stratigraphic observations identified five facies: very thin- to medium-bedded turbidite (F1), thick-bedded turbidite (F2) coarse-tail graded structureless sandstone (F3), mudstone clast breccia (F4) and carbonaceous mudstone (F5); and four architectural elements: channel (AE1), distal levee (AE2), overbank splays (AE3) and crevasse splays (AE4). These elements are assembled into a predictive depositional model that describes the initiation and evolution of locally developed splay elements within a background of thinly-bedded, fine-grained distal levee and rare channel deposits.

Channel unit (AE1) consists of two laterally-offset-stacked leveed channels. These laterally migrating channels are filled with alternating fine- and coarse-grained lateral accretion deposits, or LADs, that formed on the inner bend of laterally-migrating, sinuous, deep-marine channels. Fine LADs consist of fine-grained, thin-bedded Tcd turbidites, whereas coarse LADs consist of coarse-grained, medium- to thick-bedded structureless sandstones. Channels are bound on their margins by positive relief, wedge-shaped features termed levees. Outer bend levee deposits are thicker and more steeply inclined (into the channel) compared to their inner bend counterpart. Outer bend levees comprise two end-member stratal units: mud-rich and sand-rich. Mud-rich units consist of laterally continuous, planar based, fine-grained very thin- to medium-bedded Tcd or Tbcd turbidites. Sand-rich units are subdivided into overbank splays and crevasse splays.

Overbank splays are further subdivided into: isolated and multiple bed complexes. Isolated beds are single, thick-bedded, Tbcd or Tbd turbidites encased in thin-to medium-bedded turbidites, whereas multiple bed complexes consist of amalgamated, normally graded, coarse-grained structureless sandstone units. Both kinds of overbank splay have a low (10% or less) detrital mud matrix content. Along the outer bend, superelevation and flow stripping increased sedimentation rates and hence levee growth. Upon exiting the channel, flows bypassed the proximal levee, accelerated down its steeply-dipping backside and deposited on the lower slope of the distal levee. In the case of isolated beds, thick flows that were not completely confined to the channel, overflowed, and

under competence-driven conditions, deposited a succession of planar laminated sand. Multiple bed complexes, in contrast, are the result of a partial breach in the levee that allowed multiple flows to escape the channel and under capacity-driven conditions, deposit the graded, structureless beds. Eventually the breach was in filled (healed) and sedimentation of mostly fine, thinly-bedded turbidites resumed.

Crevasse splay deposits consist of coarse-grained, poorly-sorted, coarse-tail graded, structureless sandstones with a high (30-50%) mud matrix content. Two end member kinds are recognized: tabular and amalgamated. In tabular units, bed bases are sharp, planar and non-erosive and beds show negligible change in facies or thickness laterally. In amalgamated units, individual beds have erosive bed bases and are laterally discontinuous. Crevasse splay deposits reflect rapid, capacity-driven deposition possibly downflow of a plane-wall jet with jump. The jump formed at an abrupt change in slope downflow of a major levee breach where supercritical flow ($Fr > 1$) transitioned abruptly to subcritical flow ($Fr < 1$). The levee breach allowed most of the thickness of the flow to escape the channel and be diverted into the interchannel area. At the jump, the bed was deeply scoured and subsequently draped quickly by a layer of sediment from the collapsing sediment cloud depositing the amalgamated facies. Beyond the jump, locally-generated turbulence was damped by high sediment concentration and seafloor scour became negligible. Nevertheless, sedimentation rate remained high as the dispersion continued to collapse and deposited the matrix-rich, tabular deposits.

Acknowledgements

I would like to thank my supervisor, Bill Arnott, for giving me the opportunity to conduct this research. Your enthusiasm is contagious and made this project an extraordinary learning experience. Thank-you to the Arnott family, you made me feel like a part of your family and it made the transition of moving to a new area and starting a new life easy.

I want to thank my peers Shann Khan, Lilian Navarro, Viktor Terlaky, Mike Tilston, Jonathan Rochaleau and Lindsay Coffin for their friendship and insightful conversation. Special thanks to my field assistants, Grady Arnott and Gillian Cramm, for their friendship and hard work. Thanks to everyone who spent time with me in the Castle Creek especially field assistants Dave Anthony, Peirce Grogan, Carley Senkowski, Alexis Norwell, Jordan Clarke, Adam Tudor for all your laughter, music and food. Thanks to the McKirdy family and Yellowhead Helicopters for their support in the field.

I want to thank my committee members, Dr. André Desrochers and Dr. Claudia Schröder-Adams, for your helpful comments and insight.

I am grateful for the support of University of Ottawa staff: Wendi Adby, Paul Middlestead, and Patricia Wickham in the G. G. Hatch Stable Isotope Lab; George Mrazek for all the thin sections; and Hélène De Gouffe for administrative support.

Thanks to the Windermere Consortium, Anadarko Petroleum, Canadian Natural Resources Ltd., ConocoPhillips, Chevron, Husky Energy, Nexen Inc., and the Natural Sciences and Engineering Council of Canada (Collaborative Research and Development Grant), for funding this project.

Special thanks to Paul Mortensen for encouraging me pursue my masters and for supporting me in my career as a petroleum geologist. Thanks to Steve Hubbard for your helpful conversation.

I want to thank my family, especially my parents (Paul and Brenda Davis) and grandparents (John and Doreen Charbonneau and Alan and Linda Davis), for all their love and support. I would not have been able to do this without you.

Dedication

To my parents Paul and Brenda Davis

You taught me the value of hard work and provided me with the tools and support to succeed.

Table of Contents

Abstract iii

Résumé iv

Extended Abstract v

Acknowledgements vii

Dedication viii

Table of Contents ix

List of Figures xii

Chapter 1: Introduction

1.1: Purpose 1
1.2: Study Area 1
1.3: Paleogeography 5
1.4: Windermere Supergroup Stratigraphy 8
1.5: Age Constraints 13
1.6: Sediment Provenance 14
1.7: Origin of the Canadian Cordillera 16
1.8: Metamorphism and Structure 17
1.9: Theoretical Overview- Turbidity Currents and Turbidites 19
1.10: Depositional Environment and Modern Analogues 23
1.11: The Amazon Fan 24
1.12: Summary of Deep-Marine Systems 27
1.13: Methodology 28

Chapter Two: Facies

2.1: Introduction 32
2.2: (F1) Thin- to medium-bedded turbidite
2.2.1: Description 33
2.2.2: Petrography 35
2.2.3: Interpretation 37
2.3: (F2) Thick-bedded Turbidite 42
2.3.1: (F2a) Structured turbidite 42
2.3.2: (F2b) Structureless sandstone 44
2.3.3 Petrography 46
2.3.4: Interpretation 47
2.4: (F3) Coarse-tail graded structureless sandstone 52
2.4.1: (F3a) Amalgamated structureless sandstone 53

2.4.2: (F3b) Tabular structureless sandstone 54
2.4.3: Petrography 56
2.4.4: Interpretation 57
2.5: (F4) Mudstone clast breccia 60
2.5.1: (F4a) Mudstone clast breccia 60
2.5.2: (F4b) Irregular clast breccia 63
2.5.3: Interpretation 65
2.5.4: (F4a) Interpretation 65
2.5.5: (F4b) Interpretation 66
2.6: (F5) Carbonaceous mudstone 69
2.6.1: (F5a) Massive carbonaceous mudstone 69
2.6.2: (F5b) Carbonaceous mudstone laminae 69
2.6.3: Petrography 72
2.6.4: Interpretation 73
2.6.5: The origin and preservation of organic matter 74
2.6.6: Pyrite formation and early carbonate cements 75

Chapter 3: Architectural Elements

3.1: Introduction 77
3.2: Architectural elements in deep-marine systems 78
3.3: Channel-levee systems 81
3.3.1: Lateral accretion deposits 84
3.3.2: Channel description 87
3.3.3: Channel fill 1 90
3.3.4: Channel fill 2 94
3.3.5: Channel fill 3 99
3.3.6: Channel interpretation 101
3.4: Submarine levee deposits 103
3.5: Outer bend distal levee deposits 108
3.5.1: Fine-grained outer bend distal levee deposits 109
3.5.2: Fine-grained outer bend distal levee deposits interpretation 112
3.6: Overbank splays 114
3.6.1 Isolated overbank splays 114
3.6.2: Isolated overbank splays lateral trends 116
3.6.3: Isolated overbank splays interpretation 119
3.6.4: Multiple bed complexes (overbank splays) 120
3.6.5: Multiple bed complexes (overbank splays) interpretation 121
3.7: Crevasse splays 122
3.7.1: Amalgamated crevasse splay 123
3.7.2: Amalgamated crevasse splay interpretation 125
3.7.3: Tabular crevasse splay 126
3.7.4 Tabular crevasse splay interpretation 128

Chapter 4: Discussion

4.1: Introduction 129
4.2: Depositional history 132
4.3: Depositional model 136
4.4: General depositional model for interchannel elements 144

Chapter 5: Conclusions

5.1: Summary 149
5.2: Implications for hydrocarbon exploration 151

References 153

Appendix:

Appendix A: Detailed channel correlation 170
Appendix B: Correlation across the glacier 171

List of Figures

Chapter One: Introduction

Figure 1.1: Distribution of WSG rocks 2
Figure 1.2: Photo of the Castle Creek study area 3
Figure 1.3: Geology of the Castle Creek study area 4
Figure 1.4: Schematic cross-section of the Windermere margin 7
Figure 1.5: Comparison of modern and ancient fan systems 8
Figure 1.6: Stratigraphic correlation chart of the WSG 9
Figure 1.7: Stratigraphic column for the Castle Creek study area 10
Figure 1.8: Precambrian basement rocks of Alberta 15
Figure 1.9: Morphologic belts of the Canadian Cordillera 17
Figure 1.10: Schematic of a turbidity current 20
Figure 1.11: Idealized Bouma sequence turbidite 23
Figure 1.12: Idealized sandy and gravelly high density turbidite 23
Figure 1.13 Location of Amazon and Mississippi fans 24
Figure 1.14: Map of the Amazon Fan 26
Figure 1.15: Deep-marine depositional elements: examples from seismic 30
Figure 1.16: Deep-marine depositional elements: examples from WSG 30
Figure 1.17: Aerial photograph Castle Creek north study are 31

Chapter Two: Facies

Figure 2.1: Facies summary 32
Figure 2.2: Tabular thin-bedded turbidites (F1) 34
Figure 2.3: Tcd thin-bedded turbidites (F1) 34
Figure 2.4: Photo micrograph of the sandy portion of a thin-bedded turbidite (F1) 36
Figure 2.5: Photo micrograph of pyrite 36
Figure 2.6: Photo micrograph of the silty portion of a thin-bedded turbidite (F1) 37
Figure 2.7: Hypothetical bedform stability diagrams 39
Figure 2.8: Tbcd turbidite (F2a) 39
Figure 2.9: Tbd turbidite (F2a) 40
Figure 2.10: Flow pattern over a ripple 40
Figure 2.11: F1 thin-bedded Tcd turbidites with multiple non-climbing ripple sets 41
Figure 2.12: Climbing ripple cross-stratification 41
Figure 2.13: Origin of load and flame structures 41
Figure 2.14: Load and flame structures in outcrop 42
Figure 2.15: Thick-bedded Tbcd turbidite (F2a) 43
Figure 2.16: Shallowly scoured bed base 44
Figure 2.17: Normally graded structureless sandstone (F2b) 45
Figure 2.18: Structureless sandstone beds (F2b) with amalgamated bases 46
Figure 2.19: Photo micrograph of F2 47
Figure 2.20: Inverse grading 48
Figure 2.21: Photograph of a turbulent flow in an annular flume 49
Figure 2.22: Tabd turbidite (F2a) 51
Figure 2.23: Tbd turbidite (F2a) 51
Figure 2.24: Amalgamated structureless sandstone (F3a) 53
Figure 2.25: Breccia layer within F3a 54

Figure 2.26: Tabular coarse-tail graded structureless sandstone (F3b) 55
Figure 2.27: Large isolated mudstone clasts (F3b) 55
Figure 2.28: Photo micrograph F3 56
Figure 2.29: Plane-wall jet with jump 59
Figure 2.30: Tabular unlaminated mudstone clast breccia (F4a) 61
Figure 2.31: Angular unlaminated mudstone clast (F4a) 61
Figure 2.32: Tabular laminated mudstone clasts (F4a) 62
Figure 2.33: Tabular unlaminated mudstone clasts (F4a) with flame structures 62
Figure 2.34: Irregular mudstone clast breccia (F4b) 64
Figure 2.35: Ptygmatically folded dyke (F4b) 65
Figure 2.36: Schematic of deformation in F4b 68
Figure 2.37: Massive carbonaceous mudstone (F5a) 70
Figure 2.38: Table of TOC samples in F5 70
Figure 2.39: Massive carbonaceous mudstone (F5a) 71
Figure 2.40: Carbon-rich laminae (F5b) 71
Figure 2.41: Photo micrograph of carbonaceous mudstone (F5) 72

Chapter Three: Architectural Elements

Figure 3.1: Deep-marine architectural elements 77
Figure 3.2: Schematic diagram sandy outer bend levee distal elements 79
Figure 3.3: Table summary of deep-marine architectural elements 80
Figure 3.4: Hierarchy of submarine channel elements 81
Figure 3.5: Schematic diagram of channel evolution 83
Figure 3.6: Planform geometry meandering fluvial and deep-marine channels 85
Figure 3.7: Secondary flow pattern in a fluvial meandering channel 86
Figure 3.8: Velocity profiles for subaerial and subaqueous systems 87
Figure 3.9: LADs in channel unit 88
Figure 3.10: Stratigraphic correlation over channel unit 88
Figure 3.11: Interpreted air photo of channel unit 89
Figure 3.12: Channel fill facies association: F2b and F4a 91
Figure 3.13: Small-scale scour and mudstone drape 91
Figure 3.14: Channel fill facies association: F2b and F1 92
Figure 3.15: Interpreted photo of CH1 fill 93
Figure 3.16: Interbedded fine-and coarse-LADs 95
Figure 3.17: Structured coarse-grained end member 96
Figure 3.18: Close up of an abrupt pinch-out of a coarse-LAD 96
Figure 3.19: Coarse-LADs pinching out into fine-LADs 97
Figure 3.20: Detailed correlation of LADs within CH2 98
Figure 3.21: Abandonment fill CH2 99
Figure 3.22: Top of CH3 100
Figure 3.23: Schematic diagram LAD deposition 101
Figure 3.12: Schematic of channel stacking pattern 103
Figure 3.25: Seismic images of submarine levees 105
Figure 3.26: Straub and Morhrig model of levee development 106
Figure 3.27: Horizontal beds model of levee development 106
Figure 3.28: Potential channel overbank 107
Figure 3.29: Schematic diagram of distal levee deposition 109
Figure 3.30: Tabular thin- to medium-bedded turbidites 110
Figure 3.31: Stratigraphic correlation through tabular thin-bedded turbidite 110
Figure 3.32: Multiple ripple sets (F1) 111
Figure 3.33: Silt drapes over ripple fore sets 111
Figure 3.34: Thin-bedded “CCC” turbidites 113
Figure 3.35: Isolated overbank splay 115

Figure 3.36: Lateral facies transitions from thick- to thin-bedded turbidite 117
Figure 3.37: Outcrop photo of facies transitions 118
Figure 3.38: Schematic diagram of isolated overbank splay deposition 119
Figure 3.39: Multiple bed complex (overbank splay) 120
Figure 3.40: Schematic diagram of multiple bed complex deposition 122
Figure 3.41: Seismic image of a modern crevasse splay deposit 123
Figure 3.42: Amalgamated crevasse splay deposit 124
Figure 3.43: Stratigraphic correlation of an amalgamated crevasse splay 124
Figure 3.44: Schematic diagram of crevasse splay 125
Figure 3.45: Tabular crevasse splay deposit 126
Figure 3.46: Stratigraphic correlation through a tabular crevasse splay 127

Chapter Four: Discussion

Figure 4.1: Air photo architectural element stacking pattern 130
Figure 4.2: Stratigraphic corrletation of architectural elements 131
Figure 4.3: Vertical stratigraphic trends in F1, unit 1 133
Figure 4.4: Stacking pattern of architectural elements 136
Figure 4.5: Seismic image of Joshua channel-levee system 138
Figure 4.6: Multiple bed overbank splay complex photo and stratigraphic column 140
Figure 4.7: Isolated overbank splay photo and stratigraphic column 141
Figure 4.8: Photo micrographs comparing mud-poor and mud-rich sandstones 142
Figure 4.9: Amalgamated structureless sandstone 143
Figure 4.10: Tabular structureless sandstone 144
Figure 4.11: Schematic diagram illustrating deposition of distal levee deposits 145
Figure 4.12: Schematic diagram illustrating deposition of isolated overbank splays 146
Figure 4.13: Schematic diagram illustrating deposition of multiple bed overbank splays 147
Figure 4.14: Schematic diagram illustrating deposition of crevasse splays 148

Appendix:

Figure A.1: Stratigraphic correlation over channel unit 170
Figure B.1: Air photo of organic carbon rich intervals 171
Figure B.2: Correlation across the glacier with organic carbon-rich markers as data 172
Figure B.3: Correlation of architectural elements across the glacier 173
Figure B.4: Stratigraphic section lines through distal levee deposits 174

Chapter 1: Introduction

1.1 Purpose:

Hydrocarbon production from deep-marine sedimentary basins currently accounts for 20-30% of total global hydrocarbon production. This, in turn, has helped provide the impetus and necessary funding for advances in modern technologies, especially high-resolution 3-D seismic imaging; a tool that has significantly improved our understanding of the deep-water sedimentary record (Posamentier and Kolla, 2003). Nevertheless, these techniques still lack the resolution that high-quality outcrop-based research can provide.

Turbiditic channel fills are the most prolific deep-marine reservoirs currently being exploited, however, sandy inter-channel elements have become increasingly recognized as important reservoir facies (e.g. Clemenceau et. al., 2000). The purpose of this thesis is to provide a detailed description, from outcrop, of base-of-slope deep-marine strata deposited in the interchannel area between sinuous leveed channels. This succession comprises five unique facies that are described and interpreted herein. These facies are combined into five architectural elements, which are then used to build a predictive depositional model for the stratigraphic evolution of sandy levee elements.

1.2 Study Area:

The Castle Creek study area is located in the northern Cariboo Mountains, southern Canadian Cordillera, east-central British Columbia (Figure 1.1). The Castle Creek outcrop is a nearly complete, 2.3 km thick (perpendicular to bedding) and 7 km wide (parallel to bedding), exposure of the Neoproterozoic Upper Kaza Group and Isaac Formation of the Windermere Supergroup, hereafter termed WSG (Brown et al., 1986; Murphy, 1987) (Figure 1.2). Here, strata are exposed on the slightly overturned limb of a regional scale southwest-verging fold (Figure 1.3). The rapid retreat (<100years) of a nearby glacier and the nearly vertical dip of the bedding provides a virtually flat, lichen

and vegetation free outcrop. Beds and bedsets can be walked out for 100's of meters parallel to strike. The Castle Creek study area is separated into two parts by a glacier, and termed Castle Creek north and Castle Creek south. This study focuses primarily on a 70 m thick by 200 m wide succession of mostly mud-rich strata exposed in Castle Creek north (Figure 1.2).

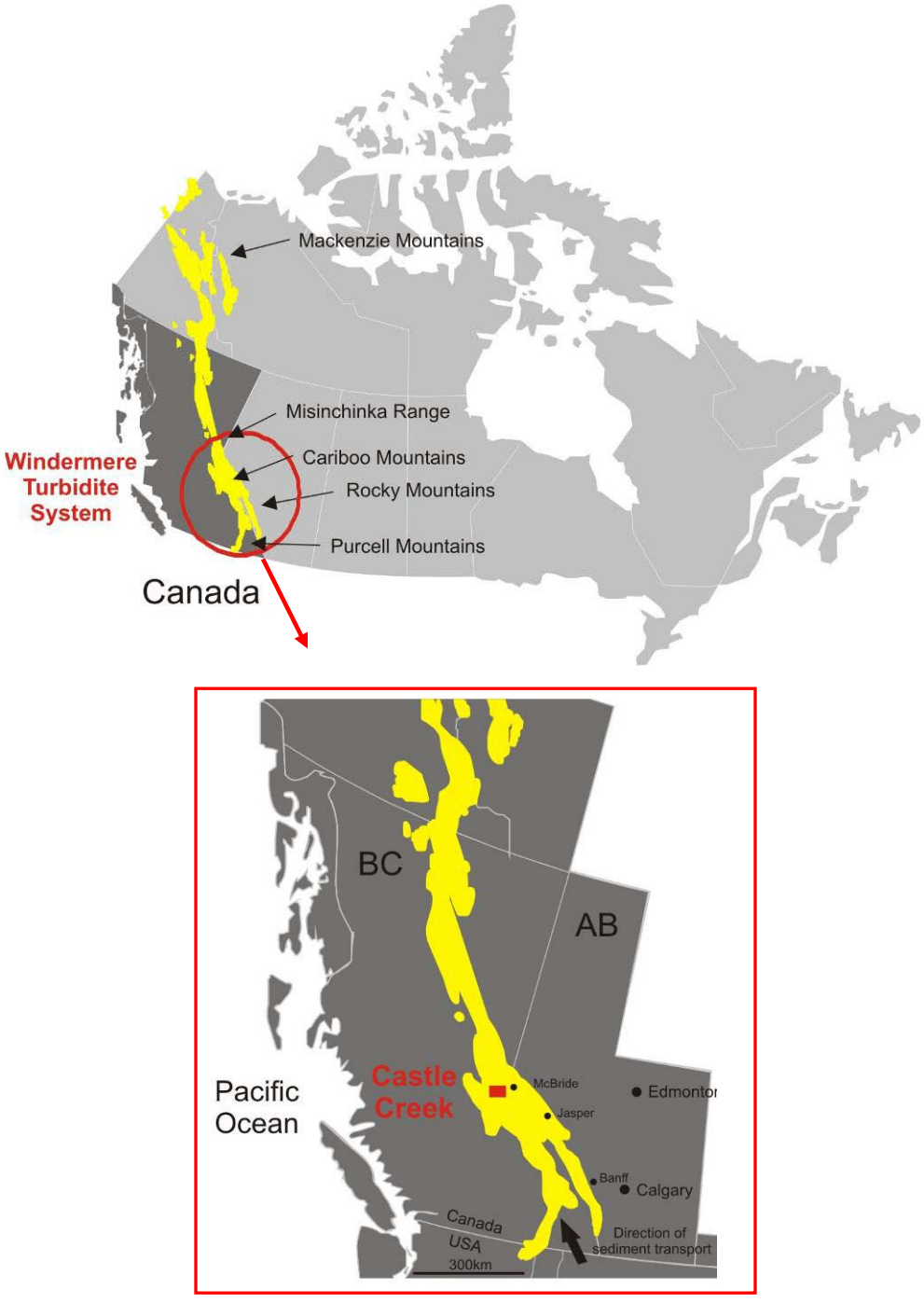

Figure 1.1: Distribution of Windermere Supergroup rocks along the Canadian Cordillera (modified from Ross et al. 1995). The deep-water portion of the Windermere (left) and the Castle Creek study area (right) are highlighted.

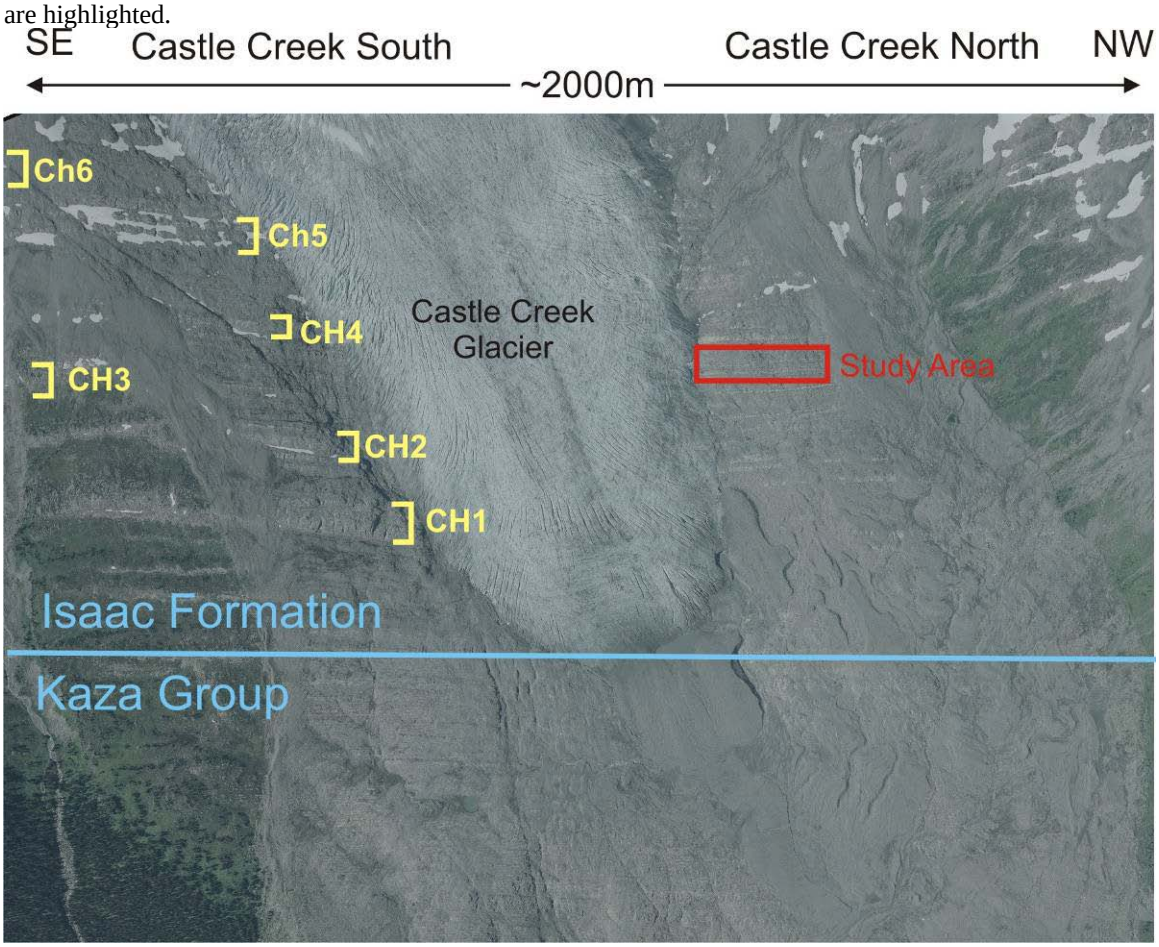

Figure 1.2: Aerial photograph of the Castle Creek region showing the location of the region. In addition, the contact between the two major stratigraphic units, (basin floor) Upper Kaza Group and (base-of-slope) Isaac Formation and the six leveed-channel complexes (IC1-6) in the Isaac Formation are shown. Note the excellent lateral continuity of strata exposed laterally adjacent to the rapidly retreating glacier.

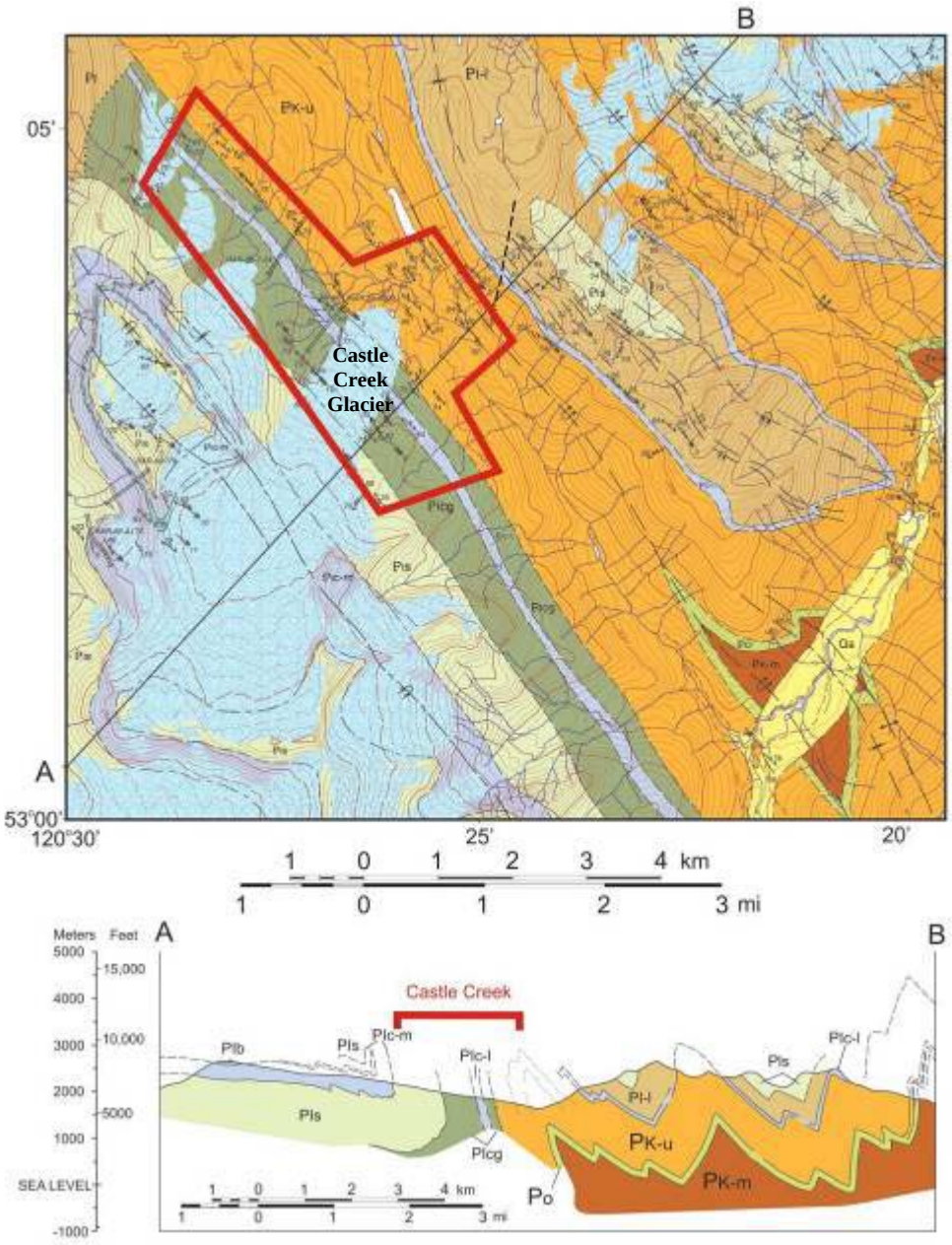

LEGEND

Pk-m = Middle Kaza Group
Po = Old Fort Point Formation
Pk-u = Upper Kaza Group
Qa = Quaternary alluvium
PI-l = lower Isaac Formation, sand-poor
Plcg = lower Isaac Formation, sand-rich
Plc-l = the lower Isaac Formation carbonate marker
PIb = black shale in the middle Isaac carbonate marker
PIc-m = the middle Isaac Formation carbonate marker
Pls = Isaac formation, shale rich

Figure 1.3: Geology in the Castle Creek study area (in red) (excerpt from the Eddy 1:50,000 map area; Ross and Ferguson, 2003). Note the near vertical dip of the strata. The Isaac Formation is shown in green.

1.3 Paleogeography:

Outcrops of the Neoproterozoic WSG extend for over 4000 km from the Sonoran Desert in north-western Mexico through the western United States and the Canadian Cordillera to the Yukon-Alaska border region (Ross et al., 1989; Ross, 1991; Link et al., 1993; Ross et al., 1995; Colpron et al., 2002) (Figure 1.1). In north-western Mexico and the western United States, the WSG consists of shallow marine siliciclastic and subordinate carbonate rocks that are exposed in discontinuous outcrops of the Sevier belt and Basin and Range Province. Further north in the southern Canadian Cordillera, the WSG consists of deep-marine slope and basin floor siliciclastics exposed within the thrust sheets of the Main Ranges. In the northern Canadian Cordillera, the WSG consists of shelf, distal shelf and upper continental slope deposits exposed in the thrust-bound panels of the Mackenzie Mountains (Eisbacher, 1981; Ross, 1991; Narbonne and Aitken, 1995; Ross, 2000).

The Neoproterozoic was a pivotal time in Earth history, and in part marked characterized by the breakup and dispersal of the supercontinent of Rodinia (Knoll and Walter, 1992; Karlstrom et al., 2001; Hoffman and Schrag, 2002). The reconstruction of Rodinia, however, is a source of much debate. Several possible conterminous parts to Laurentia (ancestral North America) have been proposed based on varying types of quantitative and/or qualitative analysis including: Siberia (Sears and Price 1978, 2000; Monger and Price, 1979), the south-western U.S. and east Antarctica (Moores, 1991; Dalziel, 1991; Borg and DePaolo, 1994) south China (Li et al., 1995, 2002), north China (Piper and Rui, 1997), Argentina (Dalziel, 1997), Australia and western U.S. (Karlstrom et al,. 1999, 2001; Burrett and Berry, 2000), and Australia and Mexico (Piper, 2000; Condie, 2001; Wingate et al., 2002).

In the Canadian Cordillera, the lower part of the WSG was deposited within a single rift basin or a complex of rift basins (Stewart, 1972) (Figure 1.4). Although the timing of rifting and its relationship to the subsequent breakup and drift of the margins of the proto-Pacific ocean remain controversial (Gabrielse, 1972; Stewart, 1976; Thompson et al., 1987; Devlin et al., 1988), two distinct crustal extension events are interpreted and have been identified based on U-Pb zircon age dates (Colpron et al., 2002). Rifting was

followed by a Late Neoproterozoic to Late Jurassic miogeoclinal platform (Price, 1994). The upper part of the WSG was deposited on a passive margin (Gabrielse, 1972). Deposition of the WSG was affected by large-basinal structures including the Windermere High; a northwest-trending offshore high that developed south of 53°N.

In the southern Canadian Cordillera, the deep water portion of the basin is represented by an extensive outcrop covering an area of ~35 000 km² (palinspastically unrestored) (Figure 1.1). Minimum palinspastic restoration of the Windermere basin suggests that the basin was originally at least 350 km wide with an areal extent of at least 100 000 km² (McDonough, 1989, Ross et al. 1989, Ross, 2000). In the Cariboo Mountains area, this deep-water part of the WSG consists of two stratigraphic units: the Kaza Group and overlying Isaac Formation. The dominance of sediment-gravity flow deposits indicates deposition below storm weather wave base (250-300 m) (Walker and James, 1992), and the vertical thickness of the stratigraphy (Upper Kaza Group, Isaac Formation and overlying Cunningham Formation), because thermally driven subsidence was negligible during deposition, implies the basin was at least 3000 m deep (Ross et al., 1995). Based on these dimensions, the deep-water Windermere basin is comparable to modern passive margin basins like the Amazon Fan, offshore Brazil and the Indonesia Fan in the Kutei basin (Saller et al., 2004, and the Mississippi Fan, offshore gulf coast, U.S.A (Barnes and Normark, 1985) (Figure 1.5).

Deposition of the WSG ended with diminishing rates of thermally-driven subsidence followed by a second major tectonic event that caused uplift and erosion during the Late Proterozoic to Early Cambrian (Narbonne and Aitken, 1995; Ross, 1991). This formed the regionally extensive sub-Cambrian unconformity (Aitken, 1969) that represents a global hiatus in the stratigraphic record, and marks the base of the Sauk Sequence (Sloss, 1963). From the late Neoproterozoic until the late Jurassic, the western margin of the North American Craton was characterized by a second passive margin, but this time the accumulation of a thick succession of mostly shallow-marine carbonate with subordinate siliciclastic strata (Ross and Arnott, 2007).

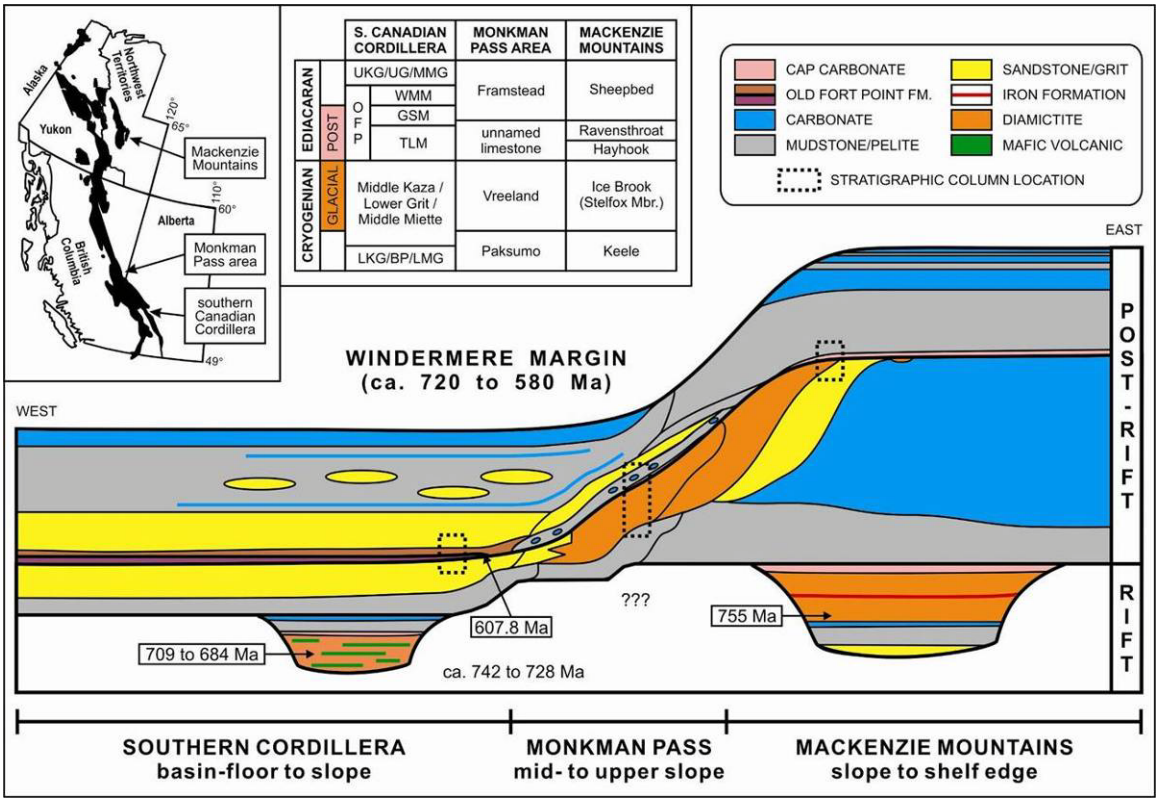

Figure 1.4: Schematic cross-section of the Windermere margin circa 600 Ma (Smith, 2009 modified from Ross et al., 1991). The study area is in the southern Canadian Cordillera where strata deposited in the most basinal (distal) part of the Windermere Basin crop out. Rift facies of the lower WSG are shown as schematic half-grabens developed in crystalline basement or underlying sedimentary rocks of the Belt-Purcell Supergroup.

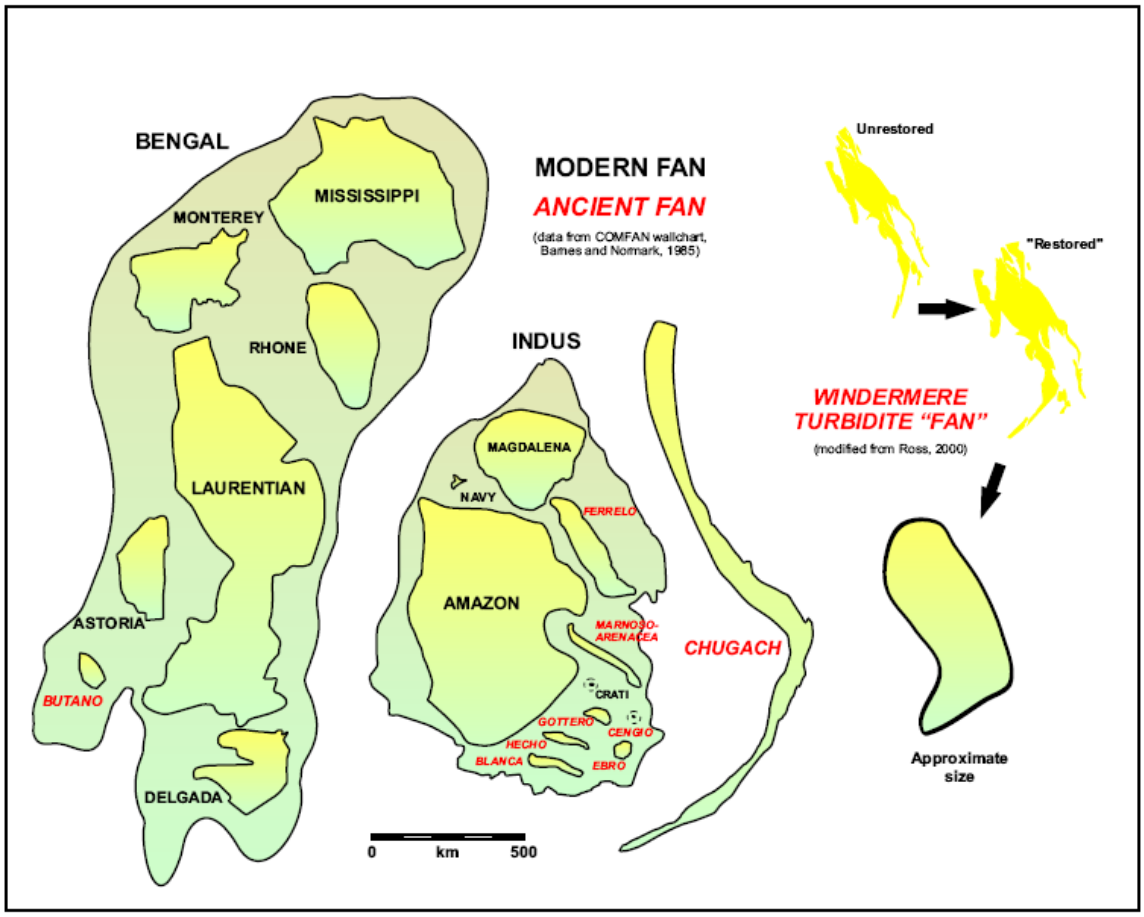

Figure 1.5: Schematic diagram comparing the areal dimension of the Windermere system (Ross, 2000) with other well-known modern and ancient deep marine fan systems from literature (Ross and Arnott, 2007).

1.4 Windermere Supergroup Stratigraphy:

Walker (1926) was the first to use the term 'Windermere System' to describe rocks of the Purcell Mountains in the Windermere area of southeastern British Columbia (Figure 1.1). Gabrielse (1972) and Reesor (1973) later modified the term to Windermere Supergroup. In the Cariboo Mountains, studies of the WSG have focused mostly on structure and regional mapping (e.g. Young et al., 1973; Campbell et al., 1973; Murphy and Rees, 1983; Murphy, 1987a,b; Ross and Murphy, 1988; Ross, 1991; Ross et al., 1995; Ross, 2000; Reid et al., 2002; Ross and Ferguson, 2003) (Figure 1.3). In the southern Canadian Cordillera, the ~9-km-thick sedimentary sequence of the WSG unconformably overlies the Middle Proterozoic Purcell Supergroup (Figure 1.6). The stratigraphy of the WSG is complex and basin wide correlation is difficult, however, the

Old Fort Point Formation, which is discussed below (Ross et. al, 1989), and two carbonate markers provide regional stratigraphic horizons (Figure 1.4 and 1.6). In the Cariboo and Purcell mountains, the WSG comprises the Toby, Irene, Horsetheif Creek formations, Kaza and Cariboo groups, the latter made up of the Isaac, Cunningham, and Yankee Belle formations (Figure 1.6). In the Castle Creek study area (Cariboo Mountains), strata of the Upper Kaza Group and Isaac Formation are well exposed (Figures 1.2 and 1.7). Detailed sedimentologic and stratigraphic mapping has been conducted here since 2000 by mostly graduate student researchers as part of the Windermere Consortium (Nilsen et al., 2007; Arnott and Ross, 2007).

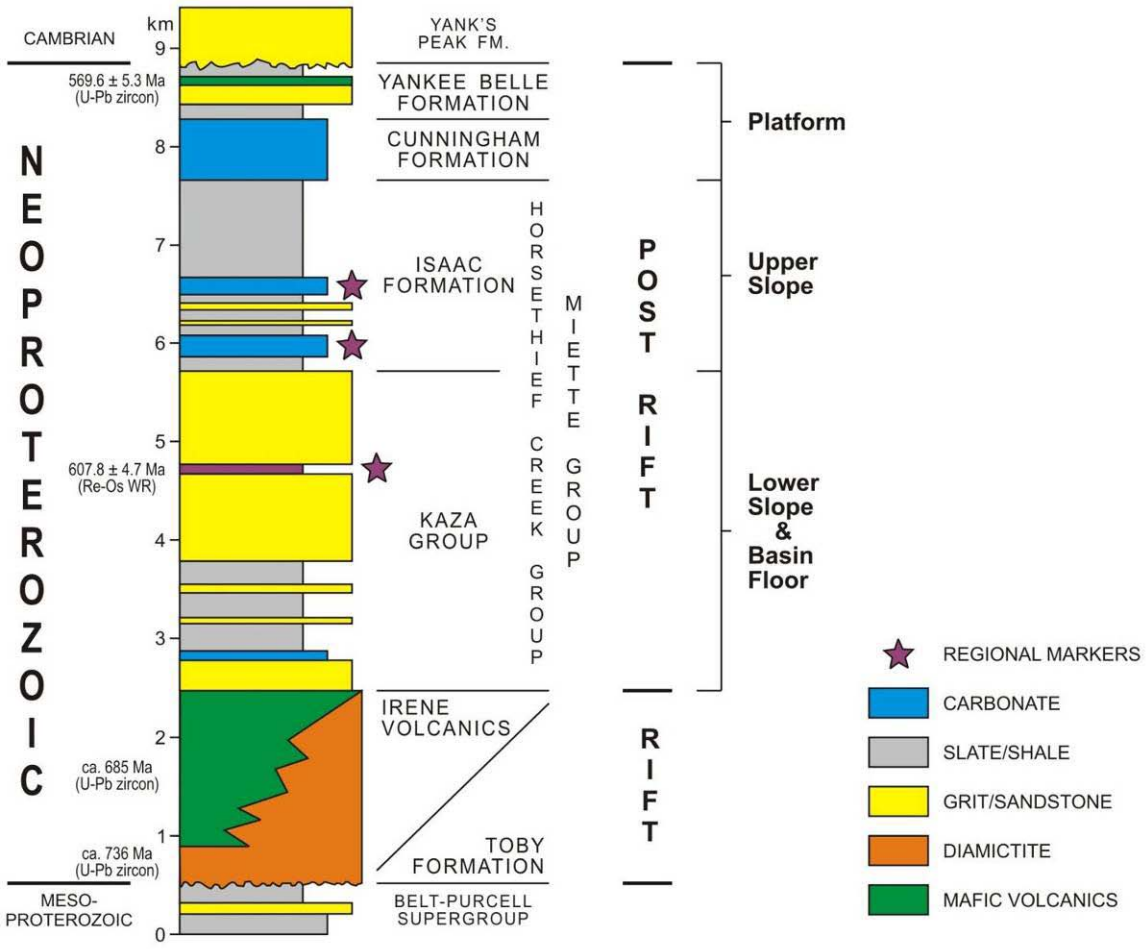

Figure 1.6: General stratigraphic column of the Windermere Supergroup (modified from Ross and Arnott, 2007) in the southern Canadian Cordillera. The deep-water carbonate horizons in the Isaac Formation (blue) and the Old Fort Point Formation (thin purple horizon in the Kaza Group) are used as regional stratigraphic markers (purple stars).

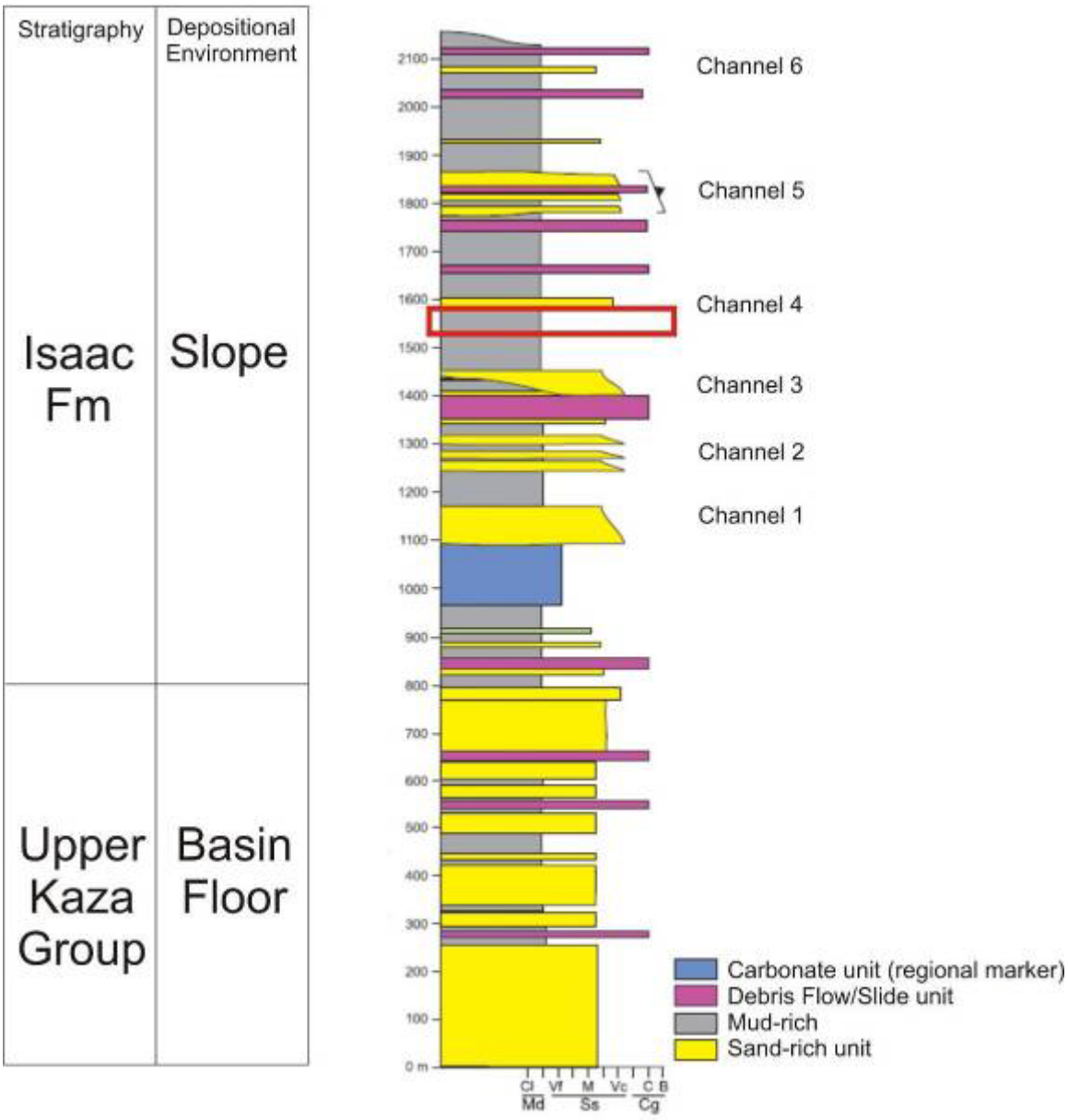

Figure 1.7: Composite stratigraphic column in the Castle Creek study area (modified from Ross and Arnott, 2007). The interval studied in this work is highlighted by the red box.

The Toby and Irene formations are exposed in the Purcell Mountains and unconformably overlie the Mount Nelson Formation. The Toby Formation consists of diamictites interpreted to be glacial in origin based on the rare occurrence of striated clasts, dropstone structures and "exotic" granitic clasts (Aalto, 1971). Further, the Toby Formation is Sturtian in age (approx. 750-700 Ma) and associated with the worldwide Sturtian glaciation (Ross et al., 1995). The Toby Formation is intercalated with mafic volcanics of the Irene Formation, and both formations are interpreted to have been

emplaced during rifting related to continental break-up of Rodinia (Ross et al., 1995).

The Kaza Group conformably overlies the Toby and Irene formations and is subdivided into the Lower, Middle and Upper Kaza groups and the Old Fort Point (OFP) Formation (Campbell et al., 1973). The Kaza Group ranges in thickness from 2 to 4 km. The Lower Kaza Group is characterized by thin, lenticular, carbonate cemented, feldspathic, coarse-grained sandstones interbedded with mudstone. The Middle and Upper Kaza groups comprise sheet-like, carbonate cemented, feldspathic, very coarse-grained sandstones to granular conglomerates interbedded with mudstone. The sandstone:mudstone ratio is approximately 75:25. These 'sheets' consist of stacked decimetre to metre thick, massive to normally graded sandstone beds that become progressively more interstratified with thin bedded turbidites over several 100 meters laterally. Deposition is interpreted to be the result of strong temporal and spatial gradients in sediment transport caused by the lateral spreading of flow on an almost featureless basin floor. In the Castle Creek study area a succession 800 m thick by ~1 km wide is exposed, which makes the outcrop an excellent analogue for seismically resolved basin floor depositional lobes and terminal splays.

The Old Fort Point Formation (OFP), which separates the Lower and Middle Kaza groups, is a unique stratigraphic marker, easily recognized by its distinctive colours and lithologies. The OFP is well exposed in the Southern Canadian Cordillera and provides a key element in reconstructing the deep-water part of WSG sedimentary basin. The OFP Formation ranges from 50-175 m thick and is separated into the Temple Lake, Geikie Siding, and Whitehorn Mountain members (Smith, 2008). The Temple Lake Member is composed of siltstone, mudstone, and rhythmic limestone-siltstone packages. It has a fairly consistent thickness that ranges from 50-125 m thick. The Geikie Siding Member, on the other hand, is composed of organic-rich mudstone-pelite, rare limestone and fine-grained sandstone. It is much thinner that the Temple Lake Member and ranges from 2-12 m thick. The Whitehorn Mountain Member is composed of heterolithic, coarse-grained diamictite, breccia, conglomerate, quartz arenite sandstone, calcareous arenite, limestone, and mudstone-siltstone. The Whitehorn Mountain Member is much less consistent in thickness and ranges from <1 to 165 m thick. Deposition of the OFP

Formation is interpreted to be related to a post-glacial eustatic sea level rise (2nd or 3rd order) that resulted in a shutdown of coarse, immature siliciclastic sediment supply to the basin (Ross and Murphy, 1988).

In contrast to the Kaza Group, the Isaac Formation has a sandstone-mudstone ratio of 25:75. The Isaac Formation is approximately 1500 m thick and consists of resistant sandstone ridges surrounded by recessive-weathering mudstone units. Sandstone and mudstone units are interpreted to represent channel fill and interchannel/levee or mass transport deposits (MTDs), respectively. Six channel-levee complexes, informally termed Isaac Channel 1-6 (IC1-6), have been identified (Figure 1.2). In the Isaac Formation, channel complexes range from 80-200 m thick. Channels commonly extend beyond the limit of the exposure and channel widths are poorly known, although at its widest IC3 is about 1.6 km wide. Generally, each channel complex is composed of 2-4 channel units. Channel units are 10-40 m thick and >1-2 km wide. Further, each channel unit is made up of a number of channel fills that typically range from 4-15 m thick and about 200-400 m wide. In some cases, like IC3, channel complexes migrate laterally and aggrade vertically resulting in a lateral offset stacking pattern. Channel complexes are separated by thick mud-rich levee deposits or MTDs. Levee deposits consist primarily of thin-bedded turbidites, intercalated with sand-rich splay units. MTDs range up to 130 m thick and consist mostly of slump, slide or debris flow deposits. MTDs are more common in the Isaac Formation than the Kaza Group (basin floor), suggesting the Issac Formation was deposited along the gravitationally unstable Laurentian continental slope margin.

In addition, two regionally correlatable carbonate marker horizons, informally termed the first and second Isaac Carbonate markers, have been identified within the Isaac Formation (Figure 1.4, 1.6 and 1.7). The carbonate horizons are up to 250 m thick and consist of thin to medium-bedded turbidites interstratified with massive calcarenites, conglomerates and breccias. These major carbonate intervals are interpreted to be re-sedimented carbonate detritus derived from a shallow water carbonate platform (Ross, 1991). The carbonate markers represent a significant change in sediment flux into the Windermere basin, and most probably relate to a major rise in relative sea level and

development of a shallow water basin CO3 platform. The carbonate factory is interpreted to have been episodically activated, or overwhelmed by siliciclastic input into the basin.

The youngest formations of the WSG are the Cunningham and Yankee Belle formations. The Cunningham Formation is up to 550 m thick and consists of oolitic intraclastic limestone and the overlying Yankee Belle Formation is up to 900 m thick and is made up of interbedded siliciclastics and carbonates (Gabriesle and Campbell, 1992). Both the Cunningham and Yankee Belle formations are interpreted to represent shallow-marine, high-energy shelf conditions (Ross et al., 1995). Taken as a whole, the WGS in the southern Canadian Cordillera forms a several kilometre-thick upward-shoaling succession composed of basin floor deposits (Kaza) overlain by continental slope deposits (Isaac), in turn overlain by shallow-marine, high-energy shelf deposits (Cunningham and Yankee Belle).

1.5 Age Constraints:

Geochronological control on the WSG is limited due to a paucity of fossils and datable horizons. Several age dates obtained from across North America are used to constrain the basal age of the WSG. For example, in the Mackenzie Mountains Rb-Sr ages obtained from mafic sills that intrude strata below the WSG are 766 ± 24 and 769 ± 27 Ma (Armstrong et al. 1982). Similarly, in northern British Columbia zircons from gneissic granites older than the WSG yield a U – Pb age of 728 Ma (Parrish and Armstrong 1983; Evenchick et al. 1984), in the Ogilvie Mountains, near the Yukon - Alaska border, zircons from the Mount Harper Volcanic Complex yield a U - Pb age of 751 Ma ± 26 (Root, 1987), and Sm-Nd mineral-whole-rock age of 762 ± 44 Ma obtained from the Huckleberry Volcanics at the base of the upper Proterozoic in northeastern Washington (Devlin et al., 1988; Ross et al., 1995), among others. The syn-rift volcanics of the Hamill/Gog Group are used as the upper limit of Windermere deposition, which based on a zircon U-Pb date is about 569.6 ± 5.3 Ma (Colpron et al., 2002). Within the WSG, a single absolute age of 607.8 ± 4.7 Ma was measured from the OFP Formation

using Re-Os isochron dating (Kendall et al., 2004), and lies between the bounding limits of about 750 and 570 Ma (Figure 1.6).

1.6 Sediment Provenance:

Early Proterozoic and Archean basement rocks of southern Alberta are interpreted to be the principal source of siliciclastic sediment for WSG in the southern Canadian Cordillera based on their location, composition and age (Ross and Bowring, 1990; Ross et al., 1994) (Figure 1.8). Paleocurrent studies indicate that the Kaza and Cariboo groups were sourced from a single sediment dispersal system with transport generally toward the northwest (Mountjoy and Aitken 1963; Charlesworth et. al., 1967; Carey 1984). The common occurrence of feldspathic sandstone and conglomerate coupled with the lack of lithic fragments suggest that the source rock was a uniform crystalline granitoid terrane. Further, crystallization ages obtained from zircon and monazite crystals present a bimodal age distribution of 1.74 –1.86 Ga and 2.55 – 3.3 Ga (Ross and Parrish, 1991). These paleocurrent indicators, lithologies and ages are consistent with the Early Proterozoic and Archean basement rocks of the Rimbey granites (1.78 – 1.85 Ga), the Loverna Domain (>2.6 Ga; 1.7 – 1.8 Ga), and the Medicine Hat Block (2.6 – 3.3 Ga) (Burwash et al., 1988; Ross and Parrish, 1991; Ross 1995) in southern Alberta. Further, the lack of zircons ages from basement rocks in northern and central Alberta is because they were thought to have been covered by shallow marine sediment during deposition of the WSG (Ross and Parrish, 1991; Ross, 1995; Ross, 2000).

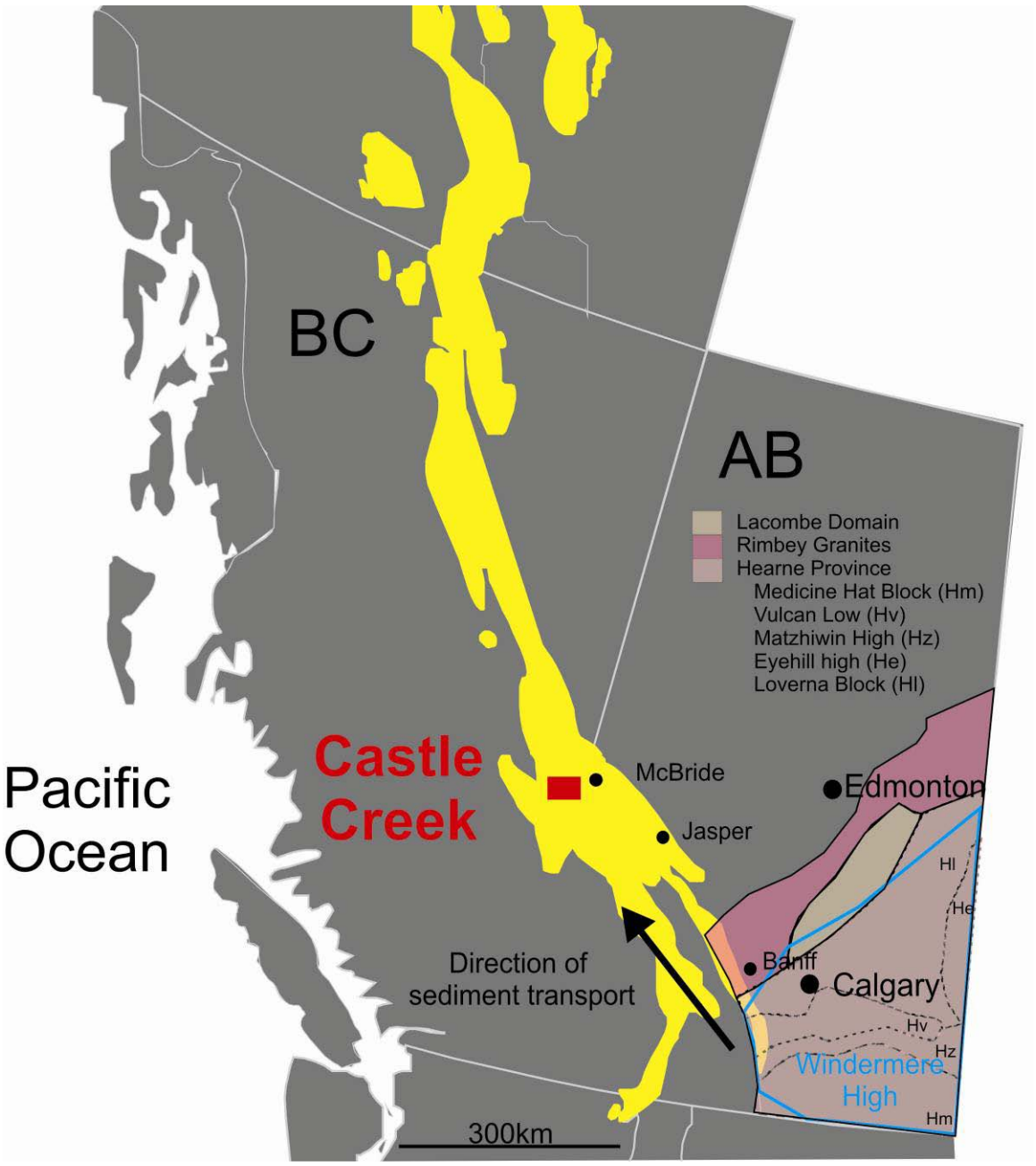

Figure 1.8: Map of Precambrian basement rocks and the Windermere High in Alberta which provided the bulk of the sediment to the deep-water part of the WSG.

1.7 Origin of the Canadian Cordillera:

Collision and accretion of allochthonous terranes formed the Canadian Cordillera. During the Late Jurassic to Early Tertiary through the accretion of allochthonous terranes produced crustal thickening by folding and thrust faulting and eventually culminated in the westward extention of the North American continent by about 500 km (Monger et al., 1985; Monger and Price, 1986; Gabrielse, et al., 1991; Reid et al., 2002). Crustal thickening loaded the continental margin and caused it to downwarp creating a foreland basin ahead of the developing orogen (Price, 1994).

The orogen consists of 5 major morphologic belts, comprising from East to West, the Foreland Fold and Thrust Belt, Omineca Crystalline Belt, Intermontane Belt, Coast Plutonic Belt and Insular Belt; (Figure 1.9) each differentiated based on their characteristic lithologic, structural, tectonic, metamorphic and physiographic attributes (Gabrielse et al., 1991). The Omineca Crysalline Belt and Foreland Fold and Thrust Belt contain autochtonous North American rocks that were deformed and metamorphosed during the growth of the Canadian Cordillera. The Omineca Crystalline Belt is separated from the Foreland Fold and Thrust Belt by a long linear valley called the Rocky Mountian Trench, which, in turn, has been divided into 2 distinct segments namely the northern (NRMT) and southern (SRMT) Rocky Mountain Trench (Monger and Price, 1979; Price, 1994). The WSG crops out in both the Omineca Crystalline and Fold and Thrust Belts.

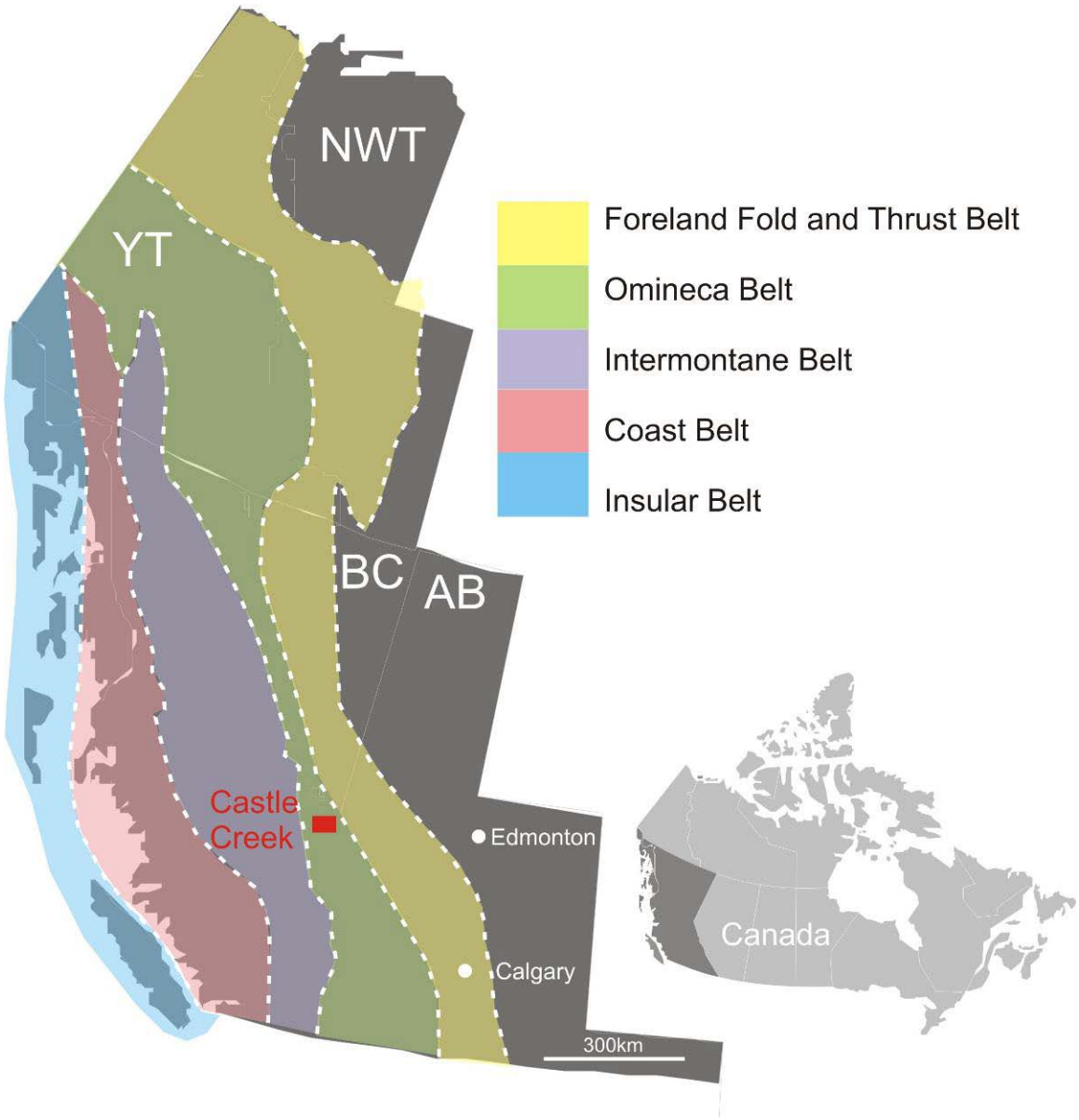

Figure 1.9: Map of western Canada showing the five major morphological belts of the Canadian Cordillera (modified from Reid et al., 2002).

1.8 Metamorphism and Structure:

Metamorphism within the Omineca Crystalline Belt is characterized by high grade (amphibolite facies), Barrovian-style metamorphic complexes typical of orogenic belts, however, it includes expansive areas where rocks were deformed and metamorphosed under low grade conditions at shallow (10-15 km) structural levels. The relationship between high grade and low grade metamorphic rocks within the Omineca

Crystalline Belt remains poorly understood. At deep structural levels the rocks are dominated by ductile features such as large thrust or fold nappes which are polydeformed. At shallow structural levels the rock is dominated by ductile to brittle structures (Campbell, 1970) (Figure 1.3).

Neoproterozoic rocks in the Cariboo Mountains are low-grade, greenschist facies rocks. The metamorphic mineral assemblage is commonly quartz + muscovite + chlorite + albite + pyrite, indicating peak metamorphic conditions within the study area were in the chlorite zone of the greenschist facies. These rocks have been affected by four major phases of deformation, D1, D2, D3 and D4, and 2 major phases of metamorphism, M1 and M2 (Murphy and Rees, 1983; Murphy, 1987 a,b). Each deformation event is associated with folding, faulting and the formation of an axial planar cleavage. The D1 event has a minor influence on the present structural geometry. The oldest structural fabric, S1, is the main evidence for D1 deformation. It formed at approximately the same time as the first stage of metamorphism, M1, and represents the axial planar cleavage of rare, local, recumbant, isoclinal east-west verging folds. The D2 event forms the main regional structure in the Cariboo Mountains and consists of overturned northwest trending, northwest plunging, southwest-verging kilometre-scale folds. It is the northwest plunge of these fold structures that exposes the southward transition to deeper structural levels and increasing metamorphic grade. In addition, a series of reverse faults are associated with the D2 event. D2 deformation is younger than M1 and is interpreted to have formed slightly before and during the second metamorphic event, M2. The age of deformation is constrained by cross-cutting relationships between the deformation events and the intrusion of the Hobson Pluton at 174 Ma. The Hobson Pluton cross cuts regional D2 structures thus constraining the age of D1 and D2 features (Pigage, 1977; Gerasimoff, 1988). The D3 event is post metamorphic. D3 folds are open, upright east-southeast to west-southwest trending folds that refolded D1 and D2 structures. The D3 deformation is also associated with reverse faults. D4 is also interpreted to be post-metamorphic deformation and has a marginal effect on the morphology and orientation of the metamorphic mineral assemblages. The D4 event formed north-south to northeast-southwest trending, steep to upright folds with open to close interlimb angles and chevron style hinge zones. These folds are generally metre to decimetre scale and refolded D1,

D2 and D3 structures. Faults associated with the D4 deformation are mainly strike slip (Campbell, 1970; Campbell et al., 1973; Ferguson, 1994; Reid, 1997).

The Castle Creek study area is exposed on the western side of the Premier Anticlinorium, part of a train of kilometre scale folds created during D2 deformation (Murphy and Journey, 1982; Murphy, 1987a, b). On the steep limb of this anticline, the beds are nearly vertical dipping at approximately 89°. Rocks in Castle Creek were metamorphosed at shallow structural levels. The development of cleavage and greenschist grade metamorphism significantly reduced the primary porosity. The resulting grain framework is typical of metamorphic rocks characterized by sutured grain contacts and the growth of metamorphic mica. The rocks in the study area were subject to temperatures of 350-450° C and pressures of 4-9 kbars (Greenwood et al., 1991).

Although rocks in Castle Creek have undergone greenschist facies metamorphism and multiple phases of deformation, primary sedimentary structures and textures are preserved on the millimetre scale allowing for detailed sedimentologic and stratigraphic study. As a consequence rocks will be classified according to the Folk classification (1959) for sedimentary rocks.

1.9 Theoretical Overview- Turbidity Currents and Turbidites:

Sediment gravity flows are currents consisting of a mixture of sediment and water that move downslope due to gravity forces and are the primary mechanism that transports sediment from the shelf to the abyssal plain (Figure 1.10). Geologists, in an attempt to understand the controls on the character and distribution of different deep-marine deposits, study the fluid mechanics of sediment gravity flows (Walton, 1967; Lowe, 1982, Stow, 1985; Postma, 1986 among others). Several classification schemes based on flow characteristics for sediment gravity flows have been proposed (Lowe, 1982; Kneller and Branney, 1995; Mulder and Alexander, 2001; Sumnar, 2008 among others). Lowe (1982) divided sediment gravity flows into 2 groups: fluid flows and debris flows. In fluid flows, the grains are kept in suspension by the fluid. Fluid flows are further subdivided into turbidity currents and fluidized flows based on the primary

mechanism that maintains large grains in suspension. In turbidity currents, grains are supported by the upward component of flow turbulence whereas in fluidized flows the grains are supported by the upward movement of the ambient fluid. Liquidified flows are intermediate between fluid flows and debris flows wherein grains are partially supported by the upward movement of pore fluid and partly supported by grain-to-grain interaction. In debris flows, on the other hand, grains are supported largely by grain-to-grain interactions. Debris flows are further subdivided into grain flows and cohesive flows. In grain flows the particles are supported by dispersive pressure from particle collisions whereas in cohesive flows the particles are supported by a cohesive matrix.

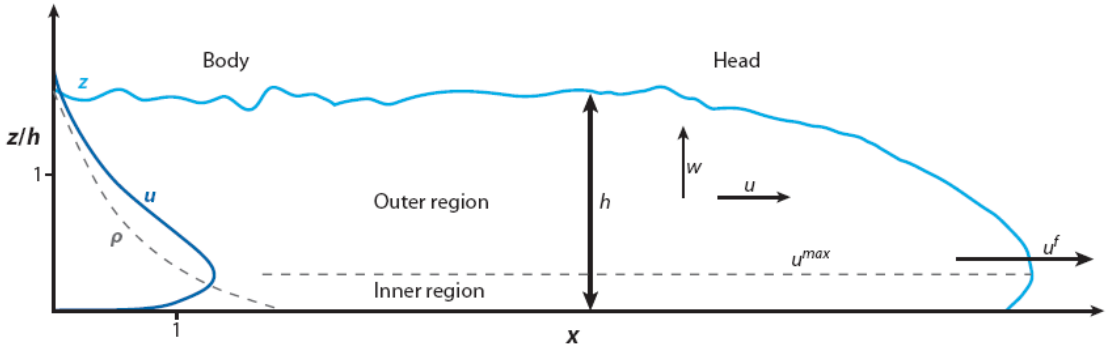

Figure 1.10: Schematic of a turbidity current, the main sediment transporter into the deep marine, showing generalized velocity and density profiles from Meiburg and Kneller, 2009. In an ideal sequence of events a turbidity current is initiated in the sediment staging area by underflow (river discharge) or failure (slump, slide or debris flow). The flow accelerates downslope eroding the substrate and incorporating sediment into the body of the flow, which in turn increases flow density and hence flow speed.

Of the four types of sediment gravity flows, turbidity currents are the most common in the deep-marine. Turbidity currents may evolve directly from the discharge of fluvial systems at the shelf edge, or follow the degradation of a slump, slide or debris flow (Kneller and Buckee, 2000). For example, the Grand Banks earthquake in 1929 destablized sediment along the Nova Scotia continental slope and formed a turbidity current that deposited over 185km^3 of sediment (which if placed in a series railway box cars would form a train that would wrap around the world over 558 times (Arnott pers. comm.)). In nature,

most turbidity currents are vertically density-stratified meaning that grain concentration and flow velocity are highest near the base of the flow and decrease exponentially upwards (Mulder and Alexander, 2001). Turbidity currents become depositional when competence and/or capacity become exceeded. In most cases, this is the result of a reduced flow velocity commonly related to a change in slope, suspended sediment load and/or sediment supply. The resulting deposit is called a turbidite; a term that was first introduced by Kuenen in 1957. As sediment falls from suspension it is then transported by traction along the bed, resulting in the formation of a consistent suite of unidirectional sedimentary structures that reflect waning flow conditions (Southard and Boguchwal, 1990; Kneller and McCaffrey, 2003). Massive sandstones are commonly associated with classical (structured) turbidites and where present, occur at the base of the turbidite (Stow and Johansson, 2000). When the aggradation rate is sufficiently high, upper stage parallel lamination is suppressed and massive beds are deposited (Arnott and Hand, 1989). Other proposed mechanisms for massive sandstone deposition include: sandy debris flows (Shanmugan 1997) and turbidity currents experiencing internal hydraulic jumps (Komar, 1971; Garcia and Parker, 1989; Garcia, 1993; Mulder and Alexander, 2001; Leclair and Arnott; 2003).

The link between the deposit (turbidite) and original flow (turbidite or other form of sediment gravity flow) is not always straightforward. Bouma (1962) proposed an idealized sequence of sedimentary structures, later termed the Bouma sequence, for deposition from a single low-density turbidity current (Figure 1.11). Low-density turbidity currents are generally considered to be turbidity currents with a low sediment concentration less than 9% and consist of clay to medium-grained sand. The idealized sequence of sedimentary structures consists of an upward fining succession that grades from a normally-graded structureless basal sandstone (Ta), to an planar laminated sandstone (Tb), overlain by a cross stratified sandstone (Tc), capped by a laminated sandstone and siltstone (Td), and finally a mudstone unit (Te). In the geological record, complete turbidite sequences are uncommon, however, the vertical succession of divisions is

always observed in the same stratigraphic order and indicates waning flow conditions.

Alternative turbidite classification schemes have been proposed for high density turbidity currents (e.g. Lowe, 1982; Mulder and Alexander, 2001). Lowe (1982) proposed a classification that A, L.subdivides turbidites based on the character of the turbidity current into three main groups: gravelly high density turbidity currents, sandy high density turbidity currents (Figure 1.12) and low density turbidity currents. Deposits of gravelly high density turbidity currents are composed of pebble to cobble gravel and are divided into three main divisions: traction (R1) forming upper stage plane bed and dune cross-stratified deposits, traction carpet (R2) forming inversely graded deposits and suspension (R3) forming normally graded deposits. Deposits of sandy high density turbidity currents are composed of coarse sand to pebble gravel and are subdivided also into three main divisions: traction (S1) forming upper stage plane bed and dune cross stratified deposits, traction carpet (S2) forming thin, horizontal, commonly inversely graded laminae, and suspension (S3 equivalent to the Bouma Ta division) forming structureless or normally graded sandstones commonly with water escape structures. Low density turbidites according to Lowe are composed of clay to medium sand grains and are equivalent to those described by Bouma (1962).

Characteristics of turbidity currents have also been studied using numerical models (Pirmez and Imran, 2003) and observations of morphologic features in modern systems (Pirmez and Flood, 1995). Based on these works, flow durations of many turbidity currents are estimated to be on the order 10s of hours to a few days with recurrence intervals of individual flows every 1–2 years. Many turbidity currents are likely supercritical, with average velocities of 2–4 ms^{-1} and initial mean low concentrations of 1%.

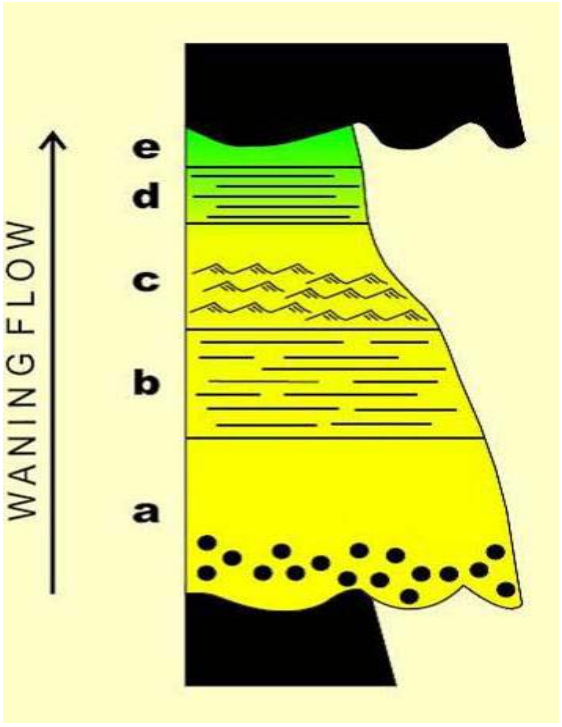

Figure 1.11: The idealized classical, or "Bouma" turbidite sequence (after Bouma 1962). (a) massive conglomerate to sand (b) parallel laminated sand (c) ripple cross-laminated sand (d) parallel laminated sand silt and mud (e) pelagic and hemiplegic mud

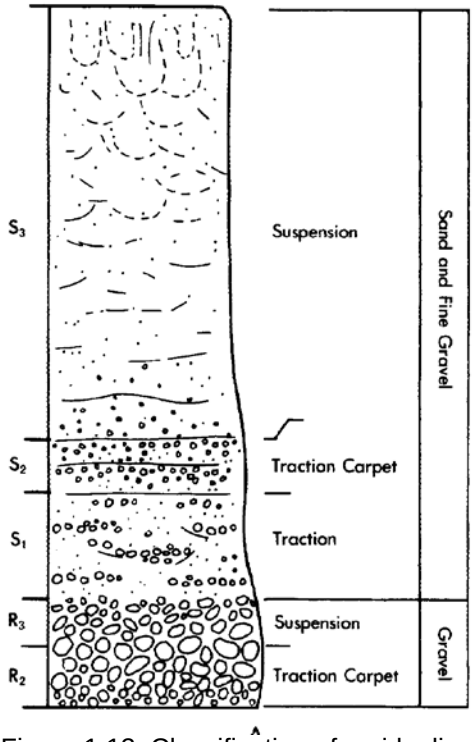

Figure 1.12: Classification of an idealized sandy and gravelly high density turbidite (Lowe, 1982).

1.10 Depositional Environment and Modern Analogues:

Many published studies of deep-marine sinuous channels come from modern systems. Comparison of data collected in modern and ancient fans can be challenging, due to differences in scale and data resolution. Further, detailed information on planform geometries of deep-marine elements is difficult to discern from 2-d outcrops. Published images of modern sinuous channels, in planform and cross-sectional view, are often highly vertically exaggerated (typically >25 times e.g. Schwenk et al., 2003) whereas channels exposed in outcrop are typically affected by compaction during burial and diagenesis. Analogues from modern systems provide an important additional data set for building reliable depositional models. Two deep-marine modern systems are reviewed here: the Amazon and the Mississippi fans (Figure 1.13).

Figure 1.13 Location of the modern Amazon and the ancient Windermere fan systems.

1.11 The Amazon Fan:

The Amazon Fan is fed by the Amazon River and is one of the world's largest submarine fan systems. It is over 800 km long, covers an area of about 330,000 km² and consists of more than 700,000 km³ of sediment (Damuth and Kumar, 1975; Damuth and Flood, 1984, 1985; Pirmez and Imran, 2003). The Amazon Fan extends off the northern Brazilian coast into the Atlantic Ocean between 3° N and 9° N and started to prograde in the middle Miocene (Castro et al., 1978). The average fan gradient decreases downslope from 0.8° on the upper fan to 0.3° on the middle fan and 0.1° on the lower fan (Damuth and Flood, 1984, 1985). The main feeder channel, the Amazon Canyon, is up to 600 m deep and begins on the continental shelf at about the 75 m isobath. The Amazon Canyon passes into a single leveed distributary channel at 1400 m water depth, and marks the up-flow end of the upper fan. The middle fan, between 2000 and 3000 m water depth, begins where the main leveed distributary channel bifurcates into two channel–levee complexes: the Western and Eastern Levee Complex (Damuth and Kumar, 1975; Damuth et al., 1983). The transition to the lower fan is defined by the point where small sand-rich distributary channels that lack levees begin to dominate the stratigraphy. Distributary channels terminate at approximately 4800 m water depth forming sandy lobes on the Demerara Abyssal Plain (Damuth and Kumar, 1975; Damuth and Flood, 1984, 1985; Damuth et al., 1988). Superimposed on this basinward progression are mass-transport

deposits (MTDs) that disrupt or bury the channel–levee systems and modify the basin topography (Figure 1.14) (Damuth and Embley, 1981; Maslin and Mikkelsen, 1998; Maslin et al., 2005). MTDs typically originate on the upper fan and comprise up to 14% (2500 km³) of the sediment on the Amazon Fan (Damuth and Flood, 1985).

The Amazon Fan developed in discrete stages (Mikkelsen and Maslin, 1997). During periods of sea-level lowstand, the Amazon River connects directly to the Amazon Canyon which allows high-frequency, low-density turbidity currents triggered by failure along shelf-edge deltas to transport sediment into the deep-basin (Damuth et al.,1988; Piper and Normark, 2001; Pirmez and Imran, 2003). During periods of sea-level highstand, such as present day, Amazon sediment is transported northward along the continental shelf and virtually no sandy sediment reaches the fan (Shipboard Scientific Party, 1995). Generally, at each successive lowstand, a new slope canyon is activated and each slope canyon feeds a single distributary channel complex where only a single distributary channel is active at any one time. The canyons tend to be stable for many thousands of years whereas the leveed channels on the middle and lower fan regions tend to switch position more frequently (Flood et al., 1991). During highstand, the system is deactivated and covered by a thin layer of pelagic sediment (Flood and Piper, 1997).

Multibeam bathymetric and GLORIA long-range side-scan sonar mapping techniques have revealed that leveed channels are highly sinuous. Sinuosity typically ranges from 1.1–2.95 (Flood and Damuth, 1987; Flood et al., 1991; Pirmez and Flood, 1995), width from 0.3–1.4 km, loop wavelength from 2–15 km and radius of curvature from 0.5–7 km (Flood and Damuth, 1987). Channel relief ranges between 200 m in proximal areas to less than 20 m near the distal fan limit. Core data indicates that channels are filled with very thick, coarse-sand beds with abundant mudstone clasts overlain by very thick, medium-grained to fine-grained sand beds that alternate with thin- to medium-bedded, fine-grained sand, silt, and mud (Normark et al., 1997). In contrast, the associated channel levees consist primarily of mud and silt. Fine-grained, thinly-bedded turbidites are common, and medium-grained, thinly-bedded turbidites were only observed near the base of levee sequences. Thinning- and fining-upward cycles within the levee packages were uncommon (Normark et al., 1997).

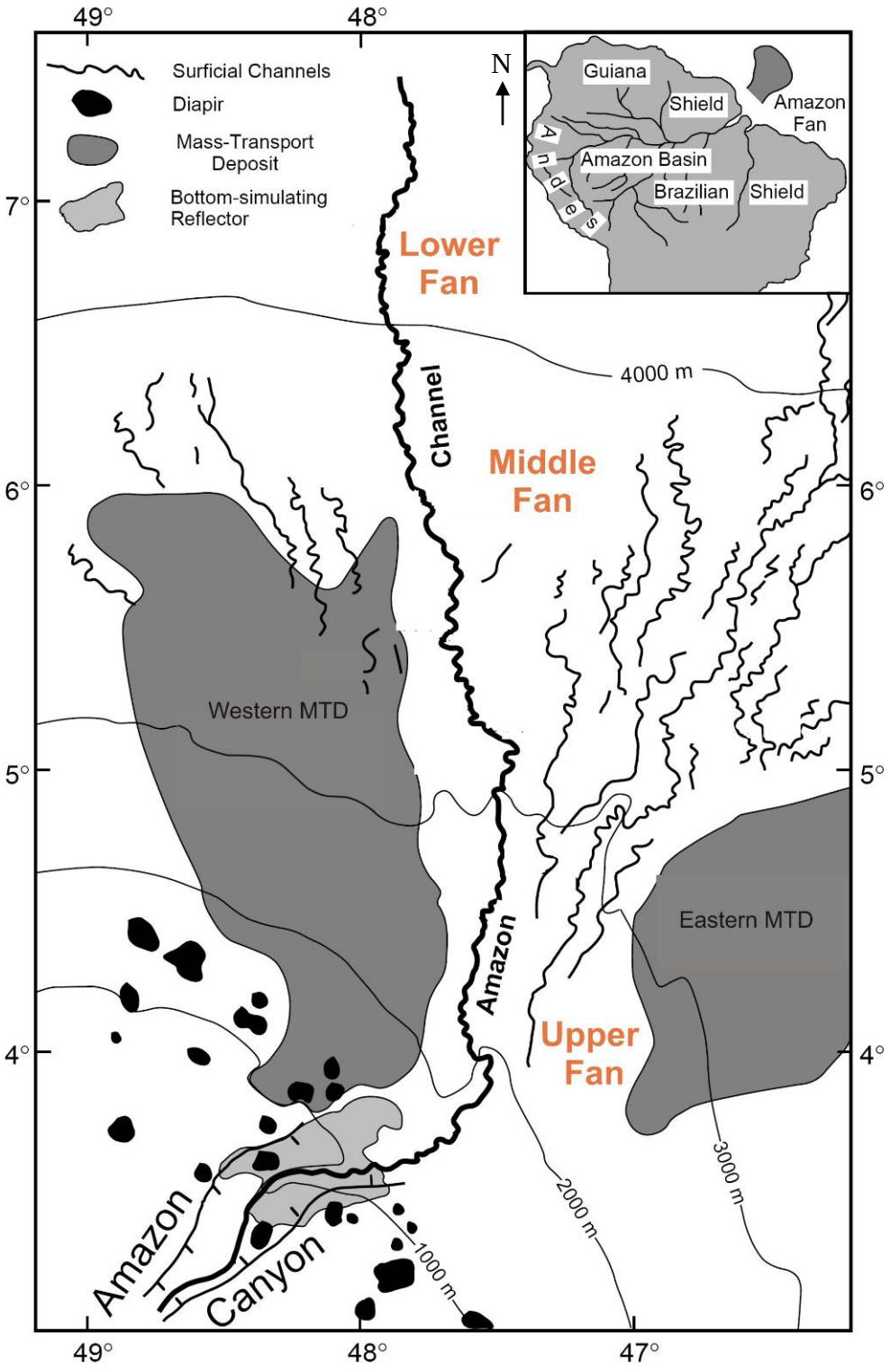

Figure 1.14: Map of Amazon Fan showing the upper, middle and lower canyon areas. The Amazon Channel (bold line) is the most recently active channel on the fan. Modified from Normark and Damuth, 1997 and Flood et al., 1995.

1.12 Summary of Deep-Marine Systems:

The majority of modern deep-water systems are located on passive margins. Sediment is typically transported by river systems to the continental shelf before being re-sedimented further basinward (Figure 1.15 and Figure 1.16). River-fed systems are strongly affected by sea-level fluctuations. During lowstand, submarine canyons tap directly into the hinterland drainage system. They are the principle conduit through which sediment is transported further downslope and eventually to the basin floor fan. As a consequence, sediment rate in the basin floor fans is high. During highstand, on the other hand, the canyon head becomes detached from the river mouth and, as a result, submarine fans become largely inactive. Basinward, canyons shallow and as a result part of the current becomes unconfined and overspills into the inter-channel area building channel-bounding levees. Leveed channels typically occur on low-angle slopes between 0.1–0.5° and may extend 100's of kilometres into the basin. These channel–levee systems are highly aggradational and stack to form channel–levee complexes (e.g. Isaac channels). Further downsystem, and once the supply of fine-grained sediment has been exhausted, the flow can no longer build levees and as a consequence the flow expands over the basin floor and forms a commonly lobate shaped depositional body composed of shallow channels and lobes (e.g. Kaza Group).

1.13 Methodology:

Data was collected over two field seasons, July-August 2008 and August 2009, using field-based outcrop analysis. Data collection included detailed field mapping using high-resolution aerial photomosaics (Figure 1.17a), bed-by-bed measurement of 52 stratigraphic sections (Figure 1.17b), and scintillometer measurements of five stratigraphic sections (Figure 1.17c). Stratigraphic section measurement included bed-by-bed description of lithology, grain size, bed thickness, primary and secondary sedimentary structures. The sedimentologic data gathered was used to identify and distinguish facies relationships. Bed-by-bed correlations and lateral and vertical facies relationships were established by physically "walking-out" bed boundaries on the ground surface between stratigraphic sections. Major marker horizons and thick sandstone beds were mapped on aerial photomosaics. These correlations allowed for the recognition of lateral and vertical facies relationships and the identification of architectural elements. All field data have been captured digitally.

A hand-held scintillometer was used to collect gamma ray spectrometry (GRS) data. The scintillometer measures the naturally emitted gamma radiation of the rock (sourced principally from potassium, uranium and thorium) and records it in counts per second (cps). Measurements were taken at 75 cm intervals and converted into smoothed gamma ray curves. These data can be subsequently rendered into synthetic seismograms, which then can be used to compare the Windermere fan system with well log and seismic data collected from other modern and ancient fan systems.

Hand samples were collected from several strategic locations for petrographic and geochemical analyses. A total of 56 samples were collected for thin section analysis. Thin sections were prepared at the University of Ottawa and evaluated with Olympus SZ61 (plane light stereoscopic) and BX41 (plane and polarized transmitted light) microscopes. Data collected from the thin sections were used to describe grain size, mineralogical constituents, alteration and microstructure. Fourteen of the thin sections were stained following the standard procedure for Alizarin Red S and potassium ferrocyanide (Dickson, 1966). Alizarin Red S staining was used to determine

the type of carbonate cement present (calcite or dolomite) and potassium ferrocyanide was used to identify iron-bearing minerals.

Geochemical analyses were conducted on 16 samples to determine the weight percent of total organic carbon (TOC). Approximately 300 mg of each sample was washed in 10% hydrochloric acid for 1 hour and then rinsed 4 times to remove the inorganic carbonate fraction, which in these rocks occurs mostly as carbonate cement. Samples were then oven dried for 24 hours at 60° C and subsequently re-pulverized into a fine powder using a laboratory ring grinder (tungsten carbide barrel). Approximately 4 mg of each sample was weighed out and wrapped in tin foil. The capsules were loaded with standards into the Vario EL III combustion elemental analyser (EA) to determine the percent carbon content in each sample. In the EA, the sample was flash combusted with oxygen at about 1800° C and carried by helium through columns of reducing/oxidizing chemicals producing N_2, CO_2, H_2O and SO_2 gases. The gases are separated by specific adsorption columns so the thermal conductivity detector can detect each gas separately. Then, an Isotope Ratio Mass Spectrometer (IRMS) was used to measure the various carbon isotopes. The IRMS measures a ratio, therefore, the amount of carbon in each sample must be between 0.02 and 0.2 mg. Using the percent carbon in each sample (from EA), the weight of sample required to obtain ~0.1 mg of carbon was calculated. Samples and standards were weighed into tin capsules and loaded into an EA interfaced with an IRMS (Delta XP Plus Advantage). In the EA the sample is flash combusted at about 1800° C (Dumas combustion) and the resulting gases carried by helium through columns of oxidizing/reducing chemicals optimised for CO_2. These gases are separated by a "purge and trap" adsorption column and subsequently sent to the IRMS interface and then to the IRMS. In the IRMS the gas was ionised as it travels through the source and then shot down a tube through a magnetic field, where as a function of its atomic mass,the path of the isotope is bent. The resulting “mass” streams are then collected and measured to determine the isotopic abundance. The results were blank corrected in order to provide more representative data. Error associated with wt% Corg values is ± 0.1% (Paul Middlestead (G.G. Hatch Stable Isotope Laboratory), 2010 pers. comun.).

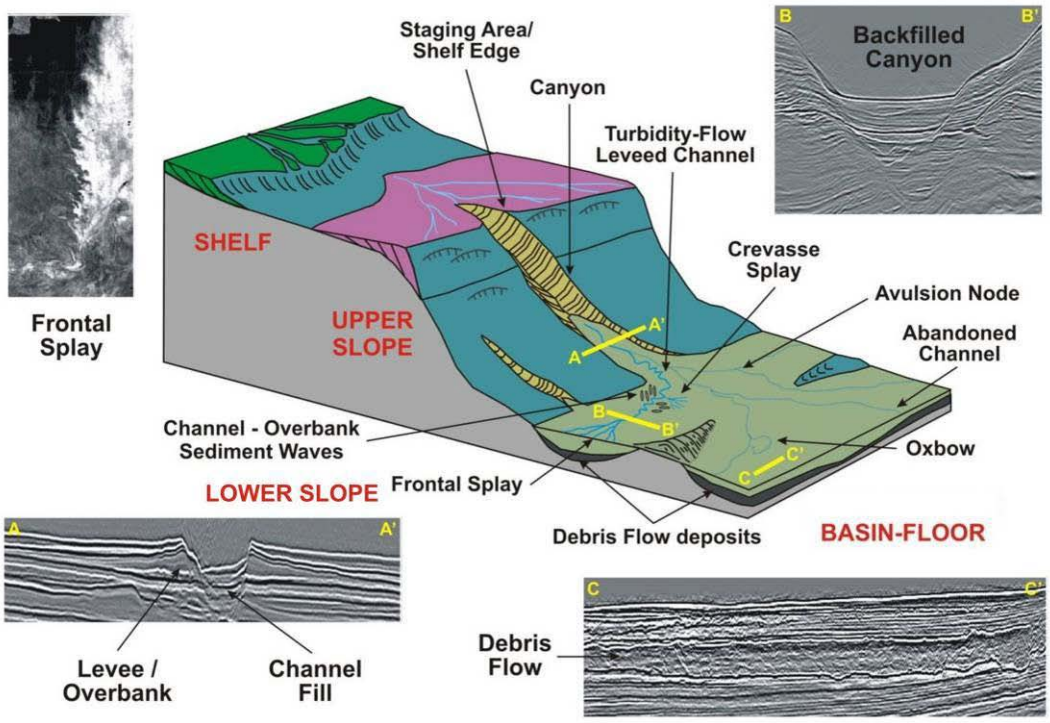

Figure 1.15: General schematic illustrating the of principal depositional elements in deep-water settings with examples from seismic (Posamentier and Kolla, 2003).

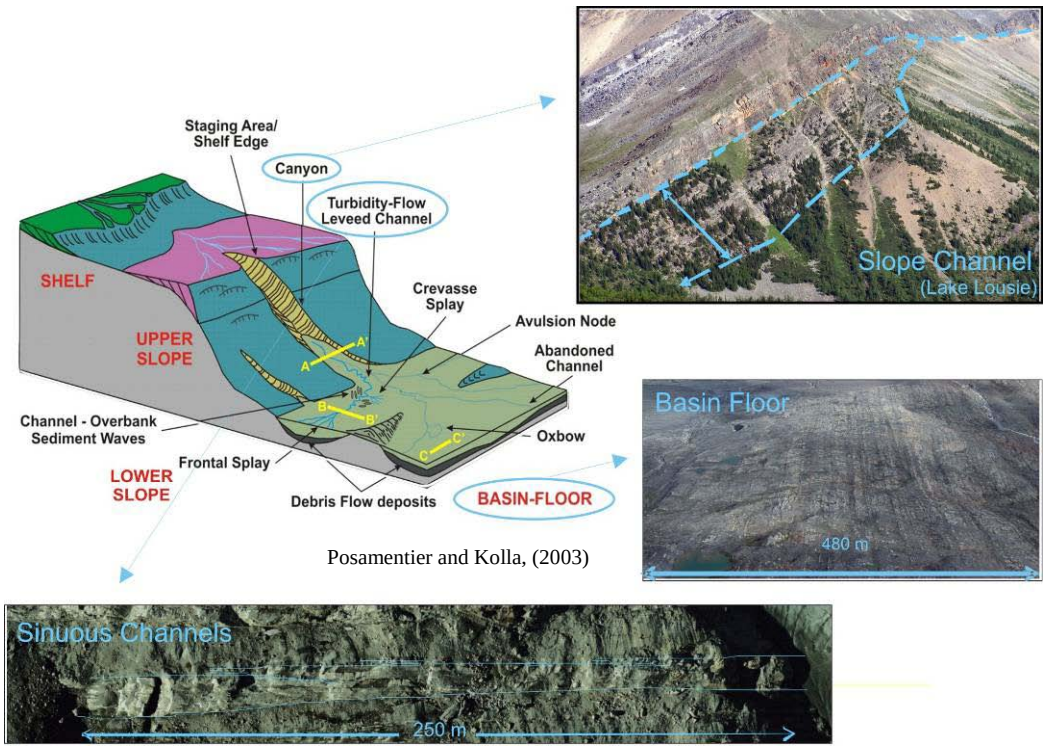

Posamentier and Kolla, (2003)

Figure 1.16: Schematic showing the of principal depositional elements in deep-water settings with examples from the Windermere System.

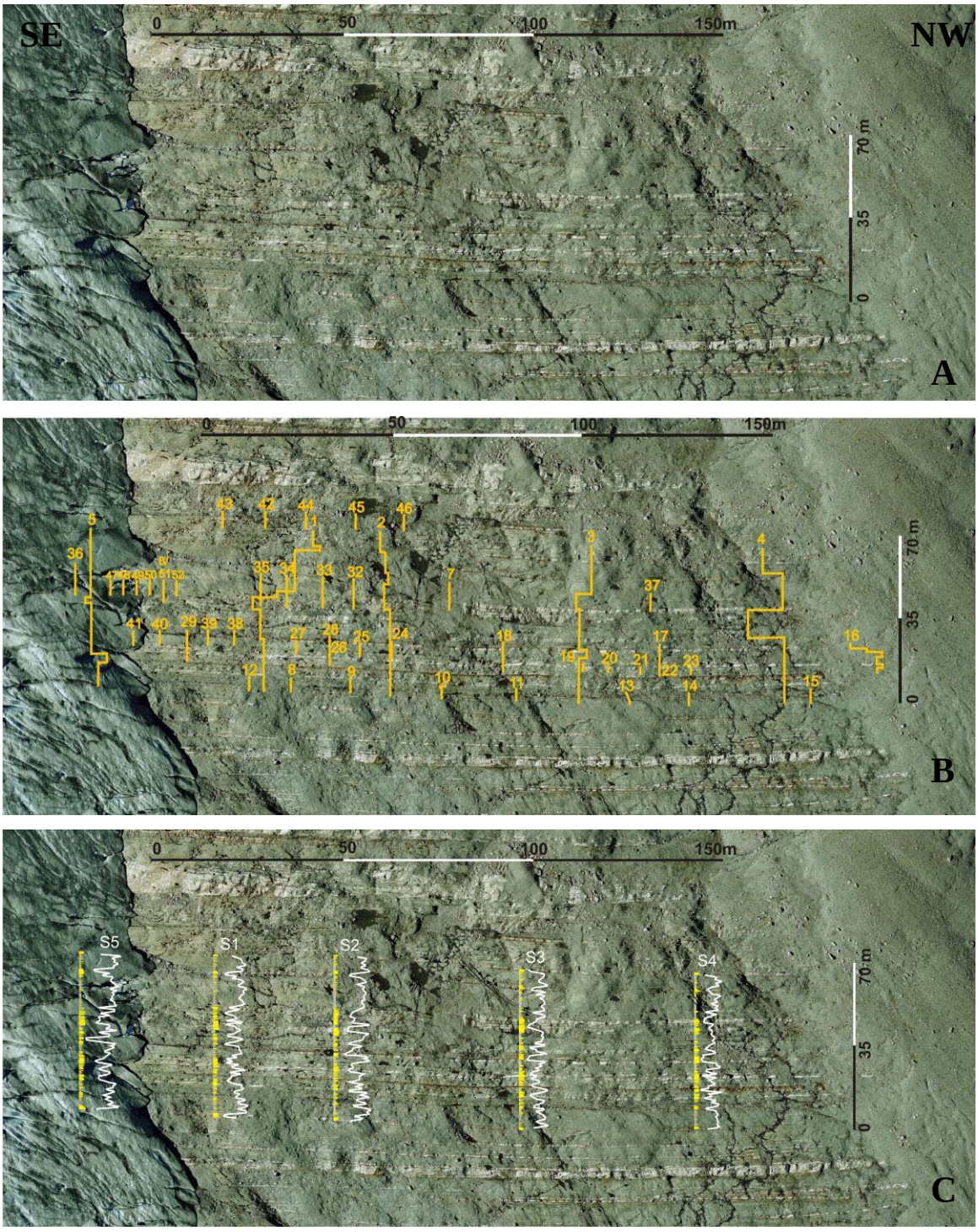

Figure 1.17: High resolution aerial photograph of the study area in Castle Creek north, Cariboo Mountains, southern Canadian Cordillera (see Figure 1.1 and 1.2 for location). (A) Uninterrupted, (B) distribution of measured stratigraphic sections. (C) Distribution of scintillometred sections and corresponding stratigraphic sections. Note the glacier has receded about 55 m laterally since the aerial photo was taken in 2003 and has exposed new outcrop.

Chapter 2: Facies Description

2.1 Introduction

Five facies have been identified through detailed stratigraphic and petrographic study. Facies are subdivided based on variations in thickness, sedimentary structures, sorting, grain size, bed contacts and composition. These facies are summarized in Figure 2.1.

Grain size is described using the Wentworth (geometric) grain size classification scale (Wentworth, 1922). Bed thickness is described using a modified Ingram (1954) classification scheme: very thin-bedded (1- 3 cm), thin-bedded (3-15 cm) medium-bedded (15-30 cm), thick-bedded (30-100 cm) and very thick-bedded (>100 cm).

Facies	Name	Subfacies	Lithology	Sedimentary Structures	Thickness	Contacts	Geometry	Bouma/ Lowe Division	Other Features	Depositional Mechanisms
F1	Very thin- to medium-bedded turbidite	N/A	m/f sand to silt subarkose	planar lamination and ripple cross stratification	1-30	sharp or loaded and non-erosive	tabular	Tbcd, Tbd, Tcd	load and flame structures	deposition from low-density, decelerating turbidity currents under traction transport conditions
F2	Thick-bedded turbidite	F2a: structured turbidites	m sand subarkose	planar lamination and/or ripple cross stratification	30-200	sharp and non-erosive	tabular	Tabcde, Tbcde, Tbde or S1	shallow scours	deposition from moderate to high density, decelerating turbidity currents under tractional conditions
		F2b: structureless sandstone	c sand subarkose	structureless, normally graded	15-170	erosional, amalgamated or partially amalgamated	lenticular	Ta or S3	compensational stacking	rapid competence-driven deposition from high-concentration turbidity currents under tractional conditions
F3	Coarse-tail graded structureless sandstone	F3a: amalgamated sandstone	vC sand subarkose	structureless, coarse-tail graded	5-125	erosional, amalgamated or partically amalgamated	lenticular	Ta or S3	compensational stacking	deposition from high-concentration turbidity currents immediately down-flow of a submerged hydraulic jump
		F3b: tabular sandstone	vC sand subarkose	structureless, coarse-tail graded	5-125	sharp or loaded and non-erosive	tabular	Ta or S3	load and flame structures	deposition from high-concentration turbidity currents down-flow of a submerged hydraulic jump (down-flow equivalent to the F3a)
F4	Mudstone clast breccia	F4a: mudstone clast breccia	boulder clasts in subarkose sand matrix	structureless, graded	5-120	erosive	lenticular	none		partially consolidated mudstone clasts eroded from underlying, laterally adjacent or up-dip strata and deposited by high-concentration turbidity currents
		F4b: irregular mudstone clast breccia	boulder clasts in subarkose sand matrix	structureless, graded	10-50	sharp, erosive, irregular	lenticular	none	clastic injections	post-depositional brecciation and soft sediment deformation from liquidization processes
F5	Carbonaceous Mudstone	F5a: massive mudstone	silt to vfs	massive	10-30	sharp and non-erosive	tabular	Td		deposition from fine-grained dilute decelerating turbidity currents under suspension conditions
		F5b: mudstone laminae	sparse m/f sand dispersed in graphitic matrix	planar lamination	0.5-5	undulose	tabular	none		deposition from decelerating turbidity currents under tractional conditions

Figure 2.1: Facies summary

2.2.1: (F1) Thin- to medium-bedded turbidite

Facies (F1) is the most abundant facies in the study area. Strata are characterised by alternating sandstones and mudstones (Figure 2.2; Figure 2.3). F1 consists of well sorted beds of medium or fine grained sandstone that fine upward to mudstone. Bed bases are sharp or loaded and non-erosive. Other structures commonly associated with loaded contacts include flames that range from 1-55 cm long and are consistently oriented toward the northwest. Beds range from 3-30 cm thick and bed sets range from 2-15 m thick. Sandstone comprises the lower 10-80% of the bed and ranges in colour from cream to dark pink. Sandstones are conspicuously planar and/or small scale cross stratified. Planar laminated sandstones range from 3-25 cm thick and are composed of medium grain sand. Laminae are less than 5 mm thick and are easily distinguished by their varying amounts of carbonate cement and slabby weathering character. Cross stratified sandstones are composed of medium and/or fine grained sand. Multiple ripple sets are typically found at the base of turbidites and range from 3-10 sets or 5-25 cm thick. Ripples rarely climb, however, where observed the angle of climb is typically less than 3°. In the uppermost part of the Tc division, individual ripple foresets are often interlaminated with finer-grained sandstone or siltstone drapes. Single ripple sets are 1-5 cm thick and either overlie planar laminated sandstone or occur at the base of thin to very thinly bedded turbidites. Laterally discontinuous (starved) ripple trains occur in some thinner Tcd beds less than 5cm thick. Often, when overlying planar laminated sandstone, cross stratification within single ripple sets is absent and only the ripple form set is discernible. Td divisions commonly overlie the Tc division and thicker Td divisions tend to overlie a thinner Tc division. Td divisions are light to dark grey and consist of massive or laminated siltstone and massive mudstone. Td divisions range from 1 to 10 cm thick and make-up the upper 20-90% of the bed. In general, beds are tabular and can be traced laterally across the outcrop.

Figure 2.2: Stacked thin- to medium-bedded Tcd and Tbcd turbidites (F1). Note the sharp, non-erosive bed bases and tabular morphology. Beds thicken and become sandier stratigraphically upward. Backpack for scale.

Figure 2.3: Thin-bedded Tcd turbidites (F1). Note that most beds consist of 1-2 ripple sets with sharp, non-erosive bed bases. Hammer for scale.

2.2.2: Petrography

Framework grains of planar laminated and cross-stratified sandstones are dominantly quartz (up to 90%) and feldspar (up to 7%) (Figure 2.4). Quartz grains are typically monocrystalline with moderate to strong undulose extinction. Feldspars commonly consist of plagioclase. Recrystallized matrix of quartz and metamorphic muscovite and chlorite comprises up to 5% of the sandstone. Locally, coarse crystalline carbonate cement comprises up to 20% of the rock volume. Carbonate cement was probably first precipitated as calcite was subsequently recrystallized as dolomite, the more stable phase. Dolomite crystals often show red alteration rims of an iron oxide, which is interpreted to give the sandstones their pink colour. Pyrite makes up to 3% of the rock and two types are observed: pyrite porphyroblasts and disseminated pyrite. Pyrite porphyroblasts are sub-idioblastic or idoblastic range from 0.5-10 mm long, where as disseminated pyrite is generally <0.1 mm long. Quartz pressure shadows and pressure fringes are commonly associated with pyrite porphyroblasts (Figure 2.5). Sandstones of Facies 1 are classified as subarkose. Siltstones and mudstones are composed primarily of quartz (up to 60%), muscovite and chlorite (up to 50%), dolomite cement (up to 30%) and pyrite (up to 3%) (Figure 2.6).

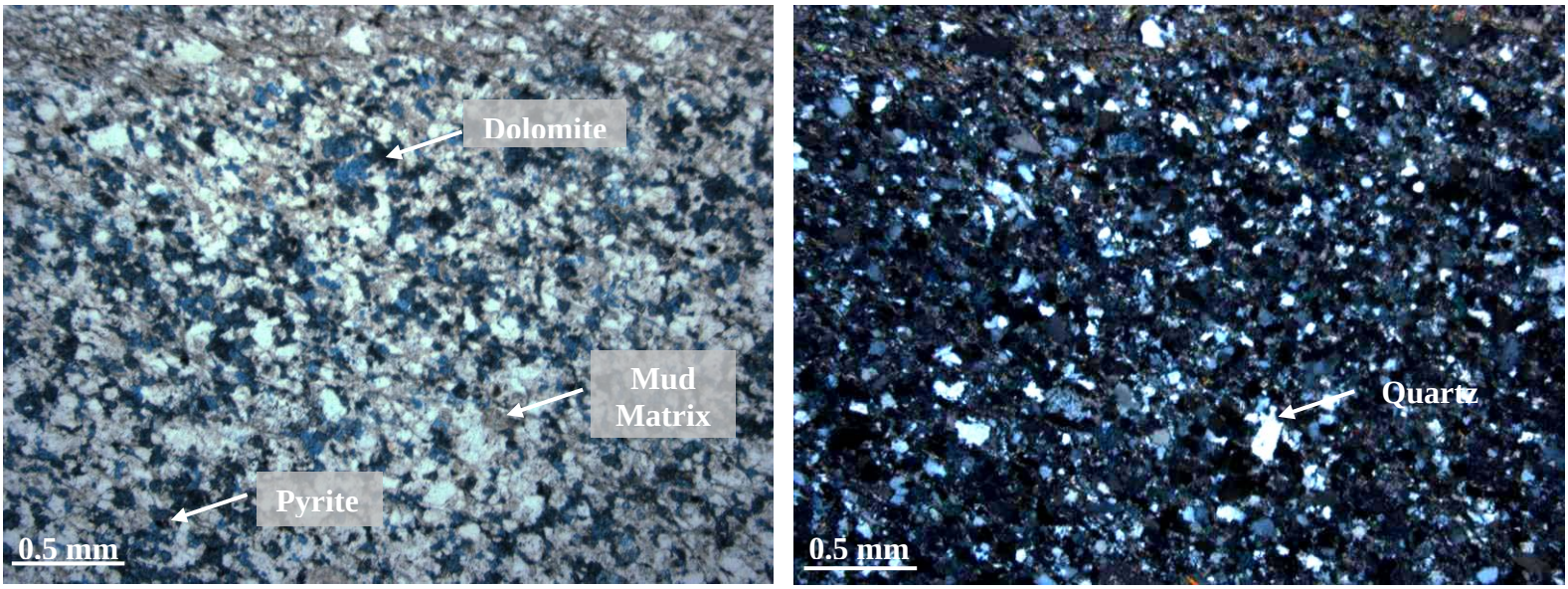

Figure 2.4: Photomicrograph of the sandy portion of a thin-bedded (Tcd) turbidite (F1). Photo A was taken under plan polarized light and photo B under cross polarized light. Main framework grain is quartz with minor feldspar and trace pyrite. Dolomite cement is stained blue by potassium ferrocyanide.

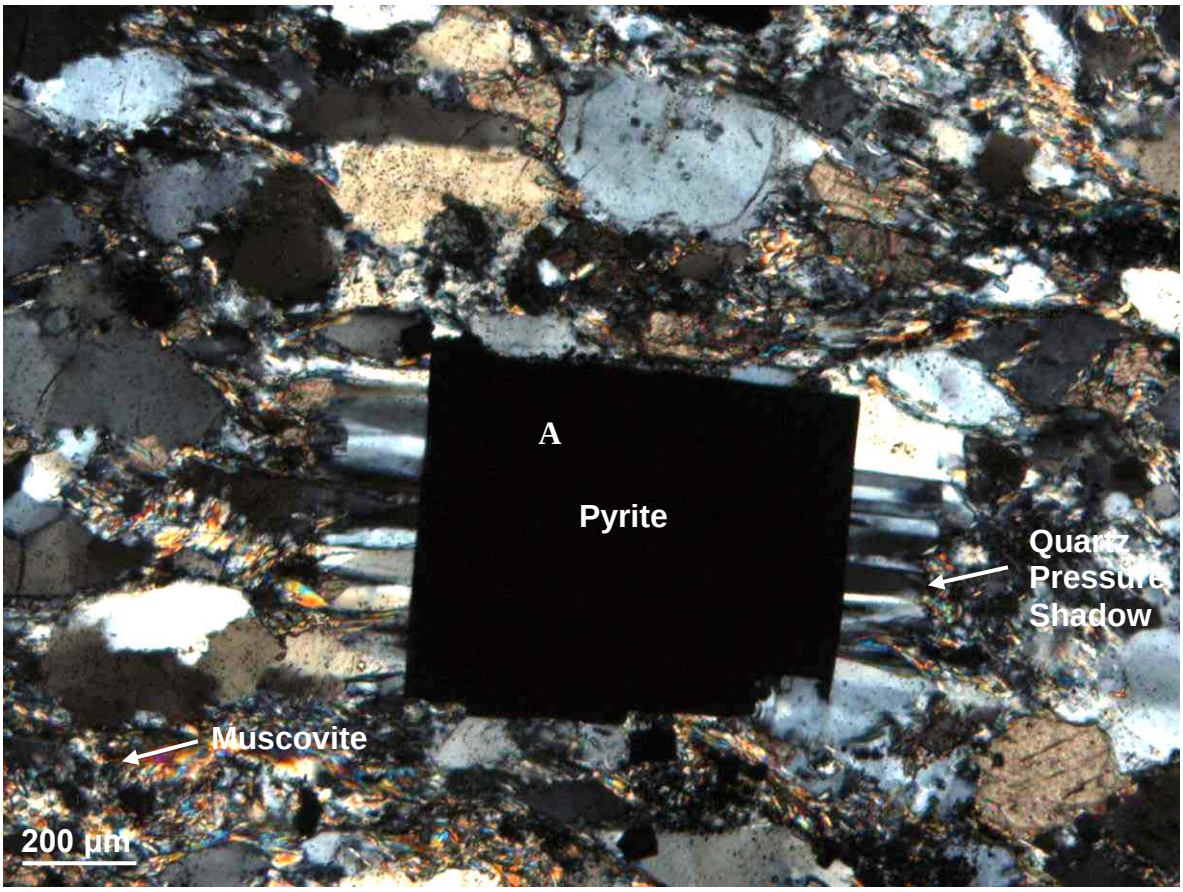

Figure 2.5: Photo micrograph of a pyrite porphyroblast with quartz pressure shadow.

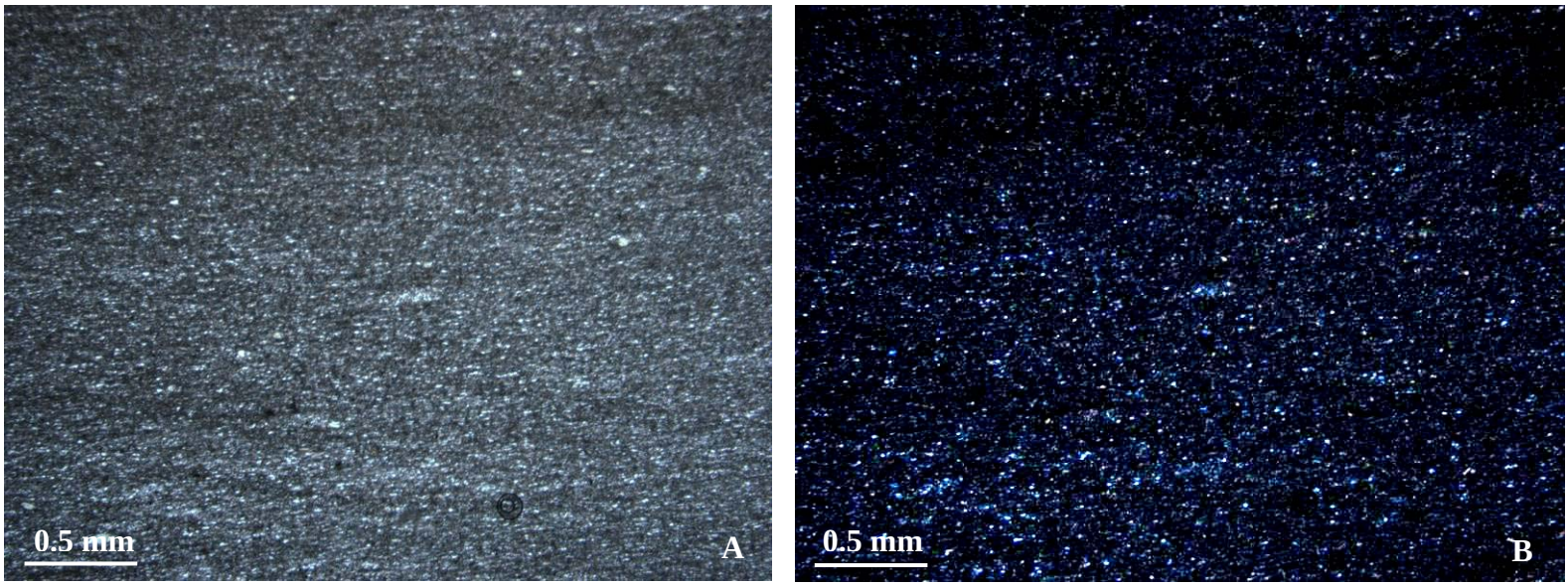

Figure 2.6: Photo micrograph of the silty portion of a thin-bedded turbidite (F1). Note the very fine grain size and abundant quartz silt grains.

2.2.3: Interpretation

Beds of F1 are interpreted to represent complete or, more commonly, partially complete Bouma turbidites. The Bouma sequence, first proposed in 1962 by Arnold H. Bouma, is an idealized sequence of sedimentary structures interpreted to represent deposition from a single decelerating turbidity current (see Ch. 1.9 p.19). The turbulent flows which deposit F1 contained clay- to medium-grained sand particles that were fully suspended by flow turbulence (Lowe, 1982). Traction transport forms upper stage planar lamination (Tb) and ripple cross stratification (Tc), while a combination of traction transport and suspension settling forms laminated and massive siltstone (Td) and suspension settling forms massive mudstone (Te). Given sufficient time under moderate to high velocity conditions, planar lamination develops as sediment is redistributed and crudely sorted during traction transport by the overlying turbulent flow (Sumnar, 2008). Intuitively, as flow velocity decreases planar lamination should transition into dune cross stratification, however, Tb deposits are commonly overlain by ripple cross stratification (Tc) or massive silt (Td) (Figure 2.7, 2.8 and 2.9). However, the typical superposition of ripple cross-stratification above planar lamination indicates the standard bedform stability diagrams developed for clear water flow must be modified for high sediment

concentration turbulent suspensions. It is only when sediment concentration becomes sufficiently reduced (due to flow waning) and angular bed forms develop, ripples most commonly form because the flow is too slow and/or the sediment too fine (due to longitudinal grading) to form dunes.

In order for angular bedforms (i.e. ripples and dunes) to form, defects must be present on the bed to divert the flow and cause flow separation. The flow separates at the bed form and reattaches to the bed at the flow reattachment point. The area between the ripple crest and the reattachment point is a zone of reverse fluid circulation, which at its top, is separated from the overlying flow by a zone of intense turbulence propagation termed a free shear layer (Figure 2.10).

Ripple cross-stratification in turbidites of F1 typically show no angle of climb (Figure 2.11). Climbing ripples form when sediment settling from suspension exceeds the bed load transport rate (Figure 2.12). Intuitively, under waning turbulent flow conditions sufficient sediment should be falling from suspension to form climbing ripples. In F1 strata, Tc turbidites are typically graded from medium- to very fine-grained sandstone. This broad range of available grain sizes suggests deposition was likely competence rather than capacity-driven deposition and instantaneous rates of sediment fallout were never high enough to result in discernible angles of climb. As flow velocity continues to decrease silt is eventually added to the bed load layer and through a combination of traction and suspension deposition creates the laminated Td layer and eventually finer silt and mud suspension deposition (Te).

Bed bases are typically planar suggesting minimal erosion of previously deposited strata, which reflects a combination of insufficiently strong turbulence and sufficiently high substrate strength. Substrate strength may be enhanced by dewatering or gravitational processes. Load structures, occasionally observed at bed bases, and are interpreted as soft sediment deformation features (Figure 2.13 and 2.14).

The persistence of sulphide minerals, principally pyrite, suggests early diagenetic bacterial reduction of seawater sulphate under anoxic/euxinic conditions (Ross et al., 1995). Their euhedral shape (Figure 2.5), however, represents Mesozoic recrystallization of the primary biogenic pyrite.

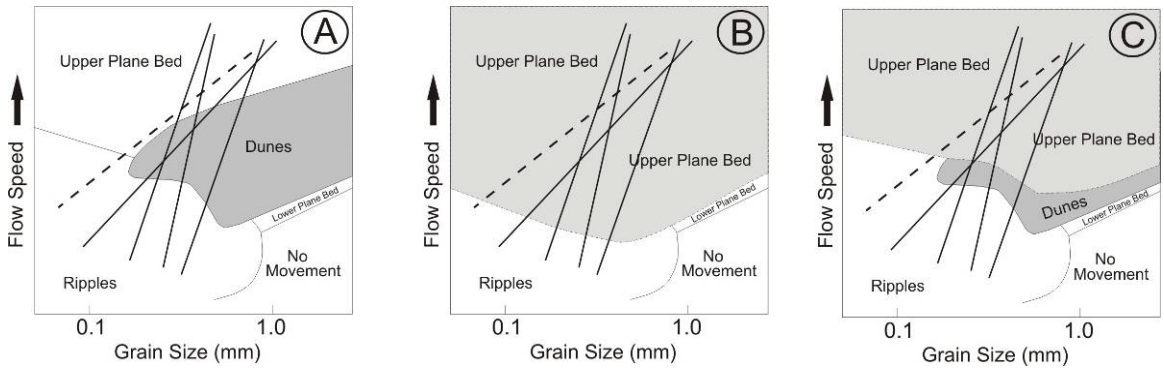

Figure 2.7: Hypothetical bedform stability diagrams from Arnott (2010) modified after Southard and Boguchwal, 1990. Solid lines sloping down to the left trace out bed form changes in a decelerating flow. (A) Hypothetical stability diagram for a clear water flow. Note the large dune stability field. All decelerating flows, except the dashed line pass, through the dune stability field before encountering the ripple field. Dunes are rare in F1 suggesting that the unidirectional bedform stability diagram must be modified for turbid flows. (B) Hypothetical stability diagram for a high-concentration turbulent suspension. The upper plane bed stability field is depressed downward into the dune and ripple stability fields. (C) Hypothetical stability diagram for a low-concentration turbulent suspension. Dunes are stable but the stability field is much narrower than in clear water.

Figure 2.8: Thick-bedded, medium-grained, Tbcd turbidite (F2a). Note thick planar laminated division (Tb) is overlain by 4 ripple sets (Tc), which in turn is overlain by massive silt (Td).

Figure 2.9: Medium grained sand Tbd turbidite. Planar lamination is overlain by massive silt (i.e. the absence of dune or ripple cross-stratification).

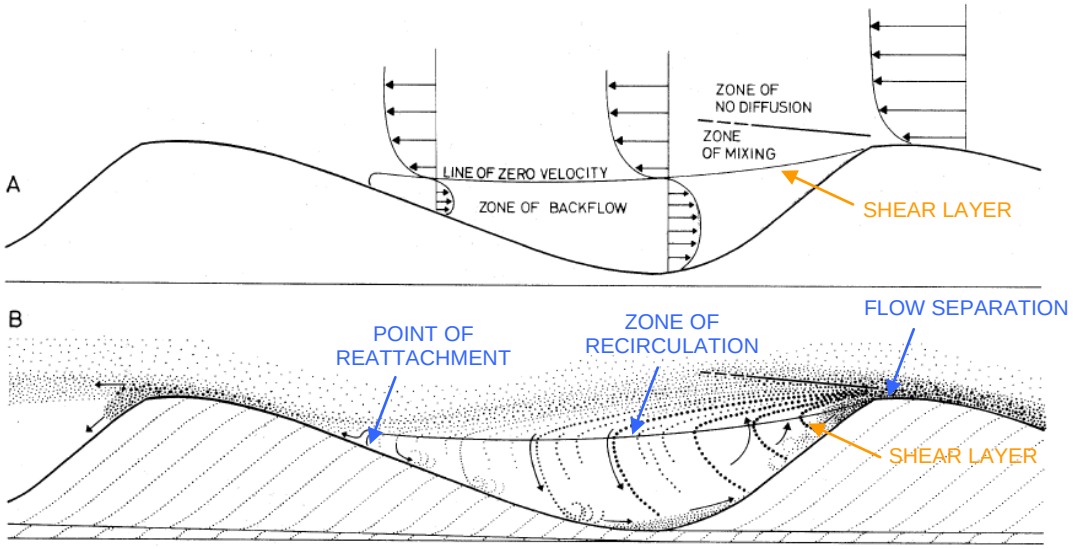

Figure 2.10: (A) Flow pattern and velocity distribution over the lee face of a ripple. (B) Flow pattern and sedimentation process. Flow accelerates over the ripple crest due to reduced cross-sectional area and entrains sediment. Flow separation occurs on the lee side of the bed form and creates a recirculation cell. A shear layer, or zone of high velocity gradient, seperates the flow-recirculation zone from the main flow (from Reinick, 1973).

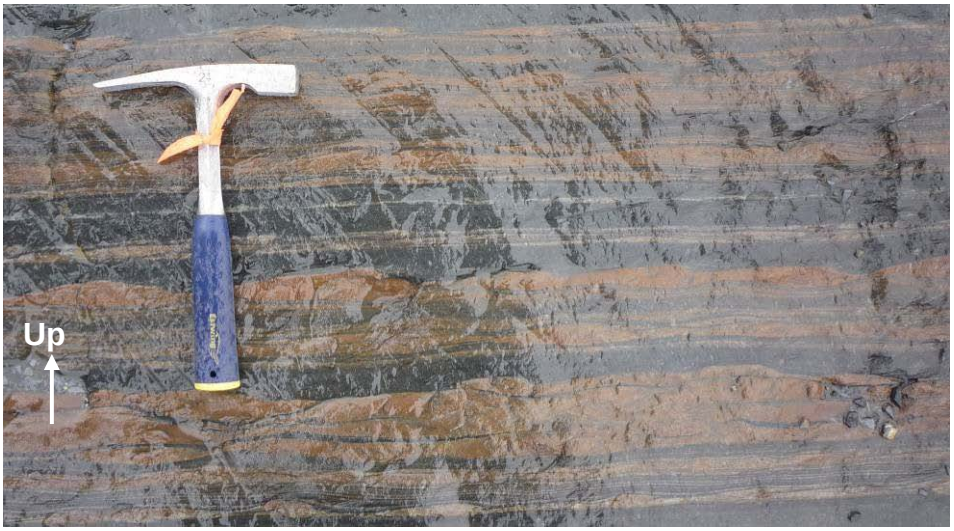

Figure 2.11: Fine-grained Tcd turbidites with multiple non-climbing ripple sets.

Figure 2.12: Rare example of climbing ripple cross-stratification. The angle of climb is ~4°.

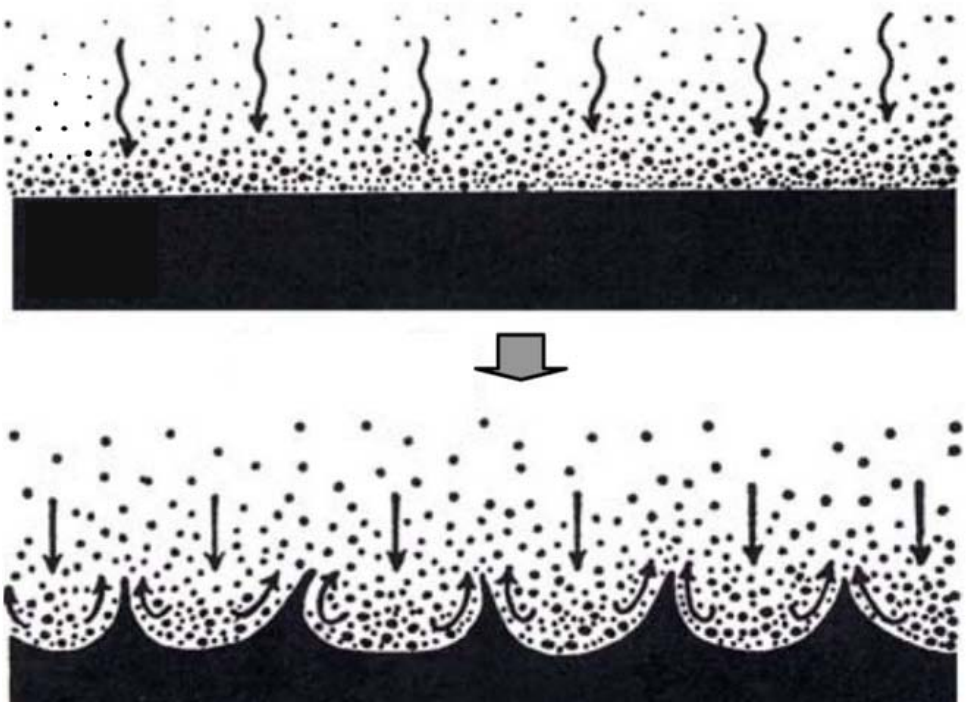

Figure 2.13: Origin of load and flame structures from Navarro (2005) modified from Ricci Lucci (1995). Previously deposited, but still water-saturated mud is displaced upward under a subsiding layer of more dense sand forming upward tapering protrusions (flames) whereas the higher density sand forms bulbous lobes (loads).

Figure 2.14: Outcrop example of flame structures from F1. Pen for scale.

2.3: (F2) Thick-bedded turbidite

Facies (F2) is subdivided into two subfacies: structured (Tabcde, Tbcde, Tbde or S1) turbidites (F2a) and structureless (Ta or S3) sandstones (F2b).

2.3.1: (F2a) Structured Turbidite

Facies (F2a) consists of interstratified sandstone and mudstone. Basal contacts are typically sharp and non-erosive. Locally, however, bed bases are erosive with scours 1-25 cm deep and 50-500 cm wide. Flame and ball-and-pillow structures are observed. Beds range from 30-200 cm thick and are typically composed of medium sand (Figure 2.15). Sandstone comprises 85-100% of the bed and is typically ungraded, well sorted and planar laminated or cross-stratified. Thin, 1-5 cm layers of structureless sandstone are observed at the base of some beds. Strata of Facies (F2a) are either diffusely or sharply planar laminated. Diffuse planar laminated sandstones are greenish to light pink in colour and weather as one large block. Laminae range from 5-30 mm thick. Sharp planar laminated sandstones are dark pink in colour and weather in slabs. Laminae are 1-5 mm thick. Planar lamination is commonly overlain by a single ripple form set or cross stratified set. Cross-stratification is typically a single small-scale (ripple) set thick that ranges from 1-5 cm thick. Rarely, sharply planar laminated sandstones are overlain by large-scale, dune cross-stratificated sandstone. Cross-stratification or planar lamination

(when cross stratification is not present) is in turn overlain by thin massive or laminated silt.

Beds are typically tabular and laterally continuous across the outcrop. One bed, however, is lenticular. It is very thick, 200 cm, in the southeast and thins to as little as 75 cm in the northwest. The bed base is shallowly scoured and the grain size ranges from coarse to fine sand with granules. Shallow scours are filled with the coarsest grain size and contain mudstone clasts (Figure 2.16). Mudstone clasts are 75% unlaminated, tabular, subangular to angular and range from 3.5 cm to 18 cm in length. In the southeast where the bed is thickest, ~180-200 cm, the lower ~25-40 cm consists of 1-10 cm thick, coarse-grained, structureless sandstone interbedded with less than 5 cm thick, coarse sand to granule inversely graded deposits. The majority of the bed is composed of a very thick, ~ 140-155 cm, planar laminated sand, which is overlain by a single ripple form set. In the northwest where the bed is thinner scouring is less common and structureless sandstone and inversely graded layers are absent. Planar lamination is overlain by 8-10 ripple sets.

Figure 2.15: Thick-bedded Tbcd turbidite (F2a). Planar laminated division is disproportionally thick comprising 90% of the bed. A single ripple set overlies the planar lamination and in turn is overlain by massive siltstone. Note the sharp non-erosive bed base. Hammer for scale.

Figure 2.16: Shallowly scoured bed base overlain by coarse-grained structureless sandstone with abundant mudstone rip-up clasts. Note the truncation of the underlying thin-bedded turbidites (F1).

2.3.3: (F2b) Structureless Sandstone

Facies (F2b) consists of normally graded, structureless, coarse to very coarse grained sandstone capped by thin siltstone (Figure 2.17). Bed bases are erosional or amalgamated typified by shallow scours (Figure 2.18). Locally, bed bases are loaded and soft sediment deformation features such as flame structures are observed. Scours are 3-40 cm deep and 10-550 cm or more wide. Loaded basal contacts characterized by flame structures are observed where sand overlies finer-grained sand or mud. Flame structures are 3-12 cm long and consistently oriented toward the northwest. Dewatering structures are notably absent. Beds range from 15-170 cm thick. Beds greater than 50 cm thick are commonly amalgamated or partially amalgamated. Amalgamation surfaces are typically difficult to identify and generally are assumed to be marked by subtle changes in grain size or mm thick dark grey siltstone layers that can only be traced laterally for at most a few meters. Beds are lenticular, laterally discontinuous and can be traced for several 10`s of meters.

Yellowish pink sandstone constitutes 85-100% of F2b. Strata are distribution graded with a progressive upward fining from coarse or very coarse grained sand to silt. Local, tabular, unlaminated mudstone clasts are observed ranging from 1-45 cm wide. Structureless sandstones are uncommonly overlain by a single ripple form set or set of ripple cross stratification. Climbing ripples were not observed overlying structureless sandstones. Beds are capped by massive siltstones 0.5-10 cm thick.

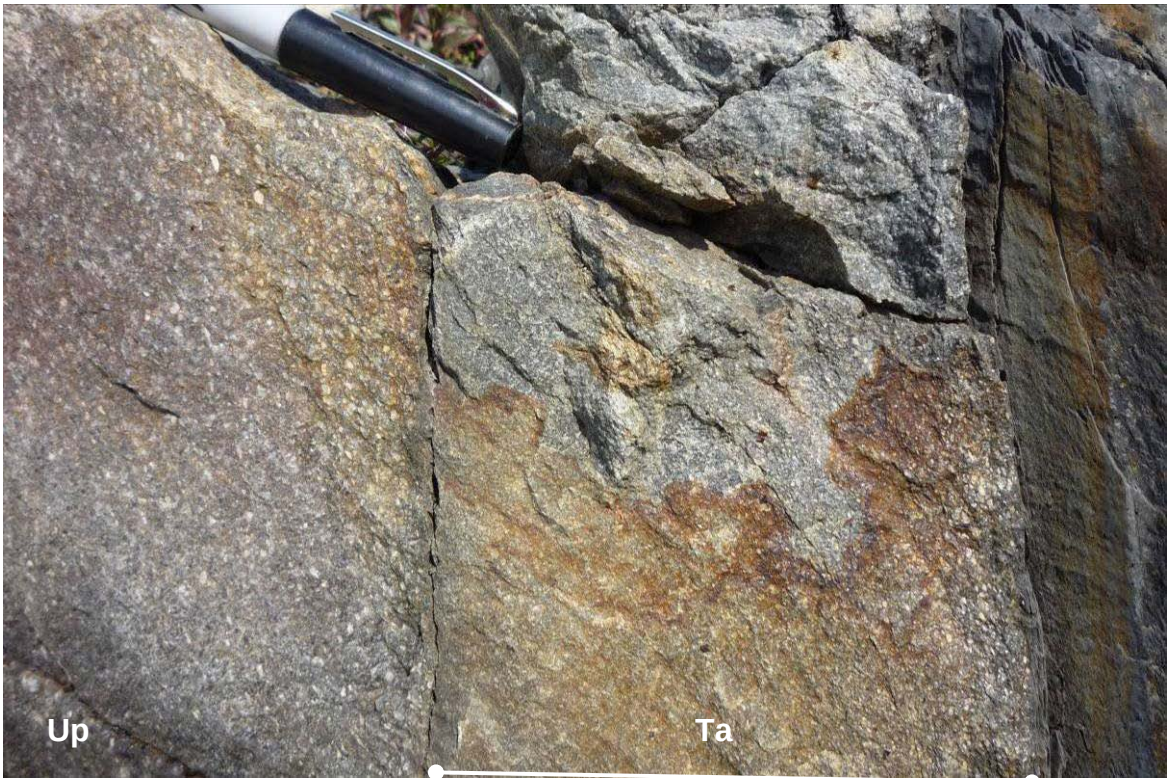

Figure 2.17: Graded structureless sandstone (F2b). Note the sharp basal contact and thin silt cap.

Figure 2.18: Structureless sandstone (F2b). Note amalgamated bed contacts (dashed white lines).

2.3.3 Petrography

Framework grains of thick-bedded turbidites are subrounded to subangular and composed mostly of quartz (up to 90%) and feldspar (up to 5%) (Figure 2.19). Quartz grains are typically monocrystalline with moderate to strong undulose extinction. Feldspars are typically albite. A recrystallized matrix of quartz and metamorphic muscovite and chlorite comprises up to 4% of the sandstone. Blocky carbonate cement is the primary pore filling cement and makes up to 40% of the rock volume. Carbonate cement was probably precipitated originally as calcite and later, during metamorphism, was recrystallized to dolomite. Two generations of carbonate cement have been indentified. The first phase is blocky dolomite cement and the second phase commonly shows red alteration rims of an iron oxide, which most likely gives the sandstones their reddish brown colour. Pyrite porphyroblasts are rare. Sandstones of Facies 2 are classified as subarkose to quartz arenite. Trace zircon is observed also.

Siltstones and mudstones are composed primarily of quartz (up to 70%), muscovite and chlorite (up to 50%), dolomite cement (up to 40%) and pyrite (up to 3%).

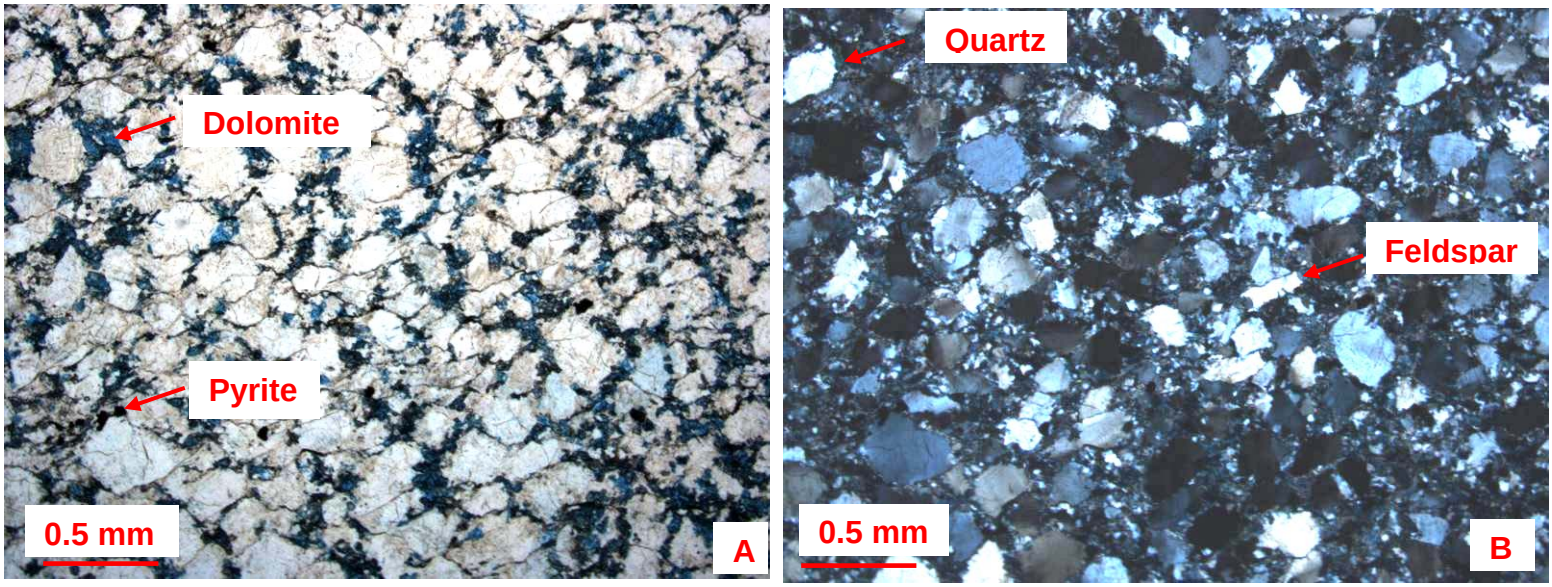

Figure 2.19: Photomicrograph of the sandy portion of a thick-bedded (Tbd) turbidite (F2). Photo A was taken under plan polarized light and photo B under cross polarized light. Main framework grains are quartz with minor feldspar and trace pyrite. Dolomite cement is stained blue by potassium ferrocyanide. Note the lack of silt and clay sized particles.

2.3.4: Interpretation

Facies (F2) is interpreted to be complete or partial Bouma turbidites deposited by a single turbidity current (Lowe, 1982). Specifically, beds are Tabcde, Tacde, Tade, Tbcde or Tbde turbidites. Facies 2 differs from Facies 1 by the occurrence of structureless sandstone, anomalously thick planar laminated divisions, the lack of multiple ripple sets and thin siltstone interbeds.

Inversely graded beds are rare, less than 5 cm thick and were observed near the base of one unique structured thick-bedded turbidite (F2a) (Figure 2.20). Tractional carpets (Hiscott and Middleton 1980; Lowe 1982) and laminar sheared layers (Sunmar, 2008) are interpreted to form inverse grading. The term 'traction carpet' was introduced by Dzulynski and Sanders (1962) and 'laminar shear layer' was introduced by Vrolijk and Southard (1997) to describe non-turbulent, high concentration layers formed at the base of unsteady turbiditity currents. Particle motion is driven by shear from the overriding turbulent flow (Bagnold, 1956) and in traction carpets, grain segregation is related to dispersive pressure caused by grain-grain interactions (Hiscott and Middleton, 1980; Lowe, 1982) whereas in laminar sheared layers, grain segregation is related to

sheared dispersion where smaller particles settle downward between larger grains (Middleton 1970; Legros 2002; Sunmar 2008). Inverse grading occurs as discrete layers within structureless sandstone. This relationship has been reported from other ancient deposits and interpreted to represent episodic deposition from highly concentrated basal layers (Lowe, 1982; Postma et al., 1988; Pickering et al., 1989). Structureless interbeds are interpreted to form by similar mechanisms as the inverse grading. Grading does not develop because either particle segregation did not occur or the grain size distribution was too restricted.

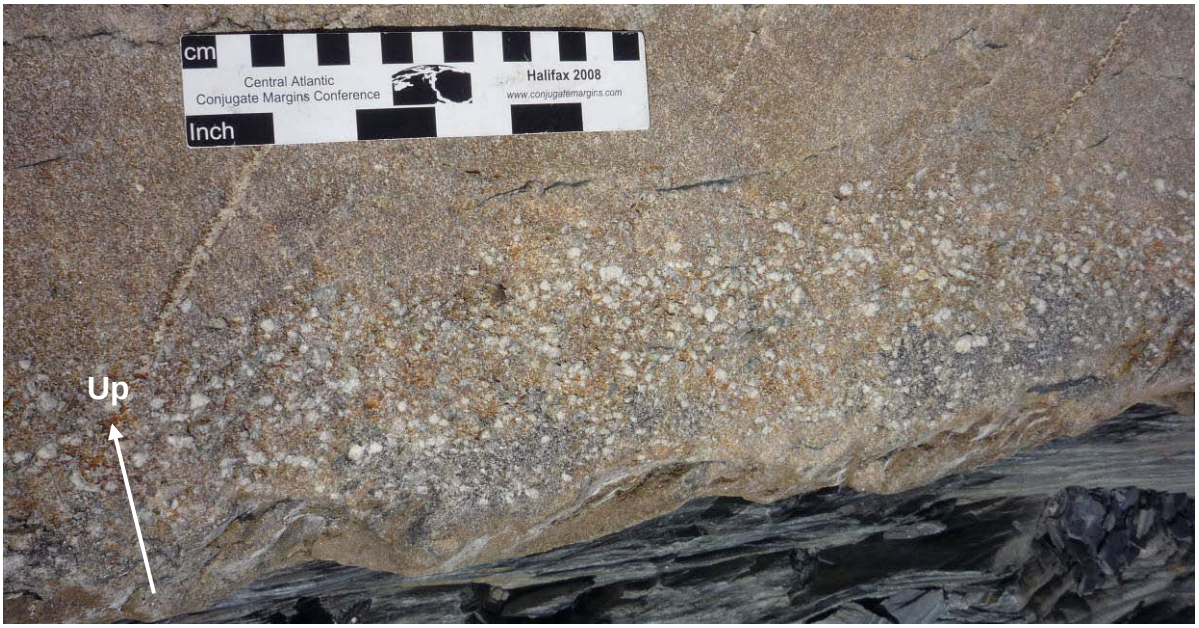

Figure 2.20: Inverse grading at the base of a 200 cm thick Tabcd turbidite (F2a).

Structureless sandstones are common within thick-bedded turbidites and compose 0-30%, or 0-40 cm, of the bed in facies (F2a), or greater than 80% or 30-150 cm, of the bed. The interpretation of structureless sandstone remains equivocal, in part, because not all structureless sandstones are formed by the same flow mechanism (e.g. Lowe, 1982; Kneller and Branney, 1995; Branney and Kokelaar, 1999; Stow and Johansson, 2000; Shanmugam, 1996, 1997; Mulder and Alexander, 2001; Arnott and Hand, 1989; Allen 1991; Leclair and Arnott, 2005; among others). The structureless sandstones of Facies 2 lack dewatering structures and have a low mud matrix content precluding deposition by suspension settling in high density turbidity currents (Lowe, 1982), or capacity-driven

deposition downflow of a submerged hydraulic jump (Leclair and Arnott, 2005) respectively. The presence of erosive bed contacts and normal grading eliminates deposition from concentrated or hyper-concentrated flows (Shanmugam, 1996, 1997; Mulder and Alexander, 2001). The structureless sandstones of facies (F2) are interpreted to form when tractional sedimentary structures such as planar lamination and/or cross stratification are suppressed by high sediment fall-out rates (Kuenen, 1966; Arnott and Hand, 1989; Leclair and Arnott, 2006; Sunmar 2008). Bedforms were buried so quickly that there was insufficient time for the bedform to amplify and migrate down system. Although flow velocity may have been within the stability field for upper plane bed, dunes or ripples high fallout rate made lamination imperceptible (Paola et al., 1989). Although the aggradation rate at which planar lamination is suppressed is highly variable and depends upon grain composition, size, shape and density (Arnott and Hand, 1989; Sunmar, 2008), sufficiently high rates of sediment fallout needed are easily achieved when high concentration flows became unconfined as they overtopped the channel banks resulting in rapid competence-driven deposition (Figure 2.21).

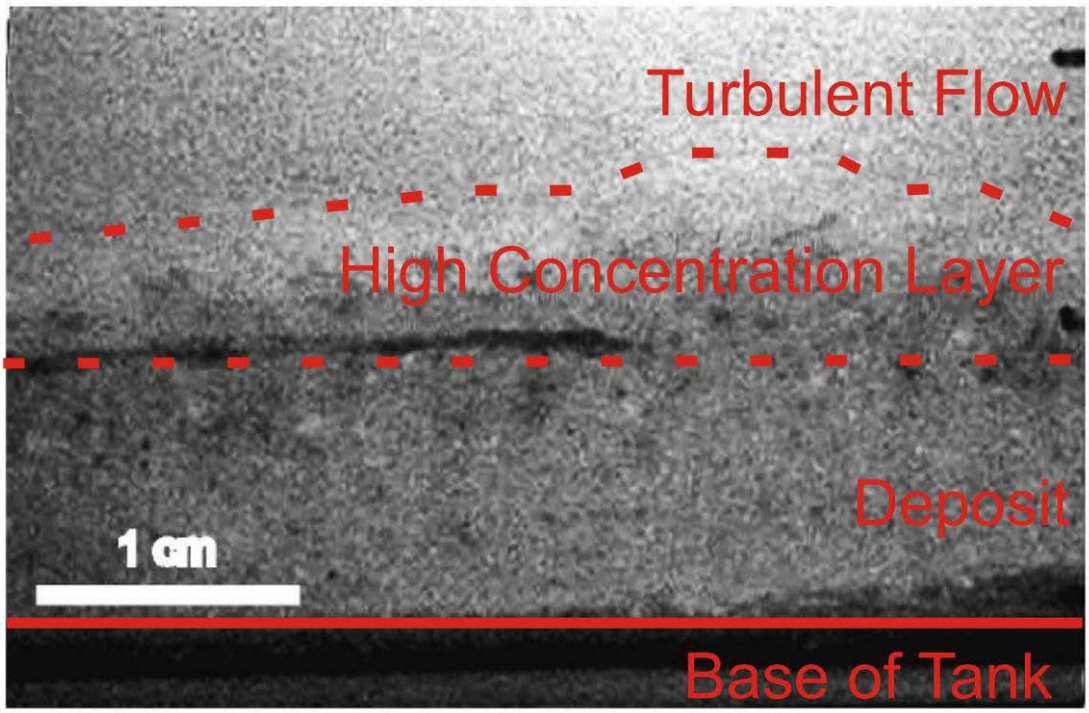

Figure 2.21: Photograph of a turbulent flow experiment in an annular flume showing a structureless sandstone deposit, high concentration basal turbulent layer and turbulent flow (from Sumnar, 2008). High rates of sediment fall out suppress the formation of traction sedimentary structures. There is insufficient time for bed forms to amplify and grow before they become buried.

Thick-bedded turbidites with a thick, basal structureless sandstone division (F2b) are in some cases overlain by thin planar laminated divisions, whereas thick-bedded turbidites with thin or absent structureless sandstone division (F2a) are overlain by thick planar laminated sandstone divisions. Discernible planar laminae form when fall-out rate decreases beyond a certain threshold. The formation of upper-stage planar laminations is attributed to the migration of low-amplitude bedwaves (Best and Bridge, 1992) or to particle sorting in laminar sheared layers (Sumnar, 2008). Two types of planar lamination were observed in Facies 2a; diffuse and sharp planar laminae. In experiments by Sumnar (2008) upper-stage planar lamination related to low-amplitude bedwaves formed only when sediment fall out rates were zero and velocity was held constant. Planar laminae were sharp and less than 1 mm thick. Laminae produced by decelerating flows were thicker, 1-4 mm thick, and more diffuse. The difference between diffuse planar laminae and sharp planar laminae might relate to differences in sediment fall out rate and/or flow steadiness. Increased sediment fall out rate and flow unsteadiness have been shown to suppress planar lamination (Arnott and Hand, 1989). In this case, the bed aggrades so quickly that particle segregation processes are exceeded and laminae become diffuse (Figure 2.22). Diffuse planar lamination is interpreted to form from flows with high sediment fall out rate and/or extreme flow unsteadiness such that the bed aggraded to quickly for planar laminations to appear sharp. Further, diffuse planar laminated sandstones are grey in colour whereas sharp planar laminated sandstones are reddish brown. Colour variation is related to the proportion of mud matrix and carbonate cement and may reflect the flow's ability to sort the sediment. The elevated sediment fall-out and aggradation rates within diffusely planar laminated sandstones may have trapped more fine grained sediment resulting in the higher content of mud matrix. Sharp planar laminated sandstones have a more open framework because they contain less mud matrix, which in turn would result in higher original permeability and hence greater transport rate of carbonate-cementing diagenetic fluids (Figure 2.23).

Figure 2.22: Example of diffuse planar lamination in a thick-bedded Tabd turbidite (F2a). Note the sharp slightly undulose bed base.

Figure 2.23: Example of sharp planar lamination from a medium-grained, thick-bedded Tbd turbidite (F2a). Note sharp none erosive base.

Utilizing the bedform stability diagram (Southard and Boguchwal, 1990), dune cross-stratification should overlie planar laminae, however, it is uncommon to observe dune cross-stratification within these thick-bedded turbidites (Figure 2.7). Dunes require sufficiently energetic flows with a minimum grain size of lower-fine sand and sediment concentration low enough for bed defects to amplify by flow separation (Collinson and Thompson, 1982). The general paucity of dunes suggests that sediment concentrations remained sufficiently high through the dune stability field that plane bed remained the stable bed form phase, which in most cases is overlain by a single ripple set. The transition from planar laminated sandstone to ripple cross stratified sandstones is interpreted to represent a change in flow sediment concentration and a decrease in flow velocity, because the grain size changes little. The grain size similarity between the dunes or more commonly ripples, the underlying parallel laminated beds and the fact that they consist of a single, non-climbing set suggests the cross stratification formed largely by reworking of the underlying bed (Kneller and McCaffrey, 2003). As the flow continued to wane silt could no longer be transported by the flow and was deposited by a combination of low energy traction and suspension deposition forming massive siltstone and mudstone deposits (Tde).

2.4: (F3) Coarse-tail graded structureless sandstone

Facies (F3) consists of sandstone with thin mudstone interbeds. Two end-member kinds of coarse-tail graded sandstones are recognized: amalgamated (F3a) and tabular (F3b). Lithologically, tabular and amalgamated sandstones are similar but differ in terms of bed geometry, basal contacts and mudstone clast character.

2.4.1: (F3a) Amalgamated structureless sandstone

Amalgamated sandstones (F3a) consist of erosively based, lenticular, laterally discontinous beds that typically extend laterally for several 10's of metres (Figure 2.24). Mudclasts within amalgamated units are < 50 cm long, subangular to angular and unlaminated and tend to be concentrated along amalgamation surfaces or near bed bases often forming breccia layers (Figure 2.25).

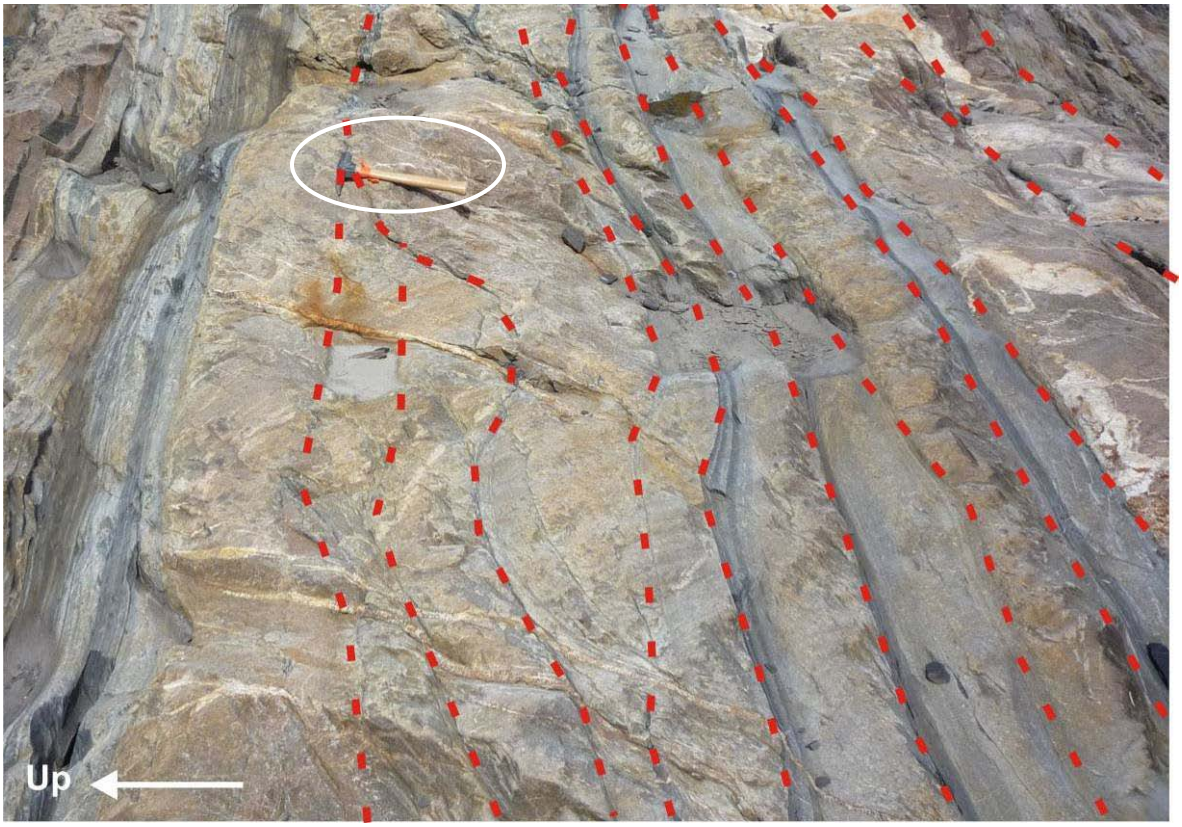

Figure 2.24: Amalgamated structureless sandstone (F3a). Note the erosive basal contacts highlighted by dashed red lines. Note hammer for scale.

Figure 2.25: Amalgamated structureless sandstone (F3a). Note the breccia bed highlighted by the dotted red line.

2.4.2: (F3b) Tabular structureless sandstone

Tabular sandstones (F3b) have sharp, non-erosive bases and extend over the entire outcrop (~200 m) and as a result bed terminations are rarely observed (Figure 2.26). Lateral changes in grain size and bed thickness are negligible, however, where beds do terminate structureless sandstones abruptly transition into ripple laminated turbidites. Bed bases are typically planar but load structures are observed locally. Tabular, unlaminated mudstone clasts are common and include a small number of large, 25-130 cm long, isolated mudstone clasts orientated parallel to bedding and dispersed throughout the upper-middle part of the bed (Figure 2.27).

Although highly variable, strata are 65-85% sandstone and range in thickness from 5-125 cm. Beds consist of a light to medium greenish grey basal layer overlain abruptly by a finer grained dark coloured top. Sandstones are composed of coarse or medium to fine grained sand that is moderately sorted and matrix supported. Primary sedimentary structures, like planar lamination or cross stratification, are not observed, instead, sandstones are structureless and ungraded or coarse-tail graded. Coarse-tail grading is characterized by a decrease in grain size of only the coarsest grain sizes and is common in thick S3 (Lowe, 1982) or Ta (Bouma, 1962) divisions of turbidites. Grading can be subtle, from lower coarse to lower medium sand. Some beds only show grading in the upper portion.

Figure 2.26: Tabular coarse-tail graded structureless sandstone (F3b). Note sharp non-erosive bed bases and isolated tabular mudstone clasts (circled). Note hammer for scale.

Figure 2.27: An example of large isolated mudstone clasts (yellow arrows) in tabular structureless sandstone (F3b).

2.4.3: Petrography

Coarse-tail graded sandstones are matrix supported with a high (30-50%) mud matrix content and framework grains to appear to 'float' in the matrix (Figure 2.28). Framework grains are composed mostly of quartz (up to 70%) and feldspar (up to 5%). Quartz grains are typically monocrystalline with moderate to strong undulose extinction. Feldspars commonly consist of plagioclase or potassium feldspar. The matrix typically consists of recrystallized quartz and metamorphic muscovite and chlorite. Locally, sparse pore-filling dolomite is the primary cement comprising up to 5% of the rock volume. The high mud content in strata of Facies 3 gives them their characteristic greenish-grey colour. Sub-idioblastic or idoblastic pyrite porphyroblasts with pressure shadows and pressure fringes of quartz comprises up to 2% of the rock.

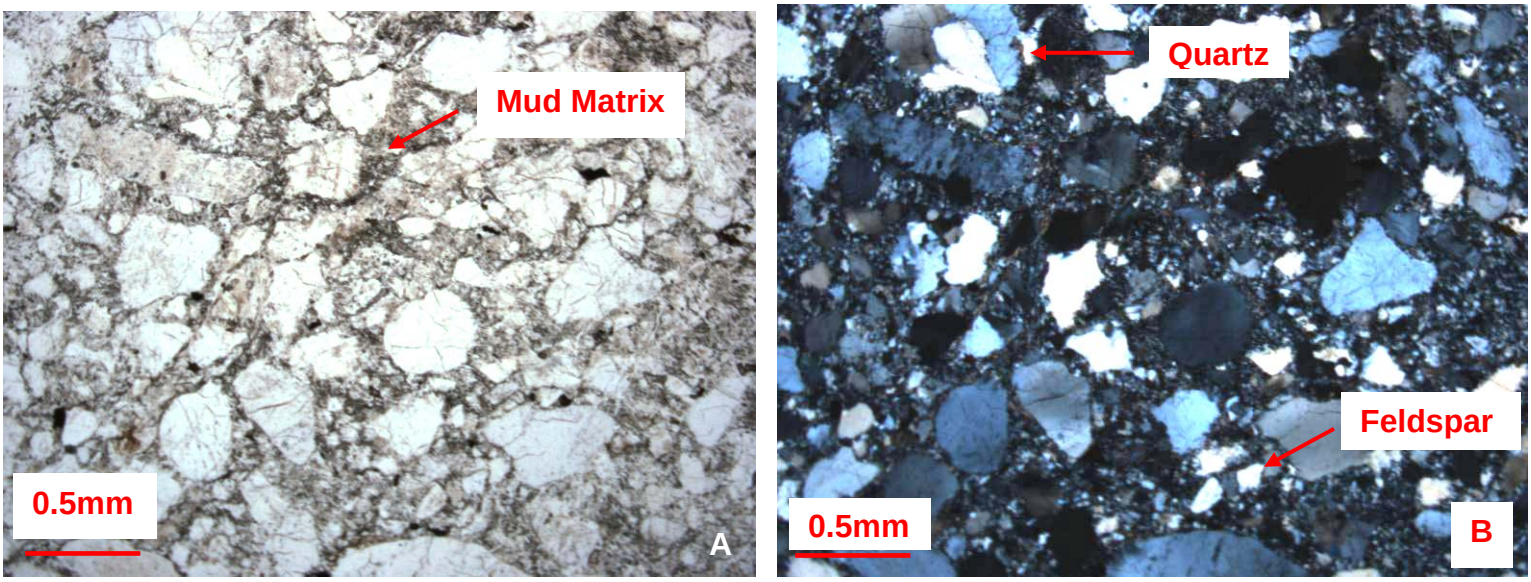

Figure 2.28: Photo micrograph of the sandy portion of a coarse-tail graded structureless sandstone (F3). Photo A was taken under plan polarized light and photo B under cross polarized light. Main framework grains are quartz with minor feldspar. The matrix comprises 30-50% of the rock volume and consists of silt and clay. Carbonate cement (dolomite), which commonly occurs locally in the strata, is absent here.

2.4.4 Interpretation:

The interpretation of structureless sandstones is a subject of considerable debate among sedimentologists in part because there are many different kinds of structureless sandstones and more than one mechanism may be responsible for their deposition. Facies (F3) consists of coarse-tail graded, structureless sandstones with a high mud matrix content. The absence of water escape structures, the high-mud matrix content and the lack of planar laminae, dune and or ripple cross-stratification precludes deposition from suspension settling in high density sandy turbidity currents (Lowe, 1982), progressive aggradation from sustained high density turbidity currents (Kneller and Branney, 1995; Branney and Kokelaar, 1999; Stow and Johansson, 2000), frictional freezing within sandy debris flows or hyperconcentrated density flows (Shanmugam, 1996, 1997; Mulder and Alexander, 2001), frictional freezing within concentrated flows (Mulder and Alexander, 2001) and rapid deposition under plane bed conditions (Arnott and Hand, 1989; Allen 1991). Characteristics of strata of F3 are similar to those described by Leclair and Arnott (2003). In their work, these authors conducted subaqueous flow experiments investigating high density (20-35% sediment volume concentration) slurries with grain sizes ranging from coarse silt to medium sand and were able to reproduce the textural characteristics of F3 strata. Specifically, these authors were able to reproduce coarse tail grading and high matrix content, but only with the installation of a hydraulic jump (Figure 2.29). In the absence of the jump, the deposits showed subtle planar stratification. In nature, hydraulic jumps commonly form at a break in slope causing supercritical flow to transition abruptly to subcritical flow. Supercritical flow is fast moving fluid defined by a Froude number >1 ($Fr = U/\sqrt{gh}$) whereas subcritical flow is slower moving fluid defined by Froude number <1. At a hydraulic jump, kinetic energy is converted into potential energy commonly associated with internal turbulence generation. In longitudinal profile, hydraulic jumps (in turbidity currents these are plane-wall jets with jump) form proximal to distal zones: zone of flow establishment, zone of transition and zone of established flow (Russell and Arnott, 2003). The zone of transition, in at or very near the hydraulic jump, is characterized by intense reworking and resuspension of sediment by turbulent eddies. Downflow of the jump the established

flow zone is dominated by high rates of capacity-driven deposition. Facies F3 consists of two end members: amalgamated (F3a) and tabular (F3b). Amalgamated sandstones have scoured bases filled by mudstone clast breccia and mud-matrix rich coarse tail graded sandstone. Tabular sandstones are mud-matrix rich coarse tail graded sandstone with sharp non-erosive bases. Tabular sandstones are more common than amalgamated sandstones. The difference between amalgamated and tabular end members is related to the proximity of the deposit to the hydraulic jump. Amalgamated units form in or immediately downflow to the hydraulic jump where energetic turbulent vortices cause intense reworking and resuspension of sediment maintaining a high sediment concentration in the basal layer and producing steep walled scours that fill almost immediately. Mudstone clast breccias typical of F3a are interpreted to be composed of rip-up clasts from erosion of the seabed. Downflow of the jump, thicker, lower-energy flow has significantly lower transport capacity and is interpreted to result in rapid sedimentation and deposition of the tabular (F3b) facies. The large isolated mudstone clasts with F3b are interpreted to have been sourced from up flow erosion within the jump. The soft-sediment deformation is interpreted to indicate syn- to very early post-depositional dewatering of the sandstones.

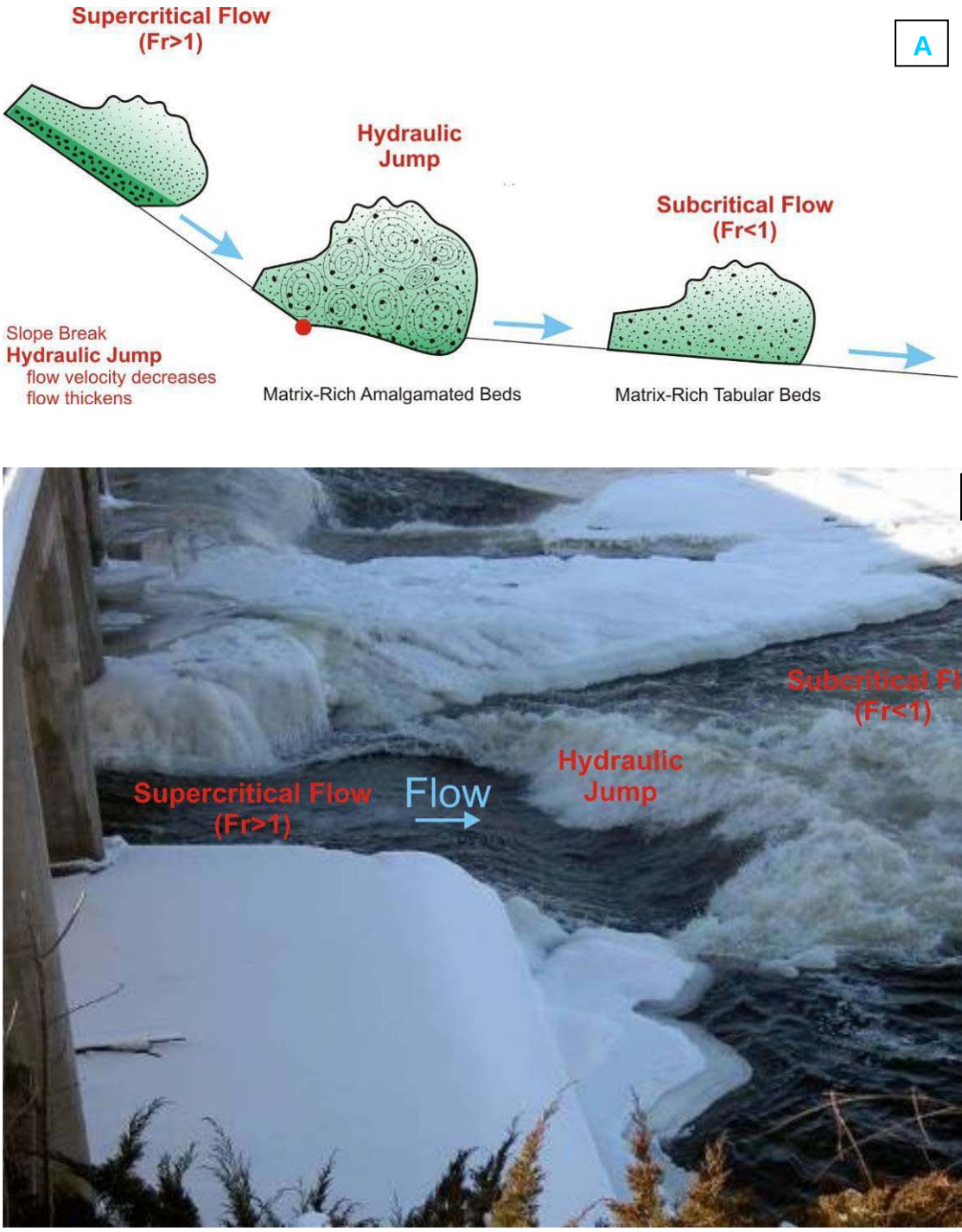

Figure 2.29: Matrix-rich coarse-tail graded structureless sandstones (F3) are deposited down flow of a plane-wall jet with jump. Plane-wall jet with jump typically forms at an abrupt change in slope where supercritical flow ($Fr > 1$) is transformed abrupty to subcritical flow ($Fr < 1$). Intense turbulence generation occurs at or near the jump and deeply scours the bed. Scours are draped with a layer of sediment from the rapidly collapsing sediment cloud depositing amalgamated structureless sandstones (F3a) and further downflow tabular structureless sandstones (F3b) are deposited. (A) Schematic diagram of turbulent flow through a hydraulic jump. (B) Example of a clear water hydraulic jump (Photo by Bill Arnott).

2.5: (F4) Mudstone Clast Breccia

Facies (F4) is composed of at least 15% clasts dispersed in a massive sandstone matrix. Based on differences in clast morphology and abundance, matrix grain size, basal contacts and facies associations, two subfacies have been identified: tabular, unlaminated mudstone clast breccia (F4a) and irregular clast breccia (F4b).

2.5.1: (F4a) Mudstone Clast Breccia

Strata of F4a range from 5-120 cm thick. Although discontinuous many beds can be traced for 10's of metres to 100's of metres laterally. Basal contacts are sharp, erosive and overlie thin-bedded turbidites (F1). In most places, breccia grades upward into structureless sandstone (F2b). Breccias are matrix-supported and consist of 15-50% mudstone clasts (Figure 2.30). Clasts are dark grey in colour and composed mostly of clay-sized particles. Two end member kinds of mudstone clasts were observed: (1) unlaminated, elongate mudstone clasts with well rounded edges (Figure 2.31) and (2) unlaminated or laminated, tabular to lensoid mudstone clasts with angular edges. Individual beds typically consist of a single clast type. Laminated clasts are less common and make up less than 10% of the clasts in a breccia unit (Figure 2.32). Clasts have an average length-to-width ratio of 5:1 and range from 0.5-110 cm in length. Elongated clasts are generally orientated sub-parallel to bedding. Some mudstone clasts show evidence of soft sediment deformation and have flame structures along their tops (Figure 2.33). The matrix consists of poorly-sorted, massive, coarse- to very coarse-grained subarkosic sandstone.

Figure 2.30: Mudstone clast breccia (F4a). Clasts are dark grey, unlaminated and tabular and supported in a matrix of coarse sand.

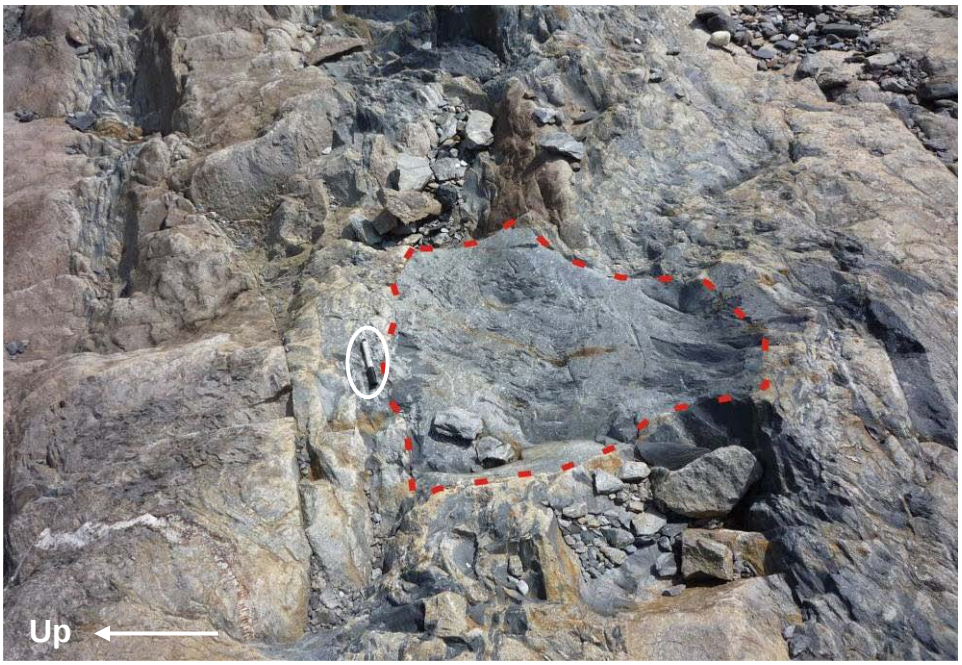

Figure 2.31: Angular unlaminated mudstone clast (F4a) highlighted by dashed red line. Pen for scale.

Figure 2.32: Tabular laminated mudstone clasts (F4a). Pen for scale.

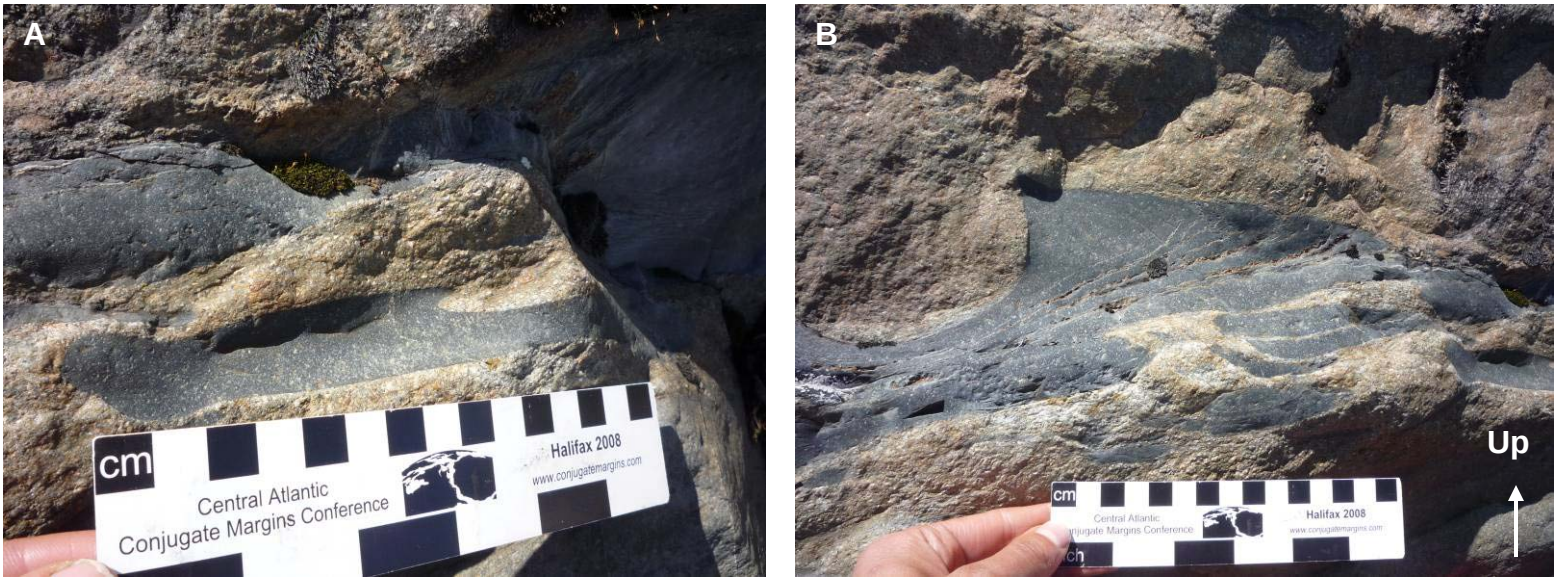

Figure 2.33: Tabular unlaminated mudstone clasts (F4a) with flame structures.

2.5.2: (F4b) Irregular Clast Breccia

Facies F4b is a clast-supported breccia comprised of angular, irregularly-shaped, unlaminated or laminated thin-bedded turbidite clasts (Figure 2.34). Beds range from 10-50 cm thick and although laterally discontinuous, can commonly be traced for several 10's of meters before pinching out into thin-bedded turbidites (F1). Upper and lower contacts are sharp, erosive, irregular and locally near vertical. Strata are commonly clast-supported and composed of 25-70% clasts. Clasts are separated by matrix sand and show no preferred orientation. The matrix consists of massive, ungraded, medium-grained subarkosic sandstone. The arrangement of clasts commonly creates a mosaic in which clasts, like jigsaw puzzle pieces, can be fit together. Clasts are commonly folded or contorted and appear partially or competely detached from other mudstone clasts or beds. Sandstone injections are common along clast margins. In laminated clasts, sand is preferentially injected along the silt or sand interbeds (Figure 2.35). Grading is generally absent. Clasts are 2-140 cm long with an average length-to-width ratio of 7:1.

Figure 2.34: Irregular mudstone clast breccia (F4b). Note the angular tapered clast edges and pigmatically folded dike.

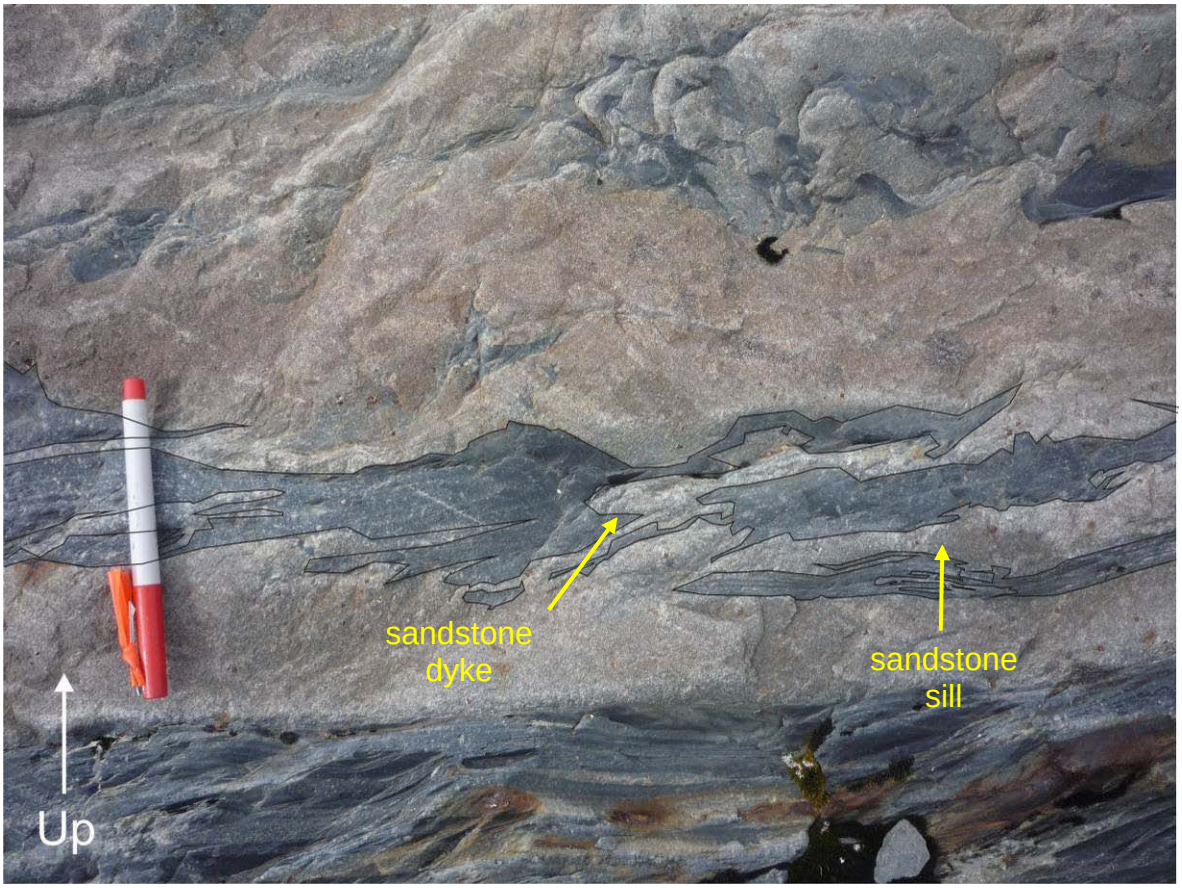

Figure 2.35: Irregular mudstone clast breccia (F4b). Note ptygmatically folded sandstone dyke that transformed upward into a sill.

2.5.3: Interpretation

The different stratal geometries, clast shapes and clast compositions observed in Facies F4 imply two different mechanisms of origin.

2.5.4: (F4a) Interpretation

The tabular, orientated mudstone clasts in facies F4a are interpreted to be intraclasts derived from upflow erosion of compacted mud-rich sediment. Clasts were eroded and re-deposited by strong, high density currents (Lowe, 1982) or hyperconcentrated flows (Mulder and Alexander, 2001). Clasts were supported in the flow by buoyancy forces, clast-to-clast interaction and hindered settling (Hampton, 1979; Postma et al., 1986; Druitt, 1995; Mulder and Alexander, 2001), but prior to deposition

had settled and become concentrated in the lower part of the flow. During transport clasts were abraded causing them to become rounded. Also, the greater abundance of unlaminated compared to laminated mudstone clasts probably relates to the ease of disaggregation of the clasts along internal interlayers of cohesionless silt and sand and preservation of the surrounding compacted mudstone. Furthermore, the disintegration of mudstone and disaggregation of silt and sand interlayers increased the viscosity of the flow, which in turn increasingly suppressed turbulence and caused the flows to deposit massive mudstone clast breccias by en-masse frictional freezing (Lowe and Guy, 2001; Baas and Best 2002).

Two main clast types were observed: unlaminated, elongate mudstone clasts with well rounded edges and unlaminated or laminated, tabular to lensoid clasts with angular edges. Variation in clast shape and the presence of lamination most probably reflects differences in distance of transport. Unlaminated, elongate mudstone clasts with well rounded edges were most likely sourced (eroded or "ripped-up") further upflow than angular, unlaminated or laminated, tabular to lensoid clasts.

2.5.5: (F4b) Interpretation

Facies F4b is interpreted to be a network of sills and dykes that intruded thin-bedded turbidites (Figure 2.36). As such breccia clasts are in fact related to in-situ brecciation with at best negligible transport. Sand intrusions similar to the dykes and sills described in facies F4b are common in deep-marine strata (Jolly and Lonergan, 2002). Requisite correlations for intrusion and in-situ brecciation include saturated unconsolidated or semi-consolidated sand sealed on all sides by low permeability mud-rich sediments and a catastrophic explusion of overpressured pore fluids. Upon explusion sand becomes suspended and transported within the now moving pore fluid (fluidization) – movement instigated by a differential pressure gradient across the bed (Huuse et al., 2005). As the pressure gradient dissipates, however, the sand-pore fluid slurry eventually arrests. The most commonly cited triggers for fluidization are seismic shocks or a sudden increase in differential lithostatic stress, for example the almost instantaneous deposition of a thick debris flow, slump or slide (Jolly and Lonergan, 2002). Triggering of fluidization has also

been attributed to tectonic stresses, storm waves, channel switching or an influx in overpressured fluid from deeper within the basin (Jolly and Lonergan, 2002).

The injection complex described in F4b was probably triggered by the local emplacement of a slump, slide or debris flow deposit – strata that are common within the Isaac Formation. Remobilized sand intruded laterally adjacent, overlying or underlying thin-bedded turbidites forming irregularly shaped mud-rich clasts surrounded on all sides by sand-rich dykes and sills. Significant deformation took place along sand and silt interlayers and sand and silt laminae most likely acted as planes of weakness along which sand preferentially injected. Clasts typically show no preferred orientation because intrusion occurred along many different and commonly cross-cutting planes.

The abundance of sills in strata of facies F4b suggests that deformation occurred at shallow burial depths. Under shallow burial conditions, the initial lithostatic pressure differential is small and dykes only propagate only a short distance before the fluid pressure equals the vertical pressure and sills develop (Jolly and Lonergan, 2002). In addition, at shallow burial depths the principal stress direction (σ) is parallel to bedding, and as a consequence encourages the formation of sills over dykes.

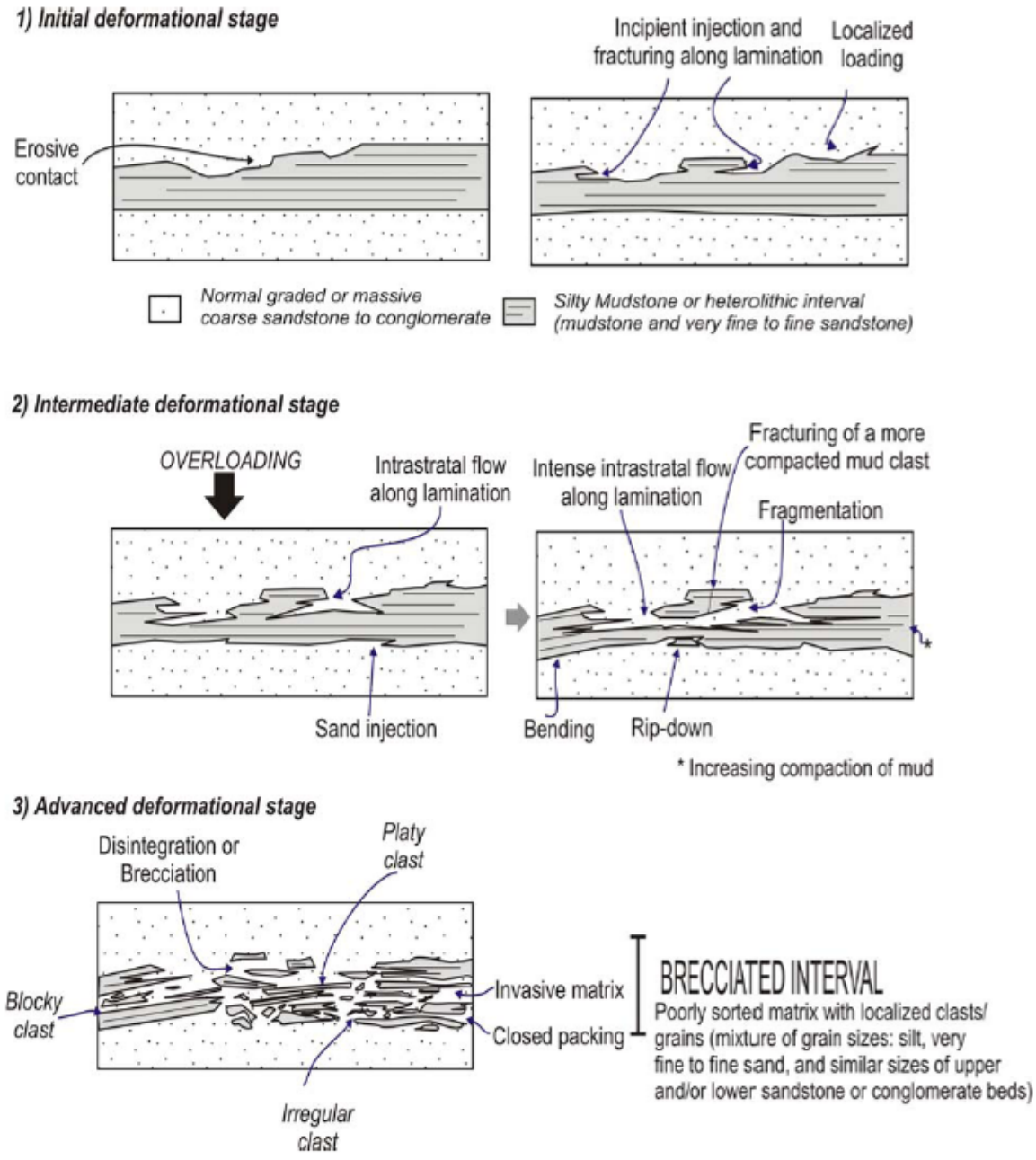

Figure 2.36: Deformation in the irregular mudstone clast breccia facies (F4b) from Navarro (2005).

2.6: (F5) Carbonaceous mudstone

Facies (F5) is a dark grey, organic-rich mudstone composed predominantly of graphite (Figure 2.37). The dark grey colour reflects elevated total organic carbon (TOC) levels. Background TOC levels in the Isaac Formation are generally on the order of 0.1%, whereas TOC levels in facies (F5) are > 0.25% (Figure 2.38). Weathered surfaces are commonly a rusty orange colour (Figure 2.39). Two end member kinds of carbonaceous mudstone are observed: massive mudstone (F5a) (Figure 2.37) and mudstone laminae or very thin mudstone interbeds (F5b) (Figure 2.39).

2.6.1: (F5a) Massive carbonaceous mudstone

Facies (F5a) consists of ungraded, massive siltstone and mudstone that range from 10-30 cm thick. Beds are tabular and laterally continuous over the study area (at least 250 m). Bed bases are undulatory or planar, sharp and non-erosive.

2.6.2: (F5b) Carbonaceous mudstone laminae

Facies (F5b) consists of graphite laminae in thin to medium bedded turbidites (F1) and thick bedded turbidites (F2). Carbonaceous interlayers range from 0.1-2 cm thick and are commonly interstratified with medium-grained sand in the planar laminated division of Tbcd or Tbd turbidites. Most abundant in the upper third of the Tb interval, interlaminations are typically straight to undulatory and oriented parallel or subparallel to bedding.

Figure 2.37: A 45 cm thick layer of carbonaceous mudstone (F5a). Note the distinctive dark grey color.

Sample ID	%C	Weight Calculated (mg)	Weight Measured (mg)	δ 13Corg	%Corg
2.1	0.46	21.739	21.473	-24.38	0.39
4.1	0.52	19.231	18.415	-24.38	0.54
5.5	0.36	27.778	27.611	-24.17	0.36
5.13	0.1	100.000	98.806	-17.89	0.09
5.15	0.14	71.429	72.492	-21.52	0.1
5.21	0.2	50.000	50.804	-18.01	0.21
5.24	0.78	12.821	12.975	-22.94	0.78
M1.1	0.41	24.390	25.213	-24.89	0.25
M1.2	0.21	47.619	46.591	-25.05	0.22
M2.1	0.7	14.286	14.253	-24.55	0.71
M2.1 dup	0.7	14.286	14.79	-24.55	0.92
M2.2	0.61	16.393	16.224	-24.7	0.57
M2.3	0.1	100.000	103.895	-25.05	0.07
M2.4	0.41	24.390	24.882	-28.45	0.38
M2.5	1.49	6.711	6.572	-24.23	0.5
M2.6	0.13	76.923	78.998	-24.89	0.13
M2.7	0.4	25.000	25.601	-14.97	0.43

Figure 2.38: Total organic carbon (TOC) data. The percent of bulk carbon (%C) was measured using an elemental analyzer. This data was then used to calculate the weight of each sample required for isotope analysis (column 3: weight calculated). Four samples (5.13, 5.15, M2.3 and M2.6), highlighted in blue, were sampled from facies F1 to measure background levels of organic carbon. One duplicate sample (M2.1 Dup), highlighted in green, was collected to ensure the accuracy of the procedure. The δ 13Corg value of M2.1 and M2.1 Dup are identical. Organic carbon percentage ranged from 0.21-0.92%. Metamorphism has reduced organic carbon content, which conservatively was originally four times the present values, or 0.84-3.68%.

Figure 2.39: Massive carbonaceous mudstone (red arrows) (F5a) overlying thick-bedded planar laminated sandstones (F2a). Rusty weathering is a result of the oxidization of abundant heavy minerals and pyrite.

Figure 2.40: Thin, undulose organic carbon-rich laminae (red arrows) in a thick-bedded, Tbcd turbidite (F2a). Note the rusty weathering.

2.6.3: Petrography

Carbonaneous mudstones consist predominantly of graphite with isolated lenses of quartz (Figure 2.41). Graphite can make up to 50% of the sample. In thin section, graphite is opaque, thin and flakey and commonly appears bent or folded. Sandstones are grain supported consisting of up to 20% matrix. Framework grains consist primarily of quartz. Quartz grains display undulose extinction and are slightly elongate parallel to bedding. The matrix is composed primarily of muscovite, chlorite and carbonate cement. Muscovite and chlorite are more common in facies (F5a) than facies (F5b) and can make up to 5% of the rock. Large (~0.3 cm), elongate chlorite grains are present in both sub-facies (F5a) and (F5b) and are oriented sub-parallel to bedding. In addition, pyrite is particularly abundant, 5-10%, in strata of facies F5.

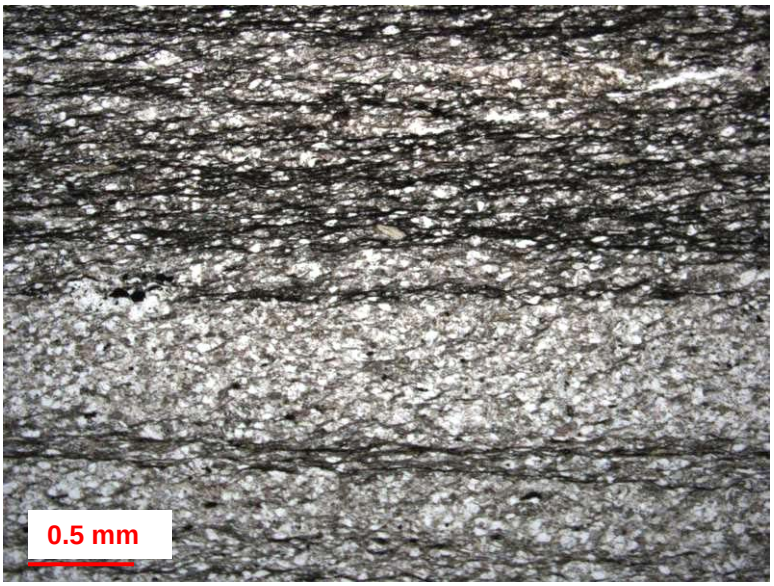

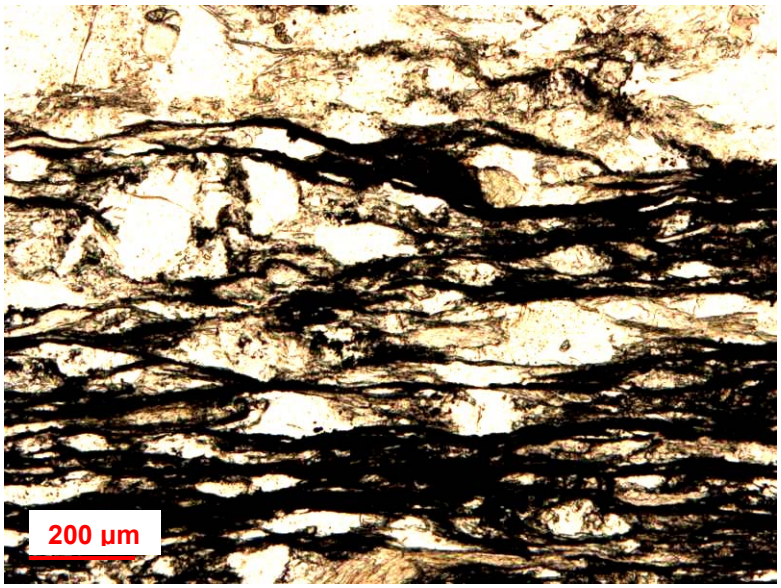

Figure 2.41: Photomicrograph under plane polarized light. (A) Fine sand interbedded with graphite. Bands run roughly parallel to bedding. (B) Close up view of lower medium sand grains floating in a matrix of graphite, which is typical of F5 strata.

2.6.4: Interpretation

Graphite is one of the most common and, at surface temperatures and pressures, the most stable allotropes of carbon. Graphite is a metamorphic mineral that forms syngenetically or epigenetically. Syngenetic graphite forms through the metamorphism of organic matter whereas epigenetic graphite forms by precipitation from C–O–H rich fluids (Crespo et al., 2004). Syngenetic and epigenetic graphite are easily distinguishable in the field as syngenetic graphite is stratabound and occurs as disseminated or massive concentrations, and epigenetic graphite occurs in veins (Luque et al. 1998) or overgrowths (Farquhar, Hauri & Wang, 1999; Satish-Kumar,Wada & Santosh, 2002; Ueno et al. 2002). The graphite in facies (F5) is stratabound and, therefore, interpreted to be syngenetic graphite. Graphite was originally deposited as organic-rich sediment and graphitisation, or the chemical conversion of organic material to graphite (Wopenka and Pasteris, 1993), most likely occurred during Mesozoic deformation.

Organic-rich strata of Facies F5 have total organic carbon contents, or TOC, of 0.21-0.92%, which are much higher than typical values (TOC <0.25%) measured in all other Windermere strata. TOC content in all WSG strata, including Facies F5, was likely reduced during burial diagenesis and later Mesozoic low-grade metamorphism as the rocks passed through the oil and subsequently gas generating windows. Hayes et al. (1983), for example, demonstrated that strata subjected to temperatures >200°C, and therefore beyond the oil and gas window, have only about 25% of their original organic carbon preserved. Accordingly, primary TOC probably ranged from about 0.84-3.68% in Facies 5 strata and <1% in background Windermere rocks, the latter being consistent with values <1% measured in modern deep marine sediments (e.g. Watanabe and Akiyama, 1998).

In addition to the Windermere Supergroup (this study, British Columbia, ~600 Ma), organic matter has also been reported from other Precambrian sedimentary basins, including: Huronian Supergroup (Ontario, 2.1-2.4 Ga), Mugford Group (Labrador, >1.97 Ga), Tyler Formation / Michigamme Slate (Michigan - 1.82 Ga) and the McArthur Basin (Australia,1.4-1.7 Ga) (Schidlowski and Aharon, 1992; Kendall et al., 2009). Moreover, evidence for life in the WSG includes fragments of calcareous crypt-algal laminites and

stromatolites in base-of-slope strata of the Isaac Formation (Navarro, 2005) and pyrite with sulphur isotope signatures indicative of bacterially-mediated sulphate reduction (Ross, 1995). Problematic, however, is the source(s) of organic matter during the Precambrian, but might include acritarchs (Vorob'eva et al., 2009) or various other kinds of ancient algae and bacteria. Future work on organic rich strata of the Windermere Supergroup, particularly those that have not undergone severe metamorphism, might attempt to analyze nitrogen and sulphur isotopes to make direct inferences regarding diet, trophic level and subsistence (ex. Frye, 1987; Sture Hansson et al., 1987; Michener, 2007), isolate steranes as biomarkers for eukaryotes (Vidal and Ford, 1985; Nagy et al., 2009), or reveal microstructure of possible biological origin using electron probe microanalysis, TEM and/or XRD (Tazaki et al., 1992).

2.6.5: The Origin and Preservation of Organic Matter

Organic rich strata (facies F5) in the Isaac Formation are mostly confined to strata of Isaac channel 4 and 6. Within these intervals the distribution of organic carbon is episodic. Organic rich intervals are a few 10's of meters thick separated by barren intervals a few 10's of meters thick. These "organic-rich episodes" are most likely related to local oceanographic conditions (km's in extent) rather than regional conditions (100's of km's) because although they can be correlated throughout the Castle Creek study area (across this study area (200 m) and across the glacier (km's)), they are absent elsewhere in the basin. Organic matter most likely originated in updip shelfal areas before being remobilized by mass movements or turbidity currents and transported basinward. Favourable periods of organic production and accumulation were probably controlled by oceanographic controls such as sea-level, upwelling and shelf transport.

In facies (F5a), organic matter was deposited with silt to mud sized grains and occurs disseminated throughout massive siltstone. As turbidity currents travel downslope silt, mud and organic material typically become concentrated in the upper and tail parts of the flow (Posamentier and Walker, 2006). At Castle Creek, silt and organic matter were deposited when overfit flows overspilled an unexposed channel, expanded, waned and deposited over the interchannel. Although, organic matter is commonly interpreted to

represent background sedimentation (i.e. Te interval), the thickness and silty nature of these strata suggests transport and deposition from high density overspilling flows.

In facies (F5b), organic matter is concentrated in bands that consistently occur within the planar laminated division of thick-bedded, medium-grain sandstone turbidites. Although metamorphism has altered the organic matter making it impossible to definitively determine the original composition, size, shape or cohesive strength of the organic matter, the association of organic matter and planar laminated medium-grained sand suggests that the organic carbon particles were hydraulically equivalent to medium sand that formed the planar lamination.

2.6.6: Pyrite formation and, early carbonate cements

Thick-bedded, organic-rich turbidite facies (F5b) are commonly associated with higher carbonate cement and pyrite content compared to their organic-poor counterparts. Oxidation of both the iron rich carbonate cement and pyrite give these sandstones their distinctive dark red and rusty orange colour. Carbonate cements in the Kaza Group and Isaac Formations are interpreted to have formed during early diagenesis because primary pore space is preserved in planar laminated sandstones and dune cross-stratified sandstone retain their primary open grain framework. Further, carbonate cemented sandstone clasts are abundant in mass movement deposits indicating that the sandstone was at least partly lithified prior to remobilization. Increased carbonate cementation can increase the alkalinity (HCO_3^-) of the pore fluids [1], which, in turn produces methane (CH_4) by methanogenesis [2].

$$4\,H_2 + H^+ + HCO_3^- \rightarrow CH_4 + 3H_2O \qquad [1]$$

$$CH_4 + SO_4^{-2} \rightarrow HCO_3^- + HS + H_2O \qquad [2]$$

Bacteria breakdown the organic matter via bacterial sulphate reduction (BSR) producing bicarbonate (Arther et. al., 1983).

$$2CH_2O + SO_4^{-2} \rightarrow H_2S + 2HCO_3^- \quad [3]$$

BSR occurs wherever there is sufficient organic carbon and dissolved sulphate under anoxic conditions. Oxidized methane increases alkalinity which further favours the precipitation of carbonate (Hesse, 1990; Boetius et. al., 2000).

$$CH_4 + SO_4^{-2} \rightarrow 2HCO_3^- + HS + H_2O \quad [4]$$

Where reactive iron (Fe^{2+}) is present, enhanced organic carbon delivery to the seafloor and shallow subsurface should promote bacterial sulphate reduction (BSR) and pyrite production as well as carbonate production (Berner, 1984). Strata of the Windermere Supergroup contain abundant iron-bearing minerals and iron-carbonate cements and hence show no evidence of the system being an iron-limited system (Smith, 2009) meaning pyrite should be abundant.

$$2HS + Fe^{2+} \rightarrow 2H^+ + Fe_2S \quad [5]$$

Although pyrite can form in the water column, most of the pyrite in the Upper Kaza Group and Isaac Formation is interpreted to have formed in the shallow subsurface as a byproduct of bacterial sulphate reduction (BSR) (Ross et al., 1995).

In summary, thick-bedded turbidites were deposited from low concentration turbidity currents. Well sorted medium sand lacking silt and mud sized particles created an open packing arrangement. Methane was generated as a consequence of early diagensis and two sources of HS^- and HCO_3^- provided sufficient reactants to form pyrite.

Chapter 3: Architectural Elements

3.1 Introduction:

In deep-marine environments, the main conceptual tool used to build predictive geologic models is architectural elements (Posamentier and Walker, 2006). These are large-scale, 3-dimensional, mappable, geomorphic features that are classified based on their external geometry and internal facies. These elements form the "building blocks" of depositional systems (Walker and James, 1992) and are used to predict lateral and vertical facies successions. Common architectural elements identified in the deep-marine include: channels, lobes, levee deposits, overbank splays, crevasse splays and debris flows (Mutti, 1992; Clarke and Pickering, 1996; Postamentier and Kolla, 2003) (Figure 1.15, 1.16 and 3.1). Sediment accumulates in the staging area, and then moves downslope through slope canyons on the proximal slope, and then into leveed channels and frontal splays, ultimately depositing on the basin floor (Posamentier and Walker, 2006).

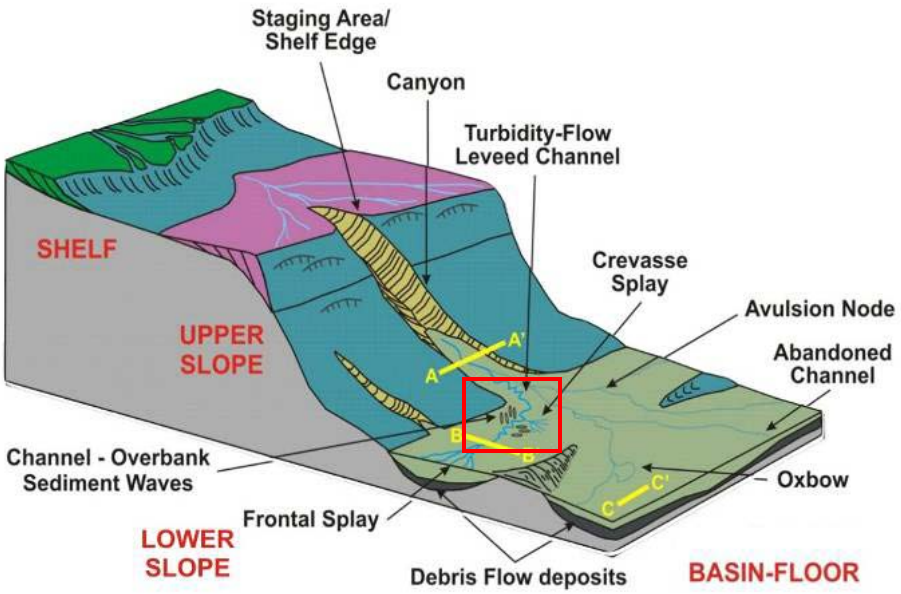

Figure 3.1: General architectural elements in the deep-marine from Posamentier and Kolla, (2003). The red box highlights the architectural elements present on the lower slope (Isaac Formation).

The objective of this chapter is to describe a suite of architectural elements and establish their geometry, dimension, facies distribution, lateral and vertical continuity. Based on the five facies identified in outcrop and described in Chapter 2, four architectural elements were identified in the study area. Some architectural elements are repeated within the study area and elements will not be presented in stratigraphic order. Vertical stacking patterns of architectural elements are discussed in Chapter 4.

3.2: Architectural Elements in Deep-Marine Systems

There are many inherent difficulties when studying deep-marine systems, including the fact that modern systems are commonly beneath several 100`s to 1000`s of meters of water making them difficult to access, and ancient systems are exposed in orogenic belts making preservation quality (level of metamorphism and structural complications) an obstacle. These limitations have made high-frequency seismic data a powerful tool for imaging modern deep-marine systems (Kolla, Bourges, Urruti, & Safa, 2001; Mayall & Stewart, 2001). Although the resolution of seismic data is improving, the detailed internal architecture of these stratigraphic features is still poorly resolved. Outcrop analogues can provide the data needed to describe the internal architecture, however, outcrops typically provide small windows of stratigraphy making it difficult to link outcrop with seismic data. Thus, large scale outcrop analogues, like those in the Windermere Supergroup, have proven helpful in merging these two data sets.

The architectural elements that populate the deep-marine, change along depositional dip from the continental slope to the basin floor. The proximal continental slope consists of deeply incised canyons that completely confine through-going turbidity currents. Downslope, from as close as 8 km from the shelf-edge staging area to the base of slope, sinuous leveed channels become increasingly common. The basin floor consists of depositional lobes that develop as flows become less confined (Posamentier, 2003). The length of the system is affected by the input grain size distribution; the more mud the system, the farther basinward the leveed-channel depositional element extends and the greater the longitudinal dimension of the system (Posamentier and Walker, 2006).

The depositional setting of this study area is well defined. The full stratigraphic section, from proximal basin floor to base of slope, is exposed in outcrop (Ross and Arnott, 2007) (see Ch 1.4). In the Castle Creek study area, the proximal basin floor (Upper Kaza Group) to base of slope (Isaac Formation) transition is exposed. This study focuses on a 75 m thick section of Isaac Formation stratigraphy deposited on the base of slope and between two unexposed sinuous leveed channels. The succession consists of a wide variety of architectural elements including: small sinuous leveed channel fills, inner bend levee deposits, outer bend levee deposits, overbank splay complexes and crevasse splay complexes (Figure 3.2; Figure 3.3).

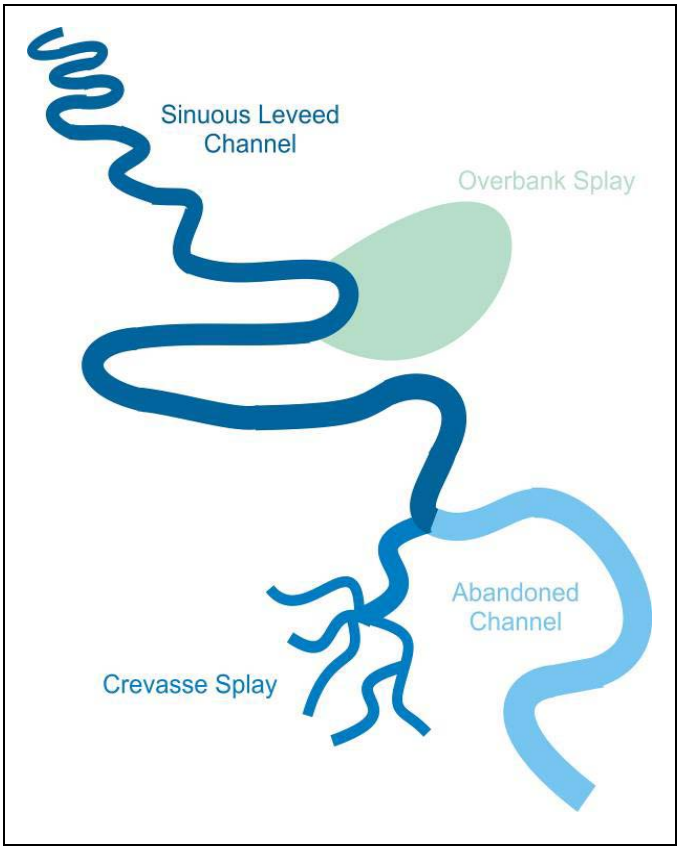

Figure 3.2: Schematic diagram of a sinuous leveed channel and associated sandy outer bend levee elements (overbank and crevasse splays). White area consists of muddy distal levee deposits.

Architectural Element	Subfacies	Thickness (m)	Facies	Description	Interpretation
(AE1) Channel	lateral accretion deposits (LADs)	3-9	F1; F2b; F4a	alternating fine LADs and coarse LADs are inclined at 1-4° towards the base of the channel	LADs are deposited on the inner bend of a laterally migrating, vertically aggrading sinuous channel by turbidity currents under traction transport conditions. Changes in channel geometry push the system out of equilibrum causing deposition of coarse LADs. Fine lads are deposited by the upper more dilute part of the flow.
(AE2) Distal Outerbend Levee	mud-rich overbank deposits	7-21	F1; F5a	laterally continous flat lying thin- to medium-bedded turbidites	Deposition from flows which overspill channel confines. Overspill results from over-fit flows. The coarser denser part of the flow remains confined to the channel and the upper dilute part of the flow escapes. Deposition occurs simultaneously along both sides of the channel under traction transport conditions.
(AE3) Overbank Splay	AE3.1: isolated splay	0.4-2	F2a; F5b	single structured thick-bedded turbidites with thick Tb division	Deposition from flow stripping, the preferential loss (overspill) of the upper, more dilute part of the flow (while the coarse, lower part of the flow remains confined to the channel) which is enhanced over the outer bend levee by superelevation. Deposition occurs under tractional transport conditions.
	AE3.2: multiple bed complexes	2-4	F2b; F4a	amalgamated structureless sandstones with low mud-matrix	A partial breach in the levee allowed coarser sediment carried in the lower part of the channelized flows to escape the confines of the channel. Rapid compedence-driven deposition occured under tractional conditions. After some number of later flows became healed (infilled), or evolved into a full channel-margin breach with associated avulsion.
(AE4) Crevasse Splay	AE4.1a: amalgamated sandstone	3.5	F3a; F4a	amalgamated coarse tail graded structureless sandstones with high mud-matrix	Deposition from high-concentration turbidity currents immediately down-flow of a submerged hydraulic jump. A levee breach allowed most of the thickness of the channelized flow to escape the channel and be diverted into the interchannel area. At some downflow break in slope, the supercritical flow (Fr > 1) passed through a hydraulic jump as it transformed quickly to subcritical flow (Fr <1) the highly turbulant flow slowed and thickened depositing matrix-rich structureless sandstone. Near the hydraulic jump flows are highly erosive depositing amalgamated sandstone.
	AE4.2: tabular sandstone	2-8	F3b	tabular coarse-tail graded structureless sandstone with high mud-matrix	Deposition further down-flow (amalgamated facies) of a hydraulic jump.

Figure 3.3: Summary of deep-marine architectural elements observed in the Castle Creek north study area.

3.3: Channel-levee systems

Submarine channels are particularly common in the geological record, and as such are well represented in the literature (eg. Mutti and Normak, 1987; Pickering et al., 1995; Garner and Borer, 2000; Sprague et al., 2002; Abreu et al., 2003; Moraes et al., 2004 and Hubbard et al., 2008). Further, channels are typically well exposed in outcrop because their sandy fill is resistant to weathering. The hierarchy of submarine channel elements, proposed by Navarro (2005) is used here to describe submarine channels (Figure 3.4). A discrete channel fill is a negative topographic element less than 10 m thick and 200 m wide which confined a number of turbulent flows (Mutti et. al, 2000). A channel unit consists of two or more genetically related channel fills. A channel complex comprises two or more channel units. A channel complex set is defined by two or more channel complexes separated by an abandonment surface or a change in facies. A channel system, the highest order hierarchical element, is delimited by two or more channel complexes.

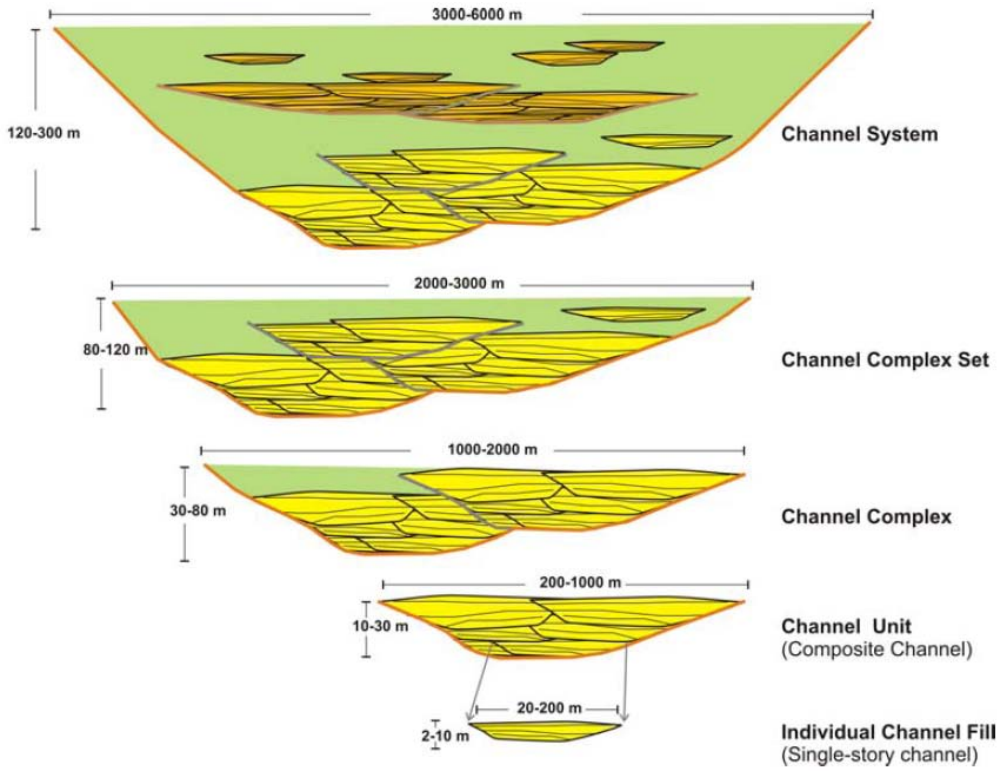

Figure 3.4: The hierarchy of submarine channel elements used to describe submarine channels (from Navarro, 2005). The channel observed in Castle Creek north and described below is classified as a channel unit.

Channels can be subdivided into three kinds: (1) erosional channels, (2) depositional channels and (3) mixed erosional-depositional channels (Mutti and Normak, 1987). Erosional channels are characterized by a local topographic low, truncation of sidewall strata and absence of channel-margin levees. They form when local erosion and removal of substrate create a topographic low. Depositional channels, on the other hand, have a channel floor which is bound by topographic highs formed levees along the sides of the conduit. Levees build up over time increasing channel confinement. Conversely, mixed erosional-depositional channels have levees bordering the channel axis, but, the channel floor may sit above or below the surrounding substrate. These mixed erosional-depositional channels are characterized by erosion at the channel base and deposition along the channel margins.

Channels are dynamic elements that evolve over time. Changes in allocyclic and autocyclic controls result in channel erosion, bypass, lateral migration, aggradation or avulsion to achieve or maintain equilibrium. As a channel develops, it goes through a series of stages which may be repeated several times: inception, bypass, fill and abandonment (Pickering et al., 1995; Clark and Pickering, 1996) (Figure 3.5). The initial stage of channel development, the inception phase, is commonly dominated by erosion involving multiple flows resulting in a complex stepped topographic low. Erosion is commonly followed by a period of bypass where the majority of flows neither erode nor deposit sediment (e.g. Mutti,1977). Although flows are considered to be in state of bypass, they may leave behind part of their sediment load. Incomplete bypass deposits, often called lag or residual deposits, consist of thin, lenticular beds (Beaubouef et al., 1999). Grain size and sedimentary structures vary depending on whether flows are primarily bypass (rework pre-existing deposits) or depositional. Incomplete bypass deposits consist of the coarsest fraction of the flow, the finest fraction of the flow, and/or mudstone intraclasts. Deposition of the coarsest fraction of the flow occurs when the flow is no longer able to transport these coarse particles due to local changes in velocity, and results in competence driven deposition. Deposition of the finest fraction of the flow occurs when the tail-end of the flow passes through the conduit. This dilute, fine-grained flow deposit silt and clay particles. Mudstone clasts, on the other hand, suggest up-dip

erosion of underlying mudstones or thin-bedded turbidites and are deposited with coarse-grained sand or gravel. Non-depositional lag deposits are formed by the reworking of older unconsolidated sedimentary deposits and often form dunes. Dunes are interpreted to indicate prolonged traction transport by the tail end of turbidity currents (e.g. Prather et al. 1998). During the channel infill phase flow efficiency decreases and net deposition ensues. Deposition occurs within the channel and channel relief decreases. Thick, amalgamated or layered structureless sandstones commonly infill the channel and either onlap the basal erosional surface or interfinger with laterally adjacent levee deposits (Navarro, 2005). During the final phase of channel development, termed channel abandonment, flow velocity and sediment flux become significantly reduced and flows are no longer able to transport coarse sediment through the channel. Flows typically deposit upward thinning, upward fining, fine-grained thin-bedded turbidites that infill any remaining topography. Channel abandonment may be the result of autocyclic controls such as channel avulsion, or allocyclic controls such as sea-level rise (Beaubouef et al., 1999).

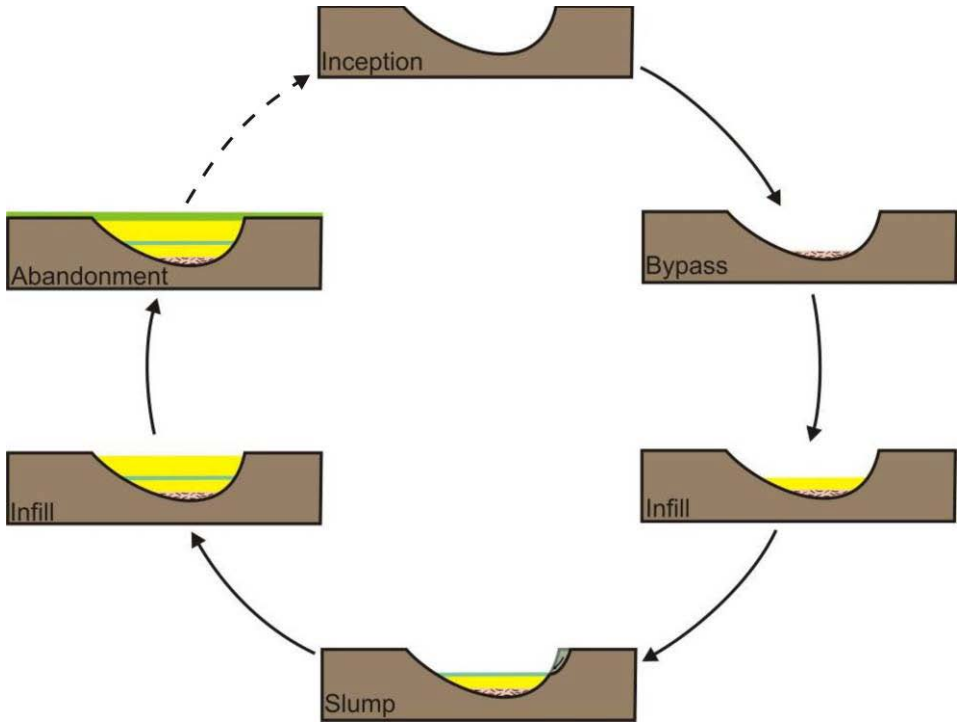

Figure 3.5: General schematic diagram of channel evolution. Channel inception creates an erosional based surface formed by a single or more likely multiple erosional events. As flow efficiency decreases, flows bypass fully or incompletely the conduit and leave behind lag deposits. Flows then become depositional during the infill phase. Finally, the system avulses and an abandonment complex infills the remaining topography.

3.3.1: Lateral Accretion Deposits (LADs)

Laterally migrating, vertically aggrading sinuous leveed channels are commonly filled with lateral accretion deposits (LADs). Due to their accessibility and similarity in planform character, fluvial lateral accretion deposits have been more extensively studied than submarine channel systems and until recently were commonly used as analogues for deep-marine channels (Figure 3.6). In fluvial systems, the point bar which includes the subaerial inner-bend levee, is formed by the lateral migration of a channel (e.g. Bridge, 2003). Erosion occurs along the outer bend, or cut bank, and is matched by deposition along the inner bend. Sediment, especially in the sand size and coarser fraction, is transported primarily as bedload transport. The resulting deposit consists of an upward-fining, upward-thinning sedimentary package described in the well-known point-bar facies model (Allen, 1964). In the fluvial realm, flow velocity is highest near the air-water interface. As a flow travels through a channel bend it will move toward the outer bank causing the surface of the flow to rise or super-elevate. Super-elevation increases pressure forces at the outer bank which then is balanced by water flow towards the inner bank along the base of the channel producing a secondary circulation. The secondary flow is directed up the surface of the point-bar to balance the pressure forces (Allen, 1970; Engelund, 1974; Johannesson and Parker, 1989) (Figure 3.7). As a result of the combination of the primary and secondary flow components and also gravity, point-bar deposits become vertically sorted - larger particles move obliquely down the point-bar surface whereas finer particles move obliquely upward.

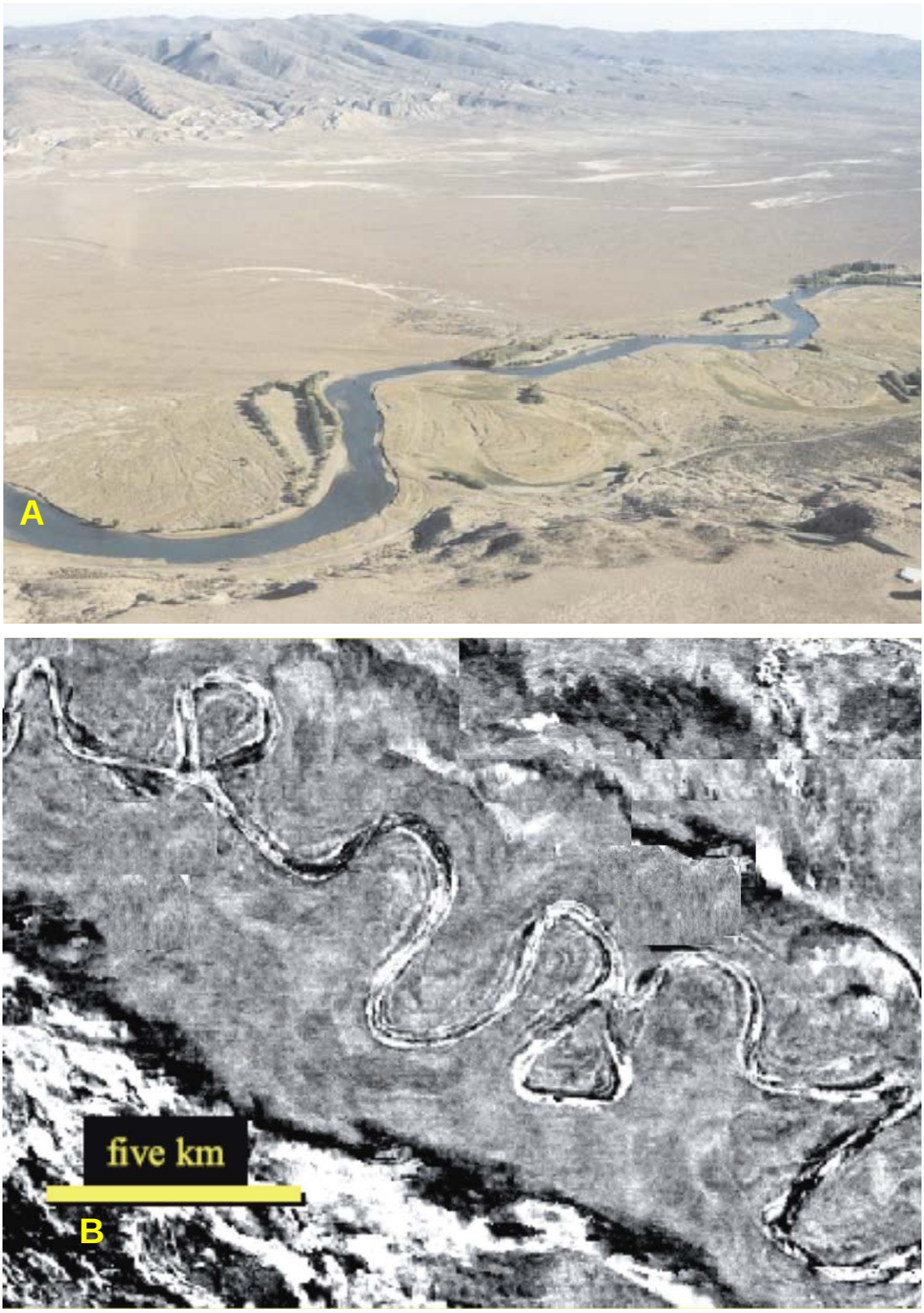

Figure 3.6: (A) An example of a meandering fluvial channel from Senguerr River, southern Argentina (Bridge, 2006). (B) Seismic image of a meandering deep-marine channel, Joshua channel, eastern Gulf of Mexico (Posamentier and Walker, 2006). Note the similarity in planform geometry.

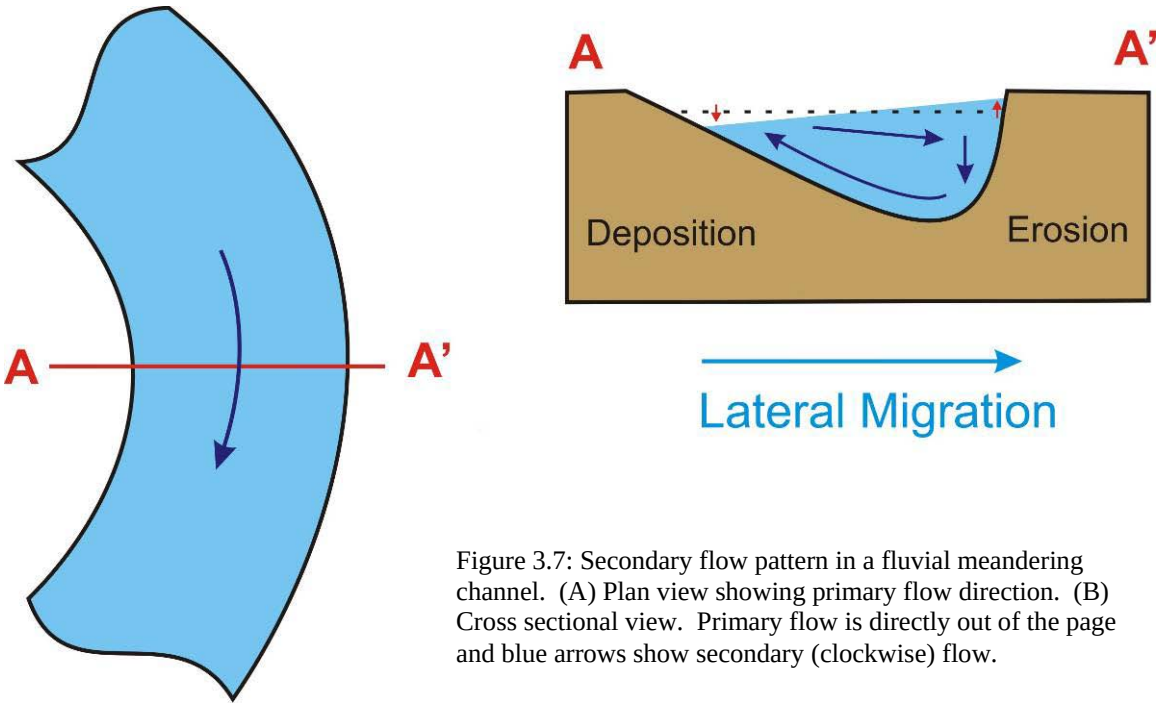

Figure 3.7: Secondary flow pattern in a fluvial meandering channel. (A) Plan view showing primary flow direction. (B) Cross sectional view. Primary flow is directly out of the page and blue arrows show secondary (clockwise) flow.

The vertical velocity profile of a sediment-gravity current differs from river currents because its maximum velocity is situated nearer the bed rather than the top of the flow (Figure 3.8). Keevil et al. (2005) suggested that this could create a secondary flow that moves in the opposite direction to that in rivers. A reversed sense of secondary circulation would strongly affect the architecture and composition of the resulting inner bank deposit thus, making fluvial meandering channel systems poor analogues for submarine meandering channel systems. Further, seismic images suggest that the spatial and temporal evolution of sinuous deep-marine channels exhibits more limited lateral migration but significantly greater aggradation (e.g. Piper and Normark, 2001; Peakall et al., 2000).

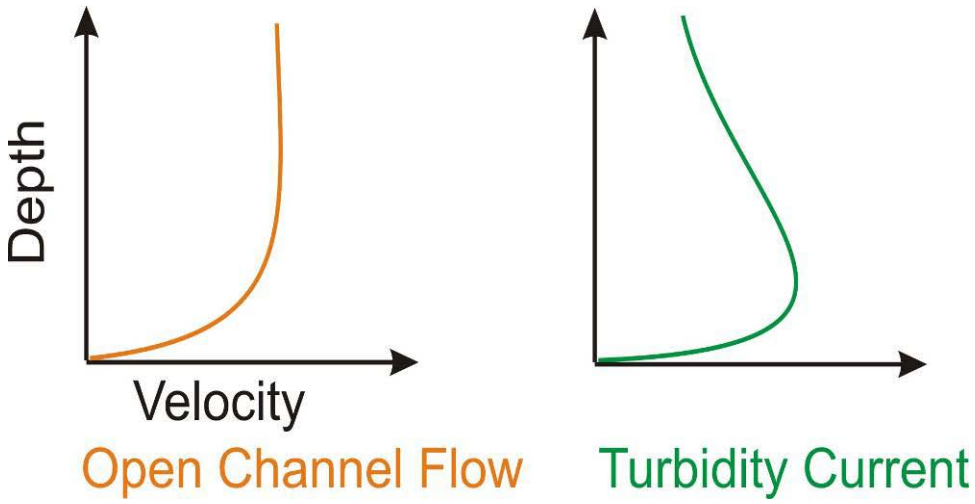

Figure 3.8: Velocity profiles for subaerial and subaqueous systems. Note that in a river the velocity maximum occurs near the top of the flow whereas in turbidity currents it is closer to base of the flow.

3.3.2: Channel description

The channel unit recognized in the study area is consists of three vertically- and laterally-offset-stacked channel fills informally named channel 1 (CH1), channel 2 (CH2) and channel 3 (CH3) (Figure 3.9). At its thickest the channel unit is 11 m thick. CH1 ranges from 2 to 5 m thick, CH2 from 3 to 7 m thick and CH3 from 2 to 3 m thick (Figure 3.10). The base of the channel unit is marked by a terraced erosional surface. The channel overlies thin- to medium-bedded turbidites (F1) and channel fill deposits do not interfinger with laterally adjacent (i.e. levee) strata. The minimum lateral extent of the channel is 200 m, extending from the edge of the glacier in the southeast to the lateral moraine in the northwest (Figure 3.11).

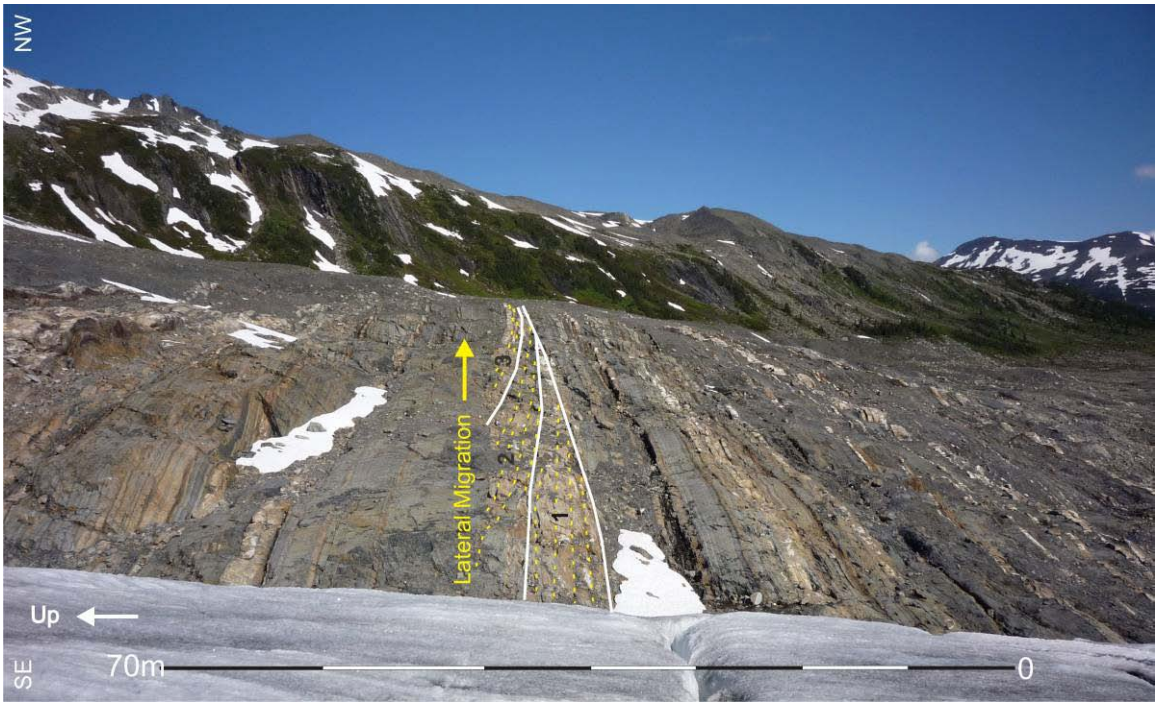

Figure 3.9: Channel unit composed of 3 channel fills (CH1, CH2 and CH3). Lateral accretion deposits (LADs) (dashed yellow lines) dip towards the base of the channel.

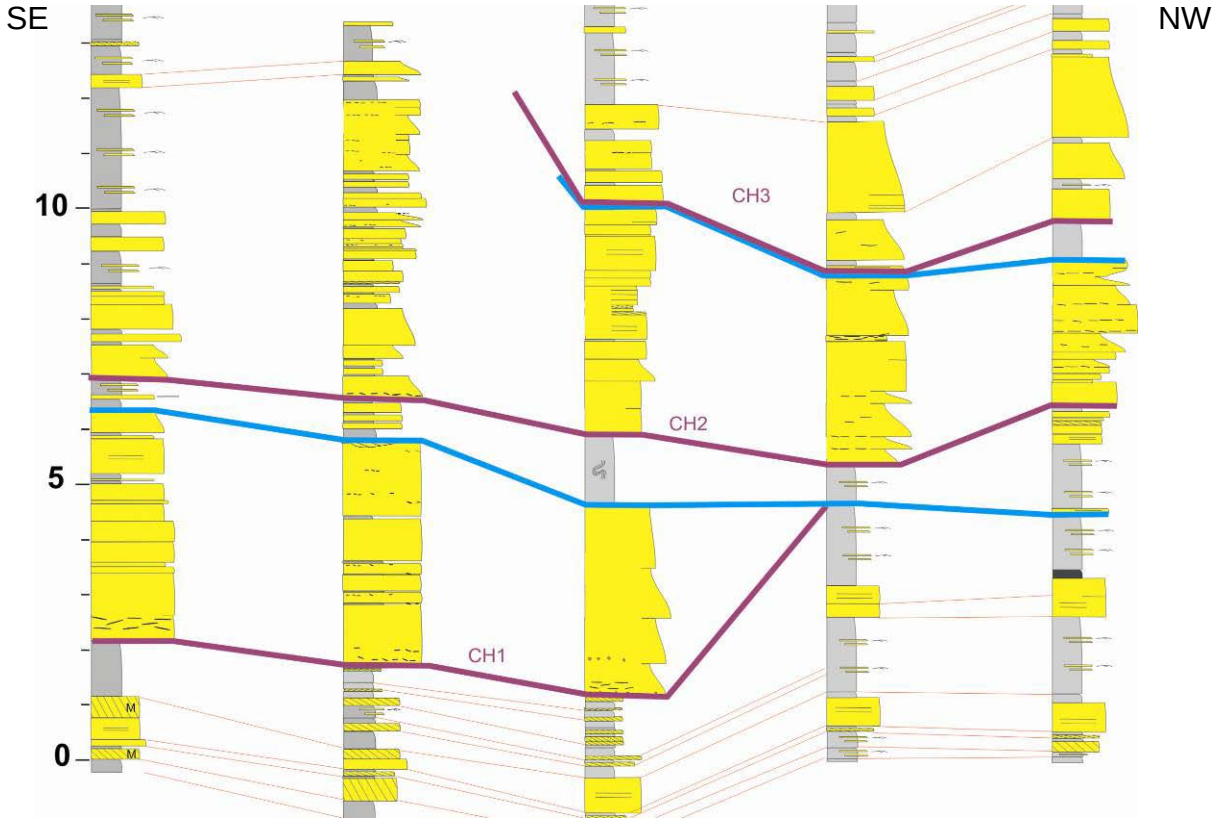

Figure 3.10: Stratigraphic correlation over channel unit. The channel unit consists of three laterally offset, stacked channel fills that are migrating toward the northwest. Note mudstones are preferentially preserved near the top of the channel fill and beds dip toward the base of the channel (detailed correlation Appendix A).

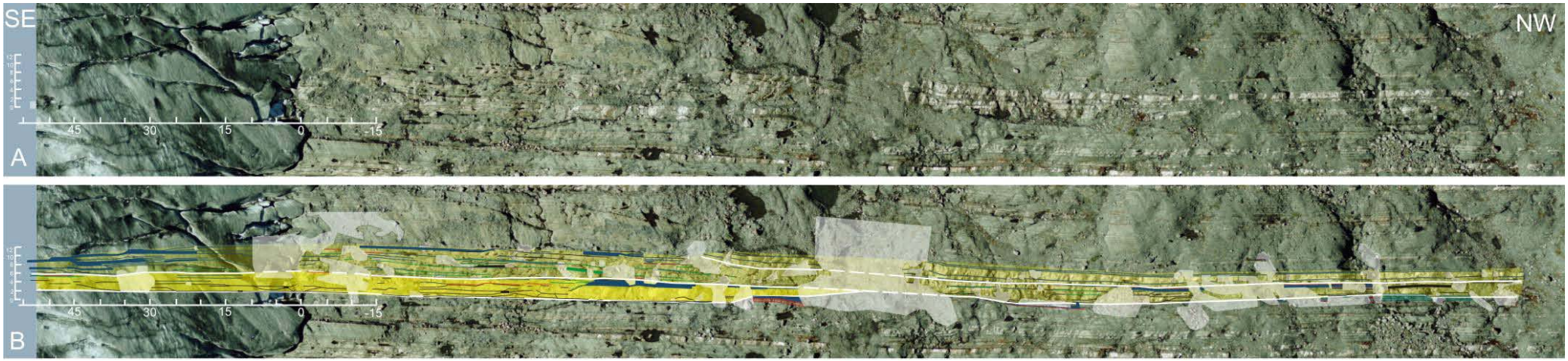

Figure 3.11: (A) Uninterpreted air photo and (B) Interpreted air photo of the channel unit. The channel unit is composed of three channel fills CH1, CH2 and CH3. Each channel fill consists of alternating coarse- (yellow) and fine-grained (blue lines) lateral accretion deposits (LADs) that dip towards the base of the channel. Coarse LADs amalgamate towards the channel fill base and contain mudstone clast breccias (black lines). Towards the top of the channel fill coarse LADs may become structured (red lines). The base of each channel unit is highlighted with a white line. Note the glacier has retreated almost 50 m since the air photo was taken (2001).

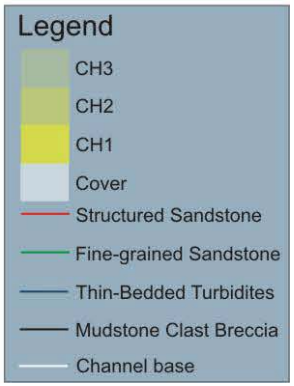

3.3.3: Channel fill 1

CH1 has an erosional basal surface, which then is overlain by sandy channel fill. The fill consists of 3 main facies associations: (1) mudstone clast breccia (F4a) and structureless sandstone (F2b), (2) thin-bedded turbidites (F1) and structureless sandstone (F2b) and (3) thin-bedded turbidites. Mudstone clast breccia (F4a) and structureless sandstone (F2b) are interbedded forming a fill unit up to 3 m thick that directly overlies the basal erosion surface. Individual beds are 30-120 cm thick with sharp, erosional bases. Mudstone clast breccias are commonly matrix supported and consist of 30-50% mudclasts (Figure 3.12). The matrix is commonly an ungraded coarse- to very coarse-grained subarkose sandstone. Clasts are dark grey, tabular, subrounded and unlaminated. Ranging from 5-120 cm long, mudstone clasts are preferentially aligned parallel to bedding (Figures 2.30-2.32). Breccias are interbedded with coarse-grained, ungraded to normally graded structureless sandstones (F2b). Occasionally, thin, 1-2 cm thick, mudstone drapes overlie small scours within the structureless sandstone facies (F2b) (Figure 3.13).

Figure 3.12: Structureless sandstone (F2b) interbedded with mudstone clast breccia (F4a). This facies association typically occurs near the base of the channel (solid yellow line). Note hammer for scale.

Figure 3.13: Structureless sandstone with erosional surface overlain by a mudstone drape and very coarse-grained sandstone.

Thin-bedded turbidites (F1) interbedded with structureless sandstones (F2b) commonly occurs stratigraphically above the mudstone clast breccia (F4a) and structureless sandstone (F2b) facies association and make up most (40-60%) of the channel fill (Figure 3.14) and form units 3-5 m thick. Thin-bedded turbidites are 1-7 cm thick, consist of laminated siltstone and become more common stratigraphically upward. Structureless sandstones are coarse-grained and ungraded or normally graded. Beds are 30-60 cm thick and laterally continuous or discontinuous. Bedding contacts are sharp and erosional, or more commonly, amalgamated.

Figure 3.14: Structureless sandstone (F2b) and thin-bedded turbidites (F1) facies association. The solid yellow line is the base of the channel. Note the amalgamated structureless sandstone near the base of the channel and the increased mud interbeds number of interbedded thin-bedded turbidites towards the top of the channel.

The thin-bedded turbidite and structureless sandstone facies association is overlain abruptly by thin-bedded turbidites. Strata consist of fine-grained, thin-bedded Tcd or Td turbidites. The unit is sharp based and ranges up to 1.7 m thick (Figure 3.15).

Figure 3.15: Interpreted photo of channel fill 1 (CH1). Near the channel base (yellow line) structureless sandstones are interbedded with mudstone clast breccias (red arrow), which then are overlain by amalgamated structureless sandstone. The channel fill is capped by a 1.7 m thick thin-bedded turbidite package. Hammer for scale.

3.3.4: Channel fill 2

The fill of CH2 consists of two end member stratal units: fine-grained, thin-bedded turbidites and coarse-grained, structureless sandstones. Fine-grained units range up to 150 cm thick and are composed of thin-bedded turbidites (F1) (Figure 3.16). Thin-bedded turbidites (F1) are mainly Tcd turbidites, <15 cm thick and consist of cross-stratified very fine- to fine-grained sand overlain by silt or mud. Cross-stratified cosets are usually 1-3 ripple sets thick and up to 5 cm thick. Individual beds are tabular with sharp, non-erosive basal contacts. Multiple-set (1-3) ripple beds transition laterally into single ripple sets.

Coarse-grained units consist of amalgamated, poorly sorted, very coarse- to coarse-grained, structureless sandstones (F2b). Near their terminus coarse-grained units consist of 2 bed types: structureless sandstone (F2b) and structured turbidite (F2a) (Figure 3.17). Beds range from 20-60 cm thick and amalgamated units are <120 cm thick. Structured turbidites exhibit tractional sedimentary structures including: planar lamination or ripple cross-stratification. Dune cross-stratification is rare. Beds terminate abruptly in fine-grained strata and the grain-size distribution shows no change near their terminus (Figure 3.18). Near their up-dip pinch-out coarse-grained strata commonly consist of 1 to 3 beds that amalgamate toward the channel base (Figure 3.19). Coarse units are lenticular in geometry with sharp, planar, erosive basal surfaces.

Fine and coarse units are interbedded near the top of the channel fill and dip at 1-6° southeast toward base of the channel (Figure 3.20). Coarse units erode locally up to several centimetres into the underlying fine-grained units and amalgamate near the base of the channel. Obliquely upward coarse units pinch out abruptly into fine-grained strata and step progressively upward across the study area. In contrast, fine-grained strata terminate obliquely downward as coarse-grained strata on either side amalgamate.

LADs are overlain in the northwest by thin-bedded turbidites and resemble the thin-bedded turbidites that cap CH1. The fine-grained, thin-bedded turbidite package ranges from 0.8 to 1.5 m thick (Figure 3.21). It is eroded out to the southeast by CH3.

Figure 3.16: Fine-grained, thin-bedded turbidites (fine-LADs) (grey strata) interbedded with coarse-grained structureless sandstones (coarse-LADs) (pink strata).

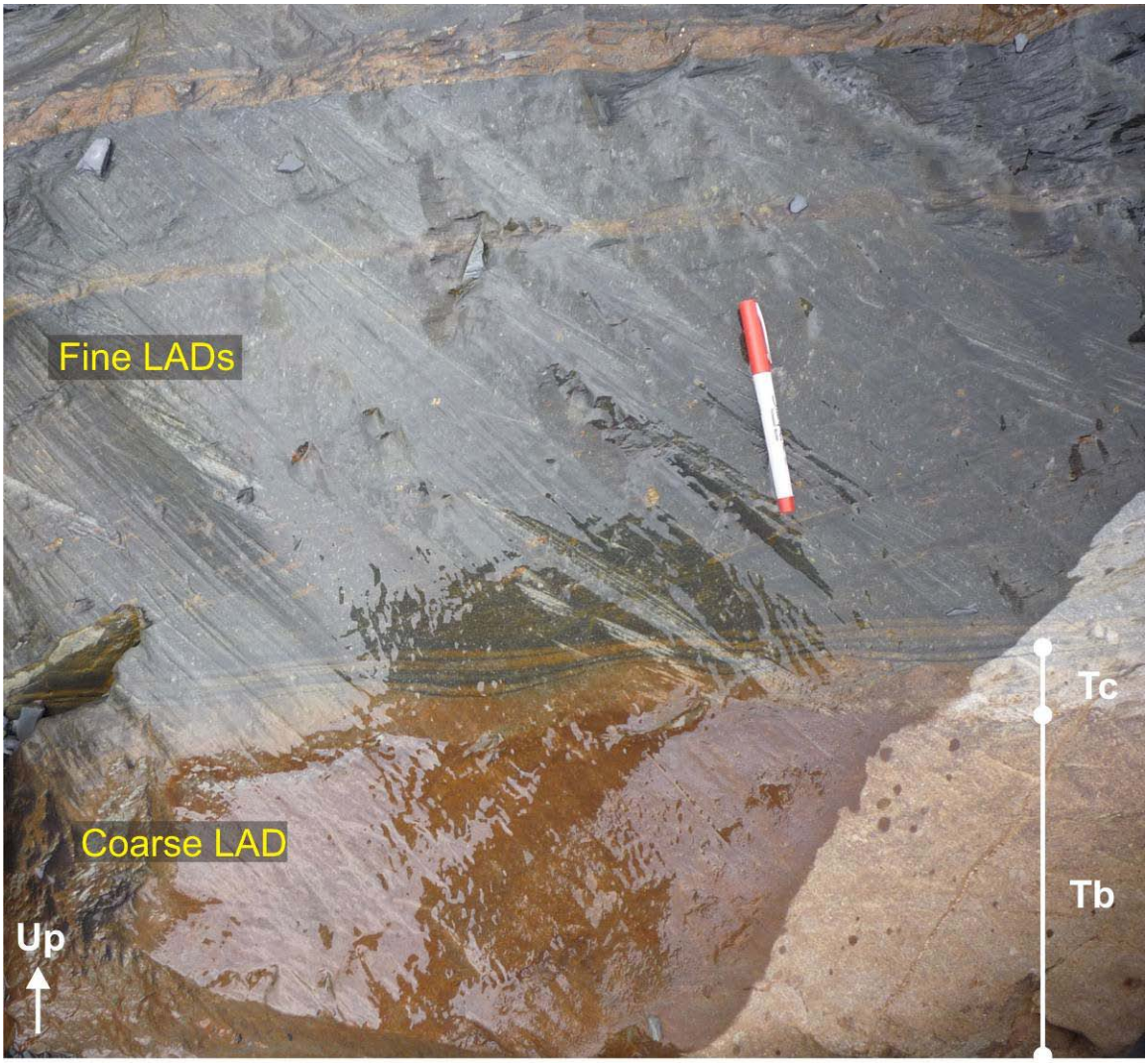

Figure 3.17: Coarse-grained, Tbcd turbidite (F2b) (pink) (coarse-LAD) overlain by fine-grained thin-bedded turbidites (grey) (fine-LADs) near the top of CH2.

Figure 3.18: Close up picture of the abrupt pinch-out of a coarse bed into thin-bedded turbidites.

Figure 3.19: Coarse-grained strata (coarse LADs) (bed bases traced by white lines) terminating abruptly into fine-grained, thin-bedded turbidites (fine LADs). Note amalgamation of at least three coarse LADs toward the top of the photo (yellow arrow). Pen for scale.

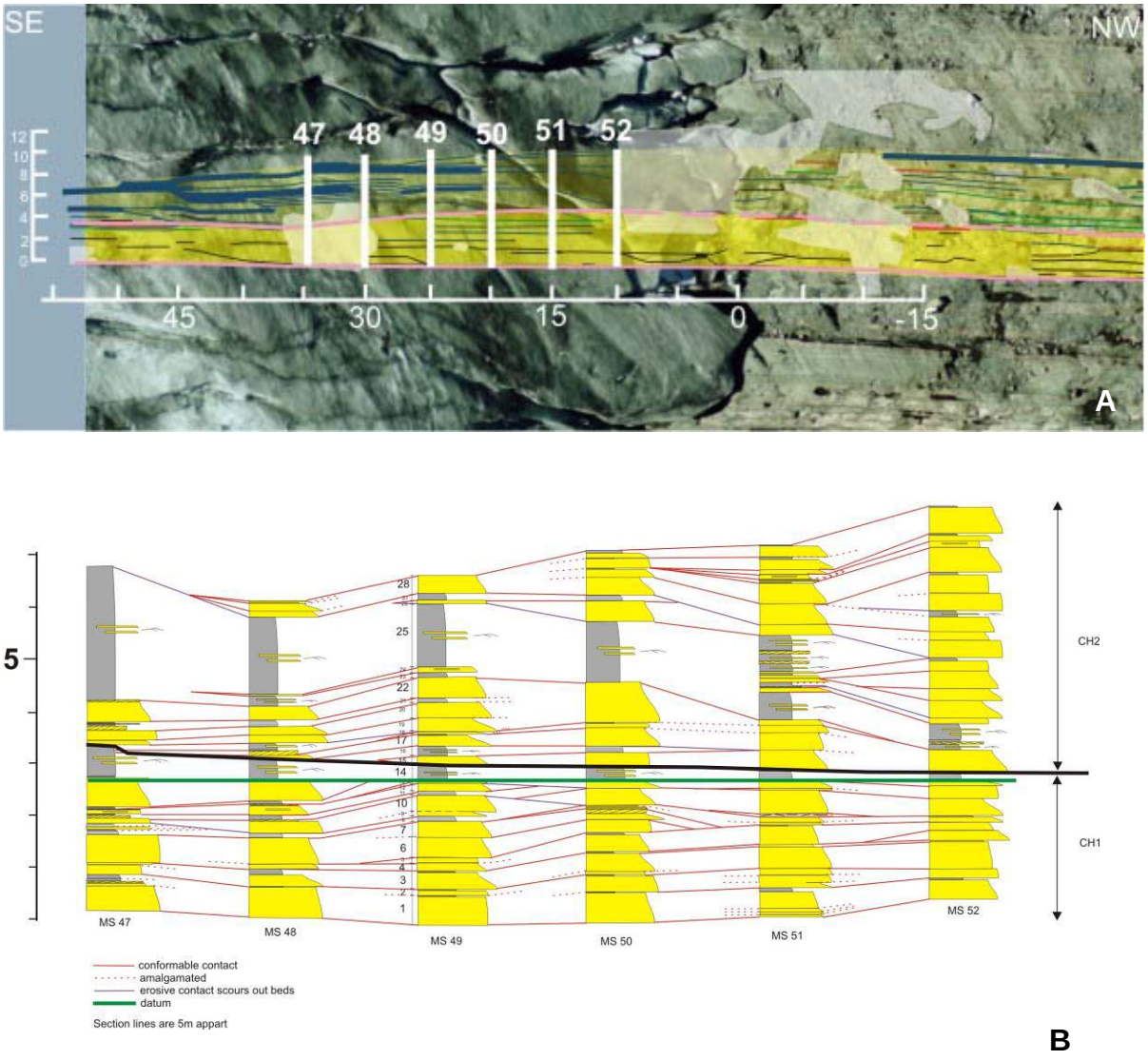

Figure 3.20: (A) Detailed air photo line drawing of channel fills CH1 and CH2. Pink lines bound CH1 and CH2. Blue lines are correlated thin-bedded turbidites (fine LADs). Note that on the left side of CH2 they dip downward toward the southeast and then become truncated toward the northwest as the coarse LADs amalgamate. (B) Stratigraphic sections showing fine (grey) and coarse (yellow) LADs. Section line locations are shown on (A).

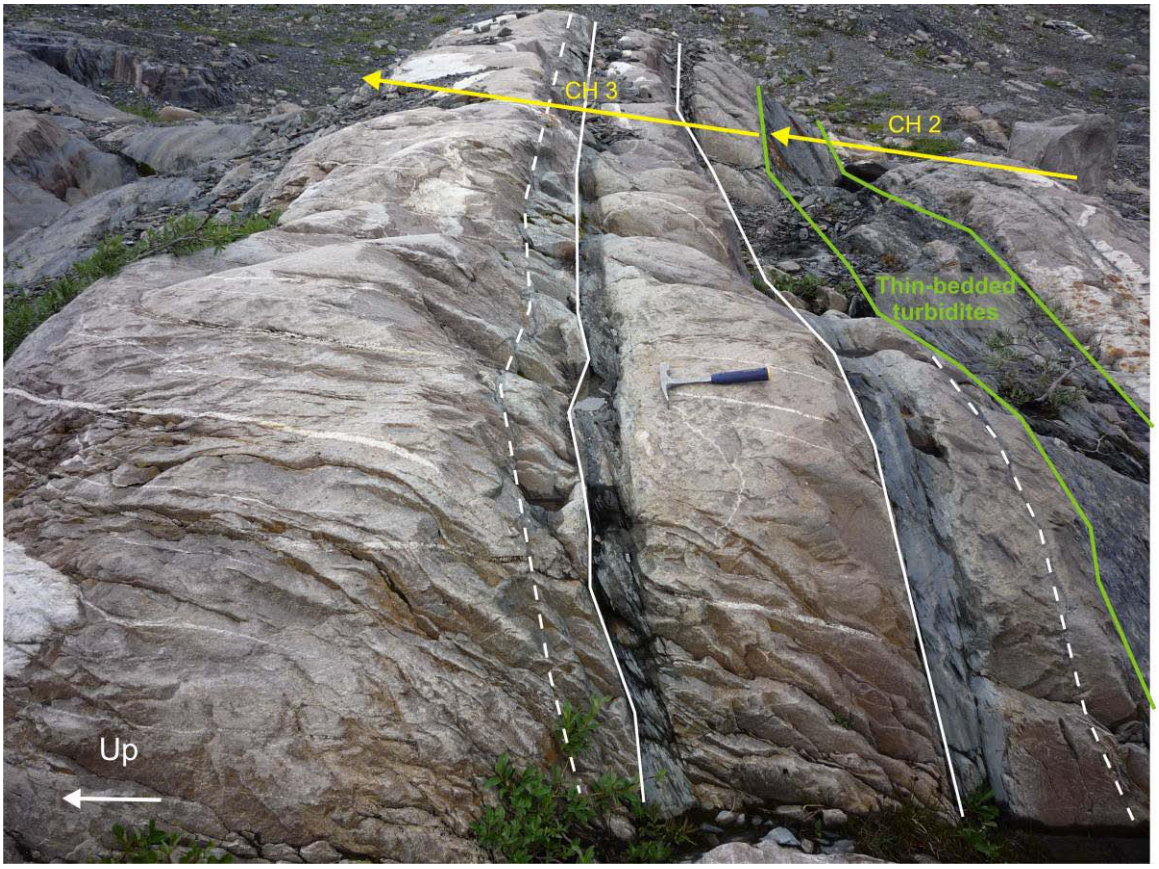

Figure 3.21: Thin-bedded turbidite strata at the top of CH2 erosively overlain by CH3. CH3 fill consists of structureless sandstones (F2b) overlain by thin-bedded turbidites (F1). Bed bases are either sharp or non-erosive (solid white lines) or amalgamated (dashed white lines). Note structureless sandstones thicken upward.

3.3.5: Channel fill 3

The youngest channel fill, CH3, is similar to CH2 and consists of two stratal units: fine-grained, thin-bedded turbidites (F1) and coarse-grained, structureless sandstones (F2b) (Figure 3.21). Fine-grained units are up to 40 cm thick and are composed of upper division, Tcd or Td turbidites. Cross-stratified cosets are usually 1-2 ripple sets thick and lesss than 3 cm thick. Coarse-grained units, on the other hand, range up to 145 cm thick and consist of structureless sandstones. Coarse-grained sandstones thin and pinch-out towards the south. Beds dip toward the channel base at 2-4°. Amalgamation of coarse-grained structureless sandstones and erosion of thin-bedded turbidites is not as common in CH3 compared to CH2 and CH1. Further, mudstone clast

breccias are also less common. The top part of CH3 consists of medium-grained, medium-bedded structureless sandstones overlain by fine-grained thin-bedded turbidites (Figure 3.22). Medium-bedded structureless sandstones thin and fine laterally into fine grained, thin-bedded turbidites. Medium- to thick-bedded turbidites are observed in the lower part of the channel fill thicken upward (Figure 3.21), however, near the top of CH3 beds thin and fine upward (Figure 3.22).

Figure 3.22: Medium-grained, medium-bedded structureless sandstones (bed bases are highlight with dashed white lines) at the top of CH3. Beds thin and fine stratigraphically upwards (yellow arrow).

3.3.6: Channel interpretation

The channel unit in the study area is interpreted to be a mixed erosional-depositional system, which at its bases scours distal levee deposits of an older channel system. The erosional surface is interpreted to represent the inception stage of channel system, and most probably represents the culmination of multiple erosive events that collectively eroded the first channel (at least in the plane of the outcrop).

The channel unit consists of three channel fills (Figure 3.11). Channels are interpreted to be filled with lateral accretion deposits (LADs) that accumulated on the inner bend of the sinuous deep-marine channel. LADs consist of alternating fine- and coarse-grained strata, fine and coarse LADs, respectively.

Fine LADs were deposited by the low-density, low-velocity tails of high-energy, equilibrium turbidity currents. Coarse-grained LADs, on the other hand, where deposited by highly-stratified, disequilibrium turbulent flows. Disequilibrium may have been the result of local changes in the channel dimension and/or sediment flux that caused flows to become locally less efficient and as a consequence deposit coarse sediment that onlapped and then became overlapped by fine LADs (Arnott, 2007). The alternation of coarse- and fine-grained LADs, therefore, records alternating episodes of disequilibrium (coarse-grained deposition) with more typical conditions of equilibrium (sediment bypass: fine-grained deposition) as the channel migrated laterally (Figure 3.23)

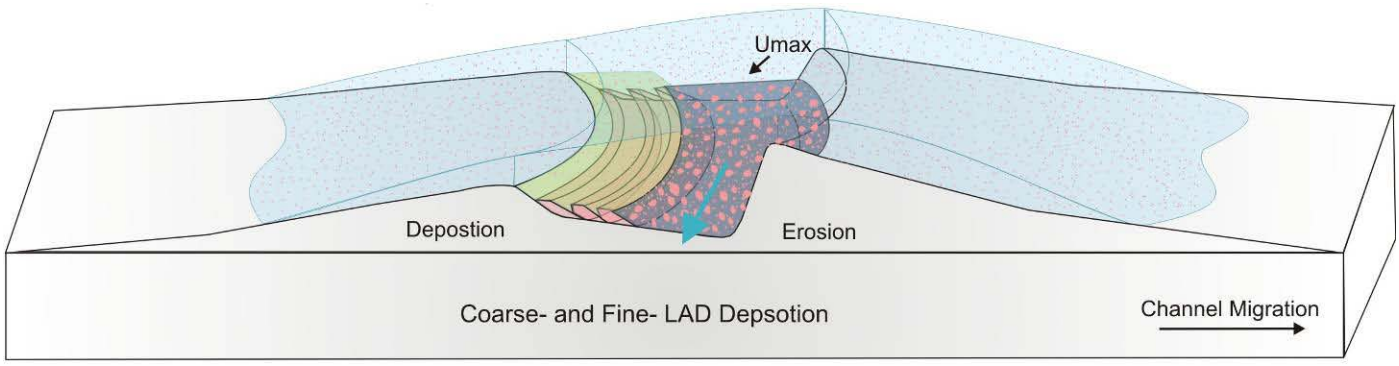

Figure 3.23: Schematic diagram illustrating deposition of coarse and fine-grained LADs. Note the turbidity current is highly density stratified. Umax is the velocity maximum and roughly corresponds to the boundary between the lower, high density, coarse grained, part of the flow and the upper, low density, fine-grained, part of the flow.

The top of the channel fills CH1 and CH2 consists of a 1.7- 2 m thick unit of fine-grained, upper division, thin-bedded turbidites. Thin-bedded turbidite units are interpreted to be partial abandonment plugs. High-density turbidity currents were diverted away from this area and only low-density turbidity currents, possibly overspilling from some active laterally adjacent channel system, flow through the area during the temporary abandonment of the channel system. These abandonment plugs are considered partial because they left a little unfilled space. The unfilled space created a topographic low, which attracted the next channel to follow, at least locally, the same channel course (Figure 3.10). CH3 is overlain by medium-bedded structureless sandstones, which thin laterally (to the south) and vertically into thin-bedded turbidites (F1). This unit is interpreted to, at least locally, be a full abandonment plug. Turbidity currents overspilling from active, laterally adjacent channel systems completely filled CH3 and as a result subsequent flow had no reason to return to this area.

The three channel fills (CH1, CH2 and CH3) are interpreted to intersect the outcrop at different angles. CH1 is interpreted to intersect the outcrop at an oblique angle to paleoflow whereas CH2 and CH3 are interpreted to intersect the outcrop almost perpendicular to paleoflow. In CH2 and CH3, LADs are observed to dip down towards the base of the channel whereas in CH1 the oblique angle prevents this observation (Figure 3.24)

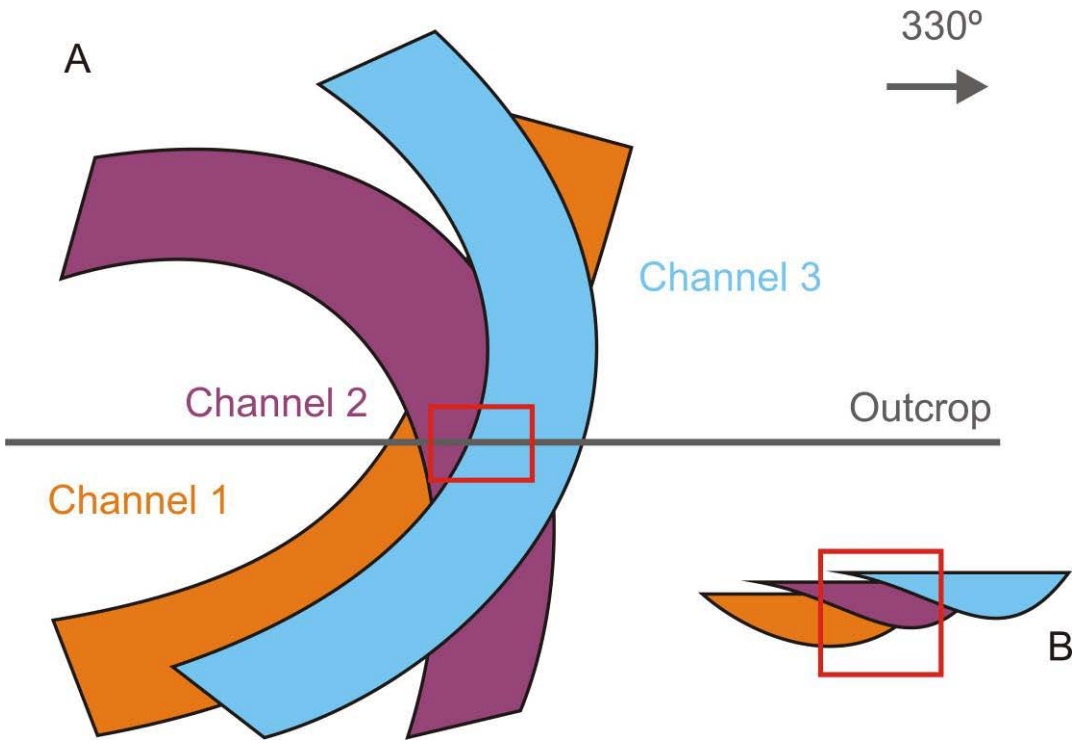

Figure 3.24: Schematic of channel stacking pattern and orientation with respect to outcrop surface (A) planform view (B) cross-sectional view. The red box outlines the outcrop extent.

3.4: Submarine levee deposits

Sinuous channels are commonly flanked by levees: wedge-shaped features with positive relief along the margins of channels (McHugh and Ryan, 2000) (Figure 3.25) that make up a significant part of the deep-marine sedimentary record (e.g. Prior et al., 1983; Damuth et al., 1988; Pirmez, 1994; Hiscott et al., 1997; Beaubouef, 2004; Navarro et al., 2007; Khan et al., in press) and form important hydrocarbon reservoirs (e.g. Tahoe and Ram/Powell fields in northern Gulf of Mexico; Clemenceau et al., 2000; Kendrick, 2000). In seismic images, submarine levees have a similar planform geometry (meander wavelength, radius of curvature and bend amplitude) to fluvial levees and as a consequence have been used as analogues for deep-marine sinuous channel migration and evolution (e.g. Leopold and Wolman, 1960; Hay et al., 1983; Clark et al., 1992; Pirmez, 1994, Hiscott et al., 1997). Recent outcrop studies, however, have identified many important differences in channel migration and evolution between fluvial and deep-marine systems. Although the systems may have similar morphologies, their scales and

internal geometries are different. Further, fluvial and deep-marine channels evolve very differently, which in part most probably relates to differences in the primary mode of sediment transport by their formative flows (e.g. Arnott, 2007). In rivers, bedload transport dominates (Deitrich and Whiting, 1989) whereas in a depositional turbidity current suspension deposition dominates (Das et al., 2004). Nevertheless, submarine levees, like fluvial levees, form when part of the flow escapes the channel and deposits sediment along the channel margin building topographic relief and increasing channel confinement (e.g. Hiscott et al., 1997).

Much of our current understanding of submarine levee morphology comes from high resolution seismic images of modern systems (e.g. Damuth and Flood, 1985; Posamentier and Kolla, 2003; Davies and Posamentier, 2005). On seismic images, levees tend to be characterized by shallowly dipping, low-amplitude continuous to discontinuous reflectors (Posamentier and Walker, 2006). Proximal to distal seismic sections of levees oriented perpendicular to channel flow exhibit a concave-up profile, commonly referred to as "gull-wing" shaped, in which levee height decays with distance from the channel (Birman et al., 2009). Levees are highly asymmetric, especially along channel meanders where the outer bend levee tends to be higher and to have a steeper slope compared to their inner bend counterpart (Posamentier, 2003; Posamentier and Kolla, 2003; Deptuck et al., 2003; Straub et al., 2008) (Figure 3.25B). Outer bend levees can be over 500 m thick at their crest and then thin laterally to less than 100 m over distances of about 10 km. The steepest segment of the levee profile is commonly 1 to 5° (Pirmez, 1994; Piper and Normark, 2001, Deptuck et al., 2003).

Two formative mechanisms have been proposed for the development of submarine levee morphology: the dipping reflectors model (Clemenceau et al., 2000; Straub and Mohrig, 2006) and the horizontal beds model (Khan et al., in press). The dipping reflectors model is based on seismic image interpretation, wherein dipping reflectors are thought to faithfully mimic the internal stratal geometry of the levee. In this model, individual beds in the proximal levee dip more steeply than their distal levee counterparts. Further, older strata dip less steeply than younger strata (Clemenceau et al., 2000; Straub and Mohrig, 2008) (Figure 3.26). The second model, the horizontal beds model, is based on outcrop data. Lateral bed-by-bed correlations over 100's of meters in

the Isaac Formation (Khan et al, in press) and published photos in the Karoo Basin (Grecula et al., 2003), Cerro Torro Formation (Beaubouef, 2004) and Rosario Formation (Kane et al., 2007) show that levee strata have no visible or measurable change in dip away from the proximal to the distal levee. Khan et al. (in press) suggest that dipping reflections on seismic may in fact reflect a lateral change lithology (i.e. lateral facies change) rather than the physical inclination of the composite strata (Figure 3.27).

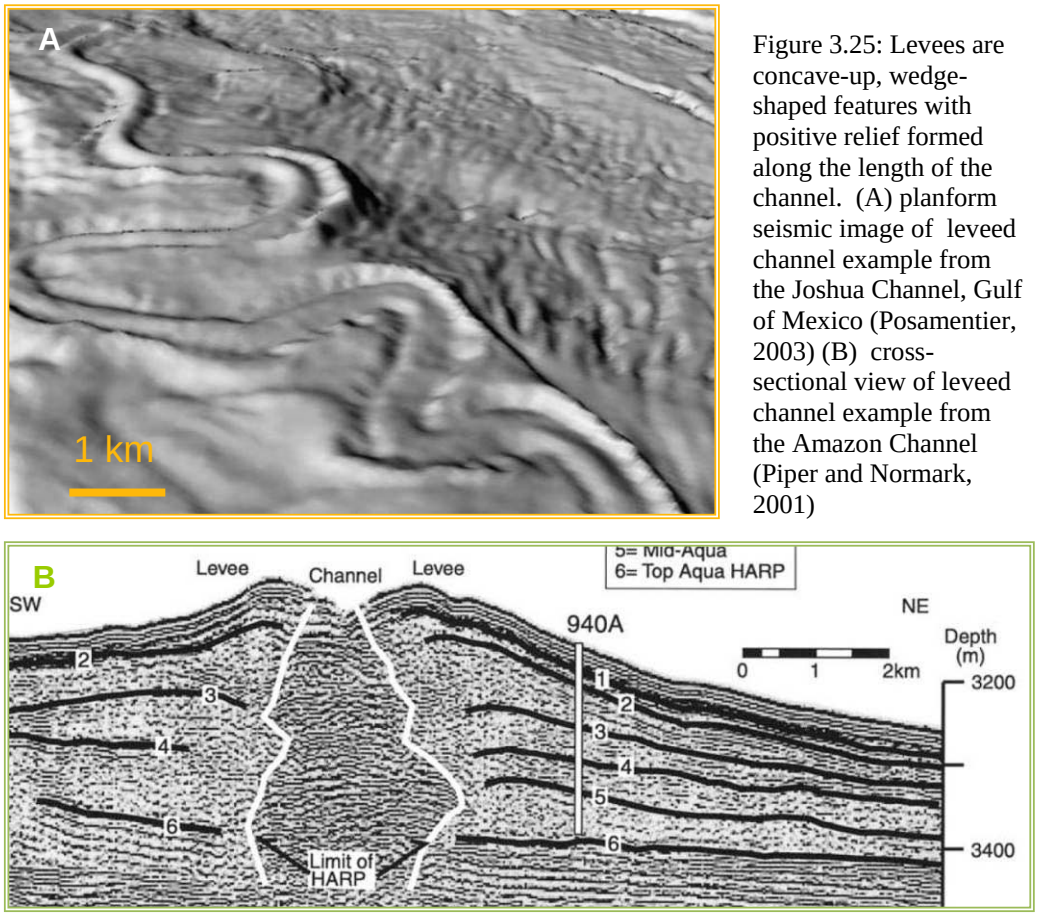

Figure 3.25: Levees are concave-up, wedge-shaped features with positive relief formed along the length of the channel. (A) planform seismic image of leveed channel example from the Joshua Channel, Gulf of Mexico (Posamentier, 2003) (B) cross-sectional view of leveed channel example from the Amazon Channel (Piper and Normark, 2001)

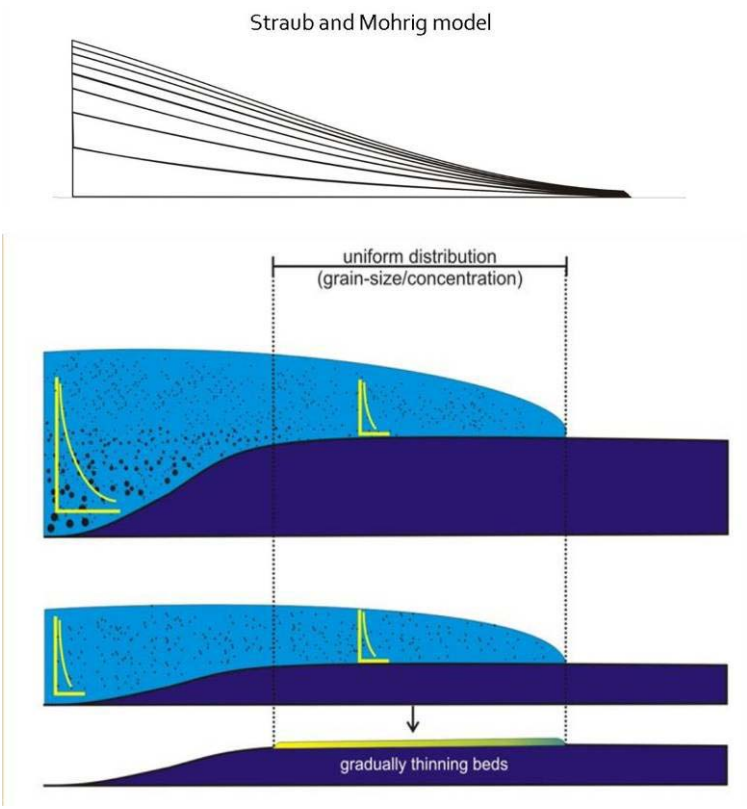

Figure 3.26: Straub and Morhrig model (2008) of levee development. Beds thin away from the channel axis. From Khan et al. (in press).

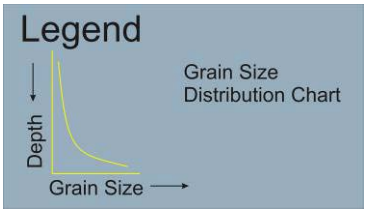

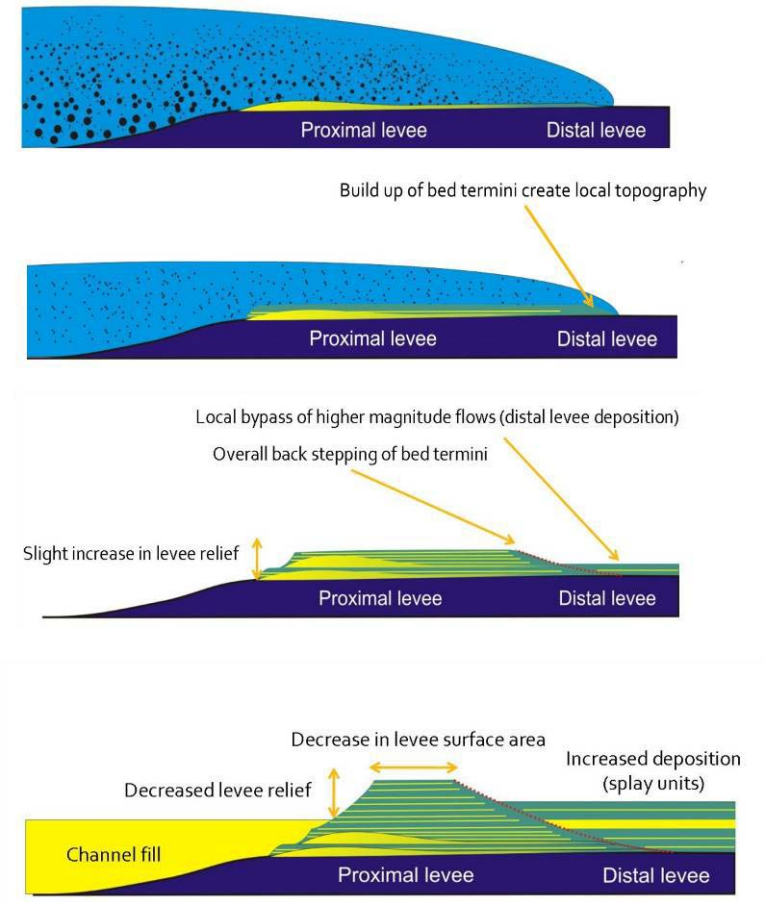

Figure 3.27: Horizontal beds model. Beds are deposited horizontally and levee relief is the result of progressively reduced distance of flow "run-out" away from the channel (from Khan et al., in press).

Irrespective of origin, levees form when flows overspill the channel and deposit sediment in the interchannel area (Figure 3.28). Overbanking processes are enhanced in deep-marine systems compared to fluvial systems because of the reduced density contrast between the associated fluids (Imran et al., 1999; Kolla et al., 2001). In fluvial systems, the large density contrast between the flow (water) and surrounding fluid (air) is so great that flow escaping the channel is limited greatly both vertically and laterally. In submarine systems, on the other hand, the density contrast is significantly smaller, thereby allowing water flow to thicken appreciably and the sediment-laden flow to expand. Overbanking, therefore, is significantly more common and better manifest in the sedimentary record of submarine systems than their fluvial counterpart extending up to 30 km from the channel margin (Pirmez et al., 2000).

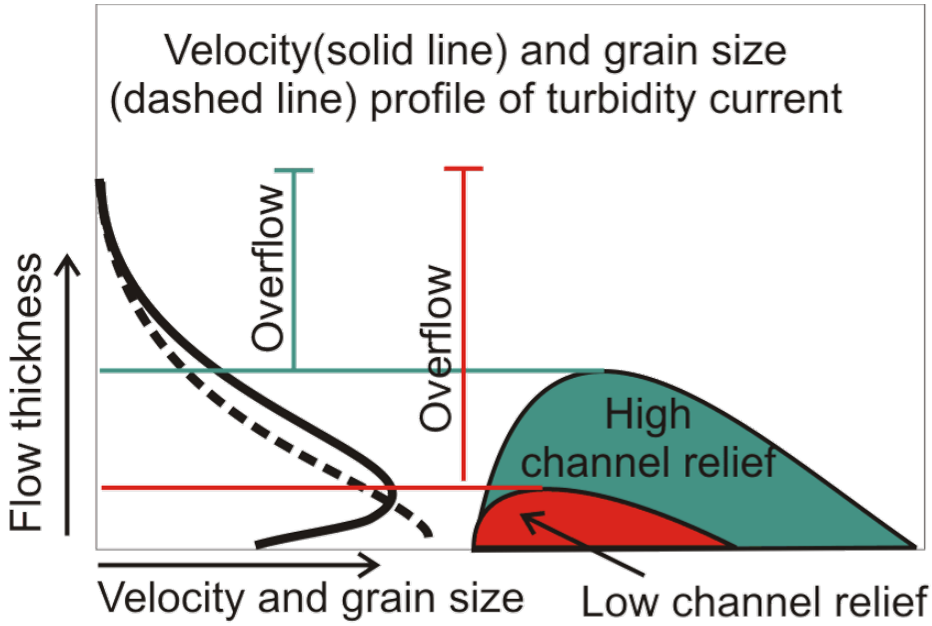

Figure 3.28: Schematic diagram illustrating potential channel overbank from Khan (unpublished).

There are three main types of overbanking processes: overspill (Clark and Pickering, 1996; Hiscott et al., 1997), flow stripping (Piper and Normark, 1983) and inertial overspill (Hay, 1987). Overspill occurs where an over-fit flow is thicker than the associated channel is deep. The finer-grained, more dilute, upper part of the flow spills out of the channel and deposits simultaneously along both sides of the channel. Flow stripping, on the other hand, occurs preferentially on the outer bends of sinuous channels.

In flow stripping, the upper part of flow becomes detached from the main through-going flow while the coarse-grained, denser, lower part of the flow remains confined to the channel. The detached upper part of the flow continues along a straight-line trajectory through the channel bend while the lower part follows the conduit through the channel bend. Flow stripping is commonly enhanced by superelevation, or the tilting of surface of the flow towards the inner bank— condition which is especially enhanced in subaqueous settings (Imran et al., 1999; Kolla et al., 2001; Straub et al., 2008). Inertial overspill, like flow stripping, occurs preferentially on the outer bend, however, as the flow moves through the channel bend, superelevation and the kinetic energy of coarse sediment carried in the lower part of the flow, enables the particles to ride up and spill over the outer bank (Straub et al., 2008).

3.5: Outer bend distal levee deposits

The external depositional geometry of levees is typically described as wedge or "gull-wing" shaped, tapering away from the channel axis. In deep-marine systems, levee deposits are characteristically highly asymmetric, especially along channel bends (Posamentier, 2003; Posamentier and Kolla, 2003; Deptuck et al., 2003). Outer bend levees are typically higher and coarser than their inner bend counterpart because the processes of overspill, flow stripping and inertial overspill (see levee introduction) are enhanced along the outer bend encouraging the flow to escape the channel. As a consequence the flow expands and loses transport efficiency resulting in high sedimentation rates.

In the study area distal outer bend levee deposits are well exposed, and two end-member kinds are recognized: fine-grained and coarse-grained deposits (Figure 3.29). Coarse-grained end-members are further subdivided into overbank and crevasse splays.

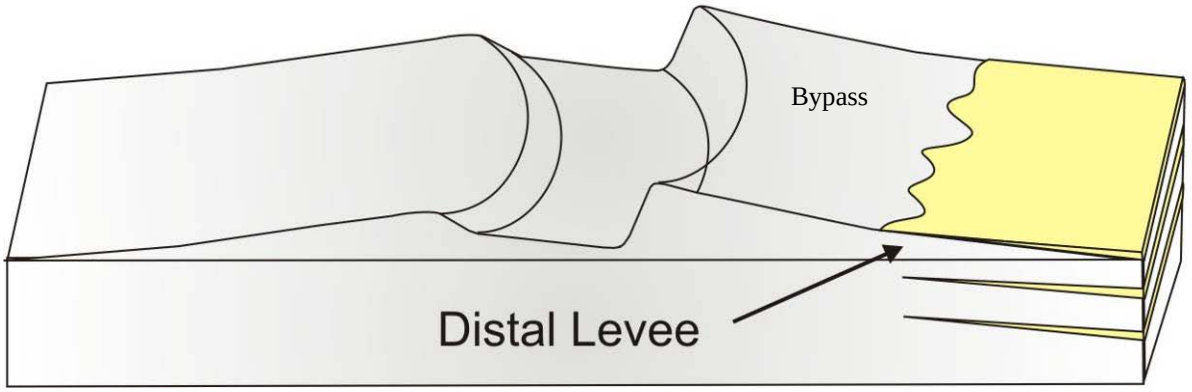

Figure 3.29: Schematic diagram showing deposition in the distal levee of fine-grained (grey) and coarse-grained (yellow) distal levee deposits.

3.5.1: Fine-grained outer bend distal levee deposits

Fine-grained units are composed primarily of very thin- to thin-bedded turbidites (F1) 1-10 cm thick. Strata consist of well-graded, Tcd turbidites locally interbedded with medium-bedded Tcd or Tbcd turbidites that show negligible change in thickness or facies laterally (Figure 3.30; 3.31). Grain size typically ranges from fine sand to mud, although, planar laminated divisions (Tb) can be composed of medium sand. Cross-stratified divisions (Tc) contain multiple (1-4), non-climbing ripple sets (Figure 3.31). In the uppermost part of Tc divisions, individual ripple foresets are commonly interlaminated with darker coloured, very fine-grained sand or silt drapes (Figure 3.32). Laterally discontinuous (starved) single ripple trains occur in some thinner, <5cm thick, Tcd beds. Td divisions consist of unlaminated to faintly parallel laminated silt or mud and range from 2 to 10 cm thick. The thickest Td divisions commonly overlie the thinnest Tc divisions. Where present, laminae consist of light grey coarse siltstone or very fine-grained sandstone and dark gray fine siltstone. Individual laminae are < 2 mm thick. Beds are tabular and laterally continuous with sharp, planar and non-erosive basal contacts. Basal contacts are locally loaded and flame structures up to 7 cm long are common.

Figure 3.30: Tabular, laterally extensive sharp based thin- to medium-bedded turbidites.

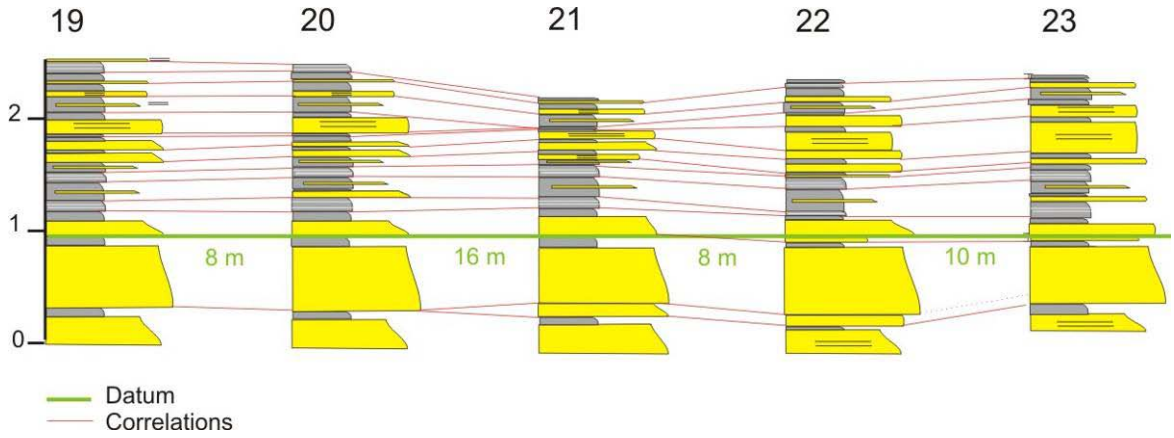

Figure 3.31: Stratigraphic correlation through tabular thin-bedded turbidites. Stratigraphic column locations on Figure 1.17b.

Figure 3.32: Multiple ripple sets in thin-bedded Tcd turbidites.

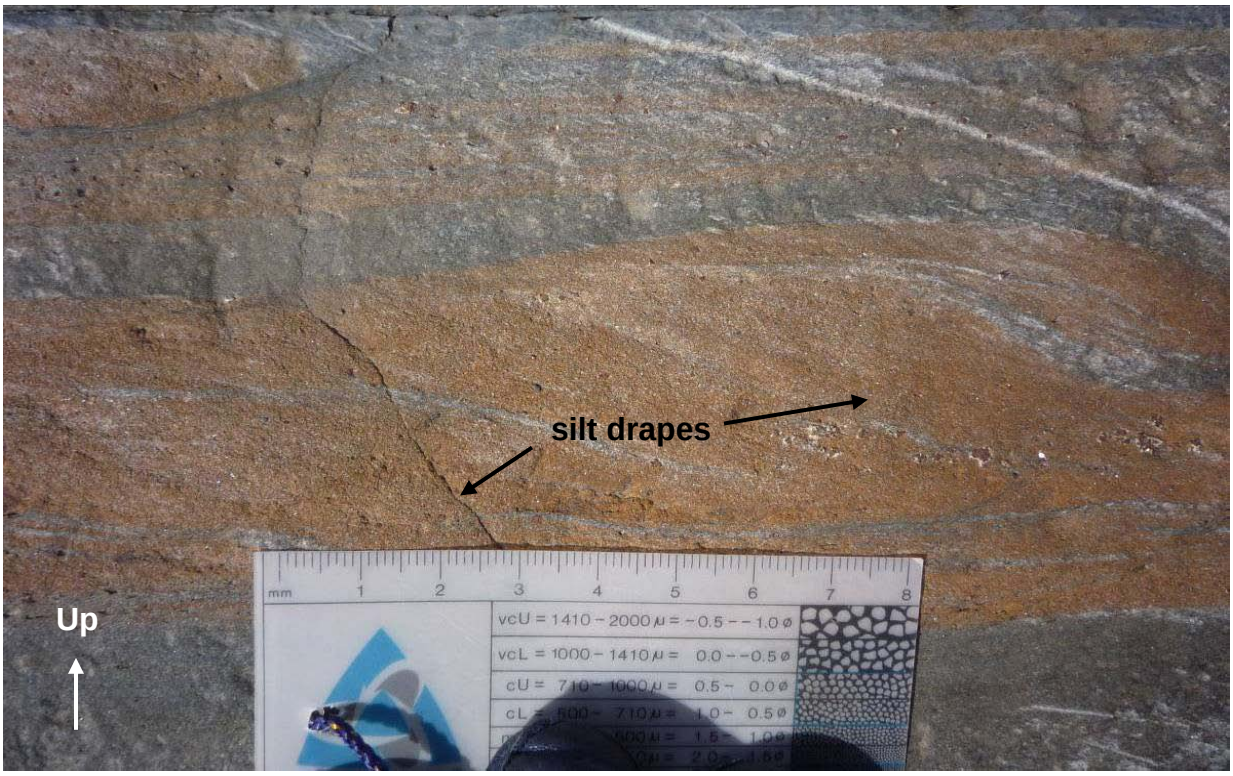

Figure 3.33: Silt drapes on ripple fore sets.

3.5.2: Fine-grained outer bend distal levee deposits interpretation

Very thin- to thin-bedded turbidites were deposited by quasi-steady, although episodic, non-erosive, low- to moderate- concentration, depletive turbidity currents through a combination of flow overspill and flow stripping (see 3.4) of the finer-grained, upper, more dilute part of the flow. The coarser-grained, lower, denser part of the flow remained confined to the channel. The reduced density contrast between turbid water and ambient (clear) sea water (Imran et al., 1999; Kolla et al., 2001) facilitates vertical flow expansion and increases the probability that a flow will exceed the depth of the associated channel. Upon escaping the confines of the channel, the flow expands but then accelerates down the high angle proximal levee slope. Subsequently, the flow slows and becomes depositional over the reduced slope of the distal levee. Through competence-driven deposition, the flow deposits an upward fining succession of ripple cross-laminated fine-sand overlain by silt.

Climbing ripple cross-stratification, convolute lamination and mud rip-up clasts (commonly termed "CCC" turbidites) are features commonly reported from ancient levee deposits (e.g. King et al., 1994; Lyons, 1994; Coleman, 2000; Cronin et al., 2000; Hickson and Lowe, 2002; Eschard et al., 2003; Grecula et al., 2003; Beaubouef, 2004; Posamentier and Walker, 2006), and are taken to be diagnostic of submarine levee deposits (Walker, 1985) (Figure 3.34). It is assumed that flows overspilling into the interchannel area will experience high sediment fallout rates (Walker, 1985). If sediment fallout rates exceed bedload transport in the ripple stability field, ripples will climb (Allen, 1982). Further, rapid deposition of sediment traps pore fluid and creates instabilities that deform primary sedimentary structures. Oddly, climbing ripples and convolute lamination are rarely observed here. The general lack of climbing ripples and convolute lamination may suggest that instantaneous deposition rates were never sufficiently high, which in turn was the result of a mixed grain-size sediment supply. Examples of climbing ripples from the literature typically occur in well sorted, fine- and very fine-grained sand (Posamentier and Walker, 2006) whereas non-climbing ripples in Castle Creek are observed in beds that grade upward from fine-grained sand to silt. Where well sorted turbidity currents become depositional, capacity-driven deposition

dominates, sediment fall out rates are high and climbing ripples easily form. However, where a range of grain sizes are present, competence-driven deposition dominates, instantaneous rates of sediment fallout are reduced and imperceptible angles of climb result (Khan, in press).

Walker (1985) also suggested that thin-bedded turbidites that lack "CCC" turbidites, indicate deposition within basin-plain settings. However, the thin-bedded turbidites described here are interpreted to be distal levee deposits associated with base-of-slope channel levee complexes (Arnott, 2007; Ross and Arnott, 2007).

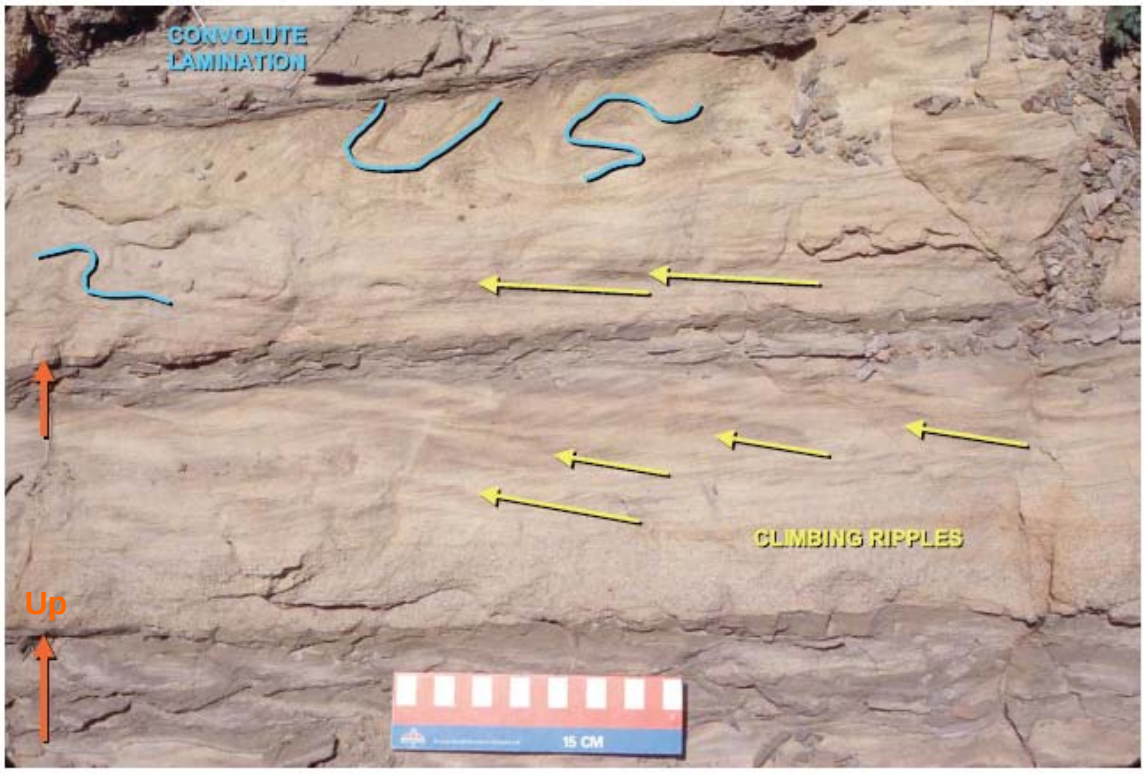

Figure 3.34: Example of thin-bedded "CCC" turbidites in the Chatsworth Sandstone (Cretaceous), Chatsworth (Simi Hills), California (from Posamentier and Walker, 2006). "CCC" turbidites consist of climbing ripples (yellow arrows), convolute lamination (outlined in blue) and mudstone clasts (absent).

3.6: Overbank Splays

Overbank splays are sand-rich lobate or tongue-shaped sediment wedges that preferentially develop on the outer bends of sinuous leveed-channels (Posamentier, 2003). Mohrig and Buttles (2007) suggest that overbanking is common in the deep-marine and plays an important role in submarine channel development. Flow overbanking is enhanced by flow stripping along outer channel bends. Based on seismic examples from the literature, overbank splays typically have areal extents of 100's of m^2 (e.g. Postmentier and Kolla, 2003). Two end members of overbank splays are recognized: isolated beds and multiple bed complexes.

3.6.1: Isolated overbank splays

Isolated beds occur as single thick- to very thickly-bedded (40-200 cm) sandstone turbidites (F2a) encased in distal levee deposits. Within the 75 m thick study area, eight randomly distributed isolated beds are recognized. Isolated beds consist of well sorted, medium-grained Tbcd or Tbd turbidites. Typically the planar laminated division is ungraded and anomalously thick, comprising 75-90% of the bed. Planar lamination is occasionally capped by a single ripple set (Figure 3.35). Isolated beds have a low (10% or less) detrital mud matrix content. Beds have a tabular geometry and basal surfaces are sharp, planar and non-erosive. Lateral thinning and facies changes are rare.

Of the eight isolated beds, three contain carbonaceous mudstone laminae (F5b) (see chapter 2.6 for a complete description). Carbon-rich laminae, 0.1-2 cm thick, are observed within the planar laminated division of medium-grained, thick-bedded Tbcd or Tbd turbidites. Organic carbon becomes more abundant in the upper third of the bed. Interlaminations are typically discontinuous, straight to undulatory and orientated parallel or subparallel to bedding.

Figure 3.35: Isolated beds are thick-bedded, planar-laminated, medium-grained turbidites (F2b). Isolated beds are typically separated by thin- to medium-bedded Tbcd or Tcd turbidites (F1). Pink coloured strata are sandstones and the grey coloured strata are mudstones. Note sharp, non-erosive bed bases.

3.6.2: Isolated overbank splays lateral trends

Isolated overbank splays typically show no lateral facies changes or thickness variations across the study area, however, one example of an isolated overbank splay element, which crops out at the base of the study area, thickens then thins significantly. Subsequent flows deposited thin- to medium-bedded turbidites which heal the topography created by the isolated bed (Figure 3.36; 3.37). The base of the bed is erosive with local scours 50-150 cm long and 2-20 cm deep. The bed is a 2 m thick turbidite (F2a) with carbonaceous mudstone laminae (F5b). In the southeastern part of the exposure the bed is 180 cm thick with common basal scours (Section 5) and then thickens to 200 cm thick over a distance of 50 m (Section 1), and then thins to 104 cm thick over the next 150 m. The northwest thinning trend is accompanied by a lateral facies change. In the southeast, the bed is composed of a 20 cm thick structureless coarse-grained sandstone with dispersed granules overlain by a 173 cm thick planar laminated medium-grained sandstone, a 5 cm thick, fine-grained, single ripple set, and a 2 cm thick massive siltstone. This is the only isolated overbank splay in the study area with a structureless sandstone (Ta) division. Laterally, the bed then consists of a 52 cm thick planar laminated medium-grained sandstone overlain by a 50 cm thick wavy laminated fine-grained sandstone and a 2 cm thick siltstone. Unlaminated or laminated mudstone clasts are observed locally. Mudstone clasts are less than 5cm long, tabular and angular. Coarser grains and mudstone clasts are more common immediately above scoured basal contacts.

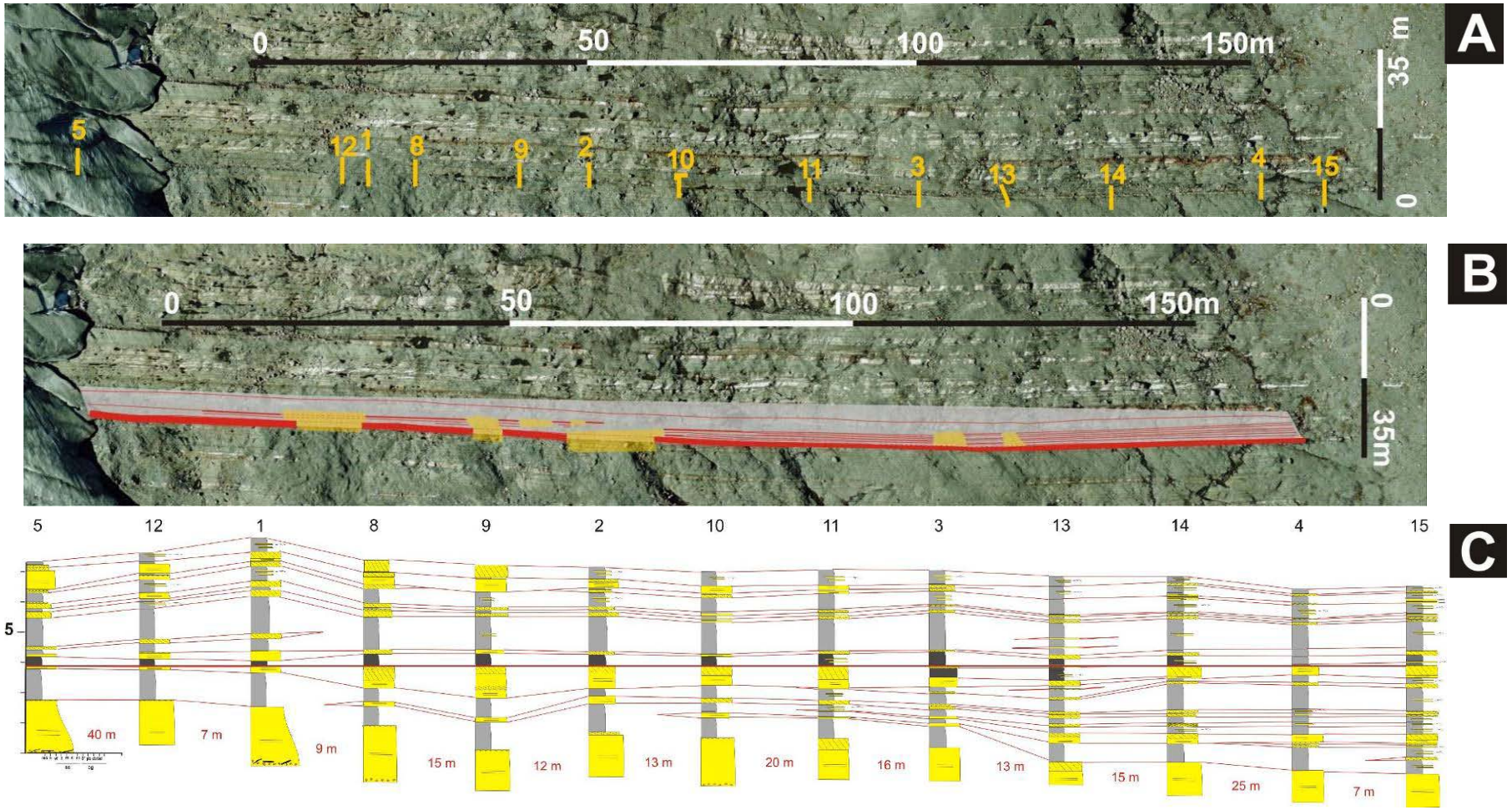

Figure 3.36: Lateral facies transition from thick-bedded Tbcd turbidite to very thin-bedded Td turbidite. (A) Uninterpreted air photo with section line locations. (B) Interpreted air photo. Red lines trace thick-bedded turbidites (F2a). Grey represents thin- to very thinly-bedded turbidites. Orange areas are covered. (C) Bed by bed stratigraphic correlation (correlated beds were "walked out" in the field).

Figure 3.37: Medium-bedded Tbcd turbidite thinning into a very thin-bedded Td turbidites. Bed bases are highlighted with yellow lines.

3.6.3: Isolated overbank splays interpretation

Isolated beds were deposited by non-erosive, low- to moderate-concentration, depletive turbidity currents through a combination of super-elevation, flow stripping, and inertial overspill. In the majority of throughgoing turbidity currents, coarse sediment was confined to the channel; only fine grained sand, silt and clay was able to escape depositing very thin- to medium-bedded turbidites (F1) in the distal levee. Periodically, a more voluminous turbidity current passed through the channel. These larger flows were not as well confined by the channel's levee and medium-grained sand particles were able to overspill onto the interchannel area (Figure 3.38). Upon exiting the channel, these flows bypassed the proximal levee, accelerated down its steep backside slope, and then, on the reduced slope of the distal levee, deposited, under competence-driven conditions, the thick succession of planar laminated, medium-grained sand followed by ripple cross-stratified fine-grained sand.

The general lack of bed amalgamation and erosional features at bed bases suggests that overbanking flows were primarily depositional. Note that flow deceleration was not accompanied by a hydraulic jump like in crevasse splays (see 3.7).

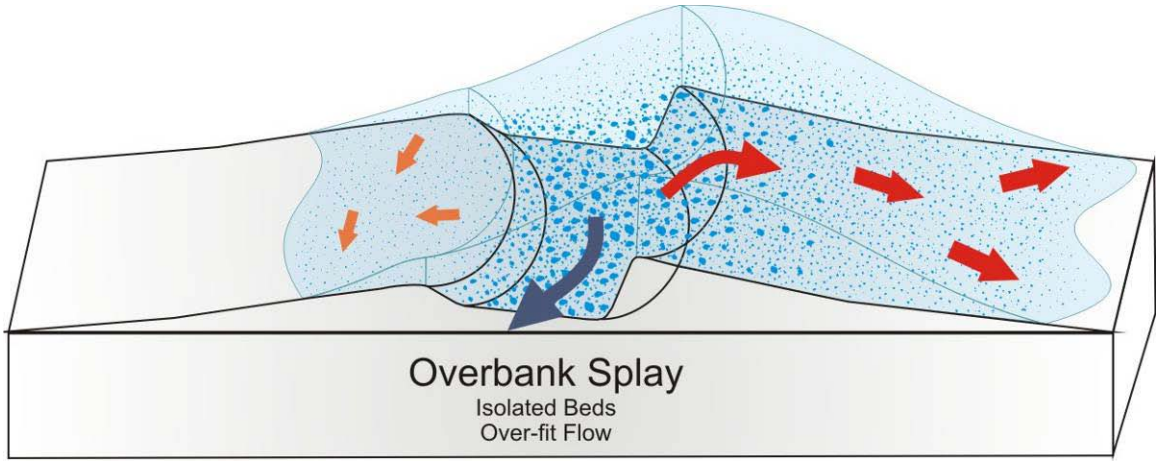

Figure 3.38: Schematic diagram of isolated overbank splay deposition. Isolated beds preferentially develop on the outer bend levee where superelevation and flow stripping are enhanced. Overspilling flow bypass the proximal levee and deposit on the distal levee under competence-driven conditions. The resulting deposits consists of a succession of planar laminated followed by ripple cross-stratified sand. Flow deceleration was not accompanied by a hydraulic jump.

3.6.4: Multiple bed complexes (overbank splays)

Multiple bed complexes were not observed in the study area but do occur in the levee deposits elsewhere at Castle Creek. Multiple bed complexes extend up to 1000 m laterally, and range from 2-4 m thick (Khan, in press) and consist of structureless sandstone (F2b) interbedded with medium- (F1) to thick- (F2a) bedded turbidites (Figure 3.39). All strata have a low (10% or less) detrital mud matrix content. Structureless sandstones (F2b) are normally graded and consist of medium-grained sandstone. Medium- (F1) to thick- (F2a) bedded turbidites are commonly planar laminated Tbcd turbidites. Beds in the uppermost part of these multi-bed complexes are commonly overlain by a single or few set thick ripple cross-stratified layer. Dune cross-stratified beds occur but are uncommon. Beds are typically amalgamated and dispersed mudstone clasts or mud clast horizons occur locally. Although, multiple bed complexes are laterally continuous over several hundreds of metres, their composite beds are laterally discontinuous and cannot be traced for more than 100 m laterally.

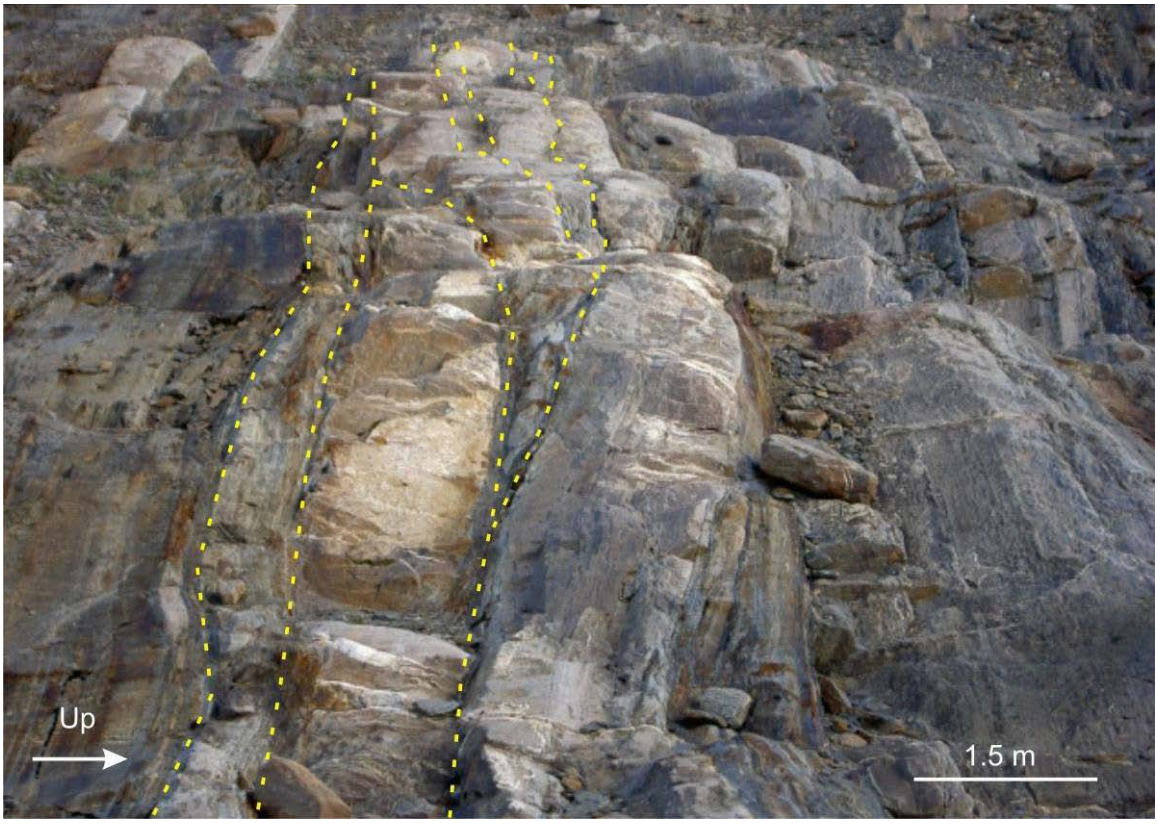

Figure 3.39: Multiple bed complex in between IC4 and IC5 south-side of the glacier Castle Creek, B.C. Individual bed contacts are traced out by dotted yellow lines (Photo by Shann Khan).

3.6.5: Multiple bed complexes (overbank splays) interpretation

Multiple bed complexes, like isolated bed splays, relate to super-elevation, overspill and flow stripping that allowed coarser sediment to escape the channel and increase sedimentation rates over the outer bend levee (Figure 3.40). Unlike isolated bed splays, however, multiple bed complexes were built up by multiple flows that apparently succeeded one another. These flows either correlate with a pulse of anomalously large flows or, more likely, a partial breach in the levee. A partial levee breach would allow coarser sediment, even in an average size flow, to escape the channel. Under these conditions coarser sediment continued to escape until after some number of flows the partial breach healed (infilled), or alternatively, evolved into a full channel-margin breach with an associated avulsion. Irrespective of the eventual outcome, the partial breach allowed coarser sediment carried in the lower part of the channelized flows to regularly escape the confines of the channel. Much of these flows were diverted into the interchannel area where they accelerated down the backside of the proximal levee and then deposited on the more shallow-dipping distal levee. Here they experienced capacity- rather than competence-driven deposition, and emplaced the common graded, structureless beds. Note that flow deceleration was not accompanied by a hydraulic jump like in crevasse splays (3.7). Also, the lack of lateral bed continuity, mudstone interbeds and paucity of traction structures is likely the result of erosion and rapid deposition that infilled topography on the distal levee.

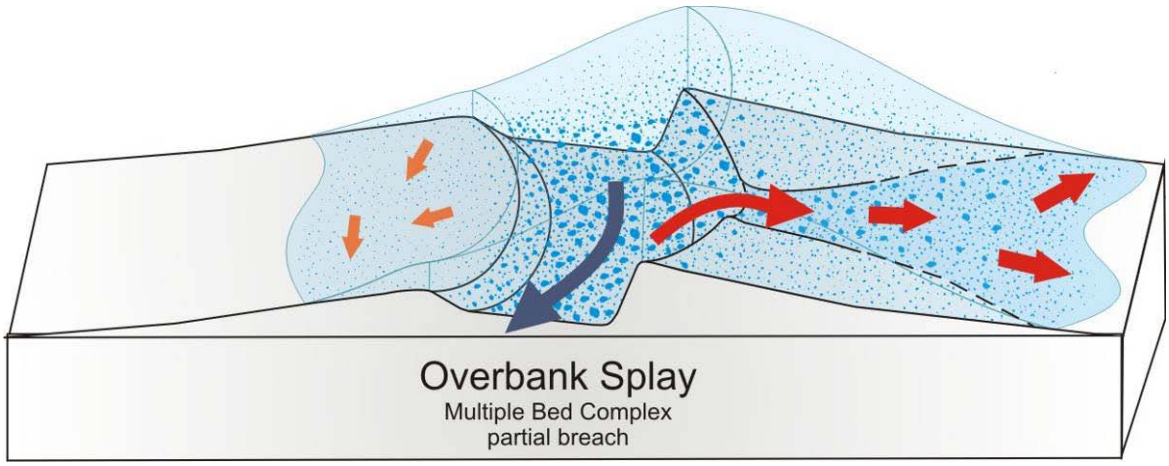

Figure 3.40: Schematic diagram of multiple bed complex development. Multiple bed complexes preferentially develop on outer bend levee where superelevation enhances overspill. A partial breach allows deeper, more coarse-grained parts of the flow to escape the channel. Successive flows bypassed the proximal levee and deposited a multi-bed complex composed of amalgamated structureless sandstone. Deceleration of successive flows was not accompanied by a hydraulic jump.

3.7: Crevasse splays

Crevasse splays are common depositional elements in both fluvial and deep-marine settings (Allen, 1970; Bridge and Jarvis, 1982; Prior et al., 1983; Damuth et al., 1988; Pirmez, 1994; Hiscott et al., 1997; Posamentier, 2003; Deptuck et al., 2003; Beaubouef, 2004; Navarro et al., 2007) and exhibit a characteristic lobate to elongate planform geometry (Figure 3.41). Crevasse splays develop following a major breach in the channel levee that diverts the flow away from the main channel into the interchannel area. Commonly, a short channel will form and leads away from the main channel, feeding a smaller distributary channel network downflow (Posamentier and Kolla, 2003; Van Wagoner et al., 2003; Posamentier and Walker, 2006). Based on seismic examples from the literature, submarine crevasse splays can be large, covering areas of several km² (e.g. Postamentier and Kolla, 2003). Crevasse splays may evolve further into an avulsion channel with the main difference being that a crevasse splay represents a temporary diversion of the main flow whereas an avulsion channel is a permanent diversion resulting in the abandonment of the main channel (Posamentier and Walker, 2006). Two end-member kinds of crevasse splays were recognized: amalgamated and tabular splays.

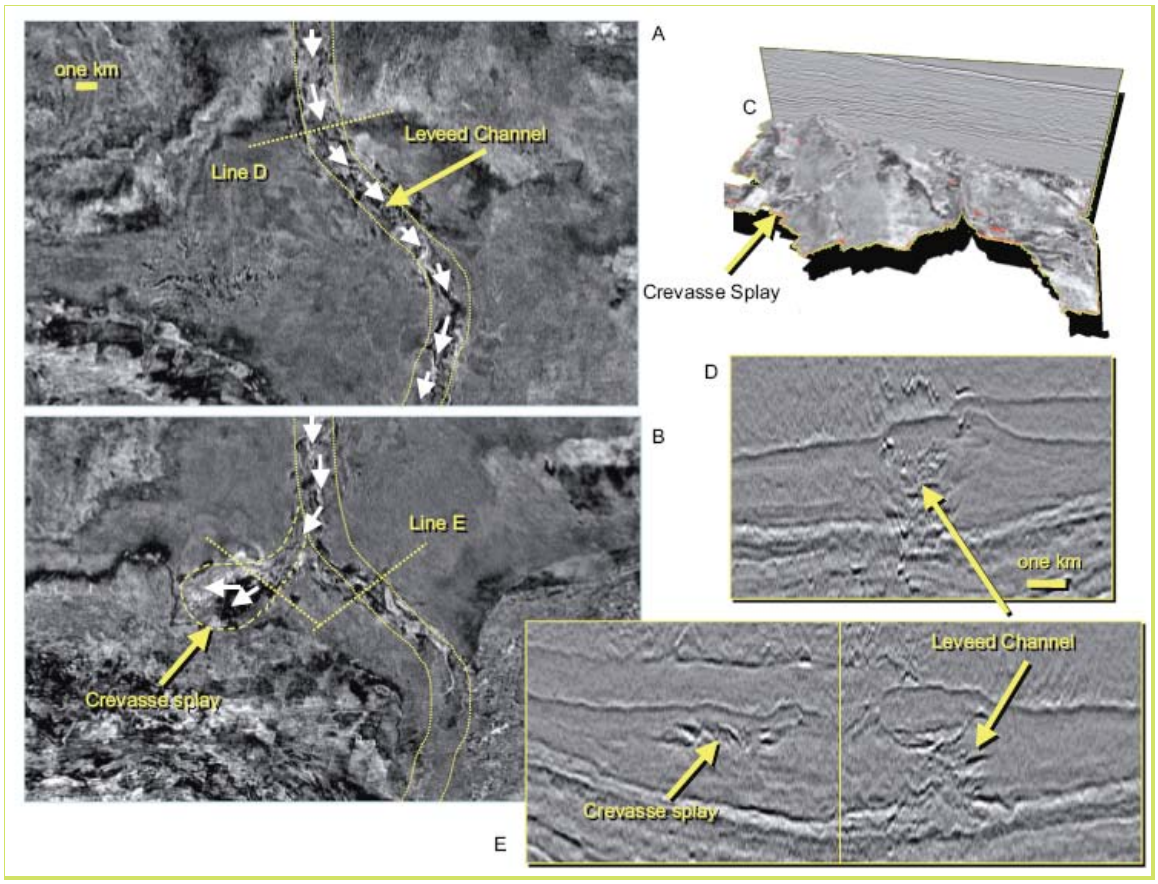

Figure 3.41: Seismic example from the Gulf of Mexico displaying a Pliocene deep-marine leveed-channel and associated crevasse splay deposit. (A) is a deeper time slice and (B) is a shallower time slice. (C) provides a 3D prospective view of the system. (D) is a cross-sectional view of the channel whereas (E) is a cross-sectional view of the crevasse splay. High-amplitude reflectors suggest the presence of sand in the channel and splay deposits (from Posamentier and Walker, 2006).

3.6.1: Amalgamated crevasse splay

Amalgamated crevasse splay deposits consist primarily of structureless sandstone (F3) capped with mudstone (Figure 3.42). Structureless sandstones (F3a) are coarse-grained, poorly sorted and ungraded or coarse-tail graded. Sandstones have a high mud-matrix content that ranges from 30-50%. Beds commonly contain tabular, unlaminated mudstone clasts < 50 cm long, and locally clasts often form breccia layers (F4a). Amalgamated units are approximately 3.5 m thick with beds ranging from 25-100 cm thick. Individual beds are discontinuous and cannot be traced for more than 150 m laterally. Bed bases are sharp and typically deeply scoured (Figure 3.43).

Figure 3.42: Amalgamated crevasse splay deposit. Numbers represent individual beds.

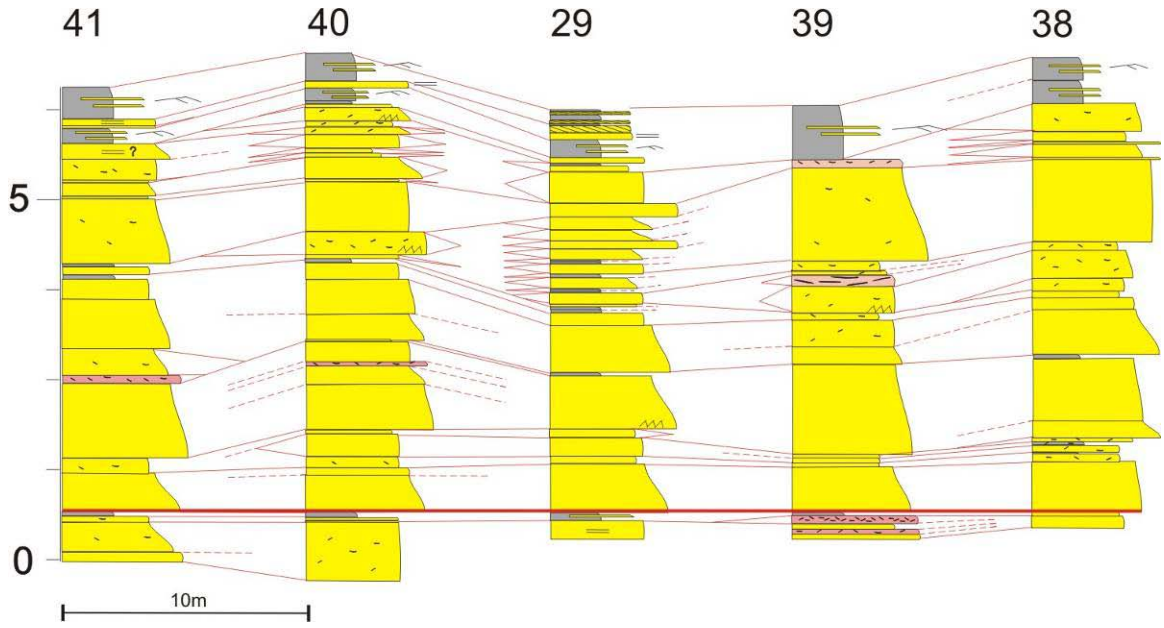

Figure 3.43: Stratigraphic correlation of an amalgamated coarse-tail graded structureless sandstone complex. Note beds are highly amalgamated and basal scour is common. Stratigraphic datum is a thin-bedded turbidite marker (dark red line) See figure 1.19B for stratigraphic column locations.

3.7.2: Amalgamated crevasse splay interpretation

The mud-rich, poorly sorted, coarse-tail graded structureless sandstones (F3) that make up crevasse splay deposits are unlike those (F2b) observed in multiple bed complexes. These differences reflect important differences in flow conditions at the time of deposition. The poorly sorted texture and high-mud content of the coarse-tail graded structureless sandstones (F3) is interpreted to reflect extremely rapid capacity-driven deposition possibly immediately downflow of a plane-wall jet with jump (e.g. Leclair and Arnott, 2003) (Figure 3.44). The jump is interpreted to have formed downflow of a major levee breach, and in the vicinity of an abrupt change in slope where supercritical flow ($Fr > 1$) passed through a hydraulic jump as it transformed quickly to subcritical flow ($Fr < 1$). The breach in the levee allowed most of the thickness of the channelized turbidity currents, including the coarse, basal part of the main flow, to escape the channel and be diverted into the interchannel area. At some downflow break in slope, the now supercritical flow underwent an internal hydraulic jump with attendant intense turbulence generation. Here the bed was deeply scoured but then became draped with a rapidly deposited layer of sediment from the collapsing sediment cloud. Scour into underlying thin-bedded turbidites of the muddy distal levee facies association likely sourced the common mudstone clasts.

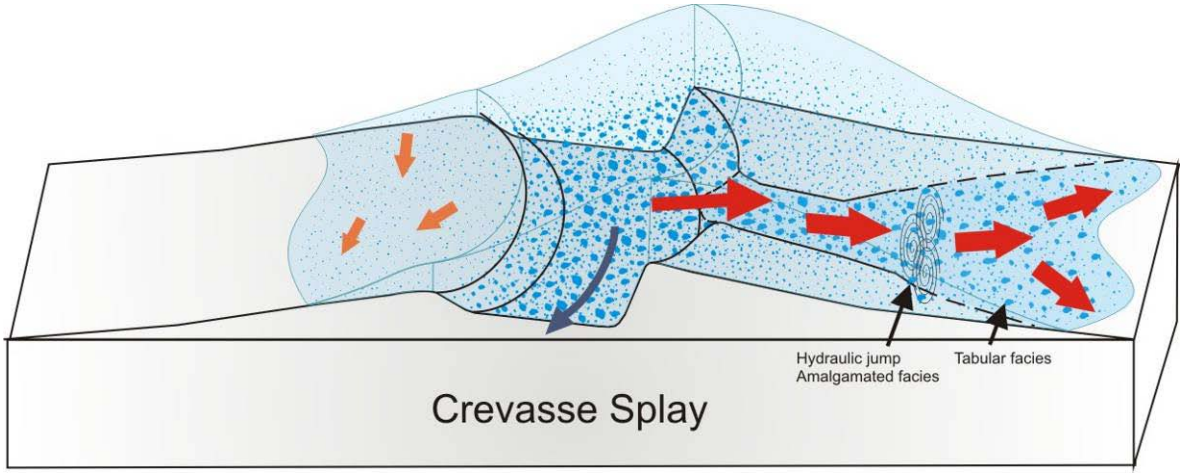

Figure 3.44: Schematic diagram of levee breach and crevasse splay deposits. The coarse, dense, lower part of the flow is able to escape the channel through a breach in the levee. At some downflow break in slope a hydraulic jump forms generating locally intense turbulence. Initially, intense turbulence generation deeply scoured the bed which then was rapidly draped with a layer of sediment from the collapsing sediment cloud (amalgamated crevasse splay). Downflow, turbulence is dampened by high sediment concentration and scour became negligible but sedimentation rate remained high as the dispersion continued to collapse, depositing the matrix-rich, tabular structureless sandstones.

3.7.3: Tabular crevasse splay

Tabular splays are the most common kind of crevasse splay deposit observed in the study area. Like amalgamated crevasse splays, tabular splays consist primarily of structureless sandstone (F3b) capped with mudstone (Figure 3.45). Sandstones are poorly sorted, ungraded or coarse-tail graded and grade upward from coarse- to medium- or fine-grained sand. The mud-matrix content is high, typically composing 30-50% of the bed. Beds commonly contain a small number of large (up to 150cm long) isolated mudstone clasts. Clasts are unlaminated and tabular with rounded edges. Tabular units range from 2-8 m thick and comprise beds 5-125 cm thick. Individual beds are tabular and laterally extensive. Bed bases are sharp, non-erosive (Figure 3.46). Soft sediment deformation features such as flame structures are observed locally.

Figure 3.45: Tabular crevasse splay deposit. Note the sharp non-erosive bed bases and large flame structures (yellow oval). Backpack for scale (Photo by Bill Arnott).

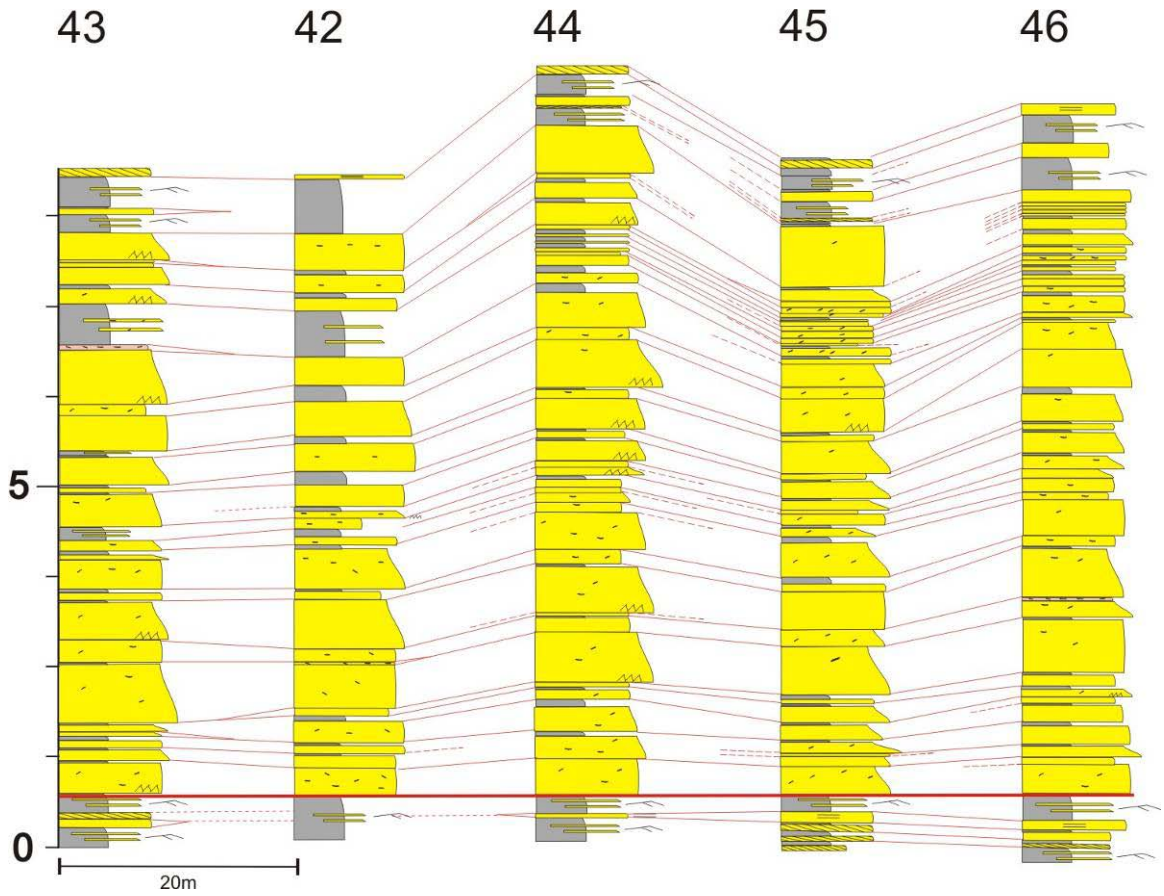

Figure 3.46: Stratigraphic correlation through tabular crevasse splay. Beds consist of coarse-tail graded structureless sandstones. Beds are typically tabular with sharp non-erosive bed bases. Note the abundant mudstone clasts. Datum is the top of succession of thin-bedded turbidites (thick red line).

3.7.4 Tabular crevasse splay interpretation

Tabular crevasse splay deposits consist of structureless sandstones that exhibit a similar suite of sedimentary structures and textures as the structureless sandstones that make up the amalgamated facies association, and as a consequence are interpreted to have been deposited under similar conditions. Tabular crevasse splays are interpreted to be related also to submerged hydraulic jumps, but further downflow of the area where the amalgamated crevasse splay element accumulated. In this more distal area much of the locally-generated turbulence formed in the jump was damped by the high sediment concentration and as a consequence seafloor scour became negligible (Figure 3.44). In addition, sedimentation rate remained high as the dispersion continued to collapse, depositing the matrix-rich, tabular deposits of the tabular crevasse splay element. Mudstone clasts were probably sourced up-dip in the hydraulic jump and transported downflow in the collapsing sediment cloud. A similar trend of amalgamated beds in the more proximal splay grading laterally into less amalgamated strata has been reported also from seismic images (Posamentier and Walker, 2006).

Chapter 4: Discussion

4.1: Introduction

This chapter is sub-divided into two parts: depositional history and depositional model. The first part, depositional history, delineates the vertical stacking pattern of architectural elements described in chapter 3 in order to provide a detailed description of interchannel deposits. The second part integrates seismic, well log and core data from the Amazon Fan with outcrop data from the Windermere System to build a predictive depositional model for splay deposits. The Amazon Fan is chosen as the modern analogue for the Windermere System because it is a well studied system with an extensive published literature, and also is a passive margin system of similar dimension to the Windermere turbidite system in the southern Canadian Cordillera (Ross and Arnott, 2007) (Figure 1.5).

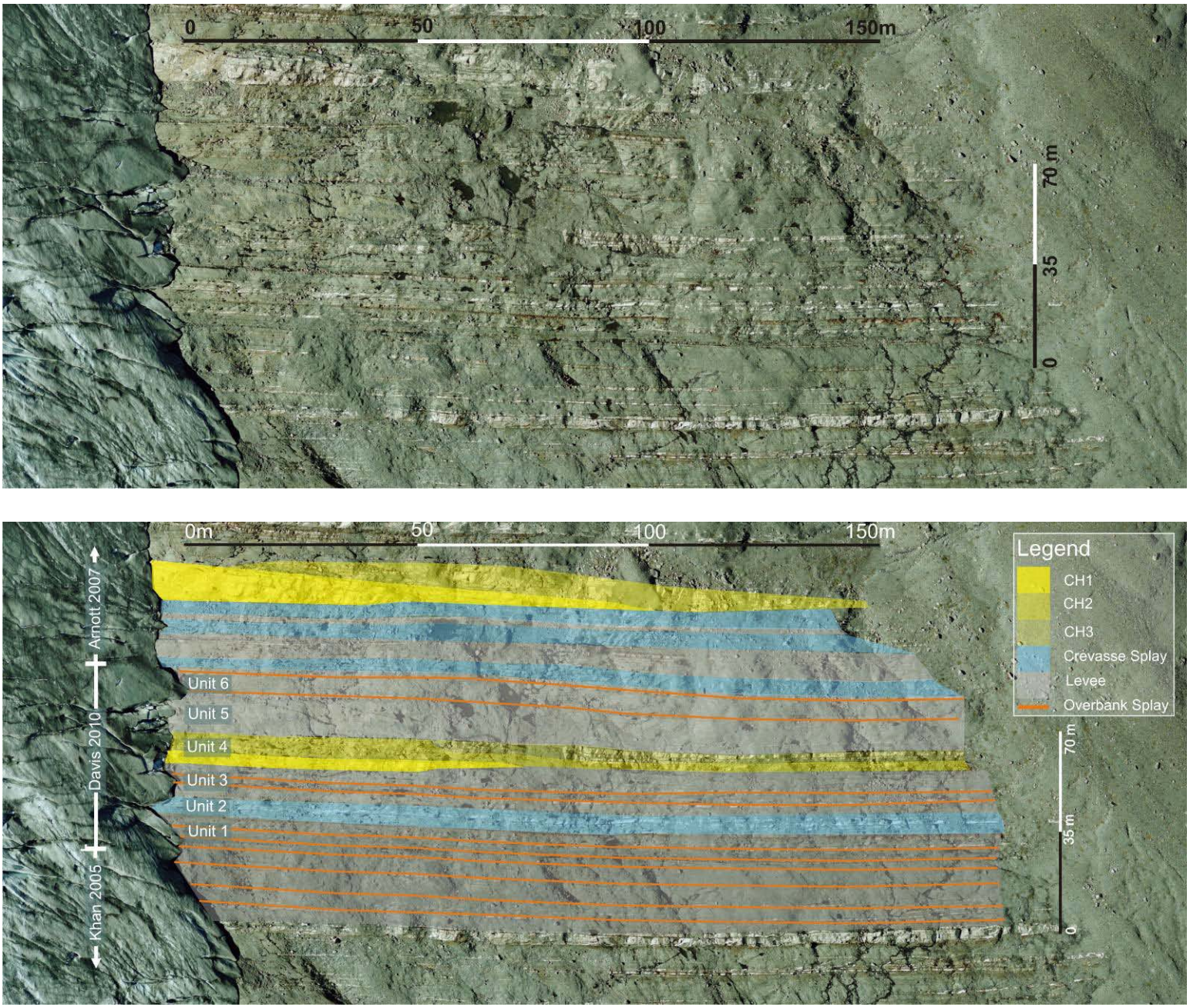

Figure 4.1: Stacking patterns of distal levee, splay and channel deposits in Castle Creek north. (A) uninterpreted (B) interpreted air photo (see text for details) (C) location of stratigraphic columns for (D) stratigraphic correlation.

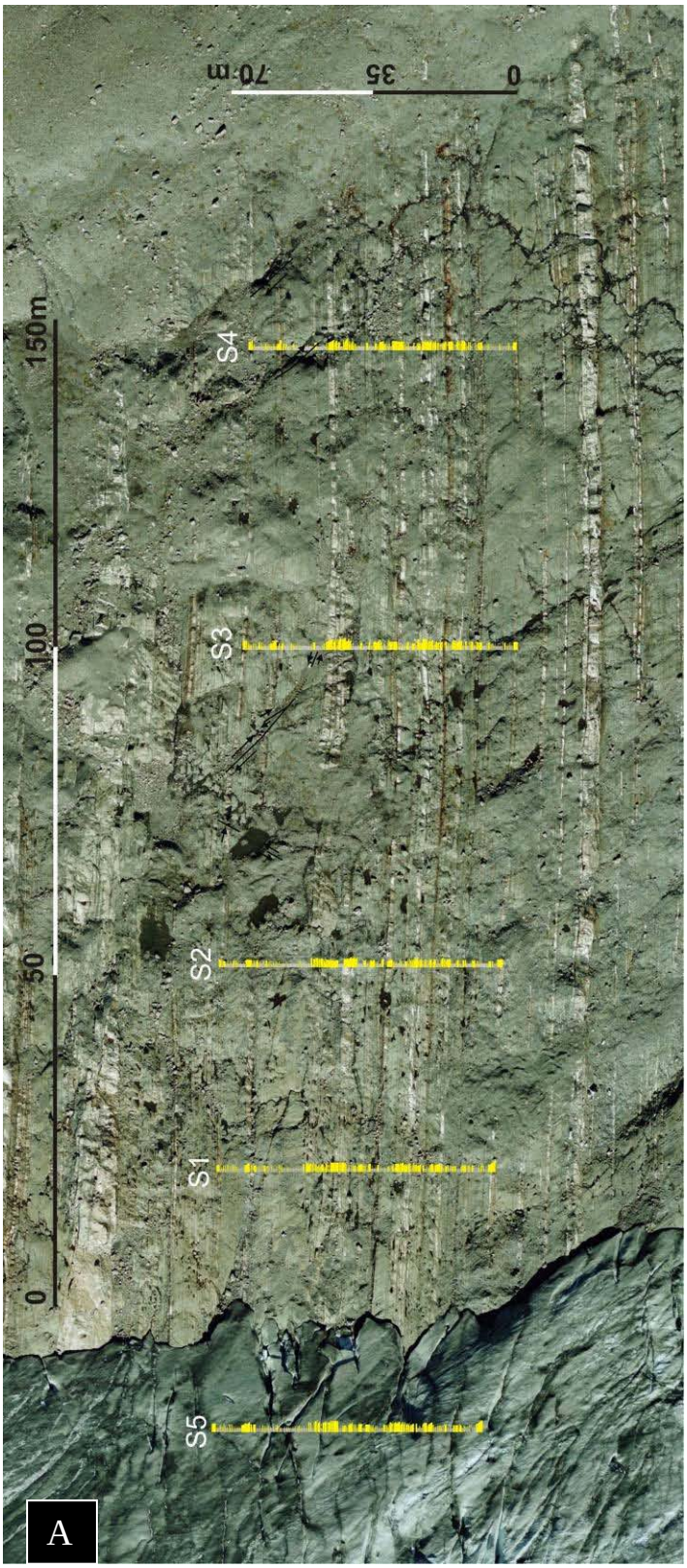

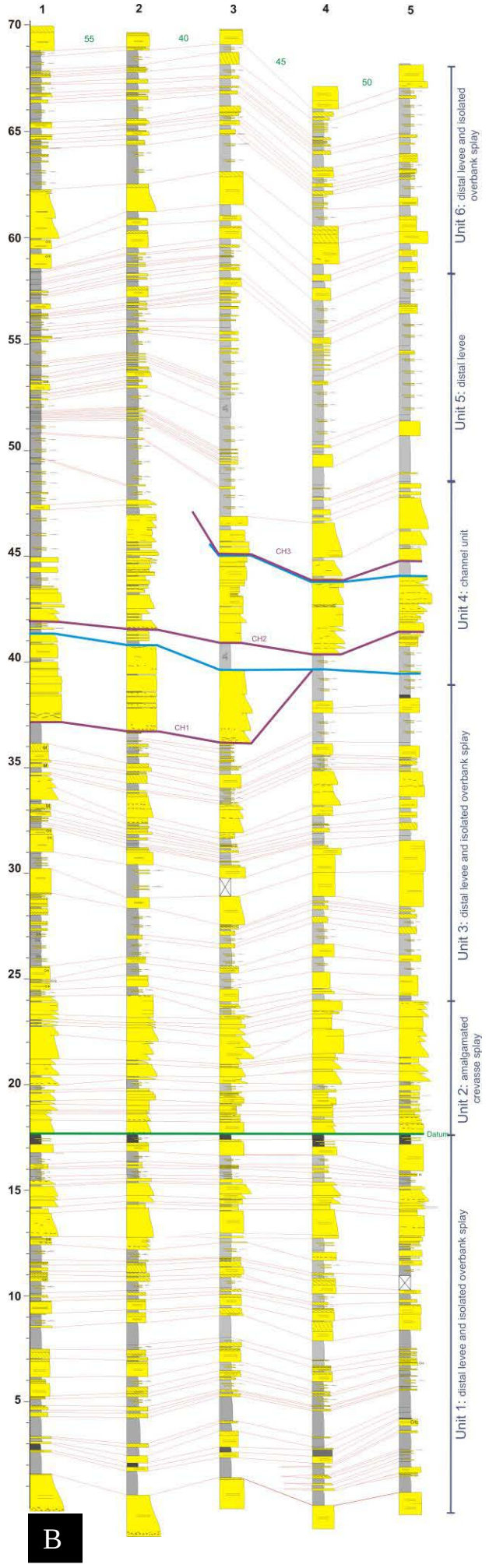

Figure 4.2: (A) Air photo of study area showing section line locations (B) Stratigraphic correlation of architectural elements observed in Castle Creek north. Datum is an organic rich mudstone (F5a).

4.2 Depositional history:

Stratigraphically below the study area is a 100 m thick succession of distal levee and overbank deposits mapped by Khan (2004-2005) (unpublished). The study area described here is approximately 200 m wide and 70 m thick and consists of distal levee, splay and channel deposits (Figure 4.1; 4.2). Immediately above the study area, a 20 m thick levee/overbank unit is overlain by a 25 m thick crevasse splay unit, in turn overlain by a 15 m thick channel unit, and was described previously by Arnott (2007).

At the base of the measured section, Unit 1, is a 21 m thick distal levee succession consisting of thin-bedded, fine-grained turbidites (F1/AE3) separated by thick-bedded, medium-grained isolated overbank splays (AE4.1). Stratigraphically upward thin-bedded, fine-grained turbidites (F1/AE3) become gradually thicker-bedded and coarser-grained with more intercalated medium-bedded, medium-grained (F1) turbidites (Figure 4.3). In addition, isolated overbank splays (AE4.1), basal scour, bed amalgamation and mudstone clasts are more common. The simplest interpretation for these upward changes is a gradual increase in flow volume and velocity. In deeper flows, a thicker part of the turbidity current occurs above the crest of the levee and overspills the channel. These overspilling flows are more sand-rich and voluminous, and hence more energetic. This, in turn, results in the deposition of thicker, coarser deposits with increased scour and bed amalgamation. Increased scour on the levee erodes older mud-rich levee deposits and forms the common mudstone rip-up clasts. The increase in grain size and volume of the overspilling flow may reflect changes in sediment supply from the upslope staging area. These changes are possibly related to a lowering of relative sea-level and/or seminal changes in weathering and/or transport characteristics within the hinterland that increased sediment supply to the deep marine. Alternatively, enhanced overspill may be related to reduced differential channel relief, caused by in-channel deposition that outpaced deposition on the levee crest. The reduced differential channel relief interpretation is more plausible based on the small vertical scale (10's of metres) of the coarsening- and thickening-upward trend. Further, stratal trends in levee deposits are rarely interpreted to be related solely to allocyclic processes, although, many authors do suggest that these processes do play some role (Beaubouef, 2004; Kane, 2007).

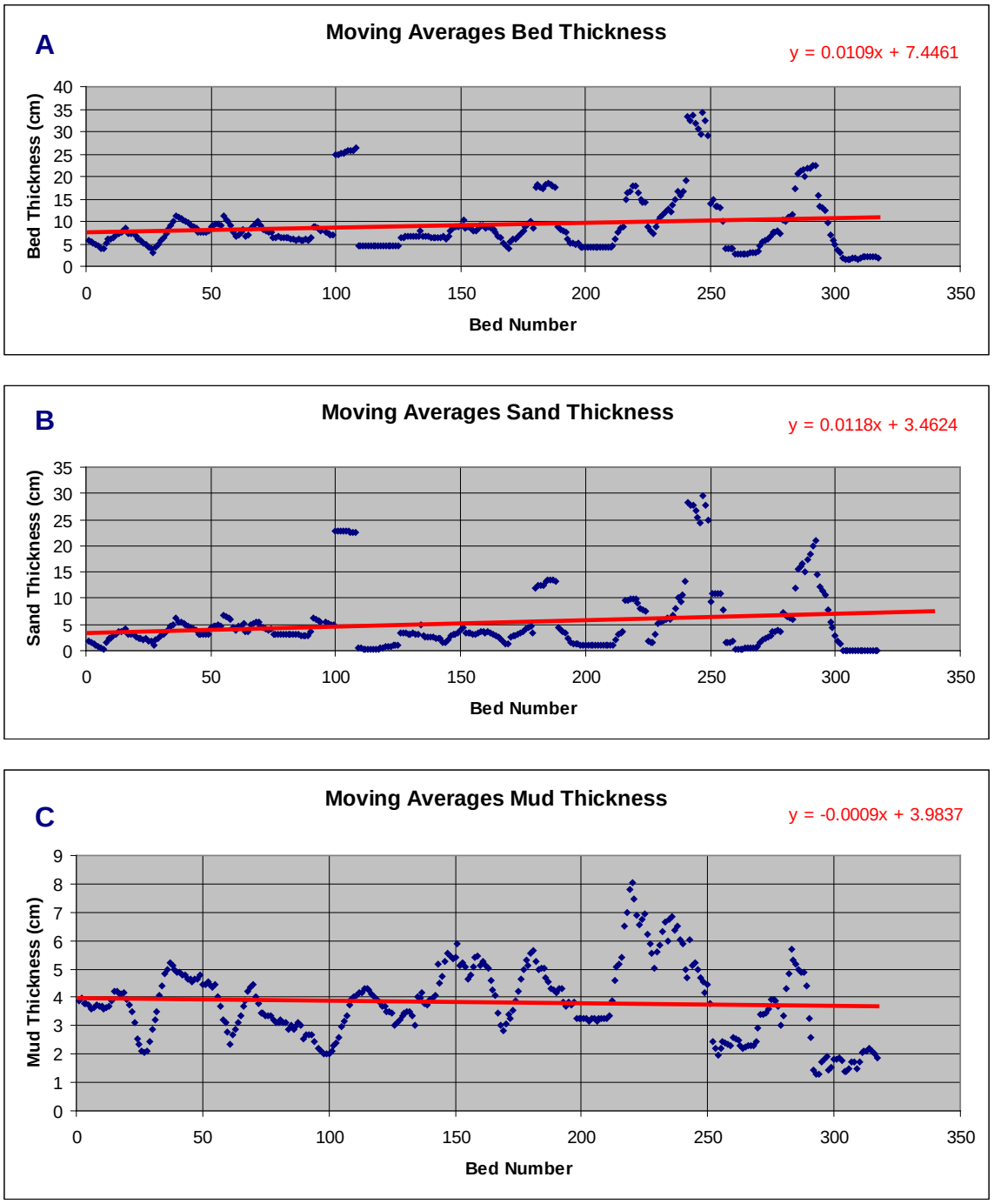

Figure 4.3: Vertical stratigraphic trends in thin-bedded, fine-grained turbidites (F1/AE3) of Unit 1. Regression lines (red) demonstrate general data trends. (A) bed thickness increases stratigraphically upward and peaks are more common stratigraphically upwards (right side of the graph). Peaks are isolated thicker bedded turbidites. (B) Sand thickness also increases stratigraphically upward, whereas (C) mud thickness decreases upward.

Distal levee and isolated overbank splay deposits of Unit 1 are overlain by a 3.5 m thick amalgamated crevasse splay unit (Unit 2) (AE5.1: mud-rich coarse-tail graded structureless sandstones) (Figure 4.4). Crevasse splays generally form downflow of a levee breach that allows a large portion of the flow to be diverted away from the channel. Levees are common sites of gravitational instability and failure. High rates of sedimentation, particularly of typically fine-grained sediment, commonly result in elevated pore pressures that reduce intrinsic shear strength. In addition, other factors including the typically steep slopes of levees, especially along the outer bend channel-margin, and erosion by overspilling flows all serve to promote failure along the levee. Crevasse splays form downflow of a breach in the levee that allows coarser-grained sediment transported in the lower part of the flow to escape the channel. In this case, the associated leveed channel is unexposed. These sand-rich strata are overlain by a thick succession of mud-rich distal levee deposits (Unit 3). The abrupt transition from sand-rich crevasse splay deposits to mud-rich distal levee deposits suggests that the levee breach healed or the channel avulsed and the flow was diverted out of the plane of the outcrop. The distal levee complex consists of very thin- to medium-bedded turbidites (AE3) and thick-bedded isolated overbank splays (AE4.1). It is 16.5 m thick in the northwest and thins to 12.5 m in the southeast due to erosion by an overlying channel complex.

The channel complex (Unit 4) is up to 11 m thick and made up of three laterally-offset-stacked channel fills composed of lateral accretion deposits (LADs). CH1 ranges from 2 to 5 m thick, CH2 ranges from 3 to 7 m thick and CH3 ranges from 2 to 3 m thick. Two end-member kinds of strata were observed and alternate at the top of the channel fill: coarse-grained structureless sandstones (coarse-LADs) and fine-grained, thin-bedded turbidites, (fine-LADs). Coarse LADs consist of 1-4 beds which pinch out at approximately the same stratigraphic horizon near the top of the channel and amalgamate towards the channel base. Interfingered with the coarse LADs are fine LADs consisting of multiple thin-bedded turbidites. Fine LADs are eroded by coarse LADs as they amalgamate in the lower part of the channel fill. Deposition of coarse-grained LADs most probably represents a change in local flow conditions or a change in channel geometry. These changes caused conditions in the local channel system to be out of

equilibrium with the throughgoing turbulent flows and resulted in deposition of coarse-grained sandstones in an attempt to regain equilibrium. Under equilibrium conditions, on the other hand, flows primarily bypassed the area and only the fine-grained dilute upper part and tail region of the flow were depositional leaving behind intercalculated fine-grained LADs that were preferentially preserved in the upper part of the channel fill. In the lower channel (Ch1) beds are highly amalgamated and dip less steeply in CH 1 than in CH 2 and CH3 (Figure 3.9). Although no paleocurrents were measured, differences in channel fill geometry indicate that each channel migrated in different directions.

Above the channel is a 7 m thick unit of thin-bedded turbidites (AE3) with no thick-bedded, isolated overbank splay deposits (AE4.1) (Unit 5). Also, the coarsest grain fraction is fine sand. The lack of overbank splay deposits and the fine grain size can be explained in a number of ways. First, these strata may have accumulated on the straight reach of a sinuous channel system. Unlike at channel bends where inertial effects promote overspill of the lower, coarser parts of the currents, only the finer upper parts overspill the levee crests in straight reaches. Alternatively, these strata may represent the more distal equivalent of coarser distal levee deposits with overbank splays, or lastly flows generally became smaller in size and as a result were unable to escape the channel (underfit). Irrespective of the interpretation, the uppermost unit in the study area is 15 m thick, and represents the resumption of overbank splay (AE4.1) deposition within a succession of fine-grained, thin-bedded distal levee deposits (AE3) formed on the outer bend of an unexposed sinuous channel (Unit 6).

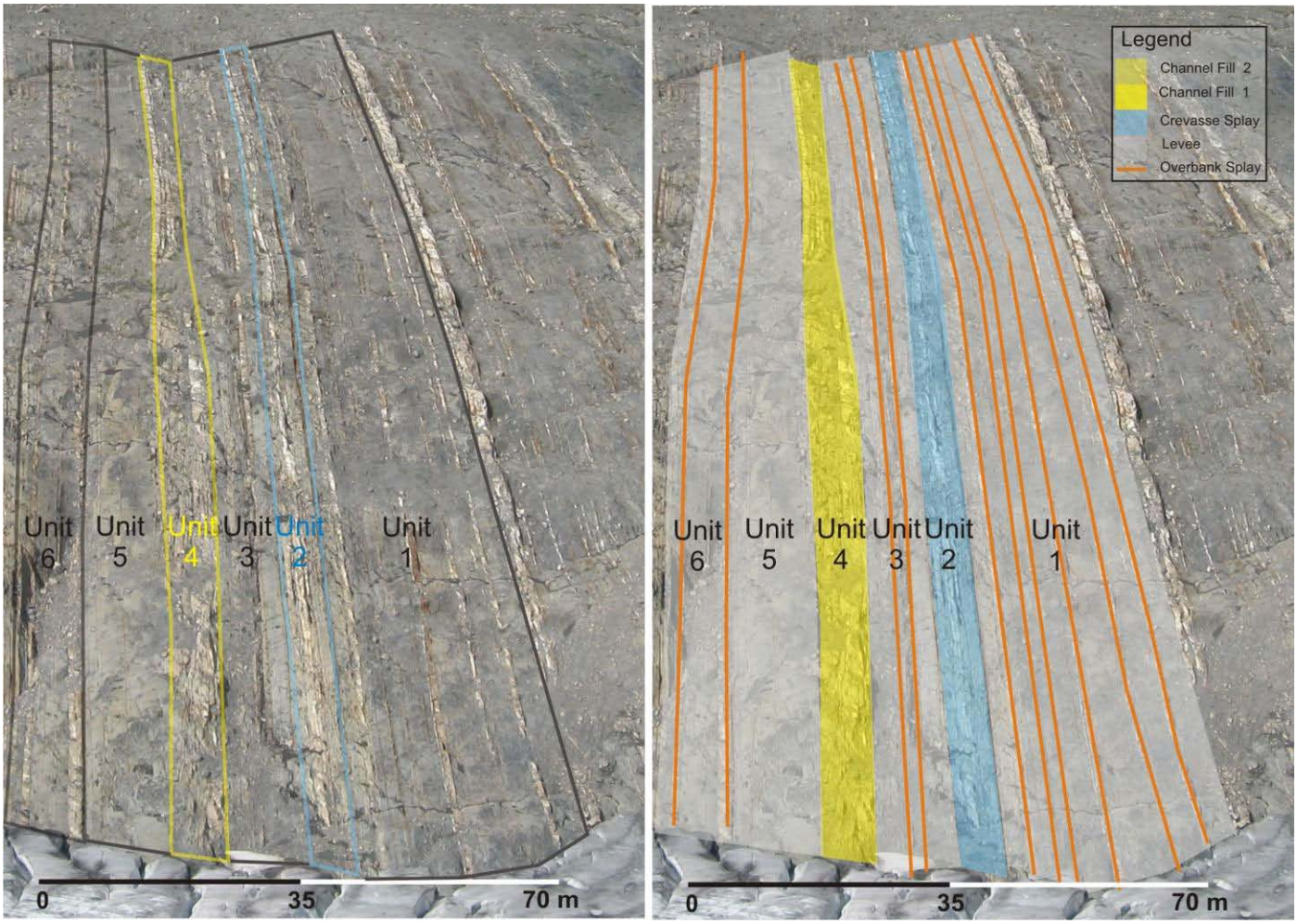

Figure 4.4: Vertical stacking of overbank splay, distal levee, crevasse and channel elements.

4.3 Depositional model:

Stratigraphic data from ancient and modern deep-marine systems are merged to define architectural elements, which then are used to build reliable, predictive depositional models. Ancient systems (outcrops) are inherently limited because they crop out in orogenic belts where metamorphic and structural deformation often obscure primary sedimentary structures and geometric relationships, in addition to being covered by vegetation and debris. Interchannel elements are particularly susceptible to these limitations because they are generally composed of more easily-deformed, recessively-weathered mud-rich strata. As a consequence, researchers turn to the modern sedimentary record to provide a supplemental dataset. Intensively studied modern systems, like the Amazon Fan, utilize high-quality integrated geophysical and

sedimentological datasets including: multibeam bathymetry, side-scan sonar, seismic profiling and core sampling. Although recent advances in geophysical techniques have significantly improved, the vertical resolution of seismic is still limited. The ancient rock record, on the other hand, provides excellent vertical resolution, but in most cases exposes a small part of not only the whole depositional system, but also the constituent architectural elements. Fortunately, the Windermere system presents a rare opportunity to make detailed millimetre- to decametre- even up to kilometre-scale sedimentological and stratigraphic observations, which are at a scale more comparable to many modern deep marine turbidite systems.

Splay elements, although commonly identified on seismic in modern deep-marine environments, are rare in outcrop. As a result a robust depositional model has not yet been proposed. Recently, splays have proven to be important hydrocarbon reservoirs (e.g. Tahoe field, North Gulf of Mexico, Kendrick, 2000; Ram/Powell field, Gulf of Mexico, Clemenceau, 2000 et al.), but are typically too thin to resolve their internal stratigraphy. As a result most earlier models for crevasse and overbank splay elements were based on models for fluvial systems, which in part relates to the interpreted similarity between deep marine channels and the much better studied meandering river channels (Flood and Damuth, 1987; Clark et al., 1992; Klaucke and Hesse, 1996; Leeder, 1999; Posamentier and Walker, 2006). Nevertheless, a number of important differences exist, including, for example, the density contrast between the ambient fluid and the flow, which in subaqueous is much reduced. This causes superelevation at subaqueous channel bends to be greatly enhanced (Komar, 1969) and as a consequence enhances processes like flow stripping and inertial run-up over the outer bend levee (Piper and Normark, 1983).

The Amazon Fan and the Windermere turbidite system are river fed passive-margin fans. The Amazon fan started to prograde in the middle Miocene (Castro et al., 1978) and extends off the northern Brazilian coast into the Atlantic Ocean between 3° N and 9° N (Figure 1.15). As one of the world's largest submarine fan systems, the Amazon Fan is 6770 km long, covers an area of 330,000 km^2 and contains more than 700,000 km^3 of sediment (Damuth and Kumar, 1975; Damuth and Flood, 1984, 1985; Pirmez and Imran, 2003) (See Ch1.11). The Windermere Supergroup in the southern

Canadian Cordillera was deposited in deep water along the passive margin of Neoproterozoic Laurentia (Ross and Arnott, 2007) (Figure 1.4). The fan was more than 350 km wide, 500 km long and had an areal extent of at least 100 000 km² (McDonough, 1989, Ross et al. 1989, Ross 2000). On submarine fans, sinuous leveed channels are common, but, levee deposits (channel bounding depositional highs) cover most of the surface commonly being an order of magnitude, or more, wider than their associated channels (Figure 4.5). On high resolution seismic images, levees are "gull-wing" shaped, typically displaying a thickening then thinning geometry with seismic reflectors dipping laterally away from the channel. Levee height above the channel floor is highly variable along the course of a channel (Posamentier, 2001). Levee thickness in highly aggradational systems can be upwards of 160 m whereas in highly erosional systems, levees can be completely absent.

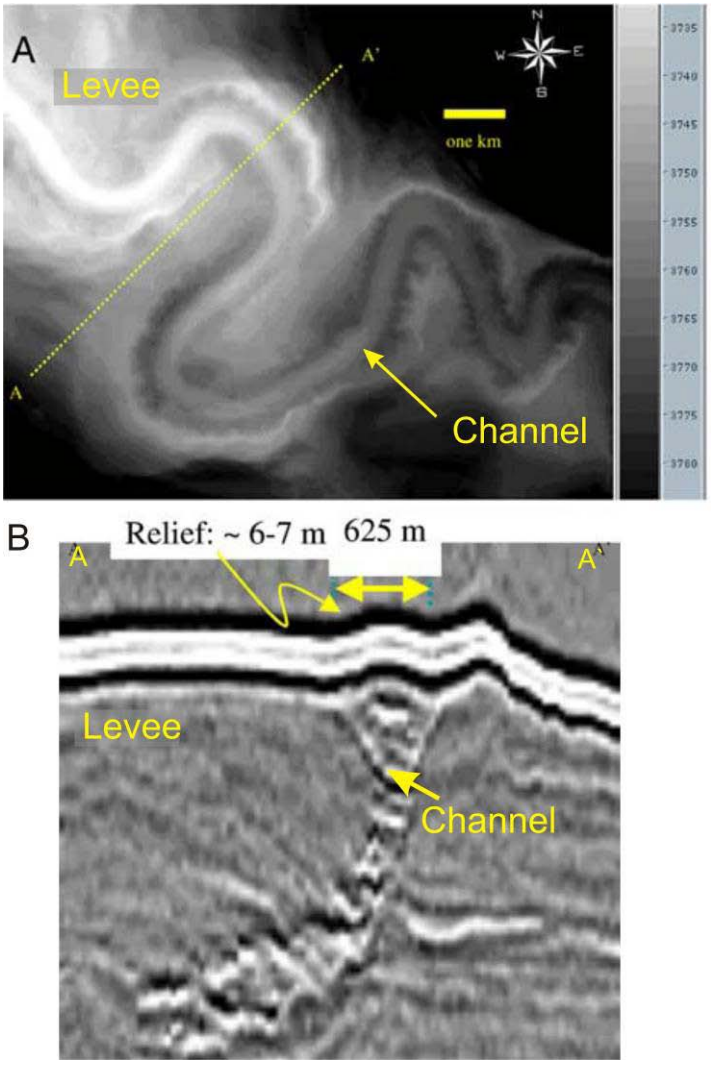

Figure 4.5: Joshua channel-levee system (A) time structure map (B) cross-section view. Note the outer bend (right) has higher relief than the inner bend and levee elements cover a greater area than channel elements.

In addition, levees are highly asymmetric, especially along channel bends where the outer bend levee is significantly higher than its counterpart along the inner bend (Posamentier, 2003; Posamentier and Kolla, 2003; Deptuck et al., 2003). Levee deposits generally consist of two end-member kinds, mud-rich and sand-rich, which are easily differentiated in seismic and in core. Mud-rich levee deposits are expressed on seismic images as low-amplitude reflections, and in core and outcrop, are composed mostly of mud intercalated with very thin- to medium-bedded cross-stratified and/or planar laminated silt and sand beds. In core, fine-grained sand beds generally occur near the base of levee sequences and both thickening- or thinning-upward trends are reported (Flood, et al., 1995; Shipboard Scientific Party, 1995). In contrast, mud-rich levee deposits in the Windermere turbidite system show little upward change in bed thickness or grain size, although one notable exception thickens and coarsens upward. In outcrop, these fine-grained thin-bedded turbidites are tabular and show negligible lateral thinning across the 200 m exposure. Further, in the Winderemere, beds show no discernible change in dip over hundreds of meters laterally or tens of meters vertically but on seismic commonly dip at angles of 1-5°.

Like in the Amazon system, sand-rich units in distal outer bend levee strata of the Windermere Supergroup are interpreted to represent overbank or crevasse splays. Two kinds of overbank splays are recognized: multiple bed complexes and isolated overbank splays. Multiple bed complexes consist of amalgamated, normally-graded, coarse-grained structureless sandstone units 2-4 m thick (Figure 4.6). Complexes are laterally continuous over several hundreds of metres, although individual beds are laterally discontinuous, typically extending less than 100 m laterally. Isolated splays are single, thick-bedded, Tbcd or Tbd turbidites bound above and below by thin- to medium-bedded turbidites (Figure 4.6). The planar-laminated division (Tb) is medium-grained, ungraded and makes up ~75-90% of the bed thickness. Beds are tabular with sharp, planar, non-erosive bases. In both isolated beds and multiple bed complexes detrital mud matrix is low (10% or less) (Figure 4.8A). Based on seismic, overbank splays are an order of magnitude smaller in area, typically hundreds m^2 compared to several km^2 for crevasse splays.

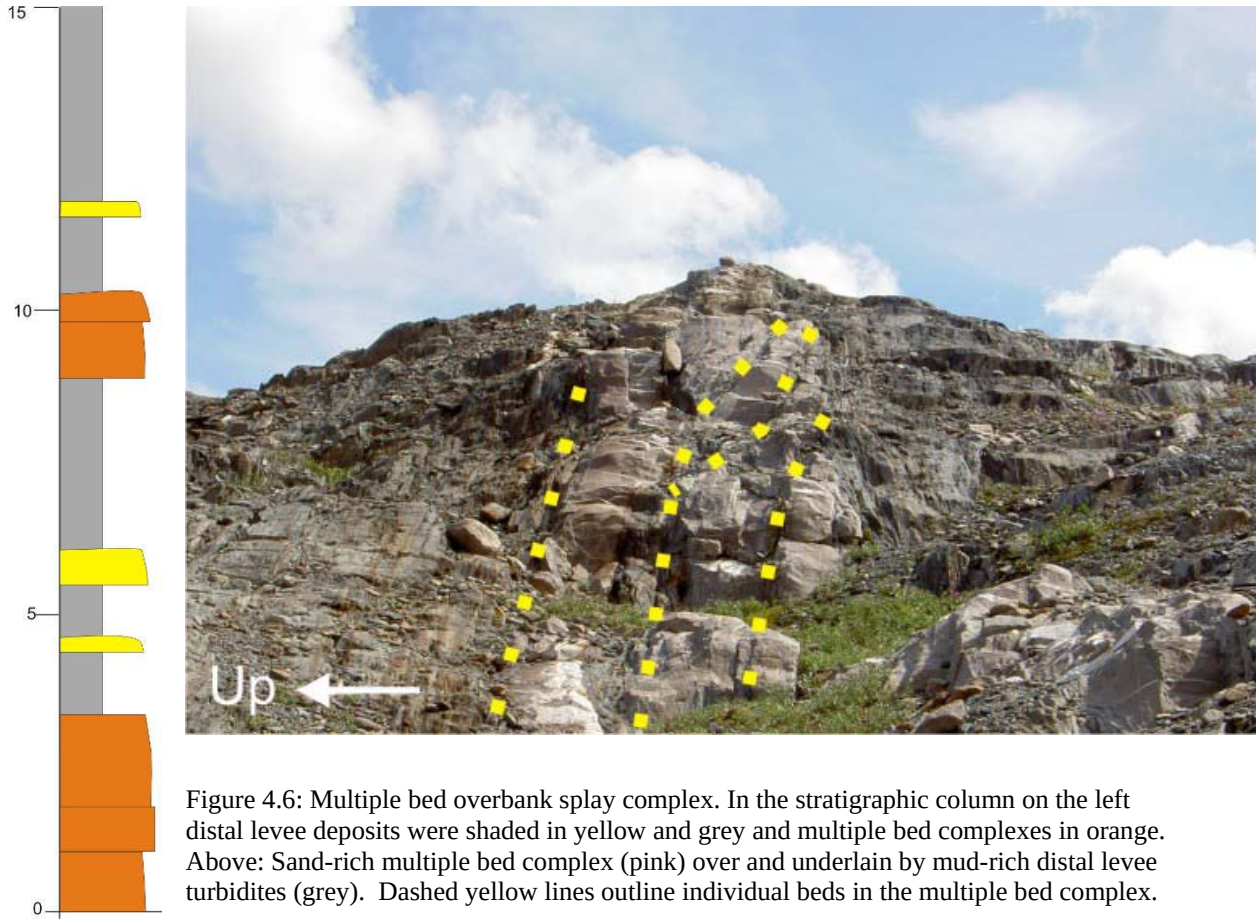

Figure 4.6: Multiple bed overbank splay complex. In the stratigraphic column on the left distal levee deposits were shaded in yellow and grey and multiple bed complexes in orange. Above: Sand-rich multiple bed complex (pink) over and underlain by mud-rich distal levee turbidites (grey). Dashed yellow lines outline individual beds in the multiple bed complex.

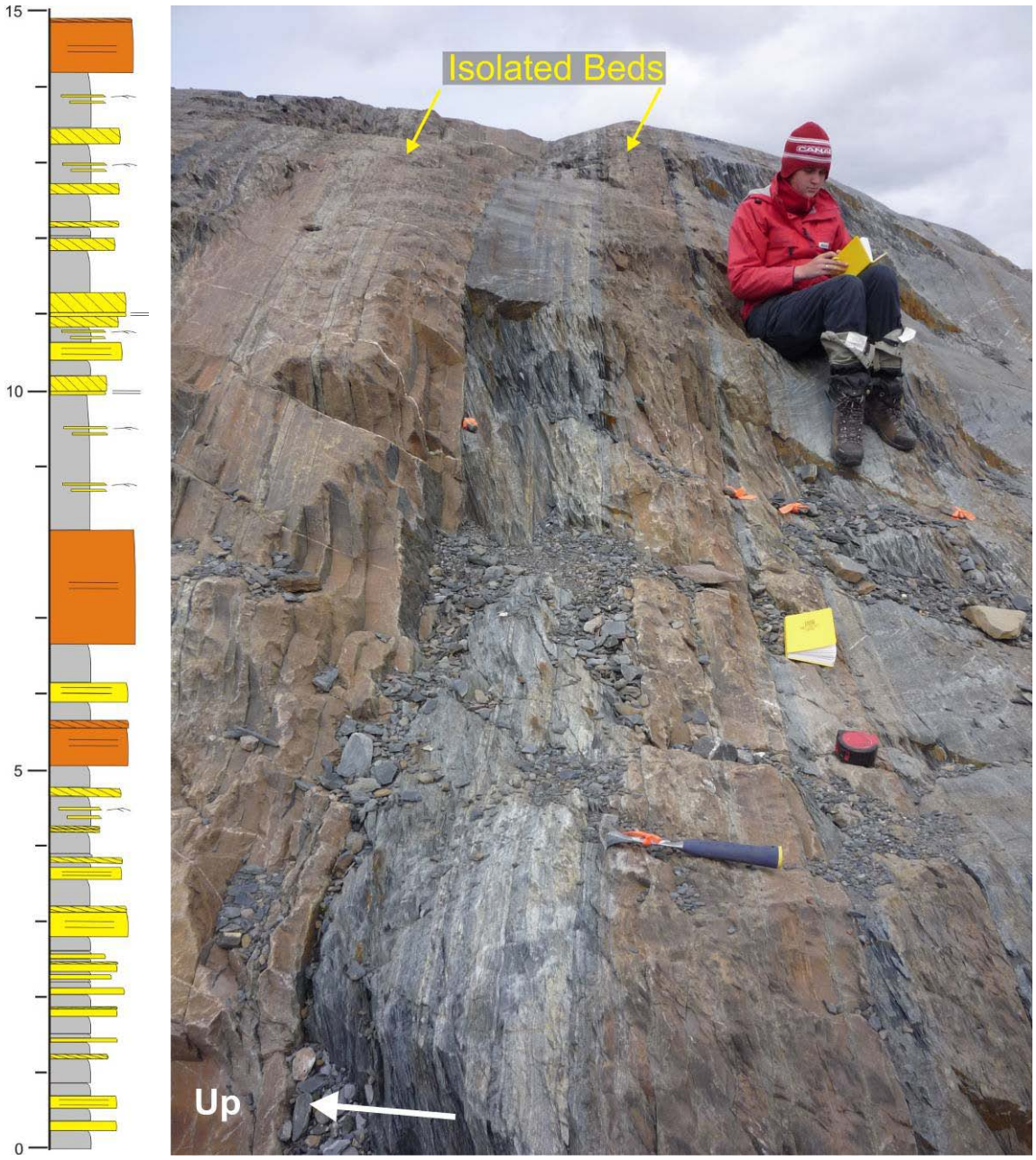

Figure 4.7: Left: stratigraphic column though distal levee deposits (yellow and grey) with isolated overbank splays (orange). Right: Photo of distal levee (grey) and isolated overbank splays (pink).

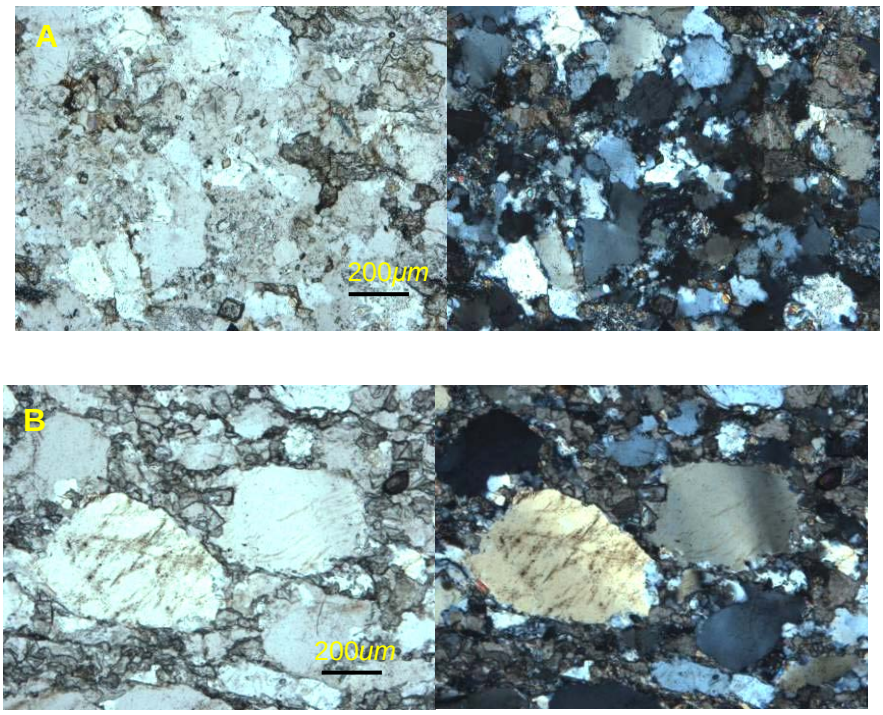

Figure 4.8: Photomicrographs of (A) mud-poor (less than 10% mud-matrix) overbank deposit and (B) mud-rich (30-50%) crevasse splay deposit.

On seismic, crevasse splay development forms relatively continuous high amplitude reflection packages, or HARPs. These sharp-based features form large, elongate, lobate elements up to 20 km long, 30 km wide and 10-50 m thick, and typically infill pre-existing interchannel lows (Pirmez et al., 2000). In this study, crevasse splays range from 2-8 m thick. In core and outcrop, crevasse splays consist primarily of medium- to very thick-bedded (5-125 cm), coarse-grained, poorly-sorted, coarse-tail graded structureless sandstones with a high (30-50%) mud matrix content (Figure 4.7B). Two kinds of crevasse splays are recognized: amalgamated and tabular. Amalgamated units consist of multiple, erosively juxtaposed beds that are discontinuous and cannot be traced for more than 150 m laterally (Figure 4.9). Mudstone clasts are small (< 50 cm), abundant and locally form breccia layers. Tabular deposits are more common and consist of single beds that form bedsets 3–7 m thick (Figure 4.10). Large isolated, tabular mudstone clasts are observed locally. Beds generally show negligible change in facies or thickness laterally. In the Amazon fan, uncommon thinly-bedded silt beds and debris flow deposits were observed but are absent in Windermere crevasse splay deposits.

Figure 4.9: Amalgamated structureless sandstone.

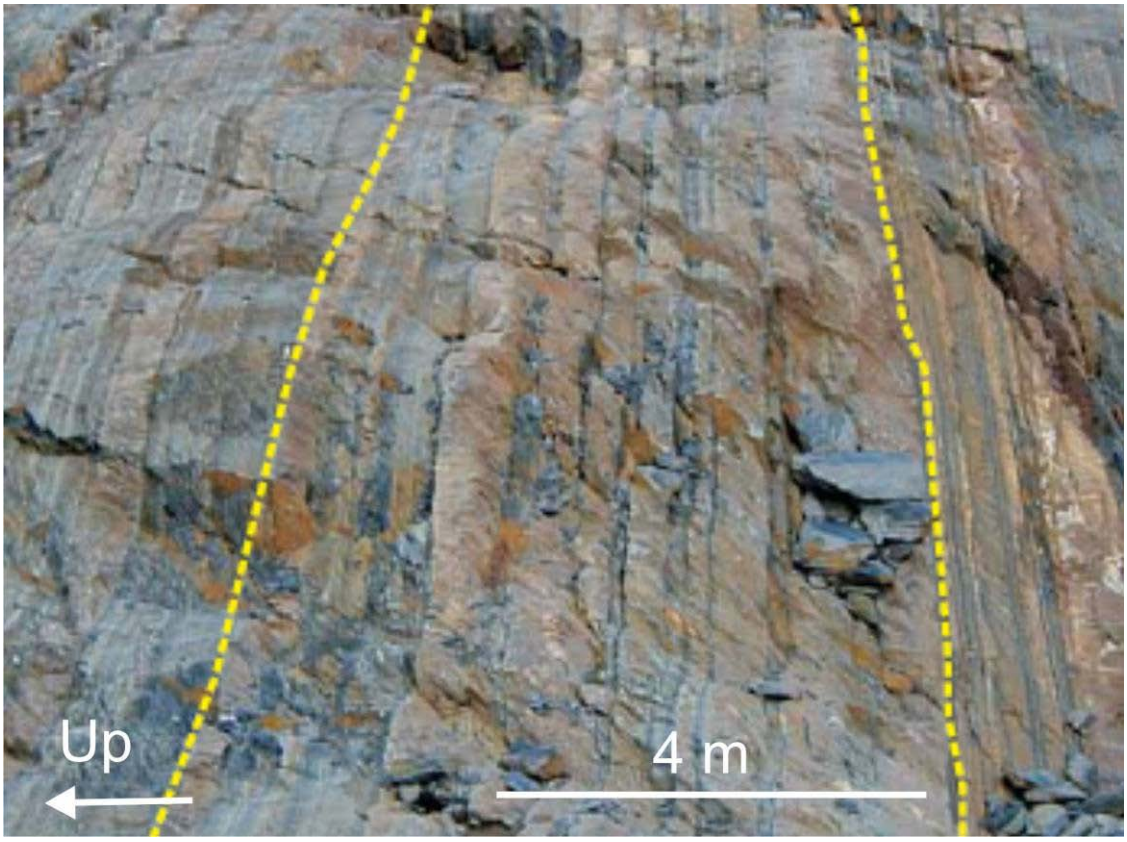

Figure 4.10: Tabular structureless sandstone. Note sharp non-erosive bed bases.

4.4: General depositional model for interchannel elements

Levee deposits are laterally extensive, channel bounding, topographically positive features that are made up of mud- and sand-rich deposits. Mud-rich levee deposits consist of fine-grained, thin-bedded turbidites deposited by dilute turbidity currents that overspilled from an adjacent channel (Figure 4.11). In the deep marine, the channelized flow thickness commonly exceeds the height of its own levees. The upper part of the current is generally fine-grained and composed of fine sand, silt and mud. As the flow overspills and becomes uncontained, velocity decreases and through competence driven deposition, deposits graded fine-grained, thin-bedded turbidites. These mud-rich strata are intercalcated with sand-rich overbank and crevasse splay deposits.

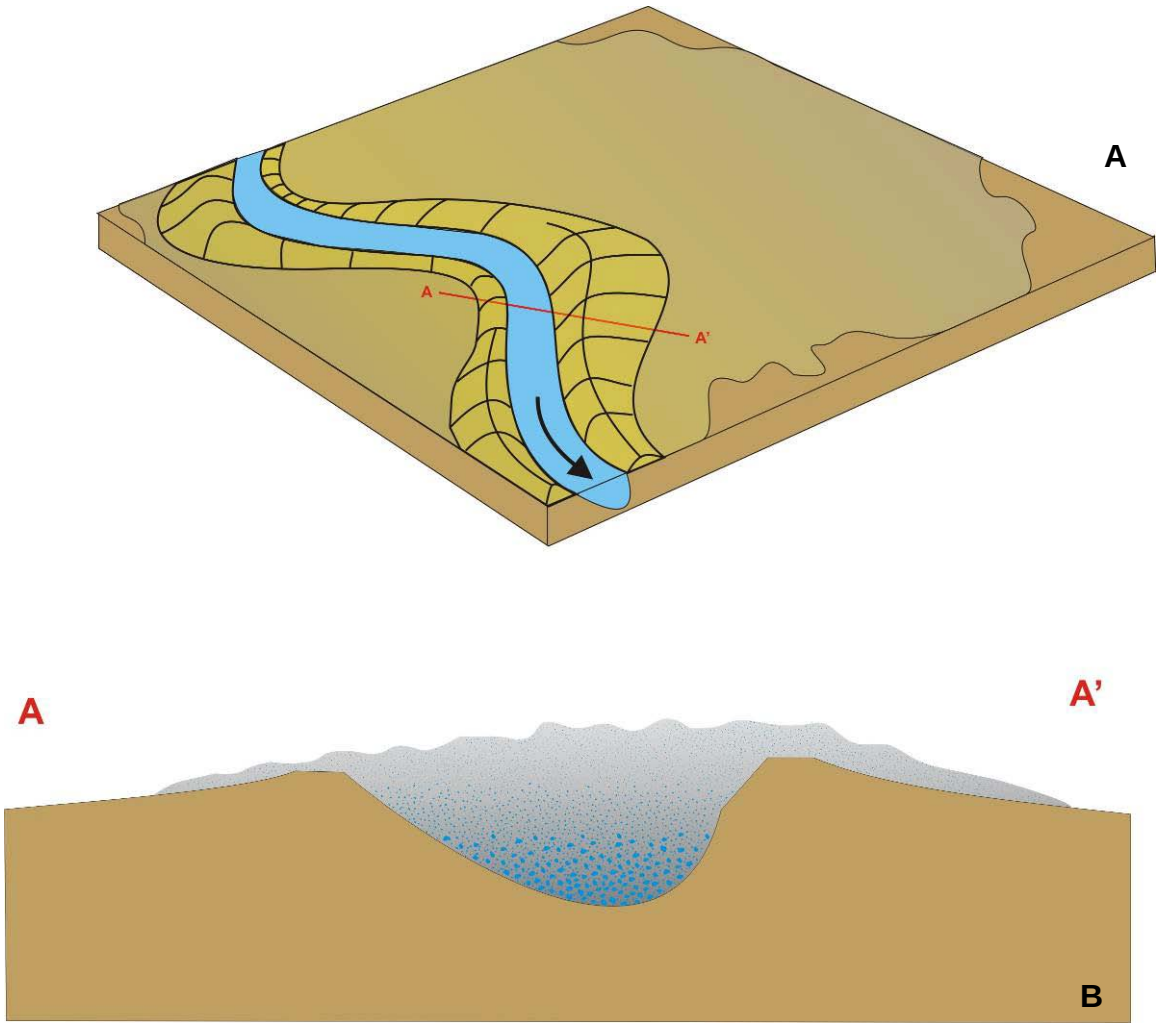

Figure 4.11: Schematic diagram illustrating deposition of mud-rich distal levee deposits. (A) Planform view of a subaqueous leveed-channel. Black arrow indicates flow direction. Thin-bedded turbidites are deposited on both sides of the channel by overspilling turbidity currents. (B) Cross-sectional view of the channel. Note the flow is stratified and coarse grains remain confined to the channel while the finer-grained dilute upper part of the flow overspills into the interchannel area.

Overbank splays form preferentially on the outer-bend levee where super-elevation, inertial run-up and flow stripping promote sediment transport out of the channel. In the case of overbank splays, overspilling flows are larger and coarser-grained than those that deposit mud-rich levee deposits. Coarser-sediments, typically medium sand, was able to escape the channel due to transport by a very large, energetic overspill (Figure 4.12) or partial breach in the levee (Figure 4.13). In the case of anomalously energetic overspill the flow bypasses the proximal levee, accelerates down the steeply-dipping levee backside and become depositional on the lower slope of the distal levee. Under competence-driven conditions, a thick succession of planar laminated sand

typically succeeded by a single-set ripple train is deposited forming an isolated overbank splay. Following a partial breach in the levee, multiple consecutive flows similarly bypass the proximal levee and deposit on the lower slope of the distal levee, building up a bedset of graded, structureless sandstone beds (multiple bed complex). After some number of flows the partial breach either heals or evolves into a full-scale breach and forms a crevasse splay. In both the overspill and partial breach scenarios, flows that exit the channel are subcritical and remain subcritical through deposition.

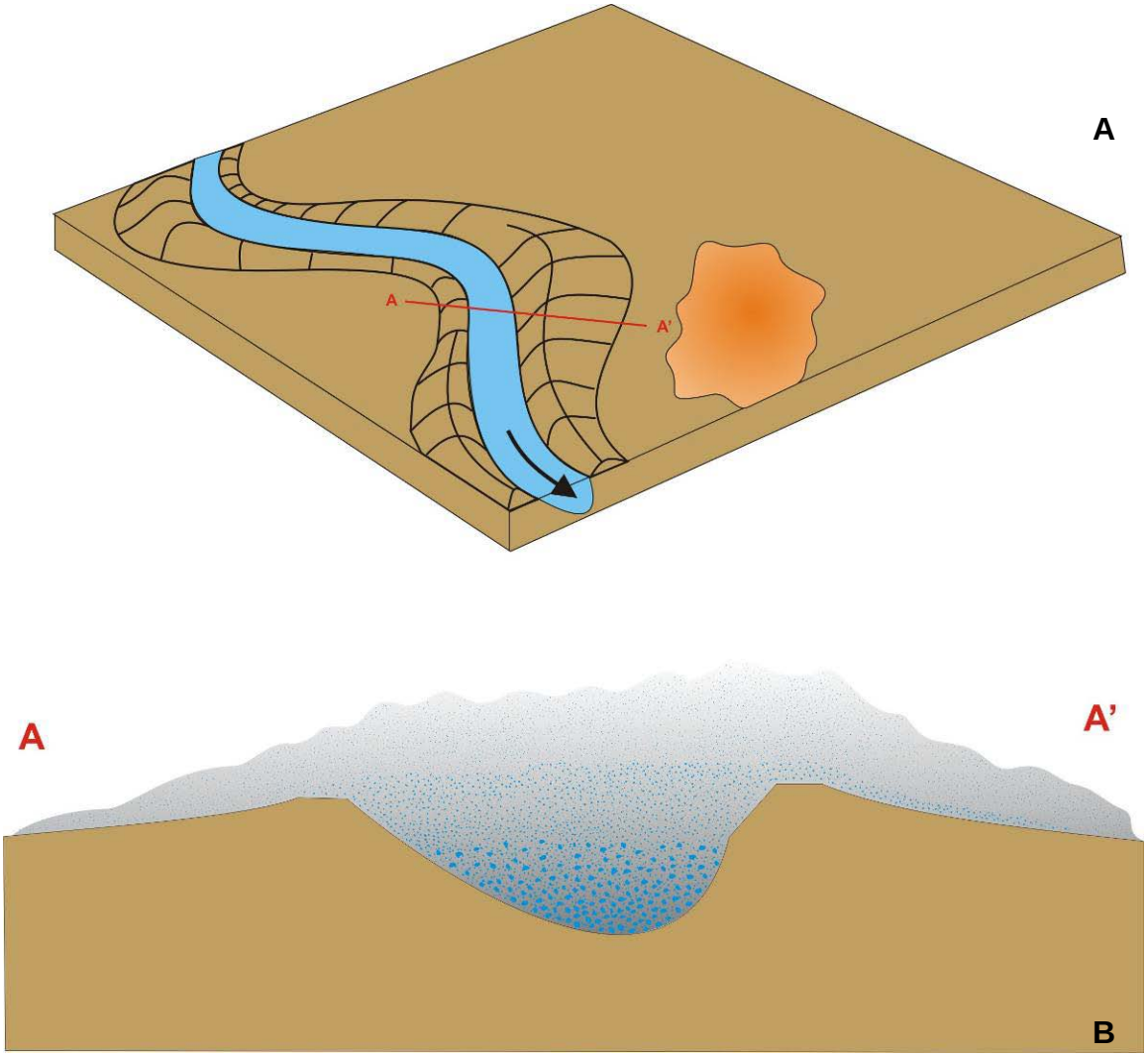

Figure 4.12: Schematic diagram illustrating deposition of sand-rich isolated overbank splay deposits. (A) Planform view of a subaqueous leveed-channel. Black arrow indicates flow direction. Isolated thick-bedded, planar laminated, turbidites are on the outer bank of the channel by overfit turbidity currents. (B) Cross-sectional view of the channel. Note the flow is stratified and coarse grains remain confined to the channel while the medium- and fine-grained sand overspills into the interchannel area.

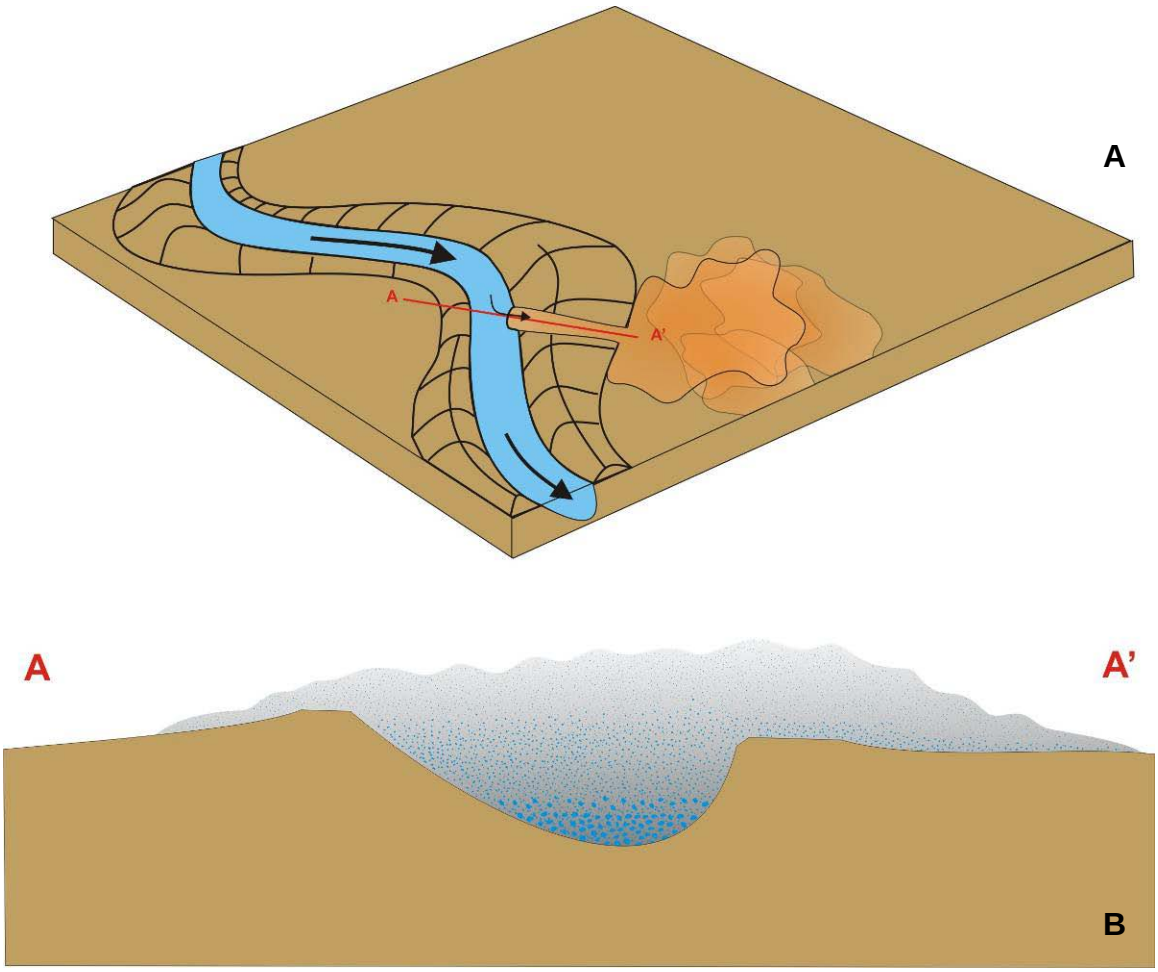

Figure 4.13: Schematic diagram illustrating deposition of sand-rich, multiple bed overbank splays. (A) Planform view of a subaqueous leveed-channel. Black arrows indicate flow direction. Multiple bed complexes consist of amalgamated structureless sandstones deposited on the outer bank of a channel. Sand particles, which are typically confined to the channel, escape through a partial breach in the levee. (B) Cross-sectional view of the channel. Note the flow is stratified. A partial breach locally reduces the levee height allowing medium- and fine-sand to escape the channel while coarse-grains remain confined.

Crevasse splays, like overbank splays, form preferentially on the outer bend levee and are deposited by unchannelized sediment-gravity flows. In the case of crevasse splays, a major levee breach allowed the full thickness of the flow to escape into the interchannel area (Kolla 2007) (Figure 4.14). Crevasse splays form sharp-based units consisting of medium- to thick-bedded, coarse-grained, mud-matrix rich, graded structureless sandstones. Mud-matrix-rich structureless sandstones reflect rapid, capacity-driven deposition possibly downflow of a plane-wall jet with jump. The jump formed at an abrupt change in slope downflow of a major levee breach where supercritical flow (*Fr* > 1) was transformed abruptly to subcritical flow (*Fr* <1). At the jump, beds were deeply

scoured and quickly draped by a layer of sediment from the collapsing sediment cloud depositing the amalgamated facies. Beyond the jump, locally-generated turbulence was damped by high sediment concentration and seafloor scour became negligible. Nevertheless, sedimentation rate remained high as the dispersion continued to collapse and deposited the matrix-rich, tabular deposits. Mudstone clasts in both the amalgamated and tabular facies were most probably sourced from erosion in the hydraulic jump.

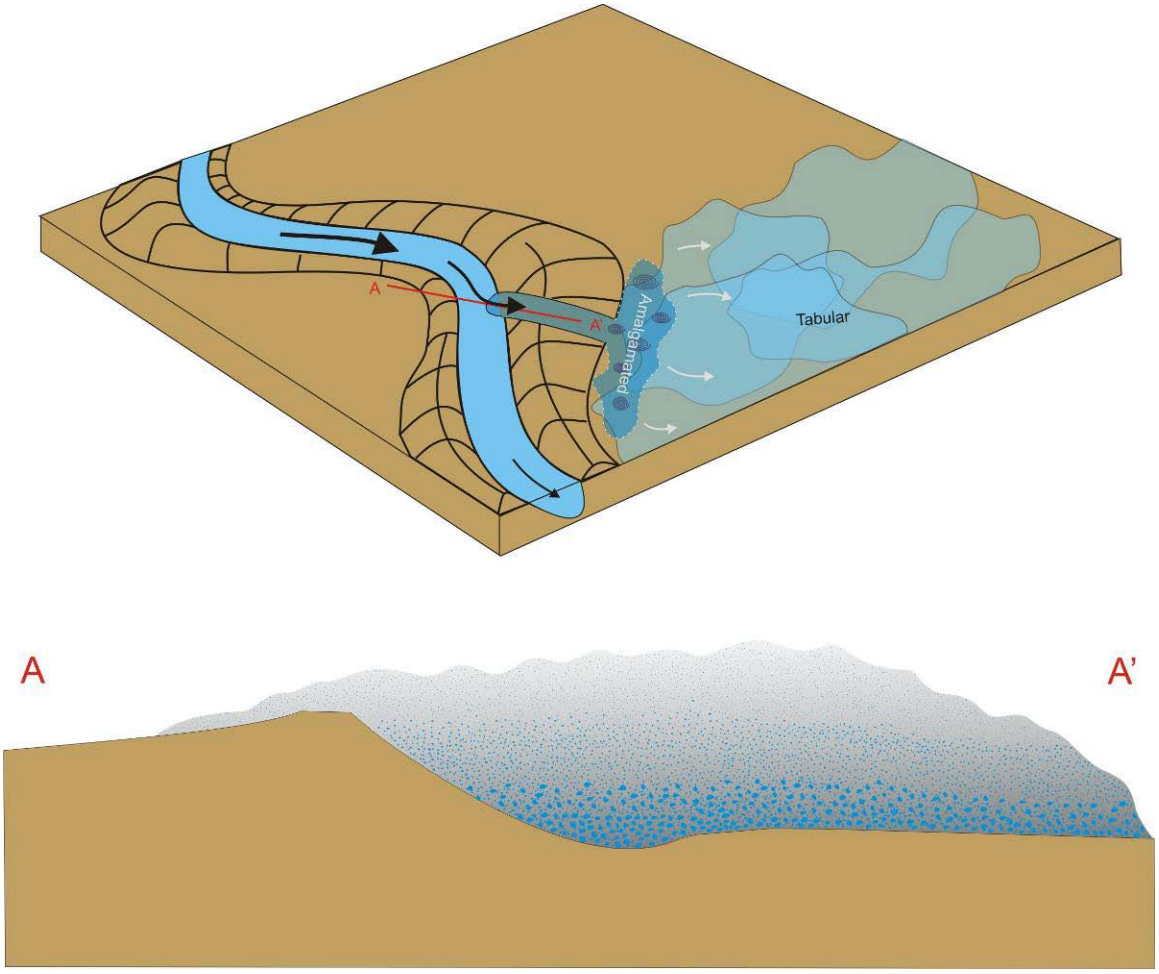

Figure 4.14: Schematic diagram illustrating deposition of sand-rich crevasse splay deposits. (A) Planform view of a subaqueous leveed-channel. Crevasse splays consist of mud-matrix-rich, coarse-tail graded structureless sandstones deposited on the outer bank of a channel. Sand particles, which are typically confined to the channel, escape through a full levee breach. (B) Cross-sectional view of the channel. Note the flow is stratified. A full levee breach locally reduces the levee height allowing coarse-sand, typically confined to the base of the channel to escape into the interchannel area.

Chapter 5: Conclusions

5.1: Summary

This study documents the stratal attributes and origin of deep-marine interchannel strata in the (base-of-slope) Neoproterozoic Isaac Formation. Based on outcrop descriptions, petrographic and organic carbon analyses, five facies were identified: very thin- to medium-bedded turbidite (most common) (F1), thick-bedded turbidite (F2) coarse-tail graded structureless sandstone (F3), mudstone clast breccia (F4) and carbonaceous mudstone (F5). Facies were further subdivided into subfacies based on differences in grain size and sedimentary structures. Petrographic analysis showed very little variation in framework grain mineralogy between facies with the exception of F5, carbonaceous mudstone, suggesting that sediment provenance changed little during deposition. The occurrence of carbonaceous mudstone layers (F5) was particularly useful for local correlations.

Facies were grouped into five architectural elements: channel (AE1), distal outer-bend levee (AE2), overbank splay (AE3) and crevasse splay (AE4). Strata are dominated by mud-rich thin-bedded turbidites (AE2). Dilute fine-grained turbidity currents overspilled an adjacent leveed channel and deposited thin-bedded turbidites over the distal levee. Alternatively, some of these strata may be the distal equivalent of thick-bedded turbidites in the proximal levee. Episodically a more voluminous, thicker flow travelled through the system, and as a consequence more of the flow thickness exceeded the levee height, and along the outer bank where super-elevation and inertial run-up enhance overspill, coarser sediment (medium-grained sand), overspilled, bypassed the proximal levee, and deposited thickly-bedded, sharp-based, non-erosive, planar-laminated turbidites (AE3.1) on the distal levee. Minor local levee collapses, caused by slumps or slides, formed a partial levee breach and allowed medium-grained sand to escape the channel. Several successive flows escaped the channel through the breach, bypassed the proximal levee and deposited medium- to thick-bedded, mud-poor, structureless sandstones on the distal levee. Flows were locally erosive and as a result bed bases are amalgamated. Multiple bed complexes consist of several stacked, mud-

matrix poor, structureless sandstones (AE3.2). Minor breaches either healed or evolved into a full-scale major levee breach. Following a major levee breach, coarse-grained sediment carried in the lower most part of a stratified throughgoing turbidity current was diverted into the interchannel area. Escaping flows were supercritical and some distance beyond the breach underwent an internal hydraulic jump. Intense turbulence within and just downflow of the jump deeply scoured the bed. Scours were rapidly draped with a layer of mud-matrix rich, coarse-tail graded structureless sandstone from the collapsing sediment cloud. Further downflow, the locally-generated turbulence is damped by high sediment concentration and scour became negligible. Sedimentation rates remained very high depositing the mud-matrix rich, tabular, non-erosive beds.

Within the study area, a channel unit composed of three thin, ~ 4 m thick, laterally-offset stacked channel fills (AE1) occurs. Channels were initiated by erosion of older, mud-rich distal levee deposits and subsequently were filled with alternating coarse and fine-grained lateral accretion deposits or LADs. LADs dip at 1-6° towards the base of the channel. Coarse LADS have erosive bed bases and consist of structureless sandstone (F2b). Towards the base of the channel, sandstones become amalgamated and interbedded with mudstone breccias (F4a). Towards the top of the channel sandstones pinch out and interfinger with thin-bedded turbidites (F1). Near the pinch out structureless beds remain coarse, but sometimes undergo a facies change to structured planar laminated turbidites or dune-cross stratified sandstone. In the oldest channel (CH1), strata dip less steeply than in the younger channels (CH2 and CH3), beds are more amalgamated and mudstone clast breccias are more common. Further, beds in CH3 have the least amalgamation and mudstone clast breccia. This is interpreted to be the result of the way of the orientation of the channel as it intersects the outcrop. CH1 is oriented oblique to the outcrop face whereas CH2 and CH3 are almost perpendicular. Channel fills are separated by mud plugs. In the area, channel fills were temporally abandoned and filled with thin-bedded turbidites. When channelization was reactivated, the subsequent channel eroded part of the previously deposited mud plug.

5.2: Implications for hydrocarbon exploration:

The first offshore rig, designed by T.F. Rowland, was patented in 1869, however, it wasn't until 1947 that the petroleum industry drilled its first offshore well off the coast of Louisiana. Since then offshore drilling and production has flourished and currently accounts for more than a third of global hydrocarbon production (Promegelle, 200?). However exploration and exploitation of hydrocarbons that are hosted in deep-marine strata and occurring in offshore areas represent a significant geologic risk and investment. To reduce exploration risk petroleum geologists integrate seismic and outcrop analogues to better understand and model subsurface reservoirs. The main contribution of this thesis is the detailed description of sandy distal levee deposits. Volumetrically, levee deposits are a major stratal component in the deep-water sedimentary record and sandy levee elements are particularly important because they have recently proven to be excellent hydrocarbon reservoirs. For example, a well producing from thin-bedded overbank-levee facies in the Ram/Powell Field, northern Gulf of Mexcio, flowed at rates up to 8.8 MBOPD and 108 MMCFD (Clemenceau et al., 2000; Kendrick, 2000). Sandy units were shown to have porosities that ranged from 15-32% and permeability from 20-1000 mD. Further, log and core data indicate pressure communication across the entire 4000 acre reservoir (Clemenceau et. al., 2000). However in spite of the demonstrated economic significance of these strata, details of their stratal make-up remain poorly understood.

In Castle Creek, sandy outer bend, distal levee deposits are divided into two end-member kinds, overbank splays and crevasse splays, which are then further subdivided into isolated overbank splays and multiple bed complexes, and amalgamated and tabular beds, respectively. Isolated overbank splay (AE4.1) deposits tend to be laterally continuous with no discernible change in grain size, sedimentary structures, sedimentary textures or bed thickness. As a result horizontal reservoir quality is probably good. However, isolated splays are separated by thin-bedded turbidites that probably reduce

vertical permeability. Multiple bed complexes (AE4.2), on the other hand, are similar to isolated splays in that they are laterally continuous and well sorted but, they are thicker, 2-4 m, and composed of multiple amalgamated sandstone beds. Although these strata are bound above and below by thin-bedded turbidites (F1), erosive juxtaposition of individual sandstone beds has removed any internal fine-grained layers, thereby improving lateral but more importantly vertical connectivity.

Crevasse splay deposits consist of coarse-tail graded, mud-matrix-rich, structureless sandstone. The high percentage (30-50%) of mud-matrix is the result of deposition from a flow that underwent an internal hydraulic jump. The transformation from supercritical to subcritical flow generates intense turbulence, which erodes the underlying substrate and vertically mixes the flow. Rapid capacity-driven deposition ensues and the flow simultaneously deposits grains of all sizes. Near the hydraulic jump beds are amalgamated, however, downflow of the jump high sediment concentration dampens turbulence reducing scour and resulting in the deposition of laterally extensive, non-erosive tabular beds. Tabular units (AE 4.2) are more common in the rock record than amalgamated structureless sandstones (AE4.1). Reservoir quality of structureless sandstones is probably fair to poor because high mud-matrix content reduces porosity and permeability and mudstone caps and breccia layers reduce vertical permeability. Nevertheless, crevasse splays are probably better reservoir facies than overbank splays despite the high mud-matrix content because of their greater thickness and larger areal expanse (10's of km^2 vs 100 m^2 respectively).

In addition to the sandy splay elements, two laterally migrating, laterally offset stacked leveed-channels were observed in this section. Channels are important hydrocarbon reservoirs and are generally the primary target of most offshore drilling projects. These channels are initiated by erosion and were subsequently filled by alternating coarse- and fine-grained lateral accretion deposits or LADs. Coarse-LADs consist of 1-4 beds that obliquely upward interfinger with poor to moderate reservoir quality fine-grained LAD. Downward, however, coarse LADs amalgamate and in the lower half to third of the fill form good reservoir quality sandstone locally reduced by mudstone breccia layers.

References

Aalto, K. R. (1971). Glacial marine sedimentation and stratigraphy of the Toby conglomerate (upper Proterozoic), southeastern British Columbia, Northwestern Idaho and northeastern Washington. *Dissertation Abstracts International, Section B: The Sciences and Engineering, 31*(9), 5423B.

Abreu, V., Sullivan, M., Pirmez, C., Mohrig, D., & Mutti, E. (. (2003). Lateral accretion packages (LAPs); an important reservoir element in deep water sinuous channels; turbidites; models and problems. *Marine and Petroleum Geology, 20*(6-8), 631-648. doi:10.1016/j.marpetgeo.2003.08.003

Aitken, J. D. (1969). Documentation of the sub-Cambrian unconformity, Rocky Mountains Main Ranges, Alberta. *Canadian Journal of Earth Sciences = Revue Canadienne Des Sciences De La Terre, 6*(2), 193-200.

Allen, J. R. L. (1964). Sedimentation in the modern delta of the river Niger, West Africa; deltaic and shallow marine deposits (int. sedimentol. congr., 6th, proc.). *Develop.Sedimentol, 1*, 26-34.

Allen, J. R. L. (1970). A quantitative model of climbing ripples and their cross-laminated deposits. *Sedimentology, 14*(1-2), 5-26.

Allen, J. R. L. (1982). Mud drapes in sand-wave deposits; a physical model with application to the Folkestone beds (early Cretaceous, southeast England). *Philosophical Transactions of the Royal Society of London, Series A: Mathematical and Physical Sciences, 306*(1493), 291-345.

Allen, J. R. L. (1991). The Bouma division A and the possible duration of turbidity currents. *Journal of Sedimentary Petrology, 61*(2), 291-295. doi:10.1306/D42676F4-2B26-11D7-8648000102C1865D

Altosaar, A.K. (2007). *Stratigraphic architecture and sedimentology of interstratified splay, levee and channel deposits: Neoproterozoic Isaac Formation (Windermere Supergroup) southern Canadian Cordillera, British Columbia*. (BSc, University of Ottawa).

Armstrong, R. L., Eisbacher, G. H., & Evans, P. D. (1982). Age and stratigraphic-tectonic significance of Proterozoic diabase sheets, Mackenzie Mountains, northwestern Canada. *Canadian Journal of Earth Sciences = Revue Canadienne Des Sciences De La Terre, 19*(2), 316-323.

Arnott, R. W. C. (2008). Depositional patterns and mechanisms on the inner-bend margin (point bar) of a sinuous deep-marine channel. *Reservoir, 35*(9), 28-30.

Arnott, R. W. C., & Hand, B. M. (1989). Bedforms, primary structures and grain fabric in the presence of suspended sediment rain. *Journal of Sedimentary Petrology, 59*(6), 1062-1069. doi:10.1306/212F90F2-2B24-11D7-8648000102C1865D

Arnott, R. W. C., & Ross, G. M. (2008). Overview of the (Neoproterozoic) Windermere Supergroup of the southern Canadian Cordillera; the world's premier ancient deep-marine turbidite system. *Reservoir, 35*(2), 35-37.

Arthur, M. A., Anderson, T. F., Kaplan, I. R., Veizer, J., & Land, L. S. (1983). Stable isotopes in sedimentary geology. *SEPM Short Course, 10*

Baas, J. H., & Best, J. L. (2002). Turbulence modulation in clay-rich sediment-laden flows and some

implications for sediment deposition. *Journal of Sedimentary Research, 72*(3), 336-340. 153

Bagnold, R. A. (1956). The flow of cohesionless grains in fluids. *Philosophical Transactions of the Royal Society of London, Series A: Mathematical and Physical Sciences, 249*(964), 235-297.

Bagnold, R. A. (1956). The flow of cohesionless grains in fluids. *Philosophical Transactions of the Royal Society of London, Series A: Mathematical and Physical Sciences, 249*(964), 235-297.

Barnes, N. E., & Normark, W. R. (1985). Diagnostic parameters for comparing modern submarine fans and ancient turbidite systems. In A. H. Bouma, W. R. Normark & N. E. Barnes (Eds.), *Submarine fans and related turbidite system*. United States (USA): Springer-Verlag, New York, NY, United States (USA).

Beaubouef, R. T. (2004). Deep-water leveed-channel complexes of the Cerro Toro Formation, upper Cretaceous, Southern Chile. *AAPG Bulletin, 88*(11), 1471-1500. doi:10.1306/06210403130

Beaubouef, R. T., & Pirmez, C. (1999). Mixed sand/mud submarine fan systems; comparing the Amazon Fan to intra-slope basin fans of the Gulf of Mexico; American Association of Petroleum Geologists 1999 annual meeting. *Annual Meeting Expanded Abstracts - American Association of Petroleum Geologists, 1999*, A10.

Berner, R. A. (1984). Sedimentary pyrite formation; an update. *Geochimica Et Cosmochimica Acta, 48*(4), 605-615.

Birman, V. K., Meiburg, E., and Kneller, B. (2009). The shape of submarine levees: Exponential or power law? *Cambridge Journals Online, 619*(1), 367.

Boetius, A., Ferdelman, T., & Lochte, K. (2000). Bacterial activity in sediments of the deep Arabian Sea in relation to vertical flux; the biogeochemistry of the deep Arabian Sea. *Deep-Sea Research.Part II: Topical Studies in Oceanography, 47*(14), 2835-2875.

Borg, S. G., & DePaolo, D. J. (1994). Laurentia, Australia, and Antarctica as a late Proterozoic supercontinent; constraints from isotopic mapping. *Geology (Boulder), 22*(4), 307-310. doi:10.1130/0091-7613(1994)022<0307:LAAAAA>2.3.CO;2

Bouma, A. H., Coleman, J. M., Bryant, W. R., & U. S. Department of the Interior, Minerals Managgement Service, Metairie, LA, United States (USA). (1985). *Recent results of the deep-sea drilling program on the Mississippi Fan, Gulf of Mexico; proceedings of the fifth annual Gulf of Mexico information transfer meeting* (07, Oceanography No. MMS 85-0008). United States (USA):

Bouma, A. H. (1962). Sedimentology of some flysch deposits; a graphic approach to facies interpretation.

Bouma, A. H., Coleman, J. M., Wright-Meyer, A. A., & Stelting, C. E. (1985). Mississippi fan; DSDP leg 96 drilling results. *Proceedings - Offshore Technology Conference, 17*, 105-112.

Bouma, A. H., Stelting, C. E., & Coleman, J. M. (1984). Mississippi fan; internal structure and depositional processes. *Geo-Marine Letters, 3*(2-4), 147-153.

Bouma, J., Jongmans, A. G., Stein, A., & Peek, G. (1989). Characterizing spatially variable hydraulic properties of a boulder clay deposit in the Netherlands. *Geoderma, 45*(1), 19-29.

Branney, M. J., & Kokelaar, P. (2002). Pyroclastic density currents and the sedimentation of ignimbrites. *Memoirs of the Geological Society of London, 27*, 143. 154

Bridge, J. S., & Jarvis, J. (1982). The dynamics of a river bend; a study in flow and sedimentary processes. *Sedimentology, 29*(4), 499-541.

Bridge, J. S. (2003). *Rivers and floodplains; forms, processes, and sedimentary record*. United Kingdom (GBR): Blackwell Publishing, Oxford, United Kingdom (GBR).

Bridge, J. S. (2006). Fluvial facies models; recent developments; facies models revisited. *Special Publication - Society for Sedimentary Geology, 84*, 85-170.

Brown, R. L., Journeay, J. M., Lane, L. S., Murphy, D. C., & Rees, C. J. (1986). Obduction, backfolding and piggyback thrusting in the metamorphic hinterland of the Southeastern Canadian Cordillera; thrusting and deformation. *Journal of Structural Geology, 8*(3-4), 255-268.

Burrett, C., & Berry, R. (2000). Proterozoic Australia-western United States (AUSWUS) fit between Laurentia and Australia. *Geology, 28*(2), 103-106. doi:10.1130/009-7613(2000)28<103:PAUSAF>2.0.CO;2

Campbell, R. B. (1970). Structural and metamorphic transitions from infrastructure to suprastructure, Cariboo Mountains, British Columbia; structure of the southern Canadian Cordillera. *Special Paper - Geological Association of Canada, 6*, 67-72.

Campbell, R. B., Mountjoy, E. W., & Young, F. G. (1973). Geology of McBride map-area, British Columbia. *Paper - Geological Survey of Canada, 72-35*, 104.

Carneiro de Castro, J., Miura, K., & Estrela Braga, J. A. (1978). Stratigraphic and structural framework of the Foz Do Amazonas Basin. *Proceedings - Offshore Technology Conference, no.10, Vol.2,* (10), 1843-1848.

Clark, J. D., Kenyon, N. H., & Pickering, K. T. (1992). Quantitative analysis of the geometry of submarine channels; implications for the classification of submarine fans. *Geology (Boulder), 20*(7), 633-636. doi:10.1130/0091-7613(1992)020<0633:QAOTGO>2.3.CO;2

Clark, J. D., & Pickering, K. T. (1996). Architectural elements and growth patterns of submarine channels; application to hydrocarbon exploration. *AAPG Bulletin, 80*(2), 194-221. doi:10.1306/64ED878C-1724-11D7-8645000102C1865D

Clemenceau, G. R., Colbert, J., & Edens, D. (2000). Production results from levee-overbank turbidite sands at Ram/Powell field, deepwater Gulf of Mexico; deep-water reservoirs of the world; Gulf Coast section Society of Economic Paleontologists and Mineralogists Foundation, 20th annual Bob F. Perkins Research. *Program and Abstracts - Society of Economic Paleontologists.Gulf Coast Section.Research Conference, 20*, 241-251.

Coleman, J. L. (2000). Reassessment of the Cerro Toro (Chile) sandstones in view of channel-levee-overbank reservoir continuity issues; deep-water reservoirs of the world; Gulf Coast section Society of Economic Paleontologists and Mineralogists Foundation, 20th annual Bob F. Perkins Research Conference. *Program and Abstracts - Society of Economic Paleontologists.Gulf Coast Section.Research Conference, 20*, 252-262.

Collinson, J. D., & Thompson, D. B. (1982). *Sedimentary structures*. United Kingdom (GBR): George Allen and Unwin, London, United Kingdom (GBR). 155

Colpron, M., Logan, J. M., & Mortensen, J. K. (2002). U-pb zircon age constraint for late Neoproterozoic rifting and initiation of the lower Paleozoic passive margin of western Laurentia. *Canadian Journal of Earth Sciences = Revue Canadienne Des Sciences De La Terre, 39*(2), 133-143.

Condie, K. C. (2001). Tectonic history of Rodinia; constraints from strontium and carbon isotopes and continental crust production rates; Geological Society of America, Rocky Mountain Section, 53rd annual meeting; Geological Society of America, south-central section, 35th annual meeting. *Abstracts with Programs - Geological Society of America, 33*(5), 19.

Crespo, E., Luque, J., Fernandez-Rodriguez, C., Rodas, M., Diaz-Azpiroz, M., Fernandez-Caliani, J. C., & Barrenechea, J. F. (2004). Significance of graphite occurrences in the Aracena metamorphic belt, Iberian Massif. *Geological Magazine, 141*(6), 687-697. doi:10.1017/S0016756804009896

Cronin, B. T., Hurst, A., Celik, H., & Turkmen, I. (2000). Superb exposure of a channel, levee and overbank complex in an ancient deep-water slope environment. *Sedimentary Geology, 132*(3-4), 205-216.

Dalziel, I. W. D. (1991). Pacific margins of Laurentia and east Antarctica-Australia as a conjugate rift pair; evidence and implications for an Eocambrian supercontinent. *Geology (Boulder), 19*(6), 598-601. doi:10.1130/0091-7613(1991)019<0598:PMOLAE>2.3.CO;2

Dalziel, I. W. D. (1997). Neoproterozoic-Paleozoic geography and tectonics; review, hypothesis, environmental speculation. *Geological Society of America Bulletin, 109*(1), 16-42. doi:10.1130/0016-7606(1997)109<0016:ONPGAT>2.3.CO;2

Damuth, J. E., & Flood, R. D. (1985). In A. H. Bouma, W. R. Normark & N. E. Barnes (Eds.), *Submarine fans and related turbidite systems* (, pp. 97) Springer-Verlag, New York.

Damuth, J. E., & Embley, R. W. (1981). Mass-transport processes on Amazon cone; western equatorial Atlantic. *AAPG Bulletin, 65*(4), 629-643. doi:10.1306/2F91999A-16CE-11D7-8645000102C1865D

Damuth, J. E., & Flood, R. D. (1984). Morphology, sedimentation processes, and growth pattern of the amazon deep-sea fan. *Geo-Marine Letters, 3*(2-4), 109-117.

Damuth, J. E., Flood, R. D., Kowsmann, R. O., Belderson, R. H., & Gorini, M. A. (1988). Anatomy and growth pattern of Amazon deep-sea fan as revealed by long-range side-scan sonar (GLORIA) and high-resolution seismic studies. *AAPG Bulletin, 72*(8), 885-911. doi:10.1306/703C9109-1707-11D7-8645000102C1865D

Damuth, J. E., Kolla, V., Flood, R. D., Kowsmann, R. O., Monteiro, M. O., Gorini, M. A., Palma, J. J. C., & Belderson, R. H. (1983). Distributary channel meandering and bifurcation patterns on the Amazon deep-sea fan as revealed by long-range side-scan sonar (GLORIA). *Geology (Boulder), 11*(2), 94-98.

Damuth, J. E., & Kumar, N. (1975). Late quaternary depositional processes on continental rise of western equatorial Atlantic; comparison with western north Atlantic and implications for reservoir-rock distribution. *AAPG Bulletin, 59*(11), 2172-2181. doi:10.1306/83D92217-16C7-11D7-8645000102C1865D

Das, H. S., Imran, J., & Mohrig, D. (2004). Numerical modeling of flow and bed evolution in meandering submarine channels. *Journal of Geophysical Research, 109*(C10), 17. doi:10.1029/2002JC001518 156

Davies, D. K. (1972). Deep sea sediments and their sedimentation, Gulf of Mexico. *The American Association of Petroleum Geologists Bulletin, 56*(11), 2212-2239. doi:10.1306/819A41FC-16C5-11D7-8645000102C1865D

Davies, R. J., & Posamentier, H. W. (2005). Geologic processes in sedimentary basins inferred from three-dimensional seismic imaging. *GSA Today, 15*(10), 4-9. doi:10.1130/1052-5173(2005)15(4:GPISBI)2.0.CO;2

Deptuck, M. E., Steffens, G. S., Barton, M., Pirmez, C., & Mutti, E. (. (2003). Architecture and evolution

of upper fan channel-belts on the Niger Delta slope and in the Arabian Sea; turbidites; models and problems. *Marine and Petroleum Geology, 20*(6-8), 649-676. doi:10.1016/j.marpetgeo.2003.01.004

Devlin, W. J., Brueckner, H. K., & Bond, G. C. (1988). New isotopic data and a preliminary age for volcanics near the base of the Windermere Supergroup, northeastern Washington, U.S.A. *Canadian Journal of Earth Sciences = Revue Canadienne Des Sciences De La Terre, 25*(11), 1906-1911.

Dickson, J.A.D. (1966). Carbonate identification and genesis revealed by staining, *Journal of Sedimentary Petrology*, 36, 13-45.

Dietrich, W. E., & Whiting, P. J. (1989). Boundary shear stress and sediment transport in river meanders of sand and gravel; river meandering. *Water Resources Monograph, 12*, 1-50.
Dolgunin, V. N., & Ukolov, A. A. (1995). Segregation modeling of particle rapid gravity flow. *Powder Technology, 83*(2), 95. doi:10.1016/0032-5910(94)02954-M

Druitt, T. H. (1995). Settling behaviour of concentrated dispersions and some volcanological applications. *Journal of Volcanology and Geothermal Research, 65*(1-2), 27.

Dzulynski, S., & Sanders, J. E. (1962). Current marks on firm mud bottoms. *Transactions of the Connecticut Academy of Arts and Sciences, 42*, 57-96.

Eisbacher, G. H. (1981). Sedimentary tectonics and glacial record in the Windermere Supergroup, Mackenzie Mountains, northwestern Canada. *Paper - Geological Survey of Canada*, (80-27), 40.

Engelund, F. (1974). Flow and bed topography in channel bends. *Journal of the Hydraulics Division, 100*(HY11), 1631-1648.

Eschard, R., Albouy, E., Deschamps, R., Euzen, T., Ayub, A., & Mutti, E. (. (2003). Downstream evolution of turbiditic channel complexes in the Pab Range outcrops; Maastrichtian, Pakistan; turbidites; models and problems. *Marine and Petroleum Geology, 20*(6-8), 691-710. doi:10.1016/j.marpetgeo.2003.02.004

Evenchick, C. A., Parrish, R. R., & Gabrielse, H. (1984). Precambrian gneiss and Late Proterozoic sedimentation in north-central British Columbia. *Geology (Boulder), 12*(4), 233-237.

Farquhar, J., Hauri, E., & Wang, J. (1999). New insights into carbon fluid chemistry and graphite precipitation; SIMS analysis of granulite facies graphite from Ponmudi, South India. *Earth and Planetary Science Letters, 171*(4), 607-621.

Feeley, M. H., Buffler, R. T., & Bryant, W. R. (1985). Depositional units and growth pattern of the Mississippi Fan. In A. H. Bouma, W. R. Normark & N. E. Barnes (Eds.), *Submarine fans and related turbidite systems* (). United States (USA): Springer-Verlag, New York, NY, United States (USA).

Ferguson, C. A. (1994). *Structural geology and stratigraphy of the northern Cariboo Mountains between Isaac Lake and Fraser River, British Columbia*. (Map, University of Calgary, Calgary, AB, Canada (CAN)). . (1997-047810) 157

Flood, R. D., Manley, P. L., Kowsmann, R. O., Appi, C. J., & Pirmez, C. (1991). Seismic facies and late quaternary growth of Amazon Submarine Fan; seismic facies and sedimentary processes of submarine fans and turbidite systems. *SEPM Midyear Meeting, Austin, TX*, United States.

Flood, R. D., & Damuth, J. E. (1987). Quantitative characteristics of sinuous distributary channels on the amazon deep-sea fan. *Geological Society of America Bulletin, 98*(6), 728-738.

Flood, R. D., Piper, D. J. W., Flood, R. D., Piper, D. J. W., Klaus, A., Burns, S. J., Busch, W. H., Cisowski, S. M., Cramp, A., Damuth, J. E., Goni, M. A., Haberle, S. G., Hall, F. R., Hinrichs, K., Hiscott, R. N., Kowsmann, R. O., Kronen, J. D.,Jr, Long, D., Lopez, M., McDaniel, D. K., Manley, P. L., Maslin, M. A., Mikkelsen, N., Nanayama, F., Normark, W. R., Pirmez, C., dos Santos, J. R., Schneider, R. R., Showers, W. J., Soh, W., & Thibal, J. (1997). Amazon fan sedimentation; the relationship to equatorial climate change, continental denudation, and sea-level fluctuations; proceedings of the ocean drilling program; scientific results, Amazon Fan; covering leg 155 of the cruises of the drilling vessel JOIDES resolution, Bridgetown, Barbados, to Bridgetown, Barbados, sites 930-946, 25 march-24 may 1994. *Proceedings of the Ocean Drilling Program, Scientific Results, 155*, 653-675. doi:10.2973/odp.proc.sr.155.246.1997

Folk, R. L. (1959). Practical petrographic classification of limestones. *Bulletin of the American Association of Petroleum Geologists, 43*(1), 1-38. doi:10.1306/0BDA5C36-16BD-11D7-8645000102C1865D

Frye, B.J.P. (1987). Stable Isotopes in Ecosystem Studies. *Annual Review of Ecology, Evolution and Systematics* 18, 293-320.

Gabrielse, H., & Campbell, R. B. (1992). Upper Proterozoic assemblages. In H. Gabrielse, & C. J. Yorath (Eds.), *Geology of the cordilleran orogen in canada* (). Canada (CAN): Geol. Surv. Can., Ottawa, ON, Canada (CAN).

Gabrielse, H. (1972). Younger Precambrian of the Canadian Cordillera. *American Journal of Science, 272*(6), 521-536.

Garcia, M. H. (1993). Hydraulic jumps in sediment-driven bottom currents. *Journal of Hydraulic Engineering, 119*(10), 1094.

Garcia, M., & Parker, G. (1989). Experiments on hydraulic jumps in turbidity currents near a canyon-fan transition. *Science, 245*(4916), 393-396.

Gardner, M. H., & Borer, J. M. (2000). Submarine channel architecture along a slope to basin profile, Brushy Canyon Formation, west Texas; fine-grained turbidite systems. *AAPG Memoir, 72*, 195-213.

Gerasimoff, M. D. (1988). *The hobson lake pluton, Cariboo Mountains, British Columbia, and its significance to mesozoic and early Cenozoic Cordilleran tectonics*. (Master's, Queen's University, Kingston, ON, Canada (CAN)). . (1990-048456)

Grecula, M., Flint, S. S., de V Wickens, H., & Johnson, S. D. (2003). Upward-thickening patterns and lateral continuity of Permian sand-rich turbidite channel fills, Laingsburg Karoo, South Africa. *Sedimentology, 50*(5), 831-853. doi:10.1046/j.1365-3091.2003.00576.x

Greenwood, B., Osborne, P. D., & Bowen, A. J. (1991). Measurements of suspended sediment transport; prototype shorefaces; coastal sediments '91. *Specialty Conference on Quantitative Approaches to Coastal Sediment Processes, Seattle, WA*, United States.

Hampton, M. A. (1979). Buoyancy in debris flows. *Journal of Sedimentary Petrology, 49*(3), 753-758. doi:10.1306/212F7838-2B24-11D7-8648000102C1865D 158

Hay, A. E. (1987). Turbidity currents and submarine channel formation in Rupert inlet, British Columbia; 1, surge observations. *Journal of Geophysical Research, 92*(C3), 2875-2881. doi:10.1029/JC092iC03p02875

Hay, A. E., Murray, J. W., & Burling, R. W. (1983). Submarine channels in Rupert inlet, British Columbia; I, morphology; sedimentology of fjords. *Sedimentary Geology, 36*(2-4), 289-315.

Hesse, R. (1990). Early diagenetic pore water/sediment interaction: Modern offshore basins. In I. A. McIlreath, & D. W. Morrow (Eds.), *Diagenesis* (pp. 277). Ottawa: Runge Press Ltd.

Hickson, T. A., & Lowe, D. R. (2002). Facies architecture of a submarine fan channel-levee complex; the juniper ridge conglomerate, Coalinga, California. *Sedimentology, 49*(2), 335-362.

Hiscott, R. N., Hall, F. R., Pirmez, C., Flood, R. D., Piper, D. J. W., Klaus, A., Burns, S. J., Busch, W. H., Cisowski, S. M., Cramp, A., Damuth, J. E., Goni, M. A., Haberle, S. G., Hall, F. R., Hinrichs, K., Hiscott, R. N., Kowsmann, R. O., Kronen, J. D.,Jr, Long, D., Lopez, M., McDaniel, D. K., Manley, P. L., Maslin, M. A., Mikkelsen, N., Nanayama, F., Normark, W. R., Pirmez, C., dos Santos, J. R., Schneider, R. R., Showers, W. J., Soh, W., & Thibal, J. (1997). Turbidity-current overspill from the amazon channel; texture of the silt/sand load, paleoflow from anisotropy of magnetic susceptibility and implications for flow processes; proceedings of the ocean drilling program; scientific results, Amazon Fan; covering leg 155 of the cruises of the drilling vessel JOIDES resolution, Bridgetown, Barbados, to Bridgetown, Barbados, sites 930-946, 25 march-24 may 1994. *Proceedings of the Ocean Drilling Program, Scientific Results, 155*, 53-78. doi:10.2973/odp.proc.sr.155.202.1997

Hiscott, R. N., & Middleton, G. V. (1980). Fabric of coarse deep-water sandstones, Tourelle Formation, Quebec, Canada. *Journal of Sedimentary Petrology, 50*(3), 703-721. doi:10.1306/212F7AC7-2B24-11D7-8648000102C1865D

Hoffman, P. F., & Schrag, D. P. (2002). The snowball earth hypothesis; testing the limits of global change. *Terra Nova, 14*(3), 129-155.

Huang, T., & Goodell, H. G. (1970). Sediments and sedimentary processes of eastern Mississippi cone, Gulf of Mexico. *The American Association of Petroleum Geologists Bulletin, 54*(11), 2070-2100.

Hubbard, S. M., Romans, B. W., & Graham, S. A. (2008). Deep-water foreland basin deposits of the Cerro Toro Formation, Magallanes Basin, Chile; architectural elements of sinuous basin axial channel belt. *Sedimentology, 55*(5), 1333-1359. doi:10.1111/j.1365-3091.2007.00948.x

Huuse, M., Cartwright, J. A., Gras, R., & Hurst, A. (2005). Kilometre-scale sandstone intrusions in the eocene of the outer moray firth (UK north sea); migration paths, reservoirs and potential drilling hazards; petroleum geology; north-west Europe and global perspectives; proceedings of the 6th petroleum geology conference. *Petroleum Geology of Northwest Europe: Proceedings of the Conference, 6*, 1577-1594.

Imran, J., Parker, G., & Pirmez, C. (1999). A nonlinear model of flow in meandering submarine and subaerial channels. *Journal of Fluid Mechanics, 400*, 295-331.

INGRAM, R. L. (1954). Terminology for the thickness of stratification and parting units in sedimentary rocks. *Bulletin of the Geological Society of America, 65*(9), 937-938. doi:10.1130/0016-7606(1954)65[937:TFTTOS]2.0.CO;2

Johannesson, H., & Parker, G. (1989). Velocity redistribution in meandering rivers. *Journal of Hydraulic Engineering, 115*(8), 1019-1039. 159

Jolly, R. J. H., & Lonergan, L. (2002). Mechanisms and controls on the formation of sand intrusions. *Journal of the Geological Society of London, 159*, 605-617. doi:10.1144/0016-764902-025

Kane, I. A., Kneller, B. C., Dykstra, M., Kassem, A., & McCaffrey, W. D. (2007). Anatomy of a submarine

channel-levee: An example from upper cretaceous slope sediments, Rosario Formation, Baja California, mexico; sinuous deep-water channels: Genesis, geometry and architecture sinuous deep-water channels. *Marine and Petroleum Geology, 24*(6-9), 540-563. doi:10.1016/j.marpetgeo.2007.01.003

Karlstrom, K. E., Ahall, K., Harlan, S. S., Williams, M. L., McLelland, J., & Geissman, J. W. (2001). Long-lived (1.8-1.0 ga) convergent orogen in southern Laurentia, its extensions to Australia and Baltica, and implications for refining Rodinia; Rodinia and the Mesoproterozoic earth-ocean system. *Precambrian Research, 111*(1-4), 5-30.

Karlstrom, K. E., Harlan, S. S., Williams, M. L., McLelland, J., Geissman, J. W., & Ahall, K. (1999). Refining Rodinia; geologic evidence for the Australia-Western U.S. connection in the Proterozoic. *GSA Today, 9*(10), 1-7.

Kastens, K. A., & Shor, A. N. (1985). Depositional processes of a meandering channel on Mississippi Fan. *AAPG Bulletin, 69*(2), 190-202. doi:10.1306/AD461C7D-16F7-11D7-8645000102C1865D

Katz, M.E., Finkel, Z.V., Grzebyk, D., Knoll, A.H., Falkowski P.G. (2004). Evolutionary Trajectories and Biogeochemical Impacts of Marine Eukaryotic Phytoplankton. *Annual Review of Ecology, Evolution, and Systematics*, 35, 523-556

Keevil, G., Peakall, J., Amos, K., Bradbury, W., & Best, J. (2005). Experimental study of the formation and development of sediment waves; AAPG 2005 annual convention; abstracts volume. *Abstracts: Annual Meeting - American Association of Petroleum Geologists, 14*, A71.

Kendall, B. S., Creaser, R. A., Ross, G. M., & Selby, D. (2004). Constraints on the timing of Marinoan snowball earth glaciation by (super 187) re/ (super 187) os dating of a Neoproterozoic, post-glacial black shale in western Canada. *Earth and Planetary Science Letters, 222*(3-4), 729-740. doi:10.1016/j.epsl.2004.04.004

Kendall, B., Creaser, R. A., & Selby, D. (2009). (Super 187) re- (super 187) os geochronology of Precambrian organic-rich sedimentary rocks; global neoproterozoic petroleum systems; the emerging potential in North Africa. *Geological Society Special Publications, 326*, 85-107.

Kendrick, J. W. (2000). Turbidite reservoir architecture in the northern Gulf of Mexico deepwater; insights from the development of auger, Tahoe, and Ram/Powell fields; deep-water reservoirs of the world; Gulf Coast Section Society of Economic Paleontologists and Mineralogists Foundation, 20th annual Bob F. Perkins Research Conference. *Program and Abstracts - Society of Economic Paleontologists.Gulf Coast Section.Research Conference, 20*, 450-468.

Khripounoff, A., Vangriesheim, A., Babonneau, N., Crassous, P., Dennielou, B., & Savoye, B. (2003). Direct observation of intense turbidity current activity in the Zaire Submarine Valley at 4000 m water depth. *Marine Geology, 194*(3-4), 151-158. doi:10.1016/S0025-3227(02)00677-1

King, P. R., Browne, G. H., Slatt, R. M., Weimer, P., Bouma, A. H., & Perkins, B. (1994). Sequence architecture of exposed late Miocene basin floor fan and channel-levee complexes (mount messenger formation), Taranaki Basin, New Zealand; submarine fans and turbidite systems; sequence stratigraphy, reservoir architecture and production characteristics, Gulf of Mexico and international. *Program and Abstracts - Society of Economic Paleontologists.Gulf Coast Section.Research Conference, 15*, 177-192. 160

Klaucke, I., & Hesse, R. (1996). Fluvial features in the deep-sea: New insights from the glacigenic submarine drainage system of the northwest Atlantic mid-ocean channel in the Labrador Sea. *Sedimentary Geology, 106*(3-4), 223-234.

Kneller, B., & Buckee, C. (2000). The structure and fluid mechanics of turbidity currents; a review of some

recent studies and their geological implications; millennium reviews. *Sedimentology, 47*, 62-94.

Kneller, B. C., & Branney, M. J. (1995). Sustained high-density turbidity currents and the deposition of thick massive sands. *Sedimentology, 42*(4), 607-616.

Kneller, B. C., & McCaffrey, W. D. (2003). The interpretation of vertical sequences in turbidite beds; the influence of longitudinal flow structure. *Journal of Sedimentary Research, 73*(5), 706-713.

Knoll, A. H., & Walter, M. R. (1992). Latest Proterozoic stratigraphy and earth history. *Nature (London), 356*(6371), 673-677.

Kohl, B., & Deep Sea Drilling Project, Leg 96 Shipboard Scientists, United States (USA). (1985). Biostratigraphy and sedimentation rates of the Mississippi Fan. In A. H. Bouma, W. R. Normark & N. E. Barnes (Eds.), *Submarine fans and related turbidite systems*. United States (USA): Springer-Verlag, New York, NY, United States (USA).

Kolla, V. (2007). A review of sinuous channel avulsion patterns in some major deep-sea fans and factors controlling them. *Marine and Petroleum Geology, 24*(6-9), 450-469. doi:10.1016/j.marpetgeo.2007.01.004

Kolla, V., Bourges, P., Urruty, J. M., & Safa, P. (2001). Evolution of deep-water tertiary sinuous channels offshore Angola (west Africa) and implications for reservoir architecture. *AAPG Bulletin, 85*(8), 1373-1405. doi:10.1306/8626CAC3-173B-11D7-8645000102C1865D ‘

Komar, P. D. (1969). A model for turbidity current flow in an enclosed basin. *EOS, Transactions, American Geophysical Union, 50*(4), 197.

Komar, P. D. (1971). Hydraulic jumps in turbidity currents. *Geological Society of America Bulletin, 82*(6), 1477-1487. doi:10.1130/0016-7606(1971)82[1477:HJITC]2.0.CO;2

Kuenen, P. H. (1957). Review of marine sand-transporting mechanisms. *Journal of the Alberta Society of Petroleum Geologists, 5*(4), 59-62.

Leclair, S. F., & Arnott, R. W. C. (2003). Coarse-tail graded, structureless strata; indicators of an internal hydraulic jump, In H.H. Roberts, N.C., Rosen, R.H., Fillon, and J.B., Anderson, eds., *Shelf margin deltas and linked downslope petroleum systems*: Gulf Coast Section SEPM 23rd Annual Bob F. Perkins Research Conference pp. 817-835.

Leeder, M. (1999). *Sedimentology and sedimentary basins; from turbulence to tectonics*. United Kingdom (GBR): Blackwell Science, Oxford, United Kingdom (GBR).

Legros, F. (2002). Can dispersive pressure cause inverse grading in grain flows? *Journal of Sedimentary Research, 72*(1), 166-170.

Leopold, L. B., & Wolman, M. G. (1960). River meanders. *Geological Society of America Bulletin, 71*(6), 769-793. 161

Li, M. Z., & Komar, P. D. (1992). Selective entrainment and transport of mixed size and density sands; flume experiments simulating the formation of black-sand placers. *Journal of Sedimentary Petrology, 62*(4), 584-590.

Li, Z., Li, X., Zhou, H., & Kinny, P. (2002). Grenvillian continental collision in south china: New SHRIMP U-pb zircon results and implications for the configuration of Rodinia. *Geology, 30*(2), 163-166. doi:10.1130/0091-7613(2002)030<0163:GCCISC>2.0.CO;2

Li, Z., Zhang, L., & Powell, C. M. (1995). South china in rodinia: Part of the missing link between Australia-East Antarctica and Laurentia? *Geology, 23*(5), 407-410. doi:10.1130/0091-7613(1995)023<0407:SCIRPO>2.3.CO;2

Link, P. K. (., Christie-Blick, N., Devlin, W. J., Elston, D. P., Horodyski, R. J., Levy, M., Miller, J. M. G., Pearson, R. C., Prave, A., Stewart, J. H., Winston, D., Wright, L. A., & Wrucke, C. T. (1993). Middle and late Proterozoic stratified rocks of the western U.S. Cordillera, Colorado Plateau, and Basin and Range province. In J. C. Reed Jr, M. E. Bickford, R. S. Houston, P. K. Link, D. W. Rankin, P. K. Sims & W. R. Van Schmus (Eds.), *Precambrian; conterminous U.S.* (). United States (USA): Geological Society of America, Boulder, CO, United States (USA).

Lowe, D. R. (1982). Sediment gravity flows; II, depositional models with special reference to the deposits of high-density turbidity currents. *Journal of Sedimentary Petrology, 52*(1), 279-297. doi:10.1306/212F7F31-2B24-11D7-8648000102C1865D

Lowe, D. R., & Guy, M. (2000). Slurry-flow deposits in the Britannia Formation (lower Cretaceous), North Sea; a new perspective on the turbidity current and debris flow problem. *Sedimentology, 47*(1), 31-70.

Lucchi, F., & Conoco, Aberdeen, England, sponsor (GBR). (1995). Contessa and associated megaturbidites; long distance (120 X 25 km) correlation of individual beds in a Miocene foredeep. In K. T. Pickering, R. N. Hiscott, N. H. Kenyon, F. Ricci Lucchi & R. D. A. Smith (Eds.), *Atlas of deep-water environments; architectural style in turbidite systems* (). United Kingdom (GBR): Chapman and Hall, London, United Kingdom (GBR).

Luque, F. J., Pasteris, J. D., Wopenka, B., Rodas, M., & Barrenechea, J. F. (1998). Natural fluid-deposited graphite; mineralogical characteristics and mechanisms of formation. *American Journal of Science, 298*(6), 471-498.

Lyons, T. W., Frank, T. D., Lohmann, K. C., & Winston, D. (1994). Carbon-oxygen isotopic trends in the Belt Supergroup (middle Proterozoic), Montana; paleoenvironmental implications; Geological Society of America, 1994 annual meeting. *Abstracts with Programs - Geological Society of America, 26*(7), 50.

Maslin, M. A., Vilela, C., Mikkelsen, N., & Grootes, P. (2005). Causes of catastrophic sediment failures of the Amazon Fan. *Quaternary Science Reviews, 24*(20-21), 2180-2193. doi:10.1016/j.quascirev.2005.01.016

McDonough, M. R. (1989). *The structural geology and strain history of the northern Selwyn Range, Rocky Mountains, near Valemount, British Columbia*. (Doctoral, University of Calgary, Calgary, AB, Canada (CAN)). . (1997-076701)

McHugh, C. M. G., & Ryan, W. B. F. (2000). Sedimentary features associated with channel overbank flow; examples from the Monterey Fan. *Marine Geology, 163*(1-4), 199-215. 162

Middleton, G. V. (1970). Experimental studies related to problems of flysch sedimentation; flysch sedimentology in North America. *Special Paper - Geological Association of Canada, 7*, 253-272.

Michener, L. K. (2007). Stable isotope ratios as tracers in marine food webs: and update. Stable Isotopes and Ecology in Environmental Science. Blackwell Publishing, Oxford, UK. 238-282.

Mikkelsen, N., & Maslin, M. (1998). Sea level controlled catastrophic sediment failures of the quaternary

Amazon Fan complex; 23rd nordiske geologiske vintermode; abstract volume. *Abstracts - Nordic Geological Winter Meeting, 23*, 323.

Mikkelsen, N., Maslin, M. A., Giraudeau, J., Showers, W. J., Flood, R. D., Piper, D. J. W., Klaus, A., Burns, S. J., Busch, W. H., Cisowski, S. M., Cramp, A., Damuth, J. E., Goni, M. A., Haberle, S. G., Hall, F. R., Hinrichs, K., Hiscott, R. N., Kowsmann, R. O., Kronen, J. D.,Jr, Long, D., Lopez, M., McDaniel, D. K., Manley, P. L., Maslin, M. A., Mikkelsen, N., Nanayama, F., Normark, W. R., Pirmez, C., dos Santos, J. R., Schneider, R. R., Showers, W. J., Soh, W., & Thibal, J. (1997). Biostratigraphy and sedimentation rates of the Amazon Fan; proceedings of the ocean drilling program; scientific results, Amazon Fan; covering leg 155 of the cruises of the drilling vessel JOIDES resolution, Bridgetown, Barbados, to Bridgetown, Barbados, sites 930-946, 25 March-24 May 1994. *Proceedings of the Ocean Drilling Program, Scientific Results, 155*, 577-594. doi:10.2973/odp.proc.sr.155.248.1997

Monger, J. W. H., Price, R. A., & Price, R. A. (. (1979). Geodynamic evolution of the Canadian Cordillera; progress and problems; geodynamics Canada. *Canadian Journal of Earth Sciences = Revue Canadienne Des Sciences De La Terre, 16*(3, Part 2), 771-791.

Moores, E. M. (1991). Southwest U.S.-east antarctic (SWEAT) connection; a hypothesis. *Geology (Boulder), 19*(5), 425-428. doi:10.1130/0091-7613(1991)019<0425:SUSEAS>2.3.CO;2

Moraes, M., Maciel, W., Braga, M. S., Vianna, A., & Marques, J. (2004). Bottom-current reworked Paleocene-Eocene reservoirs of Campos Basin, Brazil; Italia 2004; 32nd International Geological Congress; abstracts. *International Geological Congress, Abstracts = Congres Geologique International, Resumes, 32*, 317.

Mulder, T., & Alexander, J. (2001). The physical character of subaqueous sedimentary density flows and their deposits. *Sedimentology, 48*(2), 269-299.

Murphy, D. C. (1987). Kaza group, eastern wells gray park, British Columbia. *Paper - Geological Survey of Canada, 87-1A*, 735-742.

Murphy, D. C. (1987). Suprastructure/infrastructure transition, east-central Cariboo Mountains, British Columbia; geometry, kinematics and tectonic implications. *Journal of Structural Geology, 9*(1), 13-29.

Murphy, D. C., & Journeay, J. M. (1982). Structural style in the premier range, Cariboo Mountains, southern British Columbia; preliminary results; current research; part A. *Paper - Geological Survey of Canada*, (82-1A), 289-292.

Murphy, D. C., & Rees, C. J. (1983). Structural transition and stratigraphy in the Cariboo Mountains, British Columbia. *Paper - Geological Survey of Canada, 83-1A*, 245-252.

Mussa-Caleca, M. (2008). *Architecture and depositional history of a Neoproterozoic deep-water slope channel complex in a passive margin setting: Isaac Formation, Windermere Supergroup, southern Canadian Cordillera.* (MSc, University of Ottawa).

Mutti, E., & Normark, W. R. (1987). Comparing examples of modern and ancient turbidite system: Problems and concepts. In J. K. Leggett, & G. G. Zuffa (Eds.), *Marine clastic sedimentology* (pp. 1) 163

Mutti, E. (1977). Distinctive thin-bedded turbidite facies and related depositional environments in the Eocene Hecho group (south-central pyrenees, spain). *Sedimentology, 24*(1), 107-131.

Mutti, E., Tinterri, R., Di Biasi, D., Fava, L., Mavilla, N., Angella, S., Calabrese, L., Remacha, E., Maestro,

E., Oms, O., & Calvo, J. P. (2000). Delta-front facies associations of ancient flood-dominated fluvio-deltaic systems; IV congreso del grupo espanol del terciario; homenaje a joan rosell i sanuy. 4th congress of the spanish tertiary group; tribute to joan rosell i sanuy. *Revista De La Sociedad Geologica De Espana, 13*(2), 165-190.

Mutti, E. (1992). *Turbidite sandstones*. Italy (ITA): AGIP, Italy (ITA).

Narbonne, G. M., & Aitken, J. D. (1995). Neoproterozoic of the Mackenzie Mountains, northwestern Canada; Neoproterozoic stratigraphy and earth history. *Precambrian Research, 73*(1-4), 101-121.

Navarro, L. (2005). *Depositional architecture and evolution of deep-water base-of-slope and slope channel complexes in a passive-margin setting: Isaac Formation, Windermere Supergroup (Neoproterozoic), southern Canadian Cordillera.* (MSc, University of Ottawa).

Navarro, L., Khan, Z., & Arnott, R. W. C. (2007). Depositional architecture and evolution of a deep-marine channel-levee complex: Isaac Formation (Windermere Supergroup), southern Canadian Cordillera. In T. H. Nilsen, R. D. Shew, G. S. Steffens & J. R. J. Studlick (Eds.), *Atlas of deep-water outcrops* (56th ed., pp. 22) AAPG studies in geology.

Nilsen, T. H., Shew, R. D., Steffens, G. S., & Studlick, J. R. J. (2007). More effective use of outcrops in deep-water studies; 2007 AAPG annual convention & exhibition; abstracts volume. *Abstracts: Annual Meeting - American Association of Petroleum Geologists, 2007*, 101.

Parrish, R., & Armstrong, R. L. (1983). U-pb zircon age and tectonic significance of gneisses in structural culminations of the Omineca crystalline belt, British Columbia; the Geological Society of America, Rocky Mountain section, 36th annual meeting; cordilleran section, 79th annual meeting. *Abstracts with Programs - Geological Society of America, 15*(5), 324.

Peakall, J., McCaffrey, B., & Kneller, B. (2000). A process model for the evolution, morphology, and architecture of sinuous submarine channels. *Journal of Sedimentary Research, 70*(3), 434-448.

Pickering, K. T., Clark, J. D., Ricci Lucchi, F., Smith, R. N., Hiscott, R. N., & Kenyon, N. H. (1995). Architectural element analysis of turbidite systems and selected topical problems for sand-prone deep-water system. In K. T. Pickering, R. N. Hiscott, N. H. Kenyon, F. Ricci Lucchi & R. D. Smith (Eds.), *Atlas of deep-water environments: Architecture style in turbidite systems* (, pp. 1). London: Chapman and Hall.

Pickering, K., Stow, D., Watson, M., & Hiscott, R. (1986). Deep-water facies, processes and models; a review and classification scheme for modern and ancient sediments. *Earth-Science Reviews, 23*(2), 75-174.

Pigage, L. C. (1977). Rb-sr dates for granodiorite intrusions on the northeast margin of the Shuswap metamorphic complex, Cariboo Mountains, British Columbia. *Canadian Journal of Earth Sciences = Revue Canadienne Des Sciences De La Terre, 14*(7), 1690-1695.

Piper, D. J. W., & Normark, W. R. (1983). Turbidite depositional patterns and flow characteristics, navy submarine fan, California borderland. *Sedimentology, 30*(5), 681-694. 164

Piper, D. J. W., & Normark, W. R. (2001). Sandy fans; from Amazon to Hueneme and beyond. *AAPG Bulletin, 85*(8), 1407-1438. doi:10.1306/8626CACD-173B-11D7-8645000102C1865D

Piper, J. D. A. (2000). The Neoproterozoic supercontinent; Rodinia or Palaeopangaea? *Earth and Planetary Science Letters, 176*(1), 131-146.

Piper, J. D. A., & Zhang Qi Rui. (1997). Palaeomagnetism of neoproterozoic glacial rocks of the Huabei shield; the north china block in Gondwana. *Tectonophysics, 283*(1-4), 145-171.

Pirmez, C., Beaubouef, R. T., Friedmann, S. J., & Mohrig, D. C. (2000). Equilibrium profile and base level in submarine channels; examples from late Pleistocene systems and implications for the architecture of deepwater reservoirs; deep-water reservoirs of the world; Gulf Coast Section Society of Economic Paleontologists and Mineralogists Foundation, 20th annual Bob F. Perkins research conference. *Program and Abstracts - Society of Economic Paleontologists.Gulf Coast Section.Research Conference, 20*, 782-805.

Pirmez, C., & Flood, R. (1995). Amazon channel morphology and planform geometry; implications for channel meandering in the deep-sea; geological society of America, 1995 annual meeting. *Abstracts with Programs - Geological Society of America, 27*(6), 129.

Pirmez, C., Imran, J., & Mutti, E. (. (2003). Reconstruction of turbidity currents in amazon channel; turbidites; models and problems. *Marine and Petroleum Geology, 20*(6-8), 823-849. doi:10.1016/j.marpetgeo.2003.03.005

Posamentier, H. W. (2001). Braving the world of deep water exploration; challenges, technologies, and current understandings. *Reservoir, 28*(11), 10-11.

Posamentier, H. W., & Kolla, V. (2003). Seismic geomorphology and stratigraphy of depositional elements in deep-water settings. *Journal of Sedimentary Research, 73*(3), 367-388.

Posamentier, H. W., & Kolla, V. (2003). Seismic geomorphology and stratigraphy of depositional elements in deep-water settings. *Journal of Sedimentary Research, 73*(3), 367-388.

Posamentier, H. W., & Mutti, E. (. (2003). Depositional elements associated with a basin floor channel-levee system; case study from the Gulf of Mexico; turbidites; models and problems. *Marine and Petroleum Geology, 20*(6-8), 677-690. doi:10.1016/j.marpetgeo.2003.01.002

Posamentier, H. W., & Walker, R. G. (2006). Deep-water turbidites and submarine fans; facies models revisited. *Special Publication - Society for Sedimentary Geology, 84*, 399-520.

Postma, G. (1986). Classification for sediment gravity-flow deposits based on flow conditions during sedimentation. *Geology (Boulder), 14*(4), 291-294.

Prather, B. E., Booth, J. R., Steffens, G. S., & Craig, P. A. (1998). Classification, lithologic calibration, and stratigraphic succession of seismic facies of intraslope basins, deep-water Gulf of Mexico; *AAPG Bulletin, 82*(12), 707R.

Price, R. A., Mossop, G. D. (., & Shetsen, I. (. (1994). Cordilleran tectonics and the evolution of the Western Canada Sedimentary Basin. In *Geological atlas of the Western Canada Sedimentary Basin*. Canada (CAN). 165

Prior, D. B., Adams, C. E., & Coleman, J. M. (1983). Characteristics of deep-sea channel of middle Mississippi fan as revealed by a high-resolution survey; gulf coast association of geological societies and gulf coast section SEPM meeting. *AAPG Bulletin, 67*(9), 1470.

Reesor, J. E. (1973). *Geology of the lardeau map-area, east-half, British Columbia*. Canada (CAN): Geological Survey of Canada, Ottawa, ON, Canada (CAN).

Reid, L. F., Simony, P. S., & Ross, G. M. (2002). Dextral strike-slip faulting in the Cariboo Mountains, British Columbia; a natural example of wrench tectonics in relation to cordilleran tectonics. *Canadian Journal of Earth Sciences = Revue Canadienne Des Sciences De La Terre, 39*(6), 953-970.

Reid, L., Cook, F. A., Erdmer, P. (1997). Structural correlation across the suprastructure-infrastructure

transition (Cariboo Mountains, British Columbia); possible, impossible or work in progress?; lithoprobe slave-NORthern cordillera lithospheric evolution (SNORCLE) and cordilleran tectonics workshop; report of the 1997 combined meeting. *Lithoprobe Report, 56*, 181-182.

Root, K. G. (1987). *Geology of the delphine creek area, southeastern British Columbia; implications for the Proterozoic and Paleozoic development of the cordilleran divergent margin*. (Map, University of Calgary, Calgary, AB, Canada (CAN)). . (1990-052682)

Ross, G. M., Broome, J., Miles, W., Mossop, G. D. and Shetsen, I. (1994). Potential fields and basement structure; western Canada sedimentary basin. In *Geological atlas of the western Canada sedimentary basin*. Canada (CAN):

Ross, G. M., & Ferguson, C. A. (2003). *Geology and structure cross-sections, McBride, British Columbia* (14, Geologic maps No. 2004A). Canada (CAN): Geological Survey of Canada, Ottawa, ON, Canada (CAN).

Ross, G. M., & Arnott, R. W. C. (2007). Regional geology of the Windermere Supergroup, southern Canadian Cordillera and stratigraphic setting of the Castle Creek study area, Canada. In T. H. Nilsen, R. D. Shew, G. S. Steffens & J. R. J. Studlick (Eds.), *Atlas of deep-water outcrops* (, pp. 16 p.) AAPG Studies in Geology.

Ross, G., McMechan, M. E., & Hein, F. J. (1989). Proterzoic history: The birth of the miogeocline. In B. D. Ricketts (Ed.), *Western Canada sedimentary basin: A case history* (, pp. 79-104) CSPG Special Publication.

Ross, G., McMechan, M. E., & Hein, F. J. (1989). Proterozoic history; the birth of the miogeocline. In B. D. Ricketts (Ed.), *Western Canada sedimentary basin; a case history* (). Canada (CAN): Can. Soc. Pet. Geol., Calgary, AB, Canada (CAN).

Ross, G. M. (2000). *The Neoproterozoic Windermere Supergroup; an on-land continental margin turbidite system, British Columbia and Alberta* (12, Stratigraphy No. 3932). Canada (CAN): Geological Survey of Canada, Calgary, AB, Canada (CAN).

Ross, G. M. (1991). Tectonic setting of the Windermere Supergroup revisited. *Geology (Boulder), 19*(11), 1125-1128. doi:10.1130/0091-7613(1991)019<1125:TSOTWS>2.3.CO;2

Ross, G. M., & Murphy, D. C. (1988). Transgressive stratigraphy, anoxia, and regional correlations within the late Precambrian Windermere grit of the southern Canadian Cordillera. *Geology (Boulder), 16*(2), 139-143. doi:10.1130/0091-7613(1988)016<0139:TSAARC>2.3.CO;2 166

Ross, G. M., Bloch, J. D., & Krouse, H. R. (1995). Neoproterozoic strata of the southern Canadian Cordillera and the isotopic evolution of seawater sulfate; Neoproterozoic stratigraphy and earth history. *Precambrian Research, 73*(1-4), 71-99.

Ross, G. M., & Bowring, S. A. (1990). Detrital zircon geochronology of the Windermere Supergroup and the tectonic assembly of the southern Canadian Cordillera. *Journal of Geology, 98*(6), 879-893.

Russell, H. A. J., & Arnott, R. W. C. (2003). Hydraulic-jump and hyperconcentrated-flow deposits of a glacigenic subaqueous fan; oak ridges moraine, southern Ontario, Canada. *Journal of Sedimentary Research, 73*(6), 887-905.

Saller, A. H., Noah, J. T., Ruzuar, A. P., & Schneider, R. (2004). Linked lowstand delta to basin-floor fan deposition, offshore Indonesia; an analog for deep-water reservoir systems. *AAPG Bulletin, 88*(1), 21-46. doi:10.1306/E51AA024-C62F-42E4-8C217681C5F44185

Saller, A., Lin, R., & Dunham, J. (2006). Leaves in turbidite sands; the main source of oil and gas in the deep-water Kutei Basin, Indonesia. *AAPG Bulletin, 90*(10), 1585-1608. doi:10.1306/04110605127

Satish-Kumar, M., Wada, H., & Santosh, M. (2002). Constraints on the application of carbon isotope thermometry in high- to ultrahigh-temperature metamorphic terrains. *Journal of Metamorphic Geology, 20*(3), 335-350.

Schwenk, T., Spiess, V., Huebscher, C., & Breitzke, M. (2003). Frequent channel avulsions within the active channel-levee system of the middle Bengal fan; an exceptional channel-levee development derived from parasound and hydrosweep data; the bay of Bengal. *Deep-Sea Research. Part II: Topical Studies in Oceanography, 50*(5), 1023-1045. doi:10.1016/S0967-0645(02)00618-5

Sears, J. W., & Price, R. A. (1978). The Siberian connection; a case for Precambrian separation of the North American and Siberian cratons. *Geology (Boulder), 6*(5), 267-270.

Sears, J. W., & Price, R. A. (2000). New look at the Siberian connection; no SWEAT. *Geology (Boulder), 28*(5), 423-426. doi:10.1130/0091-7613(2000)028<0423:NLATSC>2.3.CO;2

Shanmugam, G. (1996). High-density turbidity currents; are they sandy debris flows? *Journal of Sedimentary Research, 66*(1), 2-10.

Shanmugam, G. (1997). Deepwater exploration; conceptual models and their uncertainties. *The Bulletin of the Houston Geological Society, 39*(7), 13.

Sloss, L. L. (1963). Sequences in the cratonic interior of North America. *Geological Society of America Bulletin, 74*(2), 93-113. doi:10.1130/0016-7606(1963)74[93:SITCIO]2.0.CO;2

Smith, M. D. (2009). *Stratigraphic and geochemical evolution of the Old Fort Point Formation, southern Canadian Cordillera: The deep-marine perspective of Ediacaran post-glacial environmental change*. (PhD, University of Ottawa).

Southard, J. B., & Boguchwal, L. A. (1990). Bed configuration in steady unidirectional water flows; part 2, synthesis of flume data. *Journal of Sedimentary Petrology, 60*(5), 658-679. 167

Sprague, A. R., Sullivan, M. D., Campion, K. M., Jensen, G. N., Goulding, F. J., Garfield, T. R., Sickafoose, D. K., Rossen, C., Jennette, D. C., Beaubouef, R. T., Abreu, V., Ardill, J., Porter, M. L., & Zelt, F. B. (2002). The physical stratigraphy of deep-water strata; a hierarchical approach to the analysis of genetically related stratigraphic elements for improved reservoir prediction; AAPG annual convention with SEPM. *Annual Meeting Expanded Abstracts - American Association of Petroleum Geologists, 2002*, 167.

Stelting, C. E., Pickering, K. T., Bouma, A. H., Coleman, J. M., Cremer, M., Droz, L., Meyer-Wright, A. A., Normark, W. R., O'Connell, S., Stow, D. A. V., & Deep Sea Drilling Project, Leg 96 Shipboard Scientists, United States (USA). (1985). Drilling results on the middle Mississippi Fan. In A. H. Bouma, W. R. Normark & N. E. Barnes (Eds.), *Submarine fans and related turbidite systems* (). United States (USA): Springer-Verlag, New York, NY, United States (USA).

Stewart, J. H. (1976). Late Precambrian evolution of North America; plate tectonics implication. *Geology (Boulder), 4*(1), 11-15.

Stewart, J. H. (1972). Initial deposits in the cordilleran geosyncline; evidence of a late precambrian (<850 m.y.) continental separation. *Geological Society of America Bulletin, 83*(5), 1345-1360. doi:10.1130/0016-7606(1972)83[1345:IDITCG]2.0.CO;2

Stow, D. A. V., & Gorsline, D. S. (. (1985). Fine-grained sediments in deep water; an overview of

processes and facies models; origins, transport, and deposition of fine-grained sediments; 1984 SEPM research conference, part II. *Geo-Marine Letters, 5*(1), 17-23.

Stow, D. A. V., & Johansson, M. (2000). Deep-water massive sands; nature, origin and hydrocarbon implications; deep-water sedimentary systems; new models for the 21st century. *Marine and Petroleum Geology, 17*(2), 145-174.

Straub, K. M., & Mohrig, D. (2008). Quantifying the morphology and growth of levees in aggrading submarine channels. *Journal of Geophysical Research, 113*(F3), @Citation F03012. doi:10.1029/2007JF000896

Straub, K. M., Mohrig, D., McElroy, B., Buttles, J., & Pirmez, C. (2008). Interactions between turbidity currents and topography in aggrading sinuous submarine channels; a laboratory study. *Geological Society of America Bulletin, 120*(3-4), 368-385. doi:10.1130/B25983.1

Sture Hansson, J.E.H., Elmgren R., Larsson U., Fry, B., Johansson, S. (1997). The stable nitrogen isotope ratio as a marker of food-web interactions and fish migration. *Ecology,* 78, 2249-2257.

Sumner, E. J., Amy, L. A., & Talling, P. J. (2008). Deposit structure and processes of sand deposition from decelerating sediment suspensions. *Journal of Sedimentary Research, 78*(8), 529-547. doi:10.2110/jsr.2008.062

Tazaki, K., Ferris, E.G., Wiese, R.G. and Fyfe, W.S. (1992) Iron and graphite associated with fossil bacteria in chert. *Chem. Geol*., 95, 313-325.

Thompson, J. A., & Ross, G. M. (1990). Feild trip 3: Late Proterozoic stratigraphy in the McBride area (British Columbia): Windermere turbidites, condensed intervals and the vanished carbonate platform. *Late Proterozoic Glaciation, Rifting, and Eustacy as Illustrated by the Windermere Supergroup,* Invermere and Valmount, British Columbia. 7.1-7.13.

Thompson, B., Mercier, E., & Roots, C. (1987). Extension and its influence on Canadian Cordillera passive-margin evolution; continental extensional tectonics. *Geological Society Special Publications, 28*, 409-417. 168

Twichell, D. C., Schwab, W. C., Kenyon, N. H., & Conoco, Aberdeen, England, sponsor (GBR). (1995). Geometry of sandy deposits at the distal edge of the Mississippi fan, gulf of Mexico. In K. T. Pickering, R. N. Hiscott, N. H. Kenyon, F. Ricci Lucchi & R. D. A. Smith (Eds.), *Atlas of deep water environments; architectural style in turbidite systems* (). United Kingdom (GBR): Chapman and Hall, London, United Kingdom (GBR).

Twichell, D. C., Kenyon, N. H., Parson, L. M., & McGregor, B. A. (1991). Depositional patterns of the Mississippi fan surface; evidence from GLORIA II and high-resolution seismic profiles; seismic facies and sedimentary processes of submarine fans and turbidite systems. *SEPM Midyear Meeting, Austin, TX,* United States.

Twichell, D. C., Schwab, W. C., Nelson, C. H., Kenyon, N. H., & Lee, H. J. (1992). Characteristics of a sandy depositional lobe on the outer Mississippi fan from SeaMarc IA sidescan sonar images. *Geology (Boulder), 20*(8), 689-692. doi:10.1130/0091-7613(1992)020<0689:COASDL>2.3.CO;2

Ueno, Y., Yurimoto, H., Yoshioka, H., Komiya, T., & Maruyama, S. (2002). Ion microprobe analysis of graphite from ca. 3.8 ga metasediments, isua supracrustal belt, west Greenland; relationship between metamorphism and carbon isotopic composition. *Geochimica Et Cosmochimica Acta, 66*(7), 1257-1268.

Vidal, G. and Ford, T.D. (1985). Microbiotas from the Late Proterozoic Chuar Group (Northern Arizona) and Uinta Group (Utah) and their chronostratigraphic implications. *Precambrian Research*, 28,

344–389.

Vorob'eva, N.G., Sergeev, V.N., Knoll, A.H. (2009). Neoproterozoic microfossils from the margin of the East European Platform and the search for a biostratigraphic model of lower Ediacaran rocks. *Precambrain Research*, 173(1-4), 163-169.

Vrolijk, P. J., & Southard, J. B. (1997). Experiments on rapid deposition of sand from high-velocity flows. *Geoscience Canada, 24*(1), 45-54.

Walker, J. F. (1926). Geology and mineral deposits of Windermere map area, British Columbia. *69 Pp,*

Walker, N. (1992). Middle Proterozoic geologic evolution of llano uplift, Texas; evidence from U-pb zircon geochronometry. *Geological Society of America Bulletin, 104*(4), 494-504. doi:10.1130/0016-7606(1992)104<0494:MPGEOL>2.3.CO;2

Walker, R. G. (1985). Mudstones and thin-bedded turbidites associated with the upper cretaceous wheeler gorge conglomerates, California; a possible channel-levee complex. *Journal of Sedimentary Petrology, 55*(2), 279-290. doi:10.1306/212F869D-2B24-11D7-8648000102C1865D

Walker, R. G., & James, N. P. (1992). *Facies models: Response to sea level change* Geological Association of Canada.

Walton, E. K. (1967). The sequence of internal structures in turbidites. *Scottish Journal of Geology, 3*, 306-317.

Watanabe, H., and Akiyama M. (1998). Characterization of organic matter in the Miocene turbidities and hemipelagic mudstones in the Niigata oil field, central Japan. *Organic Geochemistry*, .29 (1-3), 605-611.

Wentworth, C. K. (1922). A scale of grade and class terms for clastic sediments. *Journal of Geology, 30*(5), 377-392.

Williams, J. C. (1976). The segregation of particulate materials: A review. *Powder Technology, 15*, 245.

Wingate, M. T. D., Pisarevsky, S. A., & Evans, D. A. D. (2002). Rodinia connection between Australia and Laurentia; no SWEAT, no AUSWUS? *Terra Nova, 14*(2), 121-128.

Wopenka, B., & Pasteris, J. D. (1993). Structural characterization of kerogens to granulite-facies graphite; applicability of Raman microprobe spectroscopy. *American Mineralogist, 78*(5-6), 533-557.

Young, F. G., Campbell, R. B., & Poulton, T. P. (1973). The Windermere Supergroup of the southeastern Canadian Cordillera. In *Belt symposium 1973, vol. 1* (). USSR (SUN): Idaho, Univ., Dep. Geol.--Idaho Bur. Mines Geol., Moscow, Idaho.

Appendix A: *Detailed channel correlation*

Detailed stratigraphic correlation over channel unit. The channel unit consists of three discrete, vertically aggrading, laterally migrating channel fills (CH1, CH2 and CH3). Channel fills are composed of alternating coarse- and fine-grained LADs which dip toward the base of the individual channel fills. Note fine-grained LADs are more common near the top of channel fills and are eroded by coarse LADs toward the base of the channel fill. Channel fills are separated by thick mudstone units.

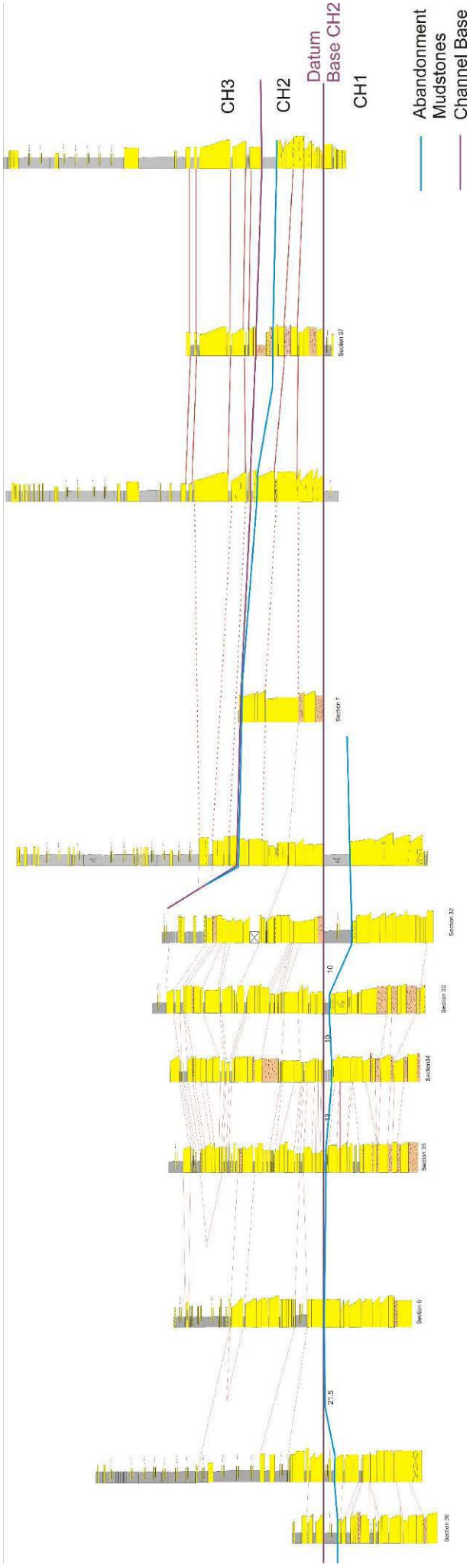

Appendix B: *Correlation across the glacier*

In part of the Castle Creek study area, a more than 1.2 km thick succession of laterally continuous base-of-slope deposit is exposed on both sides of the Castle Creek glacier. Using organic-rich carbon horizons as a datum (Figure A.1; A.2) the architectural elements described in this study, channel, distal levee and crevasse splay are correlated to similar architectural elements described by Altosaar (2007) on the south side of the glacier (Figure A.3). In addition, underlying distal levee strata (north side) described by Khan (unpublished) are correlated to distal levee deposits on the south side and overlying, channel deposits (north side) described by Arnott (2007) are correlated to Isaac Channel 4 (IC4; Figure A.1) described by Mussa-Caleca (2008). In order to aid the correlation across the glacier, control logs were measured below the study area (north side) in distal levee deposits measured by Khan (unpublished) (Figure A.4), above the study area in crevasse splay deposits described by Arnott (2007) (Figure 3.46) and on the south side in interchannel deposits described by Altosaar (2007) (Figure A.2).

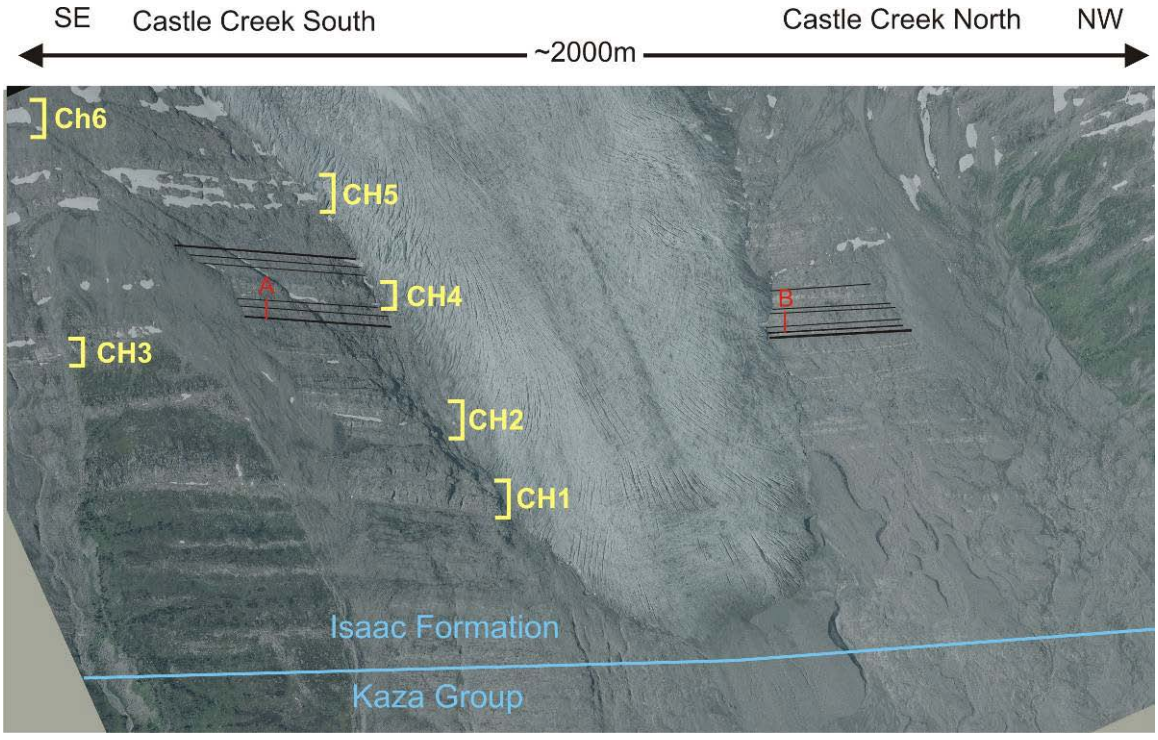

Figure B.1: Organic rich intervals used to correlate strata across the Castle Creek glacier. Stratigraphic section line locations for Figure A.2 (A and B) are displayed in red.

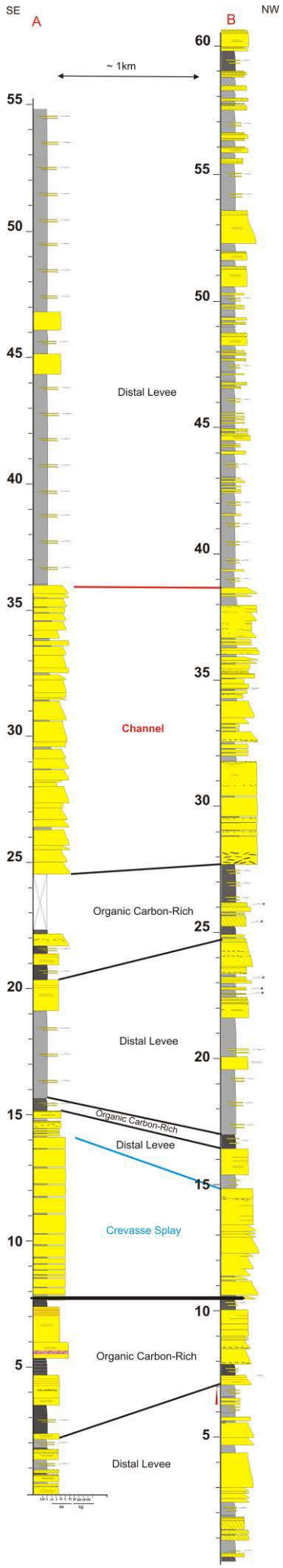

Figure B.2: Correlation across the glacier using organic carbon-rich marker horizons as the data. Section line locations are plotted in red on Figure A.1.

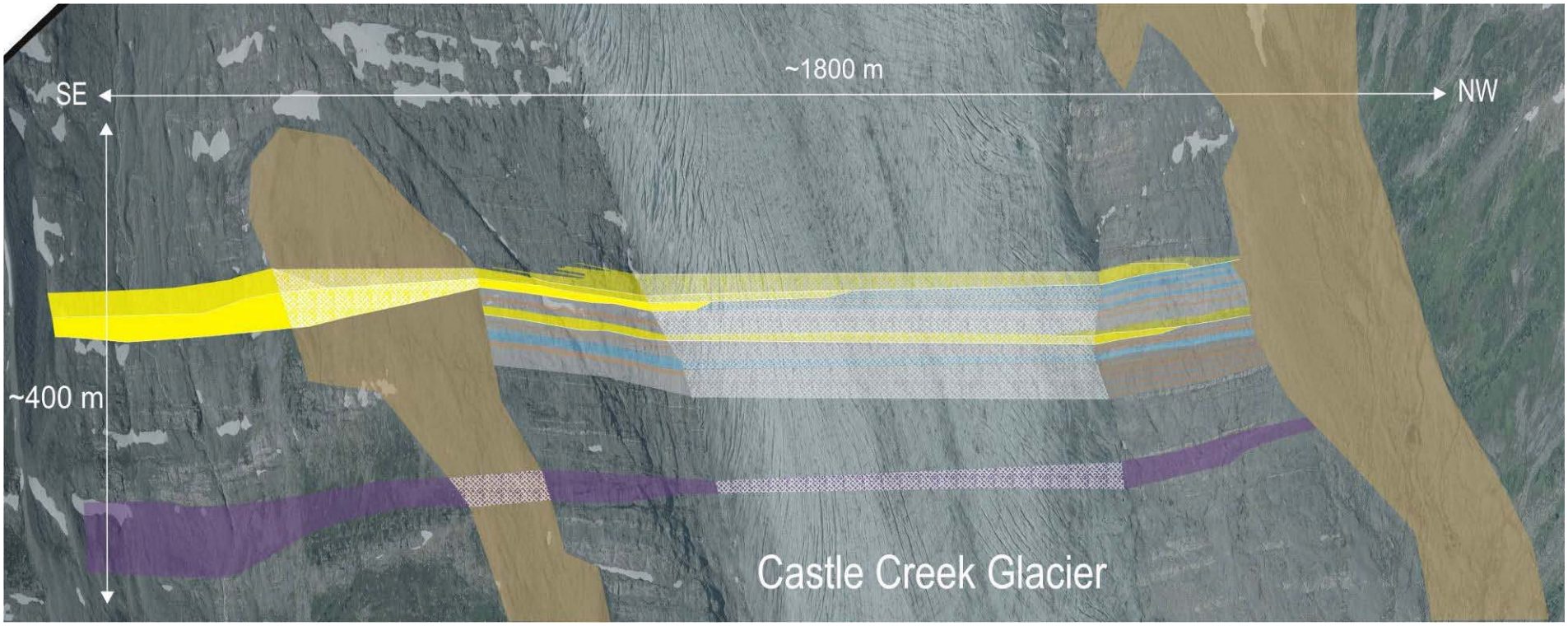

Figure A.3: Cross-glacier correlation of architectural elements including: channel, crevasse splay and levee deposits using organic carbon-rich marker beds and a debris flow (purple) as data. Vertical exaggeration 2X.

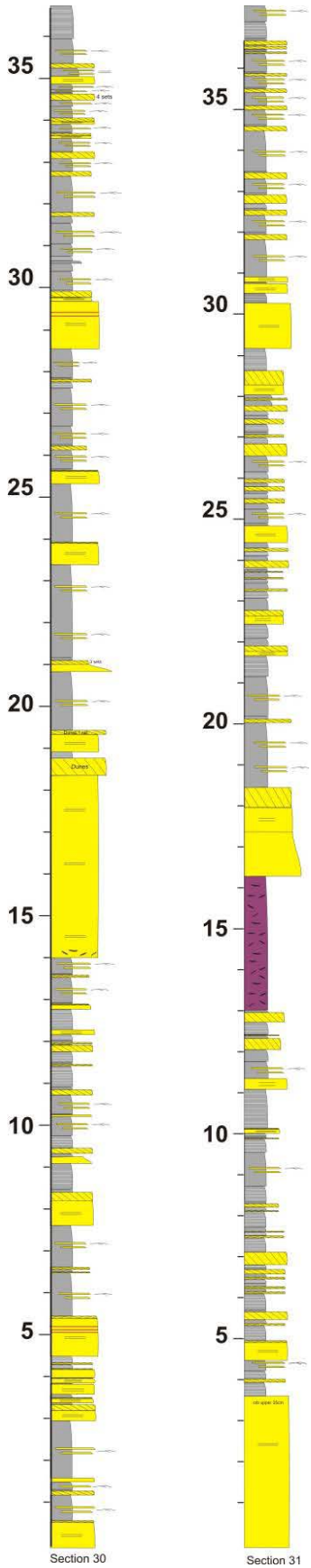

Figure B.4: Two uncorrelated stratigraphic columns measured through distal levee deposits in an area mapped by Khan (2004-2005, unpublished). The yellow represents sandstone, grey represents mudstone and purple represents debris flow deposits.